JOURNAL OF GEOPHYSICAL RESEARCH

The continuation of

TERRESTRIAL MAGNETISM AND ATMOSPHERIC ELECTRICITY
(1896-1948)

An International Quarterly

VOLUME 63 June, 1958 NUMBER 2

CONTENTS

(Contents concluded on outside back cover)

Published at

THE WILLIAM BYRD PRESS, INC.

P. O. BOX 2-W, SHERWOOD AVE. AND DURHAM ST.

RICHMOND 5, VIRGINIA

Address all correspondence to

JOURNAL OF GEOPHYSICAL RESEARCH

5241 BROAD BRANCH ROAD, NORTHWEST

WASHINGTON 15, D. C., U.S.A.

SIX DOLLARS A YEAR

SINGLE NUMBERS, TWO DOLLARS

JOURNAL OF GEOPHYSICAL RESEARCH

The continuation of

Terrestrial Magnetism and Atmospheric Electricity

(1896-1948)

An International Quarterly

Founded 1896 by L. A. BAUER *Continued 1928-1948 by* J. A. FLEMING

Editor: MERLE A. TUVE *Editorial Assistant:* WALTER E. SCOTT

Fields of Interest

Terrestrial Magnetism
Atmospheric Electricity
The Ionosphere
Solar and Terrestrial Relationships
Aurora, Night Sky, and Zodiacal Light
The Ozone Layer
Meteorology of Highest Atmospheric Levels
The Constitution and Physical States of the Upper Atmosphere
Special Investigations of the Earth's Crust and Interior, including experimental seismic waves, physics of the deep ocean and ocean bottom, physics in geology
And similar topics

This Journal serves the interests of investigators concerned with terrestrial magnetism and electricity, the upper atmosphere, the earth's crust and interior by presenting papers of new analysis and interpretation or new experimental or observational approach, and contributions to international collaboration. It is not in a position to print, primarily for archive purposes, extensive tables of data from observatories or surveys, the significance of which has not been analyzed.

Forward *manuscripts* to one of the Associate Editors, or to the editorial office of the Journal at 5241 Broad Branch Road, Northwest, Washington 15, D. C., U.S.A. It is preferred that manuscripts be submitted in English, but communications in French, German, Italian, or Spanish are also acceptable. A brief abstract, preferably in English, must accompany each manuscript. A *publication charge* of $8 per page will be billed by the Editor to the institution which sponsors the work of any author; private individuals are not assessed page charges. Manuscripts from outside the United States are invited, and should not be withheld or delayed because of currency restrictions or other special difficulties relating to page charges. Costs of publication are roughly twice the total income from page charges and subscriptions, and are met by subsidies from the Carnegie Institution of Washington and international and private sources.

Back issues and *reprints* are handled by the Editorial Office, 5241 Broad Branch Road, N.W., Washington 15, D. C., U.S.A.

Subscriptions are handled by the Editorial Office, 5241 Broad Branch Road, N.W., Washington 15, D. C., U.S.A.

Second-class mail privileges authorized at Richmond, Virginia

Journal of

GEOPHYSICAL RESEARCH

The continuation of

Terrestrial Magnetism and Atmospheric Electricity

VOLUME 63 JUNE, 1958 No. 2

THE EARTH'S MAGNETIC FIELD ABOVE WSPG, NEW MEXICO, FROM ROCKET MEASUREMENTS

BY J. P. HEPPNER, J. D. STOLARIK, AND L. H. MEREDITH

U. S. Naval Research Laboratory, Washington 25, D. C.

(Received November 16, 1957)

ABSTRACT

The absolute magnetic field was measured from ground level to an altitude of 163 km in this first rocket flight of a proton precessional magnetometer. The change in field with altitude differs significantly from that of a dipole. The field was typically quiet at firing time and an ionospheric discontinuity was not detected.

INTRODUCTION

There are numerous problems concerning the earth's magnetic field and ionospheric electric currents causing variations in the field which cannot be solved solely from surface measurements. With magnetic field measurements taken from a rocket vehicle, solutions to many of these problems are potentially possible (see, for example, reviews by Chapman [1 of "Reference" at end of paper] and Vestine [2]). As the earth's magnetic field is a principal factor in controlling the movements of electrons and ions from about 90 km to beyond the limits of our atmosphere, the study of its variations contributes to most phases of ionospheric physics. Rocket magnetic-field measurements are also of interest to the solid earth geophysicist, in that they offer the opportunity to improve the description of the earth's main field and secular variations, and to improve determinations of the depth of conducting layers in which induction currents are created by ionospheric currents.

In three flights of the NOL flux-gate magnetometer, Maple, Bowen, and Singer [3, 4] initiated the study of the earth's magnetic field using rockets. Informa-

tion on the decrease with altitude of the main field and the altitude of the equator electrojet was obtained.

Because the earth's magnetic field was a significant parameter in upper a processes, the Naval Research Laboratory was in 1953-54 concerned with selecti and/or development of a magnetometer for rocket measurements. The complicat orientation, calibration, and drift characteristics of the flux-gate type of magneto eter left much to be desired. It is fortunate that at this time Packard and Varian [of Varian Associates, Palo Alto, California, announced the invention of the prot precessional magnetometer. In 1955, development of a proton precessional ma netometer for rocket exploration was undertaken by Varian Associates und NRL sponsorship.

The first rocket model was flown to an altitude of 163 km in Aerobee NRL-3 at White Sands Proving Ground, New Mexico, 0052 MST, 5 July 1956.* Althoug the intention in this flight was merely to check the magnetometer system, excelle measurements were obtained at the rate of one measurement every 0.55 secon from one second to 367 seconds after launching, when the rocket partially brok upon reentering the atmosphere. The present report covers briefly: the operatio of the proton precessional magnetometer, the techniques for accurately countin the precession frequency, and special considerations involved in rocket installatio The decrease of field with altitude is compared to a dipole behavior. Inasmuch a a definitive discontinuity was not encountered, we assign only an upper limit t the possible magnitude of an ionospheric discontinuity at the time of flight.

THE PROTON PRECESSIONAL MAGNETOMETER

Operational Principles

A number of papers have been written pertaining to the operational theor of the proton precessional magnetometer. The nuclear induction experiments o Bloch [6] and Purcell [7] and their associates laid the foundation for future appli cations. Packard [8] presented the method for extending nuclear induction measure ments to measurements of the earth's magnetic field and gave results of early measurements at Varian Associates. Waters and Francis [9] have described thei proton precessional magnetometer, with particular emphasis on effects of field gradients across the sample. A balloon-borne magnetometer was described by Cahill and Van Allen [10] in this JOURNAL. The signal-to-noise ratio has beer treated in detail by Rempel [11]. The feasibility study for operation of the mag netometer in an earth satellite by Bloom and Johnson [12] is of particular interest as it is in some respects an extrapolation of the rocket unit used in Aerobee NRL-33 and NRL's IGY rockets. Descriptions of the rocket unit and principles involved have been presented at various meetings by Allen and Packard [13] and by the authors of this paper [14]. In view of the above, the theory will be only outlined here.

In a magnetic field of total absolute intensity (F) the proton's magnetic moments precess about the field at an angular frequency (ω) given by $\omega = \gamma_p F$, where γ_p is the gyromagnetic ratio of the proton. As γ_p is $2.67528 \pm 0.00006 \times 10^4$ sec^{-1}

*The nightglow experiment also flown in this rocket was reported in a separate paper in the March 1958 issue of this JOURNAL.

gauss^{-1}, highly accurate absolute total scalar field values result from accurate measurements of the frequency (f), where

$$f = \omega/2\pi = 4257.8(F) \quad (1)$$

Utilization of this simple relationship depends on

(*a*) Getting a sufficient number of proton moments in phase coherence to produce a detectable induced signal in a coil

(*b*) Maintaining the phase coherence for a period long enough to accurately measure f, and

(*c*) Having highly sensitive circuitry for frequency selection and amplification of the induced signal

Getting the proton moments in phase coherence may also be treated in terms of getting an excess number of protons in the higher of their two energy levels, followed by emission of frequency f, but it is usually easier to visualize a macroscopic precessing moment.

The in-phase precession is, in practice, established by creating a strong, polarizing magnetic field, **H**, through the proton sample at preferably a large angle to the earth's field, **F**. The polarization field can give the proton sample a net nuclear magnetic moment $\mathbf{M}_0 = X\mathbf{H}$, where X is the nuclear susceptibility. After time t, about equal to T_1 (the thermal relaxation time for the particular sample), sufficient polarization

$$M = M_0[1 - \exp(-t/T_1)]$$

is achieved and the polarization field is turned off sharply. The protons' moment, **M**, is then free to precess in the earth's field. The precessing moment induces a voltage of frequency $\omega = \gamma_p F$ in the surrounding coil. The induced signal will decay exponentially as $M \exp(-t/T_2)$, where T_2 ($\leq T_1$), called the transverse relaxation time, is the time required for phase incoherence. The frequency, and thus the field measurement, is independent of orientation. The signal amplitude, however, varies as $\sin^2\theta$, where θ is the angle between the coil axis and the earth's field, when the same coil is used for both the polarization current and the sensing coil.

Design Considerations

Use of the magnetometer in a rocket involved design features which would not normally be important in a surface instrument. These are outlined below.

a. *Coil orientation*: Due to the $\sin^2\theta$ signal-amplitude dependence, mentioned above, there is the possibility that a coil can get oriented such that nearly zero amplitude is obtained over much of a rocket flight. In the Aerobee rocket, where weight is not critical, it is thus advisable to use two perpendicular coils and alternately take readings from each. High amplitude signals from at least one coil are then always assured.

b. *Rocket roll and precession motions*: Although precession of **M** about the earth's field is independent of other motions, the frequency of the induced signal depends on the relative motion of **M** and the coil. If, for example, a coil is rotated such that its axis revolves in a plane perpendicular to the earth's field, the rotation frequency will directly add to, or subtract from, the precession frequency giving a detected frequency of f (proton) $\pm f$ (coil

rotation). Since a typical rocket will roll about its longitudinal axis, th detected frequency from a coil oriented with its axis perpendicular to th rocket axis will include the roll frequency. The instantaneous roll-frequenc effect is also a function of the angle between the rocket axis and the earth field. The effect, computed by Bloom [15], is illustrated in Figure 1(*a*) The rocket roll, in addition to affecting the frequency in a perpendicula coil, also modulates the precession envelope. The modulation of the envelop can serve as a measure of roll frequency in correcting for the roll effect this is not known by independent means. As the per cent modulation shown in Figure 1(*b*), increases with θ, the envelope modulation gives th roll frequency most clearly when the correction is large.

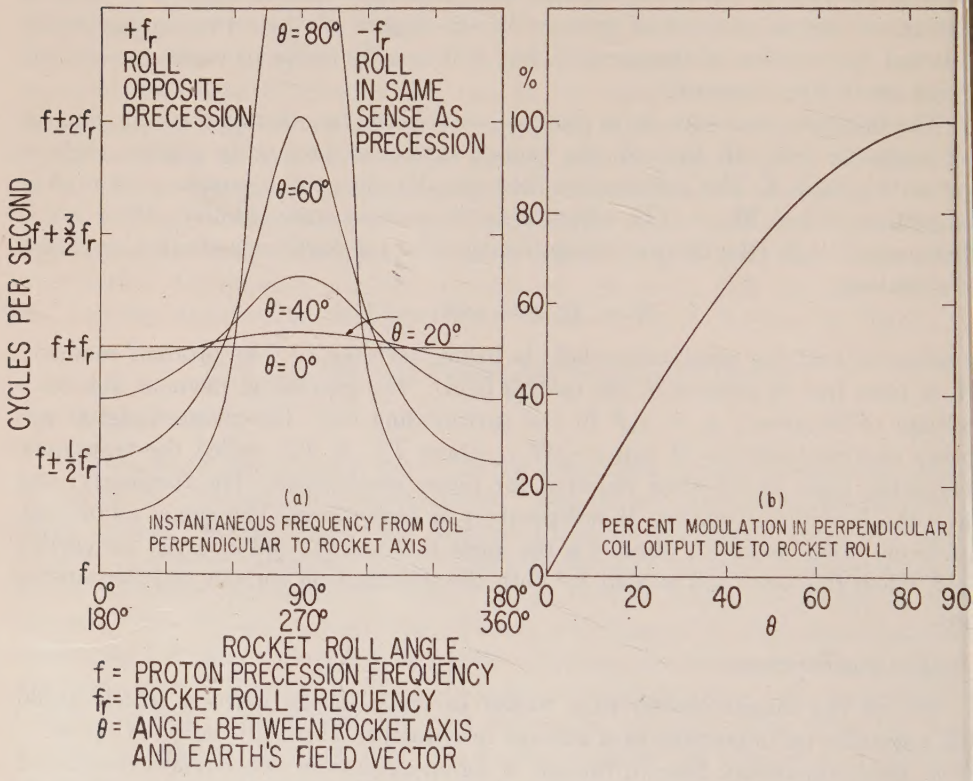

FIG. 1 (after Bloom)

A coil oriented with its axis along the rocket axis is unaffected by rocket roll, but will be affected by precession of the rocket axis. In general, precession of the Aerobee will be too slow to be of consequence and corrections are not necessary.

c. *Measurement repetition rate*: Since the rocket velocity is about a kilometer/sec (Aerobee) or mile/sec (Aerobee-Hi) in passing through the E region, the time interval between measurements must be small if sharp ionospheric discontinuities are to be accurately resolved. It is thus advantageous to have the T_1 and T_2 times short. T_2 must, however, be long enough to count

a large number of cycles when accurate measurements are desired. Thus, a compromise between resolution and accuracy is necessary.

The Rocket Magnetometer

The above considerations led to the design of a two-coil magnetometer, in which the coils are alternately polarized and read to give one reading per second from each coil. Figure 2 is a block diagram of the rocket unit. Programming of the

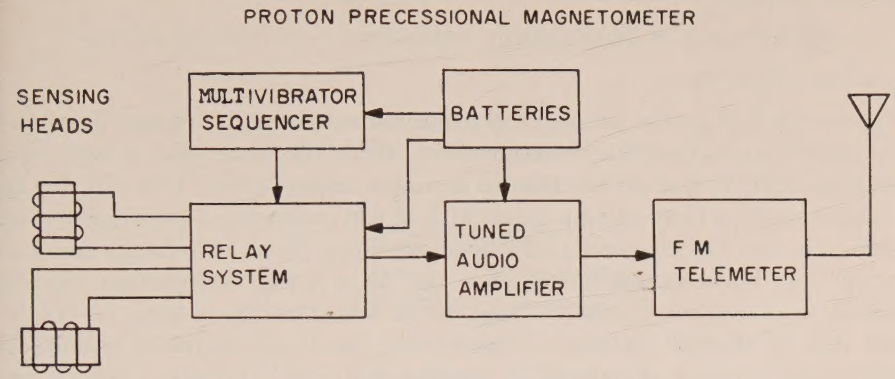

FIG. 2

switching relays was done with two multivibrator circuits. The first switched the sensing heads from batteries (for polarization current) to the amplifier (for precession signal amplification) every quarter-second. The second multivibrator, triggered from the first, alternated the sensing heads each half-second at the end of the quarter-second read interval. To obtain a quarter-second T_2 time, a kerosene-oil mixture was used for the proton sample. The band-pass of the tuned amplifier, determined primarily by the input transformer, was set at 600 cycles, with a center frequency of 2,000 cps for the White Sands firing. Over this band-

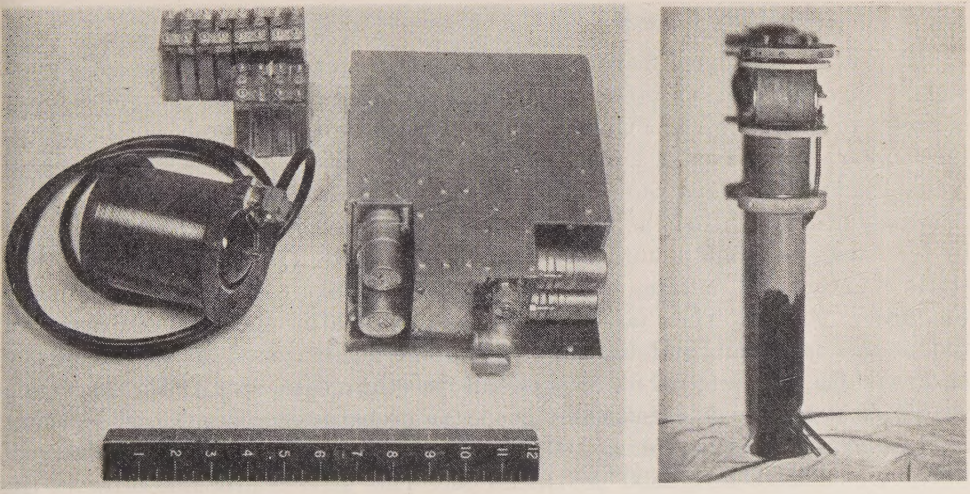

FIG. 3

width, the average signal to noise ratio was about 10 to 1. With a 12-volt, 6-ampere, polarization power and amplifier voltage gain of about 10^6, a peak to peak voltage of 1 to 3 volts was presented to the FM telemeter over a wide range of orientations.

Figure 3(*a*) is a photograph of the instrument (only one sensing head is shown). Figure 3(*b*) shows the two sensing heads in mounted position after wrapping with a Faraday shield to reduce electrical pick-up. The Zn-AgO batteries provide polarization and filament current. Dry cells for B^+ voltage are contained in the electronics package.

COUNTERS FOR PRECESSION FREQUENCY DETERMINATIONS

Design Considerations

The accuracy of proton precessional measurements is in many cases determined by the technique of frequency measurement. With any technique, a high signal-to-noise ratio, S/N, is a prerequisite to accurate measurement. It is obvious that this ratio cannot be large using a bandwidth of 600 cycles when the angle between the coil axis and the magnetic field is small. Thus, if measurements are to be obtained from both sensing heads when one is in a poor orientation, the S/N presented to a frequency counter must be increased by decreasing N. As N is largely due to thermal sources in the sensing head and amplifier circuits and amplifier tube noise, it is reduced by passing the signal through a narrow band filter, centered on the precession frequency. Selection of the precession frequency throughout a rocket flight is made more difficult by the rapid change in field values when the rocket velocity is high. For example, at velocities of 1 mile/sec and field gradients of 40 γ/mile, the frequency change is about 17 cycles in 10 seconds. Thus, if a quantity of data is to be reduced, it is desirable to have automatic means for centering the band pass.

A direct count of the precession frequency over short measurement periods does not give very accurate field values, as 1 cycle/sec = 23.486 gammas. However, using standard counting techniques, the accuracy is improved by a factor of about 50 by counting a 100-kc frequency standard gated from the precession signal.

Self-Tuning Frequency Counter

To provide the above features, a self-tuning frequency counter was designed and built by Varian Associates as a part of the magnetometer system. The counter is shown in block form in Figure 4. Since a synchronizing pulse is not provided, the counter starts its operation from receipt of the precession envelope. The signal is amplitude limited and filtered before entering the signal (or "slow") counter. A switching transient at the leading edge of the precession envelope is avoided by blanking the counters until 128 cycles have passed. The "slow" counter then starts counting and initiates the counting of the 100-kc oscillator by the 100-kc (or "fast") counter. The "fast" counter is stopped after the next 256 cycles of the precession signal, and the input is automatically tuned to the frequency observed. The time interval for 256 cycles is thus the measured quantity. Assuming that S/N at the input is reasonably good, the probable error is always ± 1 count of the 100-kc oscillator. For a 2,000-cps precession frequency, the time-interval measurement is then 0.12800 ± 0.00001 sec. This gives a probable error in the field measurement of ± 3.7 gammas.

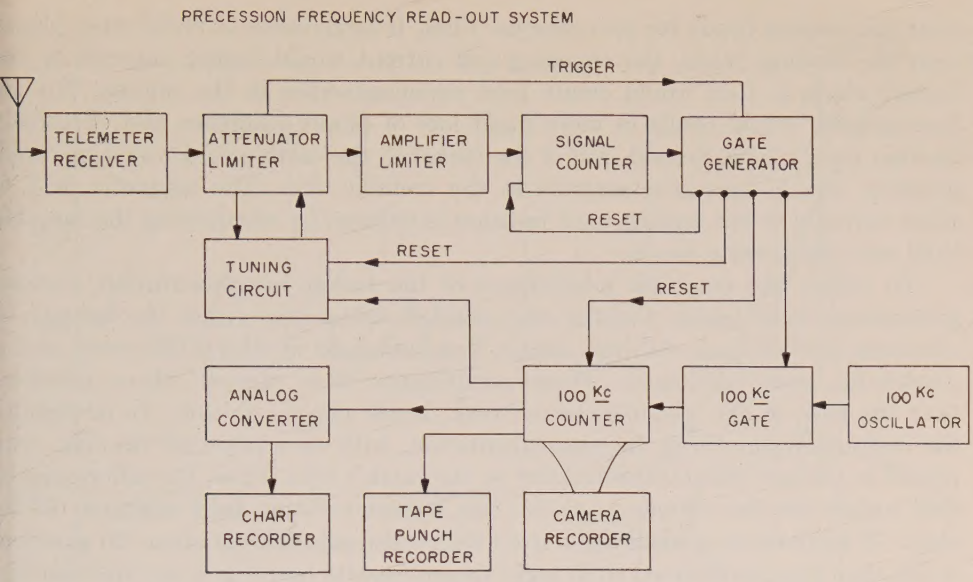

FIG. 4

Records of the binary count are obtained through photographing the counter lights or by tape punch recordings. A binary to analog converter permits recording of coarse and fine counts on a two-channel chart recorder.

Since dependence on one instrument during a rocket flight is risky, the precession signal is also recorded on magnetic tape along with a 100-kc standard. On playback, the taped 100 kc is substituted for the internal 100 kc, and the counter is used essentially as a reader. Repeated playbacks tend to reduce the ± 1 count error in counting the 100-kc standard.

Untuned Frequency Counter

A second counting system, which has been used in analyzing the flight reported here, consists essentially of a Muirhead D-669 frequency analyzer, Dynac 5095 (modified Dy 2500) computing digital indicator, and Hewlett-Packard Model 560 digital recorder. In this system, the Muirhead analyzer is used as a band-pass filter and tuned manually as tape is played back. As in the other system, the number of 100-kc cycles occurring in the time interval for a preset number of precession cycles is counted. The number is printed in digital form by the Hewlett-Packard recorder.

ROCKET INSTALLATION AND PREFLIGHT MEASUREMENTS

The nose-cone instrumentation of Aerobee NRL-33 is shown in Figure 2 of the companion paper on "Nightglow Emission ···" in the March 1958 issue of this JOURNAL. The electronics package and batteries were located in the pressurized instrumentation section. The sensing heads were mounted, mutually perpendicular, on a fiberglass structure [see Fig. 3(*b*)] inside the blackened fiberglass cyclinder at the nose of the rocket. Fiberglass rather than metallic structures were used

near the sensing heads for two reasons. First, if large areas of metal were place near the sensing heads, the changing coil current would induce currents in th metal, which in turn would create field inhomogeneities in the sample. The in homogeneity would result in more rapid loss of phase coherence and effectivel shorten the T_2 time. Second, roll of the rocket in the earth's field would, if rapi generate sizable induction currents in the metallic skin. The magnetic field c these currents at the sensing-head location is reduced by eliminating the metalli shell near the sensing heads.

To reduce the magnetic interference of the rocket instrumentation, variou precautions were taken. Coaxial and braided cables were used throughout t eliminate current loops. All iron, except that contained in relays, inductors, and dynamotor, was eliminated. These components were placed, where possible near the base of the instrumentation rack, inside conetic shields. To determin the instrumentation field, the instrumentation, with all equipment running, wa placed in various orientations relative to the earth's field. From the differences i field values for the various positions, the instrumentation field appeared to b about 70 gammas at a small angle from the rocket axis. This is about 20 gamma larger than that determined from flight measurements (see Fig. 5 and discussion). The difference is probably the result of diurnal variations between the variou ground measurements and inhomogeneities in the ground.

Measurements around the rocket proper, an Aerobee Model RTV-N-10c gave no indication of permanent or induced fields in the steel tanks. This is, in general, not true of Aerobee models which use a different steel.

FLIGHT MEASUREMENTS

Analysis: Between take-off and rocket break up following reentry, 666 measurements were taken. The signal-to-noise ratio during flight was lower than normal due to pick-up of an inductive pulse at 1,790 cycles per second from a transistor power-supply and reduced amplifier gain resulting from incomplete r-f filtering. Through narrow-band filtering (Q of 150), a good signal-to-noise ratio was, nevertheless, obtained from the vertical coil, even when $\sin^2 \theta$ was small, as well as from the horizontal coil. Only 13 measurements were discarded as being too affected by noise to be considered valid.

The discontinuity in the uncorrected field-*vs*-altitude curve, created when the rocket turned from nose-up to nose-down on reentry, gave an excellent determination of the component of the rocket instrumentation field in the earth's field direction. The difference between the descent field at the nose-down altitude and the ascent field at the same altitude checked this value. From the amplitude of the rocket-vector roll modulation as a function of θ, it was also possible to determine the angle of the rocket vector with respect to the rocket axis. The accuracy of these determinations is given in Figure 5. Since the rocket vector of Figure 5 explained the discontinuity at rocket turnover and the amplitude of roll modulation as a function of θ, it is concluded that fields due to currents created in the rocket skin by motional induction must have contributed less than 10 gammas to the measurements.

The total field contribution of the rocket vector was removed by applying the

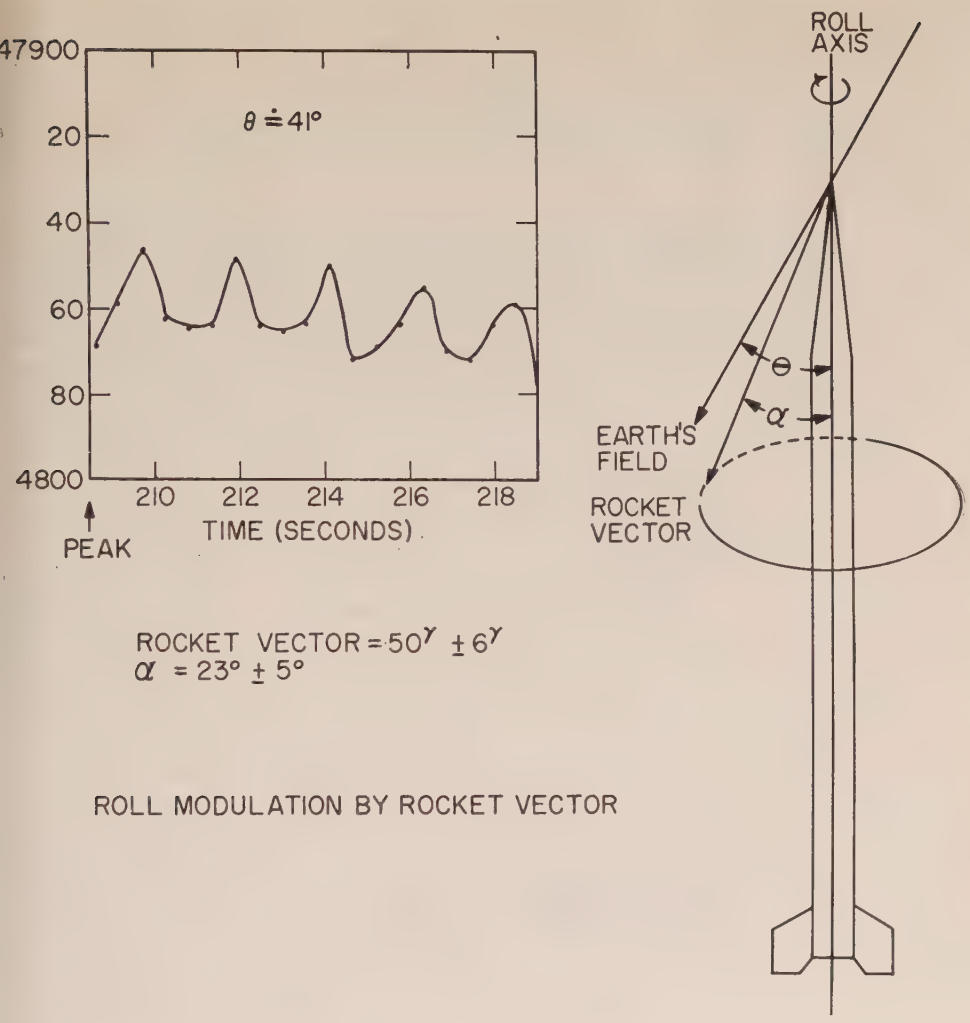

FIG. 5

correction 50 cos θ to all values. This is not exact, but gives a close average over the range of θ encountered, 25° to 42°. Exact corrections for the sake of finding discontinuities were not necessary as a consequence of the roll period being very close to the time interval required for four measurements. Thus, in looking for discontinuities, separate curves were constructed for each fourth measurement. Had there been a significant discontinuity over 1.1 seconds, two of the four curves would have deviated, and over 2.2 seconds or more, all four curves would have deviated. This technique also made more obvious the individual readings where noise affected the count accuracy.

An average correction was also used for rotation of the horizontal coil (discussed previously). The roll frequency after burn-out was practically constant at 0.45 cycle/sec; this gives an average correction of 10 gammas. At the minimum

and maximum θ, about 25° and 42°, the maximum error in the correction is abou ±1 and +4, −3 gammas, respectively.

Following these corrections, a smooth field-*vs*-time curve was drawn. Th maximum error in this curve is estimated to be less than ±10 gammas, with probable error of ±5 gammas. Using trajectory data, this was converted to fiel *vs* altitude.

The rocket trajectory was exceptionally vertical. Although the impact poin was not found, trajectory data indicate that it was 2 ± 1 miles north of the launch ing point. One consequence of this is that no accurate information was obtaine on the horizontal gradient. The descent values gradually increase over the ascen values with lower altitude, but the difference is only 36 gammas at the lowes descent altitude measured. If the field was that of a dipole, this would indicat that impact was 3 miles north. Measurements on the ground 6 miles north giv a horizontal gradient of 15 to 16 gammas/mile, indicating impact at 2.3 mile

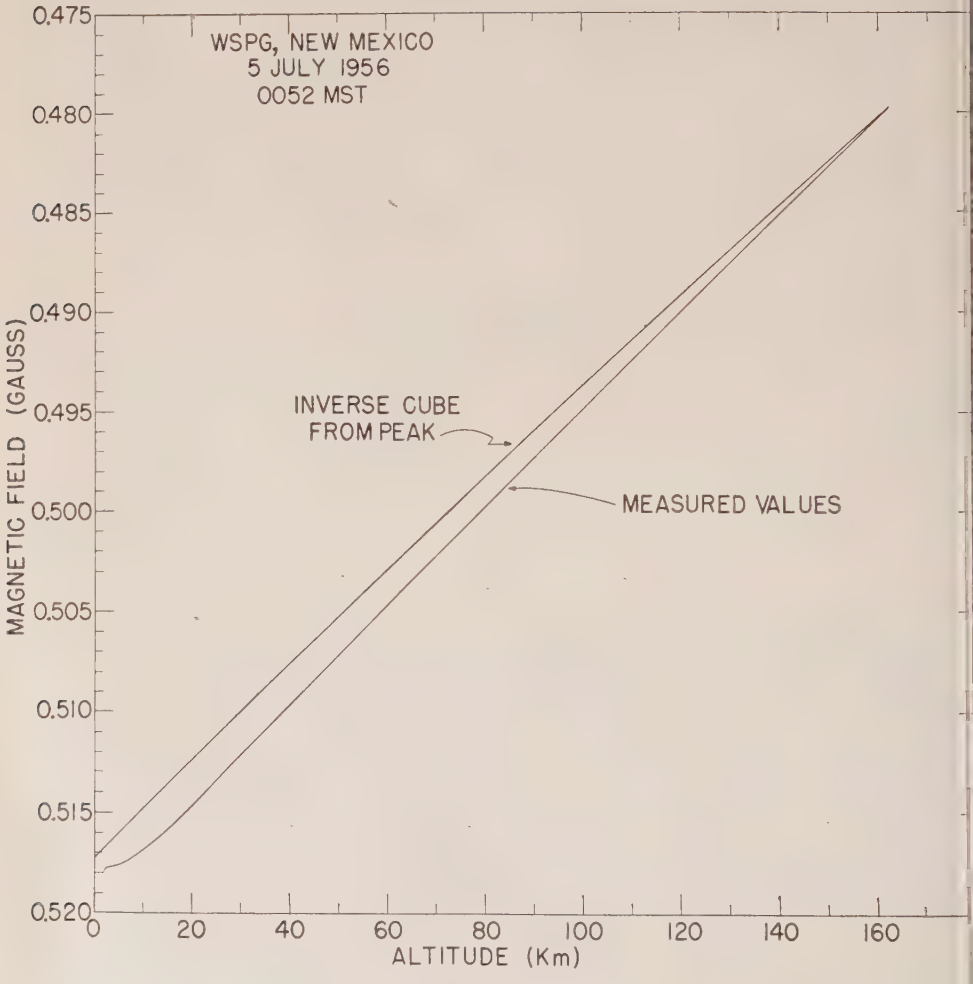

FIG. 6

north. In preference to performing latitude corrections in obtaining the field as a function of altitude, we have averaged the ascent and descent data as a function of altitude. The field-*vs*-altitude curve of Figure 6 is thus given for the latitude of a point 1 $\pm$ $\frac{1}{2}$ mile north of the launching point. At the low altitudes, below 46 km, only ascent data were available. Eighteen gammas were added to the ascent values below 46 km to match the field at the north-south mid-point of the trajectory specified above.

Field vs Altitude: For comparison with dipole behavior, an inverse cube field was matched to the peak value and computed back to sea-level. As shown in Figure 6, there is a sizable discrepancy between the measured field and a dipole behavior. For some indication of the source of this difference, the vertical gradient was computed. As shown in Figure 7, the gradient is very low near the surface

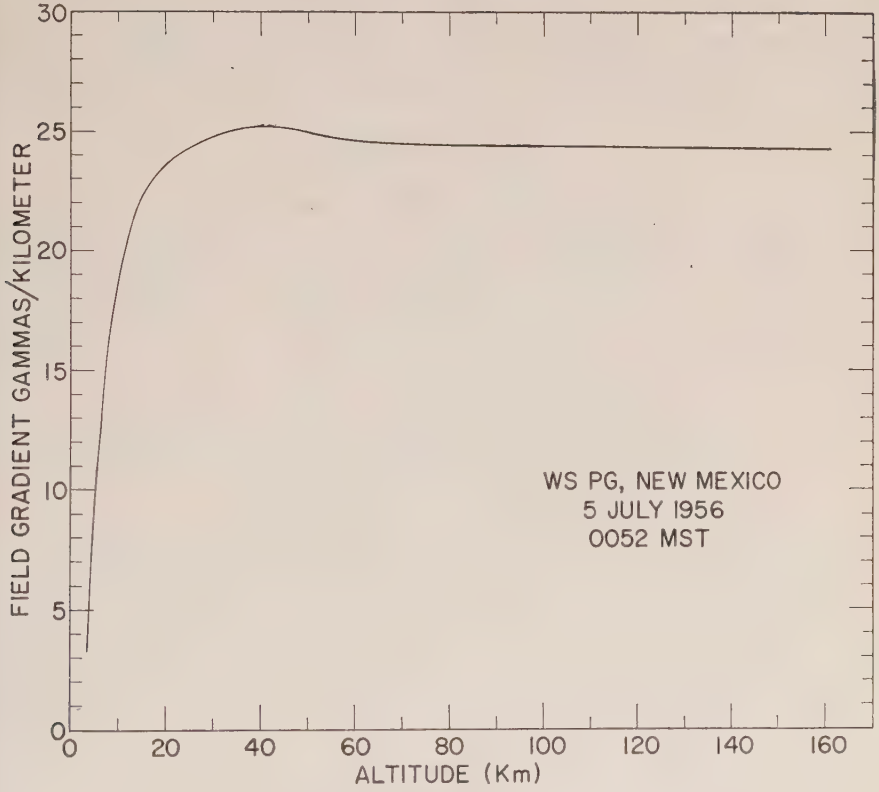

Fig. 7

(neglecting the first kilometer above the steel launching tower) and increases rapidly. The gradient becomes a maximum at 41 km, and then decreases more rapidly than would be expected up to 70 km. There is thus definite evidence that the field is anomalous up to 70 km. Above 75 km, the gradient decreases regularly, but only changes by 0.2 gamma/km between 75 and 160 km. For a dipole behavior, the gradient would decrease by 1.2 gamma/km between 75 and 160 km. Thus, at the peak altitude, the non-dipole discrepancy is still large. Since the surface

field at White Sands is about 0.046 gauss greater than the dipole value for thi magnetic latitude, such a discrepancy is to be expected if the earth's field approache the theoretical dipole at great distances.

Ionospheric Discontinuities: Magnetograms from the Tucson (Arizona) Observa tory indicate that the field was typically quiet when these measurements wer taken. A discontinuity was thus not expected in this night firing. The question o the existence of continuous, or non-variable, ionospheric currents is, however occasionally raised. Examination of this flight has not revealed departures fro a smooth curve which could with any confidence be called a discontinuity. Depar tures of about 8 gammas occurred between 75 and 77 km and again at 108-11 km during ascent, but confirmation that these were real was not found in th descent measurements. The measurements reported here do not, of course, rul out the possibility of diffuse ionospheric currents or currents at greater altitudes There is also the possibility that a more refined analysis could reveal a smal discontinuity. We estimate that a discontinuity of more than 12 gammas over a distance of 20 km or less would have been detected.

ACKNOWLEDGMENTS

The participation of scientists from Varian Associates has extended beyon that of designing and building the magnetometer and frequency counting system Mr. Lee Johnson, who designed this first rocket unit, also assisted in the rocke installation and instrumentation checks. We wish to thank Mr. Johnson an others at Varian Associates for their cooperation.

References

[1] S. Chapman, Rocket Exploration of the Upper Atmosphere (edited by R. L. F. Boy and M. J. Seaton), Interscience Publishers, Inc., New York, p. 292 (1954).
[2] E. H. Vestine, Applied Physics Laboratory, Johns Hopkins University, CM-480, NOr Contract No. 7386, June 1948.
[3] E. Maple, W. A. Bowen, and S. F. Singer, J. Geophys. Res., **55**, 115 (1950).
[4] S. F. Singer, E. Maple, and W. A. Bowen, J. Geophys. Res., **56**, 265 (1951).
[5] M. Packard and R. Varian, Phys. Rev., **93**, 941 (1954).
[6] F. Bloch, Phys. Rev., **70**, 460 (1946); F. Bloch, W. W. Hansen, and M. Packard, Phys Rev., **70**, 474 (1946).
[7] E. M. Purcell, H. C. Torrey, and R. V. Pound, Phys. Rev., **69**, 37 (1946).
[8] M. Packard, Free Nuclear Precession Magnetometer, Varian Associates, Palo Alto California, Report (1954).
[9] G. S. Waters and P. D. Francis, Signals Research and Development Establishment Christchurch, Hants, Canada, Report No. 1097 (1955).
[10] L. J. Cahill and J. A. Van Allen, J. Geophys. Res., **61**, 547 (1956).
[11] R. C. Rempel, Varian Associates, Technical Memorandum No. TMO-23, December 1956.
[12] A. L. Bloom and L. E. Johnson, Varian Associates, Palo Alto, California, Engineering Report No. 187, Contract No. Nonr-2147(00), November 1956; condensed in Electronic Ind., **16**, 76 (1957).
[13] T. L. Allen and M. E. Packard, Inst. Radio Eng., Proceedings of Wescon, San Francisco, August 1957.
[14] J. P. Heppner, J. D. Stolarik, and L. H. Meredith, presentations at Annual Meetings of the American Geophysical Union, May 1956 and 1957; abstr., Trans. Amer. Geophys. Union, **37**, 347 (1956) and **38**, 394 (1957).
[15] A. L. Bloom, Varian Associates, Palo Alto, California, Technical Memoranda (1955).

HIGH ALTITUDE INFRARED STUDIES OF THE ATMOSPHERE*

BY DAVID MURCRAY, JAMES BROOKS, FRANK MURCRAY, AND CLYDE SHAW

Department of Physics, University of Denver, Denver 10, Colorado

(Received September 14, 1957)

ABSTRACT

The results obtained from a flight with a balloon-borne infrared spectrometer are described. The spectrometer was designed to scan from the visible to 4.3 microns, but on this flight only the region from the visible to 2.7μ was obtained. In this region, the bands of interest are 1.4μ and 1.9μ H_2O bands. Spectra were obtained from the ground to 65,000 feet. The water vapor bands had completely disappeared above 46,000 feet.

I. INTRODUCTION

The work to be described in this report covers near-infrared studies of the atmosphere conducted by means of a balloon flight with a Littrow-type spectrometer. The skyhook-type polyethylene balloon provides an excellent vehicle for conducting experiments on variation of the infrared solar spectrum with altitude. It provides a relatively stable platform, and its slow ascent rate gives ample time at the various altitudes to scan the spectrum. Present balloons can attain altitudes of 100,000 feet with packages weighing in excess of 250 pounds.

II. DESCRIPTION OF THE EQUIPMENT

The spectrometer is of the Littrow type, and for this flight was equipped with a LiF prism and an uncooled PbSe cell as a detector. The optical system is shown in Figure 1. The light, chopped at 250 cycles/sec, enters the spectrometer at the entrance slit, is collimated by the spherical mirror, and passes through the prism to the Littrow mirror. It is reflected back through the prism to the spherical mirror, which focuses the radiation on the exit slit, where it falls on the detector. The spectrum is scanned by rotating the Littrow mirror. Automatic operation is accomplished by means of 28-volt D.C. motors and a cam system, which rotates the mirror through the angle necessary to scan the region of interest and then returns the mirror to its original position. The spectrometer on this flight was set to scan the region from the visible to 4.5μ. In order to get a usable signal over this range, it was necessary to provide a means of changing gains at various wavelengths, in order to compensate for the fall-off of energy with increasing wavelength. These gain changes were accomplished by means of microswitches placed on the Littrow

*This research was sponsored by the Geophysics Research Directorate of the Air Force Cambridge Research Center, Air Research and Development Command, under Contract AF 19(604)-1005.

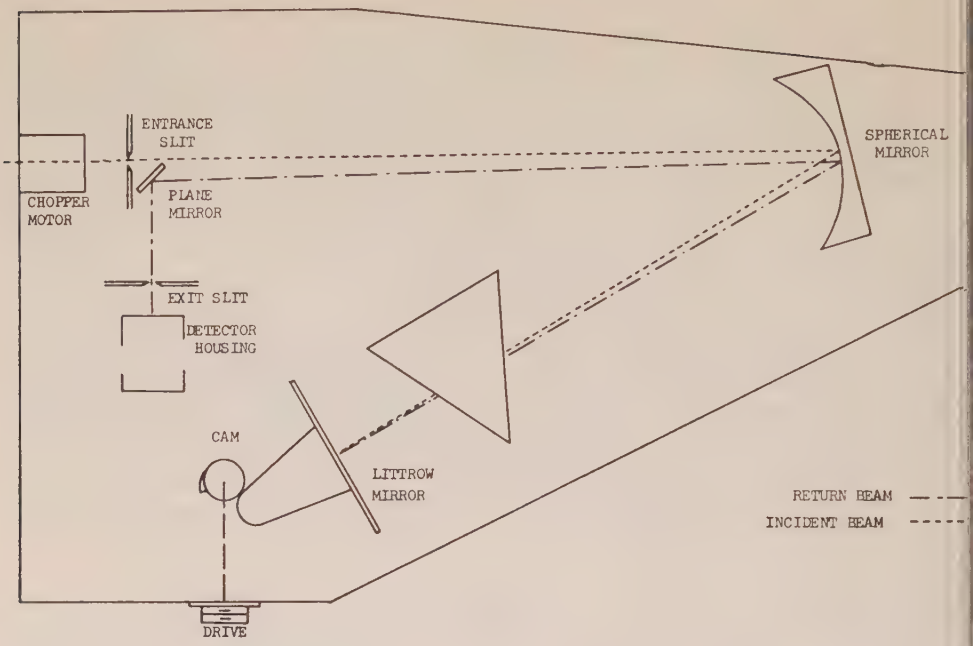

FIG. 1—Optical unit of balloon-borne infrared spectrometer

drive-shaft. The output of the second stage of the amplifier occurs as a voltage across three potentiometers, which are connected in series to act as a voltage divider. As the various microswitches are activated, the voltage occurring across the first potentiometer, the first and second potentiometer, and, finally, across all three potentiometers is applied to the output stage of the amplifier. The microswitches were adjustable so that the gain changes could be programmed to occur at any desired portion of the spectrum. On the flight described here, they were set so that a change in gain occurred at 2.7μ and at 4.3μ.

The output of the amplifier was fed to a galvanometer, and the deflection of the galvanometer was recorded on 70-mm film. In order to conserve film, microswitches which activated the film drive were placed on the Littrow drive-shaft. In this way, film was advanced only while the spectrometer was scanning a region of the spectrum of interest and record was made only of the forward scan of the spectrum. The equipment was programmed so that the spectrum was scanned in approximately 10 seconds and scans were made at the rate of one a minute. The amplifier is a low drain amplifier, designed with balloon requirements in mind The output of the amplifier is fed to the galvanometer for direct recording, and is rectified and fed to a telemetering circuit for remote recording. A radiosonde thermistor was placed on the cell-mount and its resistance was also monitored at the ground by means of telemetering. This information is needed in order to obtain intensity information about the radiation, since the cell sensitivity is temperature dependent. The sun was imaged on the slit by means of a 5-inch diameter, 30-inch focal length spherical mirror. The image was maintained on the slit by means of a biaxial pointing control, built by the Hi-Altitude Instrument

Company. This "sun seeker" is a modification of the one described by Goddard, *et al.* [see 1 of "References" at end of paper], in 1956. The entire equipment, including gondola and power-supplies for the seeker and spectrometer, weighed 230 pounds. The equipment was "greenhoused" to maintain a fairly constant temperature in the spectrometer.

III. DETAILS OF THE FLIGHT

The equipment was launched at Holloman Air Force Base, Alamogordo, New Mexico, on August 3, 1956. At the time of launch, the wind was blowing in rather strong gusts and the launch was very difficult. The launching personnel did a very good job and, in spite of the difficult conditions, got the package into the air without bouncing it against the ground. The telemetering antenna was pulled loose from the equipment and hence all contact between the balloon and the ground station was lost. Also a jolt incurred on launch moved the galvanometer slightly, causing a different portion of the light-source to be imaged on the film. This portion of the source was less intense than the original spot and hence when the galvanometer was moving rapidly (in the 2 and 3 gain positions) the trace on the film was so faint that it was practically impossible to read. The region from the visible to 2.7μ was usable on most records.

The balloon had taken quite a buffeting before take-off and may have developed slight leaks. At least the ascent rate was slower than anticipated, and when the equipment cut down (after a three-hour flight) it had only reached an altitude of 65,000 feet. The equipment came down in very rough terrain, northeast of Alamo-

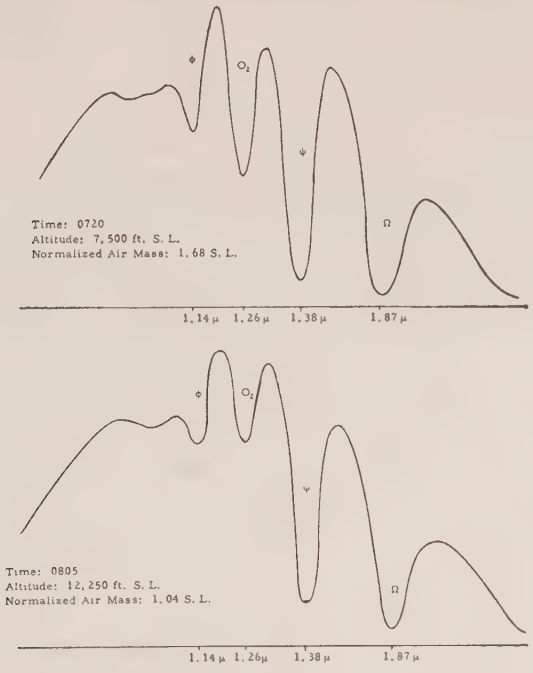

FIG. 2—High altitude near-infrared solar spectra

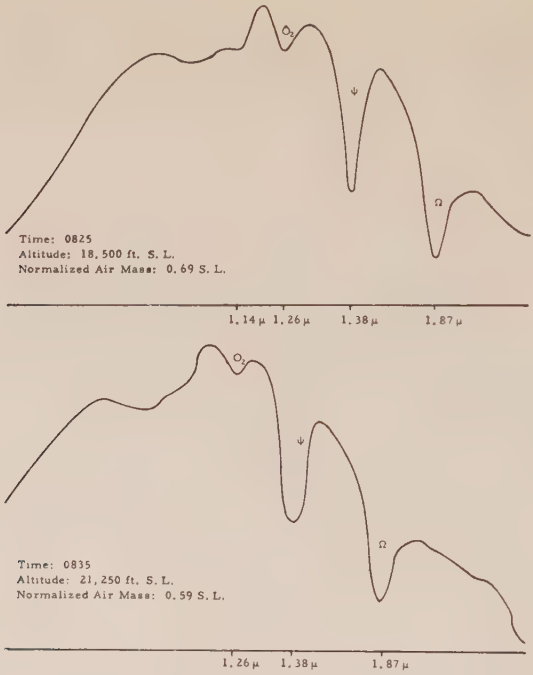

FIG. 3—High altitude near-infrared solar spectra

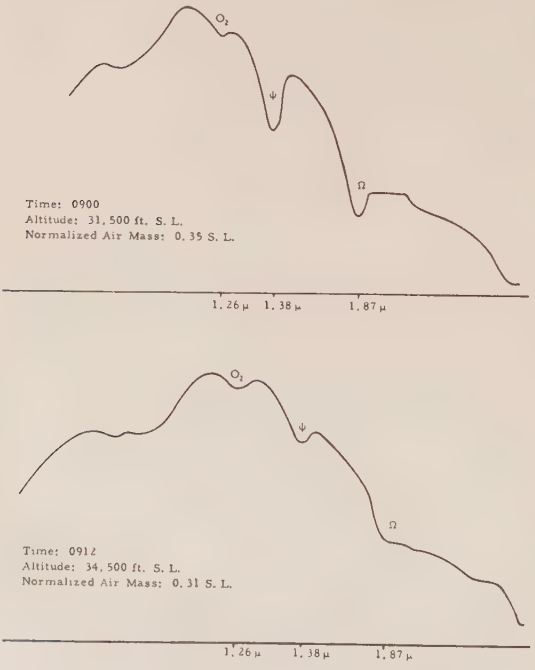

FIG. 4—High altitude near-infrared solar spectra

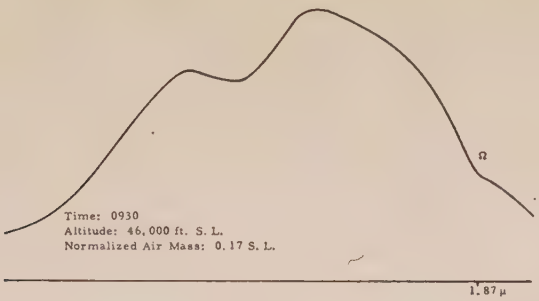

FIG. 5—High altitude near-infrared solar spectrum

gordo, and was not recovered until the following day. All mirrors and the prism were still intact. Spectra were obtained at almost all altitudes from the ground up, except for a short period during which the sun was obscured by a cloud. Because of this obstruction, no spectra were obtained from 12,000 feet to 18,000 feet.

IV. RESULTS

Representative samples of the spectra obtained are shown in Figures 2 to 5. Since the telemetering was lost, no cell temperature information was recorded, thus preventing the temperature correction necessary for comparing the intensity of the radiation received at different times. The usable spectra were enlarged and curves of fractional absorption *vs* frequency plotted for the various bands in the region. From these curves, $\int_{\nu_1}^{\nu_2} A_\nu \, d\nu$ for the various bands were obtained by means of a planimeter. In order to obtain the air mass traversed by the radiation, an exponential atmosphere was assumed, with the constants determined so as to fit the experimental values given in "The Atmosphere of the Earth and Planets" by Kuiper [2]. Since an exponential will not fit the total range of values given, the constants were determined to give a good fit in the region from the ground to 70,000 feet. The air mass was normalized by dividing by the vertical air mass above sea-level. The solar elevations were calculated without making any correction for refraction, since the solar altitudes were high enough to make this correction small. Table 1 gives the altitude at which the spectra were taken, the air mass traversed by the radiation, the $\int_{\nu_1}^{\nu_2} A_\nu \, d\nu$ for the various bands, and the amount of precipitable water vapor (abbreviated pr. mm) in the path for the Ψ and Ω bands. These last quantities were determined using the data given by Howard, *et al.* [3], and will be discussed in the next section.

V. ANALYSIS OF THE Ψ AND Ω BANDS

Figures 6 and 7 show plots of $\int_{\nu_1}^{\nu_2} A_\nu \, d\nu$ *vs* air mass for the Ψ and Ω bands. Inspection of the plots shows that an equation of the type

$$\int_{\nu_1}^{\nu_2} A_\nu \, d\nu = am^{1/2} + b$$

will fit both sets of data fairly well. The scatter is sufficient that other possible relations may fit the data.

TABLE 1—*Results of analysis of spectra obtained on balloon flight of August 3, 1956*

Altitude	Spectrum No.	Air mass	Ψ $\int A_\nu \, d\nu$	Ω $\int A_\nu \, d\nu$	ΨH_2O	ΩH_2O
feet			cm^{-1}	cm^{-1}	*pr. mm*	*pr. mm*
7,500	39	1.68	623	455	6.84	7.20
7,500	40	1.66	630	426	7.08	5.41
8,000	53	1.53	640	...	7.53	....
8,250	54	1.51	...	415	....	4.99
9,000	67	1.40	660	404	8.43	4.48
9,500	71	1.33	...	393	....	4.05
9,500	73	1.32	587	373	5.92	3.33
10,000	75	1.28	582	...	....	....
10,500	81	1.22	556	401	5.14	4.53
10,500	84	1.21	536	374	4.65	3.46
11,000	87	1.16	546	366	4.97	3.36
12,000	98	1.08	585	...	....	....
12,250	104	1.04	536	361	4.76	3.16
12,500	106	1.02	506	...	4.13	....
13,000	112	0.98	533	...	4.97	....
18,500	144	0.70	380	...	2.40	....
18,500	147	0.69	363	232	2.21	0.912
18,500	148	0.68	304	199	1.36	0.671
20,000	153	0.63	348	216	1.85	0.824
20,500	154	0.62	326	198	1.64	0.697
21,250	156	0.59	330	200	1.71	0.718
22,000	159	0.57	335	244	1.79	1.096
23,000	164	0.54	260	...	1.09	.....
23,500	167	0.52	320	194	1.67	0.708
23,750	170	0.52	272	174	1.22	0.571
24,000	173	0.51	305	217	1.55	0.906
24,250	174	0.49	267	...	1.97	.....
25,500	179	0.46	290	179	1.43	0.625
26,500	182	0.44	267	...	1.24	.....
28,500	185	0.40	213	149	0.818	0.458
31,000	191	0.35	215	179	0.864	0.692
31,500	194	0.35	...	141	.....	0.433
32,000	197	0.34	266	118	1.36	0.306
32,500	199	0.32	225	100	0.973	0.222
32,750	200	0.32	175	138	0.595	0.424
33,000	202	0.32	125	74	0.302	0.123
33,000	207	0.31	78	69	0.118	0.106
46,000	233	0.17	63	36	0.094	0.035

The work of Howard, *et al.* [3], showed that for a given quantity of water vapor w (in cm precipitable water) at a pressure P (in mm of Hg) the fractional absorption for both the Ψ and Ω bands satisfied a relation of the type

$$\int_{\nu_1}^{\nu_2} A_\nu \, d\nu = aw^{1/2}P^k \qquad \int_{\nu_1}^{\nu_2} A_\nu \, d\nu < M[\text{"Weak fit"}]$$

$$\int_{\nu_1}^{\nu_2} A_\nu \, d\nu = A \log w + B \log P + D \qquad \int_{\nu_1}^{\nu_2} A_\nu \, d\nu > M[\text{"Strong fit"}]$$

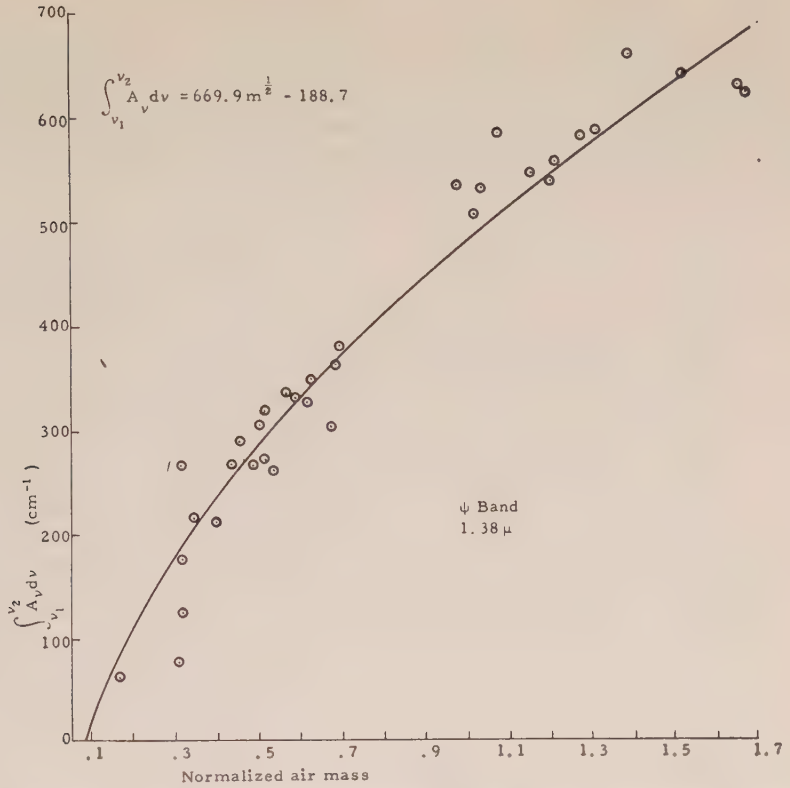

FIG. 6—Plot of the $\int_{\nu_1}^{\nu_2} A_\nu \, d\nu$ *vs* normalized air mass for the Ψ band. The curve is a least squares fit of the type $\int_{\nu_1}^{\nu_2} A_\nu \, d\nu = am^{1/2} + b$.

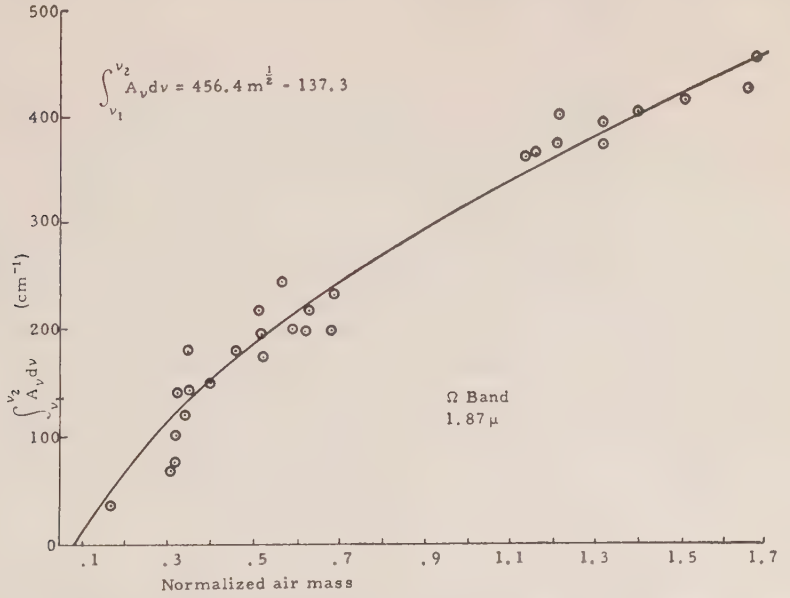

FIG. 7—Plot of the $\int_{\nu_1}^{\nu_2} A_\nu \, d\nu$ *vs* normalized air mass for the Ω band. The curve is a least squares fit of the type $\int_{\nu_1}^{\nu_2} A_\nu \, d\nu = am^{1/2} + b$.

where M is a constant characteristic of the particular band (cf. [3], Table II, p. 244). Using these relations and assuming an average value for the pressure along the absorbing path, calculations were made of the amount of water vapor in the absorbing path for both the Ψ and Ω bands. The results of these calculations are given in Table 1 and plotted in Figures 8 and 9. The values obtained by using the Ψ

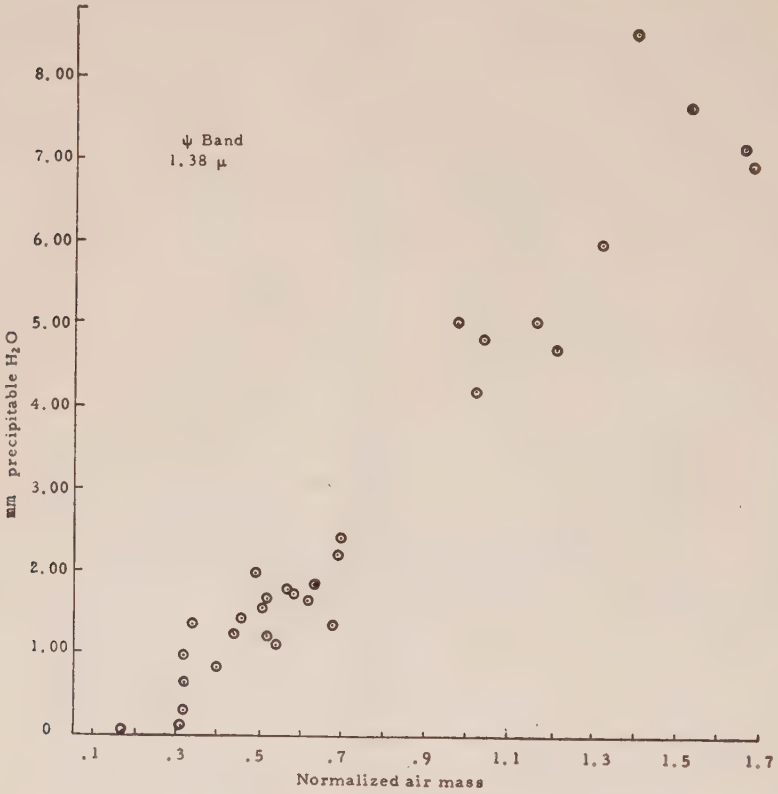

FIG. 8—Plot of mm precipitable H_2O *vs* normalized air mass as determined from the Ψ band

band seem consistently higher than the Ω band. The data for the Ψ band indicate that the water vapor is uniformly distributed with air mass to approximately 40,000 feet. Above 46,000 feet, the Ψ and Ω bands are absent from the spectra. If it is assumed that above this altitude no absorption takes place, a relation of the type $W = \alpha(m - m_0)$ between the water vapor traversed and air mass may be assumed. The pressure along the absorbing path is also proportional to air mass, and the addition or subtraction of a small amount to the pressure is going to make only slight differences in the $\int_{\nu_1}^{\nu_2} A_\nu \, d\nu$. If it is assumed then that P is also proportional to $(m - m_0)$, the above relations become

$$\int_{\nu_1}^{\nu_2} A_\nu \, d\nu = a[\alpha(m - m_0)]^{1/2}[B(m - m_0)]^k = a'(m - m_0)^{1/2+k}$$

and

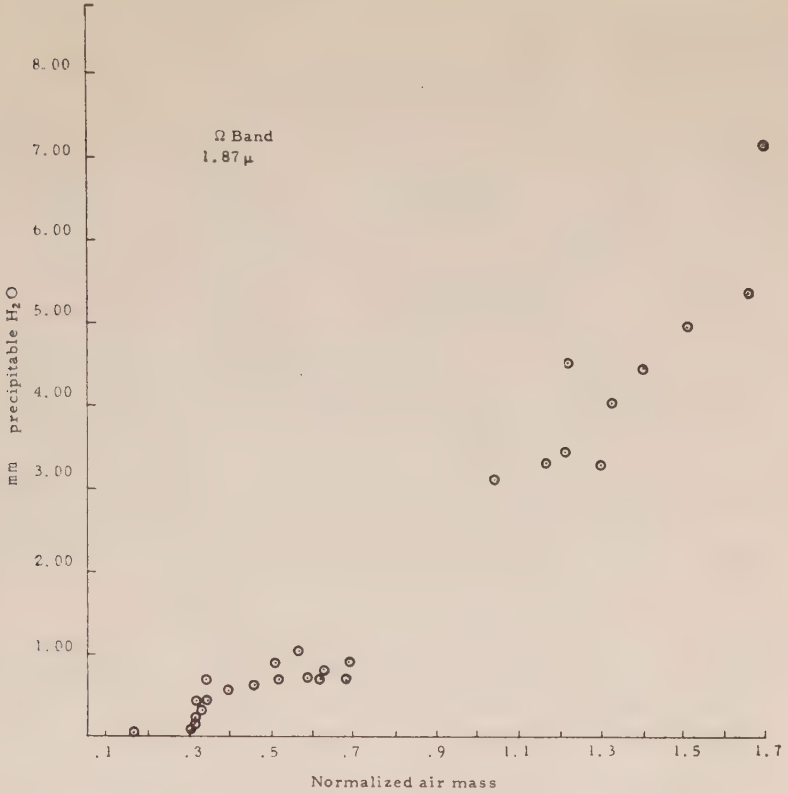

FIG. 9—Plot of mm precipitable H_2O *vs* normalized air mass as determined from the Ω band

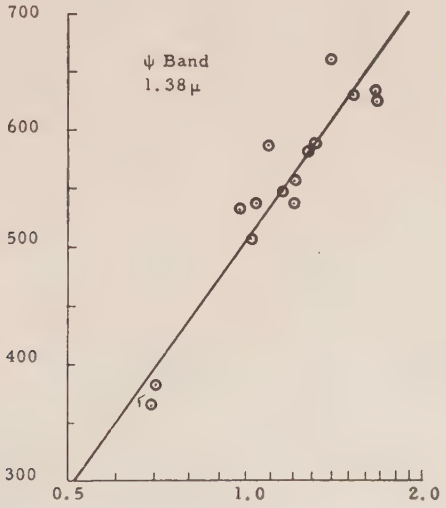

FIG. 10 -Plot of $\int_{\nu_1}^{\nu_2} A_\nu \, d\nu$ *vs* normalized air mass for the strong fit regions of the Ψ band. The curves are least square fits of the type $\int_{\nu_1}^{\nu_2} A_\nu \, d\nu = A \log m + B$.

$$\int_{\nu_1}^{\nu_2} A_\nu \, d\nu = A \log [\alpha(m - m_0)]$$

$$+ B \log [B(m - m_0)] + D = A' \log (m - m_0) + D'$$

for the weak and strong fit regions. On the basis of these assumptions then, the plot of the $\int_{\nu_1}^{\nu_2} A_\nu \, d\nu$ *vs* air mass should be a straight line on semi-logarithmic paper for $\int_{\nu_1}^{\nu_2} A_\nu \, d\nu > M$, and for $\int_{\nu_1}^{\nu_2} A_\nu \, d\nu < M$ should fit the relation given for

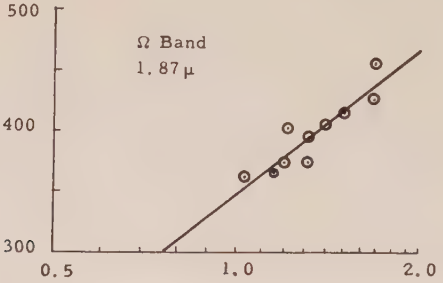

FIG. 11—Plot of $\int_{\nu_1}^{\nu_2} A_\nu \, d\nu$ *vs* normalized air mass for the strong fit region of the Ω band

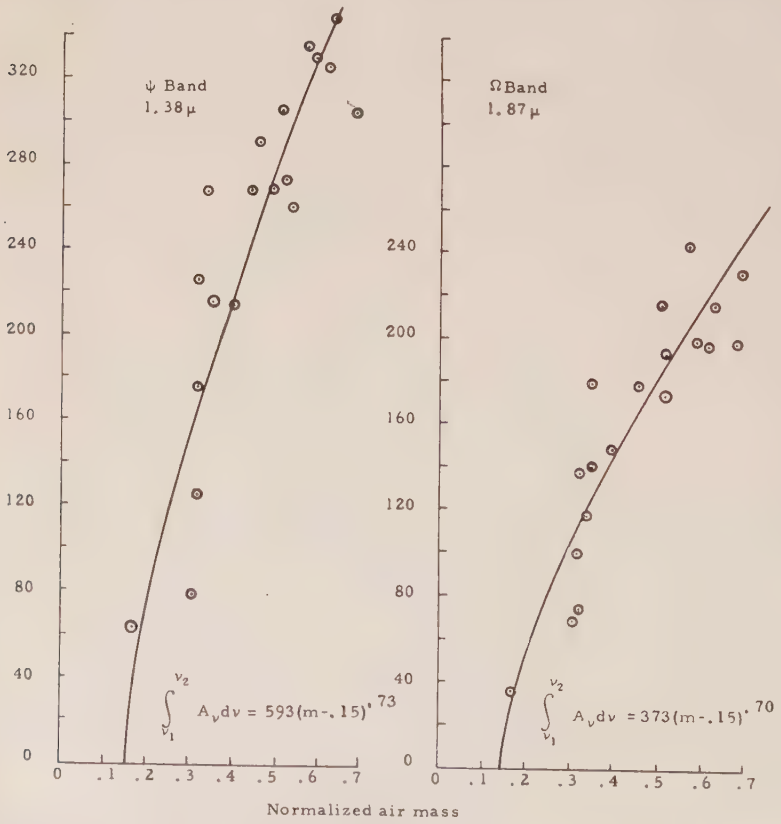

FIG. 12—Plot of $\int_{\nu_1}^{\nu_2} A_\nu \, d\nu$ *vs* normalized air mass for the weak fit regions of Ψ and Ω bands. The curves are least square fits of the type $\int_{\nu_1}^{\nu_2} A_\nu \, d\nu = A(m - 0.15)^n$.

the weak fit. Figures 10 and 11 show the semi-log plots for the strong fit regions. In both cases, the drawing of a straight line through the data seems justified. Figure 12 shows the weak fit regions for the Ψ and the Ω bands. A least squares fit was calculated using an equation of the form

$$\int_{\nu_1}^{\nu_2} A_\nu \, d\nu = a'(m - 0.15)^n$$

with a and n determined to give the best fit. In both cases, the value of n turns out to be 0.7. Since the water vapor enters to a 0.5 power, it appears that for atmospheric absorption the relations as given by Howard, *et al.* [3], are still applicable, except for the changing of the exponent on the pressure dependence from 0.3 to 0.2 in the weak fit region and a possible change in the multiplicative constant. In the strong fit region, the equations also appear to be still applicable with some adjustment of the pressure constants. In any study such as this, the scatter is generally large and the justification of some of the conclusions are open to question. On the basis of Howard's work and the agreement of the Ψ and Ω bands for all regions, the conclusions appear reasonable in spite of the scatter.

VI. ACKNOWLEDGMENTS

The authors wish to thank Air Force Cambridge Research Center for the support of this research, Hi-Altitude Instrument Company for cooperation on the flight, Dr. David Gates for the original design of the spectrometer, and Dr. Robert Talley of NOL and Dr. E. D. McAlister of Eastman Kodak Company for the loan of PbSe cells. In addition, Walter Williams aided greatly in the reduction of the data.

References

[1] A. Goddard, Jr., M. Juza, T. Maher, and F. Speck, Balloon-borne system for tracking the sun, Rev. Sci. Instr., **27**, 381-385 (1956).

[2] G. Kuiper (Ed.), The Atmospheres of the Earth and Planets, University of Chicago Press, Chicago (1952).

[3] J. Howard, D. Burch, and D. Williams, Infrared transmission through synthetic atmospheres, J. Optical Soc. Amer., **46**, 186-190, 237-245, 334-338, 452-455 (1956).

RAY-TRACING TECHNIQUE IN A HORIZONTALLY STRATIFIED IONOSPHERE USING VECTOR REPRESENTATIONS

By R. J. Marcou (1), W. Pfister (2), and J. C. Ulwick (2)

(1) *Boston College, Newton, Massachusetts;*
(2) *Air Force Cambridge Research Center, Bedford, Massachusetts*

(Received December 21, 1957)

ABSTRACT

Vector expressions are derived for tracing oblique ray paths, taking into account the full effect of the earth's magnetic field. The method is an extended analytical treatment of Poeverlein's two dimensional case based upon crystal optics. In particular, the unit vector **S** in the direction of the ray and the vector expressions for the equivalent path of the wave packet and the group refractive index are derived. A method for high speed computers is described for ray tracing in a horizontally stratified ionosphere, for determining, by an iteration process, the index of refraction and wave normal direction, and for determining electron-density distributions from rocket data.

I. INTRODUCTION

Experimental data of radio propagation between a rocket and an arbitrary station on the ground can be analyzed conveniently by tracing a ray path between those end-points and by integrating travel time, or whatever is measured, along this path.

Methods are available for tracing ray paths in a horizontally stratified ionosphere when the earth's magnetic field is taken into account. One method by Poeverlein [see 1 and 2 of "References" at end of paper], for the two dimensional case, utilizes a graphical procedure employed in crystal optics to construct the ray paths. This method has been extended to the three dimensional case by Mullaly [3]. Another method by Booker [4, 5] is an analytical treatment. Millington [6, 7] also employs this method in a revised form which facilitates calculations.

In this paper, vector expressions are derived in Section II for tracing the ray path, using the principle of crystal optics on which Poeverlein's graphical method is based. In particular, an expression is derived for the unit vector **S** in the direction of the ray, from which the angle between the ray direction and the coordinate axes, or any prescribed direction, may be obtained. For propagation in a stratified ionosphere, the fundamental quartic of Booker can be utilized for the determination of the wave normal direction and index of refraction. An alternate solution, making use of the vector concept, is described in Section III. Vector expressions are derived in Section IV for the equivalent path of the wave packet and the group refractive index. Finally, in Section V, a method for high speed computers utilizing these formulas to determine electron-density distributions from rocket data is described.

GLOSSARY OF SYMBOLS

N = number of electrons per cubic centimeter
ω = angular frequency of the wave
H = magnetic field intensity of earth (emu)
$\mathbf{M} = \frac{\mathbf{H}}{H}$ = unit vector in direction of earth's field
$\omega_N^2 = \frac{4\pi Ne^2}{m}$ = square of angular plasma frequency
$\omega_H = \frac{|e|}{mc} H$ = angular gyrofrequency
$a = \frac{\omega_N^2}{\omega^2}$ (Booker's x; Poeverlein's a_N)*
$h = \frac{\omega_H^2}{\omega^2}$ (Booker's y^2; Poeverlein's a_H^2)*
$\mathbf{S}$ = unit vector in direction of wave packet propagation
$\mathfrak{u}$ = wave propagation vector
$|\mathfrak{u}| = \mu$ = index of refraction
μ' = group refractive index
α = angle between wave normal and earth's magnetic field
ψ = angle between ray direction vectors and earth's magnetic field
ϵ = $\tan \alpha / \tan \psi$
γ = aximuth of plane of incidence measured from x-z plane
γ_H = azimuth of magnetic meridian plane measured from x-z plane
B = angle between ray direction and horizontal plane
Γ = azimuth of plane of ray measured from x-z plane
β = angle between wave normal and horizontal plane
I = angle between earth's magnetic field and horizontal plane (inclination)

II. CONNECTION BETWEEN RAY DIRECTION AND REFRACTIVE INDEX IN AN IONOSPHERIC MEDIUM

According to Hamilton's well-known principal, ray directions can be found by drawing normals to the μ-surface, which in turn is obtained by plotting in space polar coordinates the value of the refractive index as a function of the direction of the wave normal.

The refractive index is expressed by the Appleton-Hartree formula

$$\mu^2 = 1 - \frac{2a(1-a)}{2(1-a) - h\sin^2\alpha \pm \sqrt{h^2\sin^4\alpha + 4h(1-a)^2\cos^2\alpha}} \quad \text{.....(1)}$$

(case of negligible collisions)

*The Subcommission III*d* on Magneto-Ionic Nomenclature has recommended the following be used:

$$X = \frac{\omega_0^2}{\omega^2}$$

$$Y = \frac{\omega_H}{\omega}$$

It also can be written in the form

$$(1 - \mu^2 - a)\{(h + a - 1)(1 - \mu^2 - a) + ah\} + ah(1 - \mu^2)\mu^2 \cos^2 \alpha = 0 \quad \ldots\ldots(2)$$

Let the μ-surface be represented vectorally by

$$\underline{\mathbf{u}} = \underline{\mathbf{u}}(\alpha, x)$$

where α is the angle between $\underline{\mathbf{u}}$ and $\mathbf{M}$, a unit vector in the direction of the earth's magnetic field, and x is the angle between the $\underline{\mathbf{u}}\mathbf{M}$-plane and any arbitrary fixed $\underline{\mathbf{u}}_0\mathbf{M}$-plane, measured in the direction of $\underline{\mathbf{u}} \times \mathbf{M}$. Then,

$$\frac{\partial \underline{\mathbf{u}}}{\partial \alpha} \quad \text{and} \quad \frac{\partial \underline{\mathbf{u}}}{\partial x}$$

are vectors, tangent to the α and x curves, respectively, and thus tangent to the μ-surface. Therefore,

$$\frac{\partial \underline{\mathbf{u}}}{\partial x} \times \frac{\partial \underline{\mathbf{u}}}{\partial \alpha}$$

is a vector perpendicular to the μ-surface at the point (α, x) and pointing outwardly from the μ-surface.

The unit vector $\mathbf{S}$ in the direction of this vector is given by

$$\mathbf{S} = \frac{\dfrac{\partial \underline{\mathbf{u}}}{\partial x} \times \dfrac{\partial \underline{\mathbf{u}}}{\partial \alpha}}{\sqrt{\left(\dfrac{\partial \underline{\mathbf{u}}}{\partial x} \times \dfrac{\partial \underline{\mathbf{u}}}{\partial \alpha}\right) \cdot \left(\dfrac{\partial \underline{\mathbf{u}}}{\partial x} \times \dfrac{\partial \underline{\mathbf{u}}}{\partial \alpha}\right)}} \quad \ldots\ldots(3)$$

To calculate $\partial \underline{\mathbf{u}}/\partial \alpha$ and $\partial \underline{\mathbf{u}}/\partial x$, we chose two unit vectors $\mathbf{e}_1$ and $\mathbf{e}_2$ having the properties that

$$\mathbf{e}_1 \cdot \mathbf{e}_2 = \mathbf{e}_1 \cdot \mathbf{M} = \mathbf{e}_2 \cdot \mathbf{M} = 0$$

Then, we may write

$$\underline{\mathbf{u}} = \mathbf{e}_1 \mu \sin \alpha \cos x + \mathbf{e}_2 \mu \sin \alpha \sin x + \mathbf{M} \mu \cos \alpha \quad \ldots\ldots(4)$$

from which we find that

$$\left.\begin{aligned} \frac{\partial \underline{\mathbf{u}}}{\partial x} &= \mathbf{M} \times \underline{\mathbf{u}} = -\underline{\mathbf{u}} \times \mathbf{M} \\ \text{and} \quad \frac{\partial \underline{\mathbf{u}}}{\partial \alpha} &= \frac{\underline{\mathbf{u}}}{\mu}\left(\frac{\mathrm{d}\mu}{\mathrm{d}\alpha} + \mu \cot \alpha\right) - \mathbf{M} \mu \csc \alpha \end{aligned}\right\} \quad \ldots\ldots(5)$$

and also

$$\frac{\partial \underline{\mathbf{u}}}{\partial x} \times \frac{\partial \underline{\mathbf{u}}}{\partial \alpha} = \left(\frac{\mathrm{d}\mu}{\mathrm{d}\alpha} \cos \alpha - \mu \sin \alpha\right)\underline{\mathbf{u}} - \mu \frac{\mathrm{d}\mu}{\mathrm{d}\alpha} \mathbf{M} \quad \ldots\ldots(6)$$

This vector is in the direction of the unit vector $\mathbf{S}$, normal to the μ-surface at the point (α, x). The vector

$$\frac{\underline{\mu}}{\mu} - \frac{\frac{d\mu}{d\alpha}\cos\alpha\mathbf{M}}{\frac{d\mu}{d\alpha}\cos^2\alpha - \mu\sin\alpha\cos\alpha}$$

evidently has the same direction as (6), and if we define a new parameter

$$\epsilon = 1 - \frac{\frac{d\mu}{d\alpha}}{\frac{d\mu}{d\alpha}\cos^2\alpha - \mu\sin\alpha\cos\alpha} \quad \ldots\ldots(7)$$

which is a measure of the degree of isotropy, we may write

$$\mathbf{S} = \frac{\frac{\underline{\mu}}{\mu} - (1-\epsilon)\cos\alpha\mathbf{M}}{\sqrt{\sin^2\alpha + \epsilon^2\cos^2\alpha}} \quad \ldots\ldots(8)$$

The unit vector **S** given by (8) gives the ray direction at the point (α, x) of the μ-surface [8].

To find $(1-\epsilon)$, we make use of (2). Differentiating (2) with respect to α and solving for $d\mu/d\alpha$, we find

$$\frac{d\mu}{d\alpha} = -\frac{ah(1-\mu^2)\mu\sin\alpha\cos\alpha}{2(1-\mu^2-a)(h+a-1) + ah\sin^2\alpha + 2ah\mu^2\cos^2\alpha} \quad \ldots\ldots(9)$$

Substituting (9) in (7), we find

$$1 - \epsilon = \frac{ah(1-\mu^2)}{2(h+a-1)(1-\mu^2-a) + ah(1+\mu^2\cos^2\alpha)} \quad \ldots\ldots(10)$$

or

$$\epsilon = \frac{ah\mu^2 + ah\mu^2\cos^2\alpha + 2(h+a-1)(1-\mu^2-a)}{ah + ah\mu^2\cos^2\alpha + 2(h+a-1)(1-\mu^2-a)} \quad \ldots\ldots(11)$$

and making use of (2), (11) may be put in the form

$$\epsilon = \frac{(h-1)(1-\mu^2)^2 + a^2}{\left(\frac{h}{1-a} - 1\right)(1-\mu^2)^2 + a^2} \quad \ldots\ldots(12)$$

Thus, any of the formulas (10), (11), or (12), together with (8), will give the direction of the ray.

It is easy to give a simple geometric interpretation of the parameter ϵ. If **i**, **j**, **k** form a right-handed system of mutually perpendicular unit vectors with **i** and **j** in the horizontal plane, then we may write the unit vector **M** in the direction of the magnetic field and the phase propagation vector $\underline{\mu}$,

$$\mathbf{M} = \mathbf{i}\cos I\cos\gamma_H + \mathbf{j}\cos I\sin\gamma_H - \mathbf{k}\sin I \quad \ldots\ldots(13)$$

$$\underline{\mu} = \mu(\mathbf{i}\cos\beta\cos\gamma + \mathbf{j}\cos\beta\sin\gamma + \mathbf{k}\sin\beta) \quad \ldots\ldots(14)$$

We find

$$\mathbf{M}\cdot\frac{\underline{\mu}}{\mu} = \cos\alpha = \cos\beta\cos I\cos(\gamma - \gamma_H) - \sin\beta\sin I \quad \text{.....(15)}$$

$$\mathbf{M}\cdot\mathbf{S} = \cos\psi = \frac{\epsilon\cos\alpha}{\sqrt{\sin^2\alpha + \epsilon^2\cos 2\alpha}} \quad \text{.....(16)}$$

and from (15) we find the simple relation connecting ψ, α, and ϵ

$$\epsilon = \frac{\tan\alpha}{\tan\psi} \quad \text{.....(17)}$$

III. DETERMINATION OF THE WAVE NORMAL IN A STRATIFIED IONOSPHERE

Equation (8) allows one to trace a ray in a horizontally stratified ionosphere provided one has information about the index of refraction μ and the wave normal angle β. If departure angles of the ray and an electron-density distribution are assumed, the index of refraction and the wave normal angle can be determined by the simultaneous solution of the Appleton-Hartree equation and Snell's law. This solution leads to the fourth degree equation given by Booker [5]. One may, however, employ the following method, which is equivalent to the solution of Booker's equation.

The problem is to find direction (β_i , γ_i) and absolute value μ_i of the wave propagation vector in a layer (the j^{th} layer) of electron density N_i for a given direction (β_0 , γ_0) in a medium free of electrons. According to Snell's law, $\gamma_i = \gamma_0$ or the azimuth of the wave propagation vector stays constant. The problem is reduced to two dimensions—the plane of incidence. The first choice now is an arbitrary elevation angle β_{j1} . The corresponding μ_{j1} can be computed. The intersection of the tangent to the μ-surface at the end-point of $\underline{\mu}_{j1}$ and the vertical at a

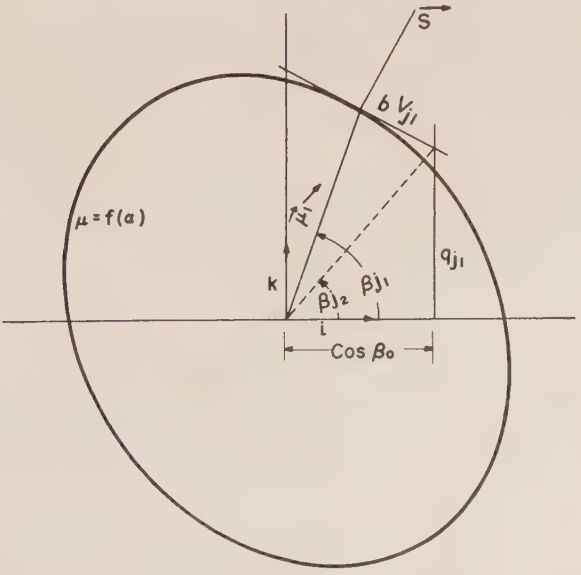

FIG. 1—Cross-section of the μ-surface in the plane of incidence

distance $\cos \beta_0$ from the origin, determines a new elevation angle β_{i2} (Fig. 1). The procedure can be repeated successively until β_{in} converges to the wave normal angle β_i , given by the intersection of the μ-surface itself with the vertical.

In order to derive the formulas for this procedure, we use the **i**, **k** plane as plane of incidence, **k** being in a vertical direction. We have now oriented our coordinate system so that $\gamma = 0$. Using the notation of Figure 1, we obtain

$$\mathbf{u}_{i1} + b_{i1}\mathbf{V}_{i1} = \mathbf{i} \cos \beta_0 + \mathbf{k}q_{i1} \quad \text{.....(18)}$$

V_{i1} is any vector in the plane of incidence tangent to the μ-surface, given by

$$\mathbf{V}_{i1} = [\mathbf{j} \times \mathbf{S}_{i1}]$$

b_{i1} and q_{i1} are the two unknowns which can be computed from the vector equation (18) or the two **i** and **k** component scalar equations

$$\mu_{i1} \cos \beta_{i1} + b_{i1}(\mathbf{i} \cdot \mathbf{V}_{i1}) = \cos \beta_0$$

$$\mu_{i1} \sin \beta_{i1} + b_{i1}(\mathbf{k} \cdot \mathbf{V}_{i1}) = q_{i1}$$

Eliminating b_{i1} and solving for q_{i1} gives

$$q_{i1} = \mu_{i1} \sin \beta_{i1} + \frac{(\mathbf{k} \cdot \mathbf{V}_{i1})}{(\mathbf{i} \cdot \mathbf{V}_{i1})} (\cos \beta_0 - \mu_{i1} \cos \beta_{i1})$$

Now

$$(\mathbf{k} \cdot \mathbf{V}_{i1}) = -(\mathbf{i} \cdot \mathbf{S}_{i1})$$

and

$$(\mathbf{i} \cdot \mathbf{V}_{i1}) = (\mathbf{k} \cdot \mathbf{S}_{i1})$$

Then, we may write

$$q_{i1} = \mu_{i1} \sin \beta_{i1} - \frac{(\mathbf{i} \cdot \mathbf{S}_{i1})}{(\mathbf{k} \cdot \mathbf{S}_{i1})} (\cos \beta_0 - \mu_{i1} \cos \beta_{i1})$$

or, according to (8) and (13), (14),

$$q_{i1} = \mu_{i1} \sin \beta_{i1} - \frac{\cos \beta_{i1} - (1 - \epsilon_{i1}) \cos \alpha_{i1} \cos I \cos \gamma_H}{\sin \beta_{i1} + (1 - \epsilon_{i1}) \cos \alpha_{i1} \sin I} (\cos \beta_0 - \mu_{i1} \cos \beta_{i1}) \quad \text{.....(19)}$$

and in general for the n^{th} approximation

$$q_{in} = \mu_{in} \sin \beta_{in} - \frac{\cos \beta_{in} - (1 - \epsilon_{in}) \cos \alpha_{in} \cos I \cos \gamma_H}{\sin \beta_{in} + (1 - \epsilon_{in}) \cos \alpha_{in} \sin I} (\cos \beta_0 - \mu_{in} \cos \beta_{in}) \quad \text{.....(20)}$$

If the axis of the coordinate system is not fixed in the plane of incidence, $\cos \gamma_H$ in the former equation has to be replaced by $\cos (\gamma - \gamma_H)$.

Now β_{i2} can be determined from

$$\tan \beta_{i2} = \frac{q_{i1}}{\cos \beta_0} \quad \text{.....(21)}$$

Then α_{i2} , $1 - \epsilon_{i2}$, and μ_{i2} can be computed from equations (15), (10), and (1), respectively. The next step is the computation of q_{i2} , using equation (20).

The n^{th} approximation to β_i is obtained from

$$\beta_{in} = \arctan \frac{q_{i(n-1)}}{\cos \beta_0} \qquad (22)$$

and for $n \longrightarrow \infty$

and

$$\left.\begin{aligned} q_{in} &\longrightarrow \mu_i \sin \beta_0 = q_i = \mu_{3i} \\ (\cos \beta_0 - \mu_{in} \cos \beta_{in}) &\longrightarrow 0 \end{aligned}\right\} \qquad (23)$$

IV. EQUIVALENT PATH LENGTH AND RAY PATH

In geometrical-optical considerations, one assumes that the extent of any inhomogeneity in the ionosphere is large compared to the wavelength of the waves. Thus, the propagation of waves may be treated from the point of view of ray theory.

The wave function of angular frequency may be expressed as

$$e^{i\omega t} \cdot e^{-i\varphi(x,y,z)\omega/c} \qquad (24)$$

The phase of this wave is given by

$$\omega ct - \omega\varphi(x, y, z) \qquad (25)$$

The wave propagation vector for this wave is defined by

$$\text{grad } \varphi = \nabla \varphi(x, y, z) = \mathfrak{y}$$

Let $\mathbf{R}$ be the position vector from the transmitter to any point $P(x, y, z)$. Then,

$$\nabla \varphi \cdot d\mathbf{R} = d\varphi = \mathfrak{y} \cdot d\mathbf{R}$$

and

$$\varphi = \int_0^{P_1} \mathfrak{y} \cdot d\mathbf{R} \qquad (26)$$

Although the integration path between the two limits is arbitrary, it is convenient to choose a specific path, the ray path. Therefore, $P(x, y, z)$ is restricted to a point on this path and is a function of the arc lengths measured from the transmitter. We obtain now

$$\varphi = \int_0^{s_1} \mathfrak{y} \cdot \mathbf{S}\, ds \qquad [27)$$

Substituting (27) in (25), we obtain the phase of the wave (24) in the form

$$\omega ct - \int_0^{s_1} \omega(\mathfrak{y} \cdot \mathbf{S})\, ds \qquad (28)$$

where $\mathfrak{y}$ is given by (14) or the equivalent form

$$\mathfrak{y} = \mathbf{i}\mu_1 + \mathbf{j}\mu_2 + \mathbf{k}\mu_3 \qquad (29)$$

From (29) and (13), we find

$$\mu \cos \alpha = \mu_1 \cos I \cos \gamma_H + \mu_2 \cos I \sin \gamma_H - \mu_3 \sin I$$

Eliminating $\mu \cos \alpha$ from the Appleton-Hartree or the μ-surface equation (2), we obtain an equation which may symbolized by

$$\mu(\mu_1 , \mu_2 , \mu_3 , \omega) = 0 \qquad (30)$$

where μ_1 , μ_2 are constant for a given ray (Snell's law). Solving this equation for μ_3 , we have

$$\mu_3 = \mu_3(\mu_1 , \mu_2 , \omega)$$

Thus, μ_3 may be considered a function of the independent variables μ_1 , μ_2 , ω. If we call $P(\mu_1 , \mu_2 , \omega)$ the phase of the wave (24), we have from (28)

$$P(\mu_1 , \mu_2 , \omega) = \omega ct - \int_0^s \omega(\mathbf{\mu} \cdot \mathbf{S}) \, ds \qquad (31)$$

This is the phase for a wave of angular frequency ω and incident directions given by μ_1 , and μ_2 .

For the ray path, according to Kelvin's principal of stationary phase, we must have

$$dP(\mu_1 , \mu_2 , \omega) = 0$$

Thus, since μ_1 , μ_2 , ω are independent,

$$\frac{\partial P}{\partial \mu_1} = 0 \qquad \frac{\partial P}{\partial \mu_2} = 0 \qquad \frac{\partial P}{\partial \omega} = 0 \qquad (32)$$

Making use of (31), the equations (32) give

$$\left.\begin{aligned} a \cdots & \int_0^s \left(\frac{\partial \mathbf{\mu}}{\partial \mu_1} \cdot \mathbf{S} \right) ds = 0 \\ b \cdots & \int_0^s \left(\frac{\partial \mathbf{\mu}}{\partial \mu_2} \cdot \mathbf{S} \right) ds = 0 \\ c \cdots & ct - \int_0^s \frac{\partial}{\partial \omega} \{\omega(\mathbf{\mu} \cdot \mathbf{S})\} \, ds = 0 \\ & \qquad \text{S constant} \end{aligned}\right\} \qquad (33)$$

The first two of these equations define the position of the ray path. The last equation gives the equivalent path length of the ray. It also defines the group refractive index μ' along the ray

$$\mu' = \frac{\partial}{\partial \omega} \{\omega(\mathbf{\mu} \cdot \mathbf{S})\}_{\text{S constant}} \qquad (34)$$

and the group velocity, which is given by (c/μ') S.

We may put this equation in a form more usable for computations. Noting that

$$\left.\begin{aligned} \frac{d\mathbf{R}}{ds} &= \mathbf{S} \\ \mathbf{k}\cdot\frac{d\mathbf{R}}{ds} &= \frac{dz}{ds} = \mathbf{k}\cdot\mathbf{S} \\ ds &= \frac{dz}{\mathbf{k}\cdot\mathbf{S}} \end{aligned}\right\} \quad \ldots\ldots(35)$$

we obtain from (29)

$$\frac{\partial \underline{\mathbf{u}}}{\partial \omega} = \mathbf{k}\,\frac{\partial \mu_3}{\partial \omega} \quad \ldots\ldots(36)$$

since μ_1 , μ_2 , are not functions of ω. Now,

$$\frac{\partial(\underline{\mathbf{u}}\cdot\mathbf{S})_{\mathbf{S}\text{ constant}}}{\partial \omega} = \frac{\partial \underline{\mathbf{u}}}{\partial \omega}\cdot\mathbf{S} = \mathbf{k}\cdot\mathbf{S}\,\frac{\partial \mu_3}{\partial \omega} \quad \ldots\ldots(37)$$

Substituting (35), (36), and (37) in (32c), we obtain

$$ct = \int_0^z \left(\frac{\underline{\mathbf{u}}\cdot\mathbf{S}}{\mathbf{k}\cdot\mathbf{S}} + \omega\,\frac{\partial \mu_3}{\partial \omega}\right) dz \quad \ldots\ldots(38)$$

$\partial\mu_3/\partial\omega$ is obtained by differentiating (30) with respect to ω and

$$\frac{\underline{\mathbf{u}}\cdot\mathbf{S}}{\mathbf{k}\cdot\mathbf{S}}$$

from equation (8). Combining and simplifying, (38) becomes

$$ct = \int_0^z \frac{1}{\mu}\cdot\frac{1 - (1-\epsilon)\mu^2\cos^2\alpha - \dfrac{(1-\mu^2-a)^2(1-\epsilon)}{ah(1-\mu^2)}}{\sin\beta + (1-\epsilon)\cos\alpha\sin I}\,dz \quad \ldots\ldots(39)$$

If one utilizes the phase path instead of the group path in an experiment, then one starts with formula (27), which gives the phase path. This may be written corresponding to formula (38) for the group path as follows:

$$\varphi = \int_0^z \frac{\underline{\mathbf{u}}\cdot\mathbf{S}}{\mathbf{k}\cdot\mathbf{S}}\,dz \quad \ldots\ldots(40)$$

and the formula for the phase path equivalent to the group path formula (39) is given by

$$\varphi = \int_0^z \mu\cdot\frac{1 - (1-\epsilon)\cos^2\alpha}{\sin\beta + (1-\epsilon)\cos\alpha\sin I}\,dz \quad \ldots\ldots(41)$$

V. DETERMINATION OF ELECTRON DENSITY DISTRIBUTION

The preceding formulas have been used for the analysis of experimental data from a rocket program to obtain electron-density distributions. These experimental data consist of delay times of pulsed signals between the rocket and a ground station as a function of rocket position. The method of analysis is essentially a trial and error method, using the IBM 704 high speed computer.

For the evaluation, the ionosphere is divided into layers of uniform thickness and constant electron density. The stepwise evaluation begins with the rocket in a position at the top of the first layer. The position of the rocket with respect to the ground station, the delay of the pulse at this position, the frequency of the pulse, and the intensity and inclination of the earth's magnetic field are known. The relative positions of the rocket with respect to the ground station and the earth's magnetic field are fixed in a *xyz* coordinate system, with the positive x axis chosen in the direction of geomagnetic north. The origin of the coordinate system is the position of the ground station.

The procedure can best be understood by looking at a flow chart (Fig. 2). It starts with an estimate of the electron density N_j in the j^{th} layer. The first

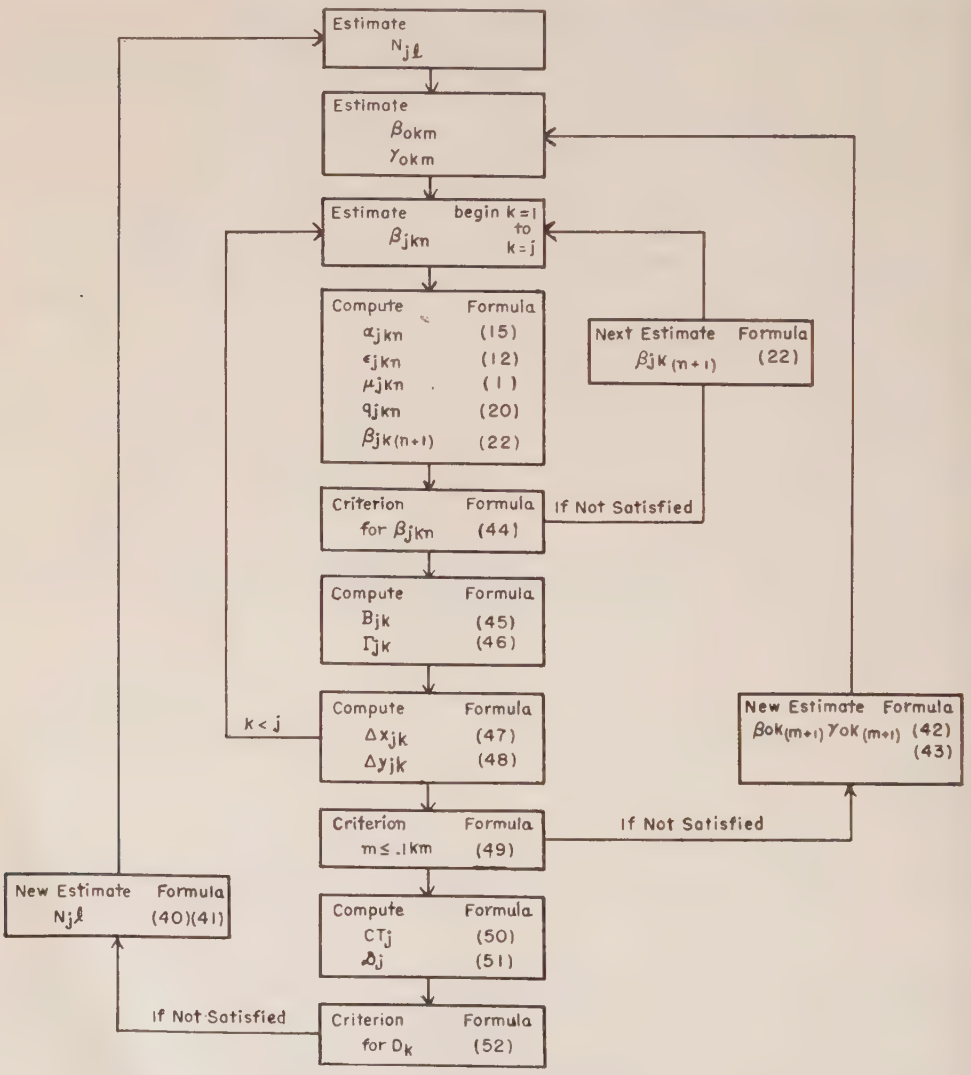

FIG. 2—Flow chart for determination of electron-density distribution

estimate chosen is $N_{i1} = 0$. The delay time $\mathfrak{D}_{i1}$ computed with this estimate allows one to make a good second estimate, provided the effect on the delay is nearly proportional to the electron density. Therefore,

$$N_{i2} = N_{(i-1)} \frac{D_i - \mathfrak{D}_{i1}}{D_{i-1} - \mathfrak{D}_{(i-1)}} \quad \text{.....(42)}$$

where D_i is the experimental delay for the j^{th} layer. For the first layer, this formula is replaced by $N_{12} = 1 \times 10^4$ electrons/cm^3. The following approximations just use a linear interpolation of the previous estimates:

$$N_{il} = N_{i(l-1)} \frac{D_i - \mathfrak{D}_{i(l-2)}}{\mathfrak{D}_{i(l-1)} - \mathfrak{D}_{i(l-2)}} + N_{i(l-2)} \frac{D_i - \mathfrak{D}_{i(l-1)}}{\mathfrak{D}_{i(l-2)} - \mathfrak{D}_{i(l-1)}} \quad \text{.....(43)}$$

The next step in the flow chart is an estimate of the departure angles $\beta_{0,k}$, $\gamma_{0,k}$ of the k^{th} ray to hit the rocket trajectory at the top of the j^{th} layer. The first estimate is the departure angle for the layer underneath $\beta_{0k1} = \beta_{0(k-1)}$; $\gamma_{0k1} = \gamma_{0(k-1)}$. The second estimate assumes a linear relation of the change of departure angle with rocket height.

$$\beta_{0k2} = 2\beta_{0(k-1)} - \beta_{0(k-2)} \; ; \quad \gamma_{0k2} = 2\gamma_{0(k-1)} - \gamma_{0(k-2)} \quad \text{.....(44)}$$

For the first two layers, this formula is replaced by an angle determined by the straight-line connection to the rocket.

The following approximations use a linear interpolation of the rocket coordinates x_i and y_i with respect to the coordinates of the two previous ray estimates:

$$\sum_0^{j=k} \Delta x_{jkm} \quad \text{and} \quad \sum_0^{j=k} \Delta y_{jkm}$$

or

$$\left.\begin{aligned}
\beta_{0km} = {} & \frac{\beta_{0k(m-2)}\left\{x_i\left(x_i - \sum_0^{j=k} \Delta x_{jk(m-1)}\right) + y_i\left(y_i - \sum_0^{j=k} \Delta y_{jk(m-1)}\right)\right\}}{x_i\left(\sum_0^{j=k} \Delta x_{jk(m-2)} - \sum_0^{j=k} \Delta x_{jk(m-1)}\right)} \\
& + \frac{\beta_{0k(m-1)}\left\{x_i\left(x_i - \sum_0^{j=k} \Delta x_{jk(m-2)}\right) + y_k\left(y_k - \sum_0^{j=k} \Delta y_{jk(m-2)}\right)\right\}}{+ y_i\left(\sum_0^{j=k} \Delta y_{jk(m-2)} - \sum_0^{j=k} \Delta y_{jk(m-1)}\right)} \\
\gamma_{0km} = {} & \frac{\gamma_{0k(m-2)}\left\{y_i\left(x_i - \sum_0^{j=k} \Delta x_{jk(m-1)}\right) - x_i\left(y_i - \sum_0^{j=k} \Delta y_{jk(m-1)}\right)\right\}}{y_i\left(\sum_0^{j=k} \Delta x_{jk(m-2)} - \sum_0^{j=k} \Delta x_{jk(m-1)}\right)} \\
& + \frac{\gamma_{0k(m-1)}\left\{y_i\left(x_i - \sum_0^{j=k} \Delta x_{jk(m-2)}\right) - x_i\left(y_i - \sum_0^{j=k} \Delta y_{jk(m-2)}\right)\right\}}{- x_i\left(\sum_0^{j=k} \Delta y_{jk(m-2)} - \sum_0^{j=k} \Delta y_{jk(m-1)}\right)}
\end{aligned}\right\} \quad \text{.....(45)}$$

The ray of this departure angle is now constructed, respectively, through the layers $j = 1$ to $j = k$. The method to find the wave normal angle β_{jk} is outlined in Section IV. As a first estimate for β_{jk}, the value of the previous layer $\beta_{(j-1)k}$ has been chosen. The successive approximations have been carried up to an accuracy which is justified by the experimental errors in the delay time readings. The criterion used is

$$| \beta_{jkn} - \beta_{jk(n-1)} | \leq 1 \text{ minute of arc} \quad \text{.....(46)}$$

For each wave normal angle and additional to the values α_{jk}, ϵ_{jk}, μ_{jk}, the ray directions are computed according to the formula

$$\sin B_{jk} = \mathbf{k}\cdot\mathbf{S} = \frac{\sin \beta_{jk} + (1 - \epsilon_{jk}) \cos \alpha_{jk} \sin I}{\sqrt{1 + (\epsilon_{jk}^2 - 1) \cos^2 \alpha_{jk}}} \quad \text{.....(47)}$$

$$\tan \Gamma = \frac{\mathbf{j}\cdot\mathbf{S}}{\mathbf{k}\cdot\mathbf{S}} = \frac{\cos \beta_{jk} \sin \gamma_{0k}}{\cos \beta_{jk} \cos \gamma_{0k} - (1 - \epsilon_{jk}) \cos \alpha_{jk} \cos I} \quad \text{.....(48)}$$

The horizontal projections of the rays in the j^{th} layer element of height Δz are

$$\Delta x_{jk} = \Delta z \cos \Gamma_{jk} / \tan \beta_{jk} \quad \text{.....(49)}$$

$$\Delta y_{jk} = \Delta z \sin \Gamma_{jk} / \tan \beta_{jk} \quad \text{.....(50)}$$

When passing the $j = k^{\text{th}}$ layer, the ray has to meet the criterion of hitting the rocket at position x_i, y_i, which has been chosen as

$$m = \sqrt{\left(\sum_0^{j=k} \Delta x_{jk} - x_i\right)^2 + \left(\sum_0^{j=k} \Delta y_{jk} - y_i\right)^2} \leq 0.1 \text{ km} \quad \text{.....(51)}$$

Once the path has been determined, the time of transit of a pulse along this path is computed by formula (39), written as a summation with the proper notation in the following way:

$$cT_k = \frac{z_0}{\sin \beta_{0k}} + \Delta z \sum_{i=1}^{k} \frac{1}{\mu_{ik}} \frac{1 - (1 - \epsilon_{jk})\mu_{jk}^2 \cos^2 \alpha_{jk} - \dfrac{(1 - \mu_{jk}^2 - a_j)^2 (1 - \epsilon_{jk})}{a_j h_j (1 - \mu_{jk}^2)}}{\sin \beta_{jk} + (1 - \epsilon_{jk}) \cos \alpha_{jk} \sin I} \quad \text{.....(52)}$$

The delay is computed by subtracting from this time, the time of travel of a pulse traveling at the velocity of light along the straight path between the rocket and ground station as follows:

$$\mathfrak{D}_i = T_k - \frac{1}{c} \sqrt{x_{ik}^2 + y_{ik}^2 + z_{ik}^2} \quad \text{.....(53)}$$

If the following criterion is satisfied, then the estimated electron density is considered satisfactory:

$$| D_i - \mathfrak{D}_i | \leq \cap \quad \text{.....(54)}$$

$\cap$ is determined by the limit of accuracy of the delay readings in microseconds. The values for $\cap$ in microseconds are chosen as follows

$$\cap = 0.005 \quad \text{if} \quad 0.1(D_i - D_{i-1}) = f < 0.005$$

$$\cap = f \quad \text{if} \quad 0.005 < f \leq 0.05$$

$$\cap = 0.05 \quad \text{if} \quad f > 0.05$$

If this criterion is not satisfied, the procedure is repeated again from the beginning with a new estimated electron density until it is satisfied. Then the electron density for the layer is known and the procedure is repeated for the next and each succeeding layer until, layer by layer, the electron-density distribution is determined. It is worth while to note that for the computing program it is possible to insert known electron-density profiles to obtain delay data.

The procedure outlined has been used quite successfully to analyze the data from a number of flights. One of them is reported in an accompanying paper [9].

VI. ACKNOWLEDGMENT

The authors are indebted to Dr. George Gassman, who did much of the preliminary work on the method of analysis for high speed computers.

References

[1] H. Poeverlein, Ber. Bayer Acad., 175 (1958).
[2] H. Poeverlein, Zs. angew. Phys., **1**, 517 (1950).
[3] R. F. Mullaly, Report of the Physical Society Conference on the Physics of the Ionosphere held at the Cavendish Laboratory, Cambridge, September 1954, p. 384 (1955).
[4] H. G. Booker, Proc. R. Soc., A, **155**, 235 (1936).
[5] H. G. Booker, Phil. Trans. R. Soc., **237**, 411 (1938).
[6] G. Millington, Proc. Inst. Elec. Eng., **98**, Pt. 4, 1 (1951).
[7] G. Millington, Proc. Inst. Elec. Eng., **101**, Pt. 3, 193 (1954).
[8] W. R. Hamilton, Trans. R. Irish Acad., **17**, 144 (1837).
[9] W. Pfister and J. C. Ulwick, G. Geophys. Res., **63**, 315 (1958).

THE ANALYSIS OF ROCKET EXPERIMENTS IN TERMS OF ELECTRON-DENSITY DISTRIBUTIONS

BY W. PFISTER AND J. C. ULWICK

Geophysics Research Directorate,
Air Force Cambridge Research Center,
Bedford, Massachusetts

(Received December 21, 1957)

ABSTRACT

Rocket ionosphere experiments give the relative delay of a pulsed signal as a function of rocket position. These data are used in an analysis to obtain the electron-density distribution with respect to height. This analysis, which takes into account the effects of the earth's magnetic field and the obliquity of the ray paths, is for the smooth, horizontally stratified ionosphere. The actual ionosphere, however, has an irregular or "blobby" structure evident in our delay records. The data then must be smoothed over a height interval corresponding roughly to the size of the blobs.

The delay data from USAF Aerobee No. 38, which was launched at 1210 hours MST on 26 June 1953, at Holloman Air Development Center, New Mexico, are analyzed for rocket ascent and descent for two frequencies, 4.05 and 4.87 Mc. The electron-density distribution from rocket descent data for both frequencies are in good agreement and show peaks at 106, 111, 117, and 128 km. For rocket ascent, an intense irregularity apparently was present around 98 km, with a minimum horizontal extension of 3.5 km and a maximum intensity of about 6×10^4 electrons/cm^3. The P'-f record taken at launch time compares very well with the electron-density distribution from rocket descent.

INTRODUCTION

The use of a pulse delay method in a rocket experiment for measuring the electron density in the ionosphere goes back to 1946, when V-2 rockets were first available for upper air research. The method was first proposed by Dr. M. H. Nichols, then at Princeton University [see 1 of "References" at end of paper]. The experiments have been carried out in a joint effort by the United States Air Force and its contractors, the University of Michigan (Prof. W. G. Dow) and the University of Utah (Prof. L. B. Linford).

Thus far, useful data for the determination of electron densities have been obtained from two V-2 rockets and ten Aerobee rockets (3 standard, 4 intermediate, and 3 hi). A summary of this information is given in Table 1. Only part of the records obtained on these rocket flights have been analyzed, and the results

TABLE 1

Rocket type	No.	Date launched	Time	Maximum altitude
			hours MST	*km*
V-2	15	Nov. 21, 1946	1000	111
V-2	24	Apr. 17, 1947	1621	140
Aerobee (standard)	38	June 26, 1953	1210	133
Aerobee (standard)	39	July 1, 1953	1052	134.5
Aerobee (standard)	45	Nov. 3, 1953	1115	121
Aerobee (intermediate)	67	June 13, 1956	1351	140
Aerobee (intermediate)	68	June 18, 1956	1342	137
Aerobee (intermediate)	69	June 21, 1956	1148	146
Aerobee (intermediate)	70	June 26, 1956	1126	110
Aerobee (hi)	78	June 18, 1957	0700	171
Aerobee (hi)	79	June 25, 1957	0704	205
Aerobee (hi)	89	Nov. 7, 1957	0905	...

reported are only of preliminary nature. The first analysis was done by E. Beth on V-2 rocket No. 24, and reported at the Conference of Ionospheric Physics in 1950 [1]. He noticed that the measured time delay fluctuates considerably after the rocket has reached a height of 95 km. His conclusion was that the ionosphere is very irregular and patchy in the interval between 95 and 110 km, while the small irregularities in the region above 110 km have negligible effects on the measured time delays.

Records obtained from later flights indicated that the fluctuations of the time delay are caused by small clouds of higher electron density, and that the smoothing process has to be done by weighting the smaller time delays. The results have been reported by J. R. Lien, *et al.*, who found a bifurcation of the *E* region in the case of V-2 No. 24 and Aerobees Nos. 38 and 39 [2]. In view of the discrepancy of this result with the general concept of the *E* layer and with findings of the Naval Research Laboratory from their rocket experiments [3], [4], a re-evaluation of the data analysis was desirable.

Part of the new, very careful analysis has been reported at several scientific meetings. The analysis, even of the earlier rockets, is still not completely done. The only rocket from which all available records have been analyzed is Aerobee No. 38, which has been chosen as the subject of this publication.

DESCRIPTION OF EXPERIMENT

The experimental procedure used is described in detail by O. C. Haycock [5], so only a review is presented here to provide background information.

This experiment consists of the measurement of the time retardation of a pulsed rf signal by the ionosphere. The delay times of pulses transmitted to and from the rocket are measured relative to an undelayed signal of higher frequency. The lower frequency pulses from the ground to the rocket are transmitted successively on seven frequencies in the range from 4 to 5 Mc from a 50-kw transmitter. The complete low-frequency, ground-to-rocket transmitting cycle consists

of two 8-μsec pulses being successively transmitted at each of the seven frequencies; the next two successive pulses are then blanked for identification purposes, and then the cycle is repeated. The low-frequency transmissions from the rocket to the ground are from a 4-kw grid-modulated transmitter and consist of 8-μsec pulses at a frequency of 6 Mc. The higher frequency comparison pulses for the upward and downward transmissions at 470 and 493.5 Mc, respectively, are part of the Air Force Cambridge Research Center multi-purpose beacon system [6]. Figure 1 shows the timing schedule of the pulses.

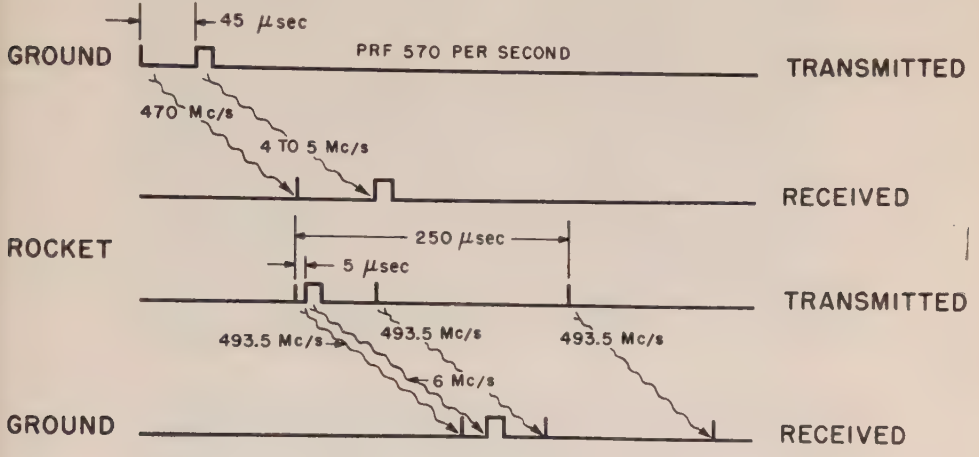

FIG. 1—Timing schedule of pulses

The 4- to 5-Mc pulse is transmitted, as shown, 45 μsec after the 470-Mc beacon interrogation pulse. When the rocket is below the ionosphere, the pulses arrive at the rocket with the same time separation as at departure; after the rocket enters the ionosphere, however, the separation in time increases due to the relative delay of the 4- to 5-Mc pulse. When received at the rocket, the 4- to 5-Mc pulse triggers the triangulation beacon during the time interval normally reserved for the first-channel telemetering reply. The second-channel telemetering pulse is transmitted, as normal, 250 to 400 μsec after the beacon reply pulse (generated at the rocket by the arrival of the 470-Mc interrogation pulse). The pulse repetition rate of the system is 570 pps.

In addition to the three 493.5-Mc pulses, a 6-Mc pulse is transmitted from the rocket 5 μsec after the beacon reply pulse. As with the upward transmission, this pulse will arrive at the ground stations with an unchanged time separation, except when the 6-Mc pulse is delayed by passage through the ionosphere. The 6-Mc pulse is recorded both by Mitchell frame cameras and modified General Radio moving-strip cameras, while the telemetered pulses are recorded on Fairchild oscilloscope cameras.

Figure 2 shows the geographical location of the ground transmitting and receiving sites with respect to the Aerobee launching tower at Holloman Air Development Center, New Mexico, for USAF Aerobee No. 38, the results of which are discussed in this paper. The basic function of these stations for all Aerobee flights is to record the time difference between the arrival of a pulse synchronized with the 470-Mc

interrogation pulse to the rocket and the 493.5-Mc reply pulse from the rocket. The information obtained from the four ground stations provides the necessary data to enable the calculation of the XYZ coordinates of the rocket by the so-called Inyokern method. In addition, the four stations were equipped with 6-Mc receivers to record the difference in arrival times between the 493.5-Mc and 6-Mc pulses from the rocket, thus providing four transmission paths at this frequency. The telemetering data, which include the delay data for the upward transmissions, are recorded from the 493.5-Mc receivers at Two Buttes and Army 2. The Two Buttes station also is the location of the 4- to 5-Mc and 470-Mc ground transmitters. As is shown in Figure 2, the launching direction for all Aerobees is in the northwest quadrant, to satisfy range safety requirements.

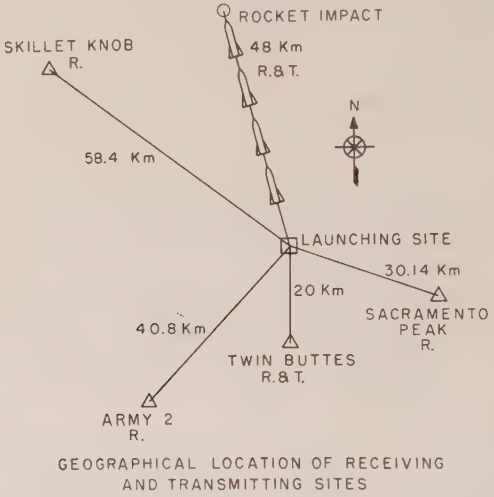

Fig. 2—Geographical location of receiving and transmitting sites

DELAY DATA RECORDING

The recordings of information are made by photographing the oscilloscope sweeps initiated by the 493.5-Mc beacon reply pulse. Figure 3 shows an example of the pulse-time telemetering record from Aerobee No. 38 at 165 seconds after rocket launch, which corresponds in this flight to a rocket altitude of 133 km. Time is advancing to the right. The 493.5-Mc pulses intensity-modulate the scope, resulting in the dots shown. Those at the bottom of the record are due to the beacon reply pulse and are spaced 1/570 second apart, the repetition period

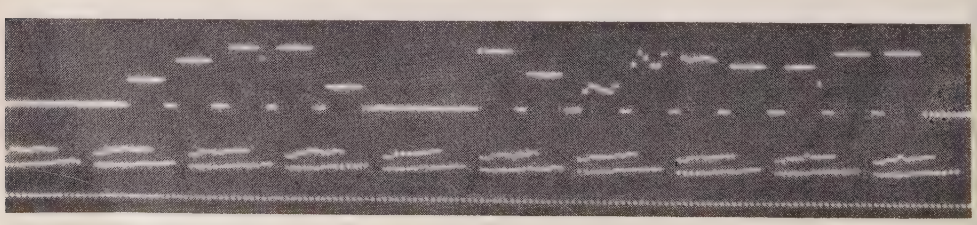

Fig. 3—Telemetering record at 165 sec time of flight for Aerobee No. 38

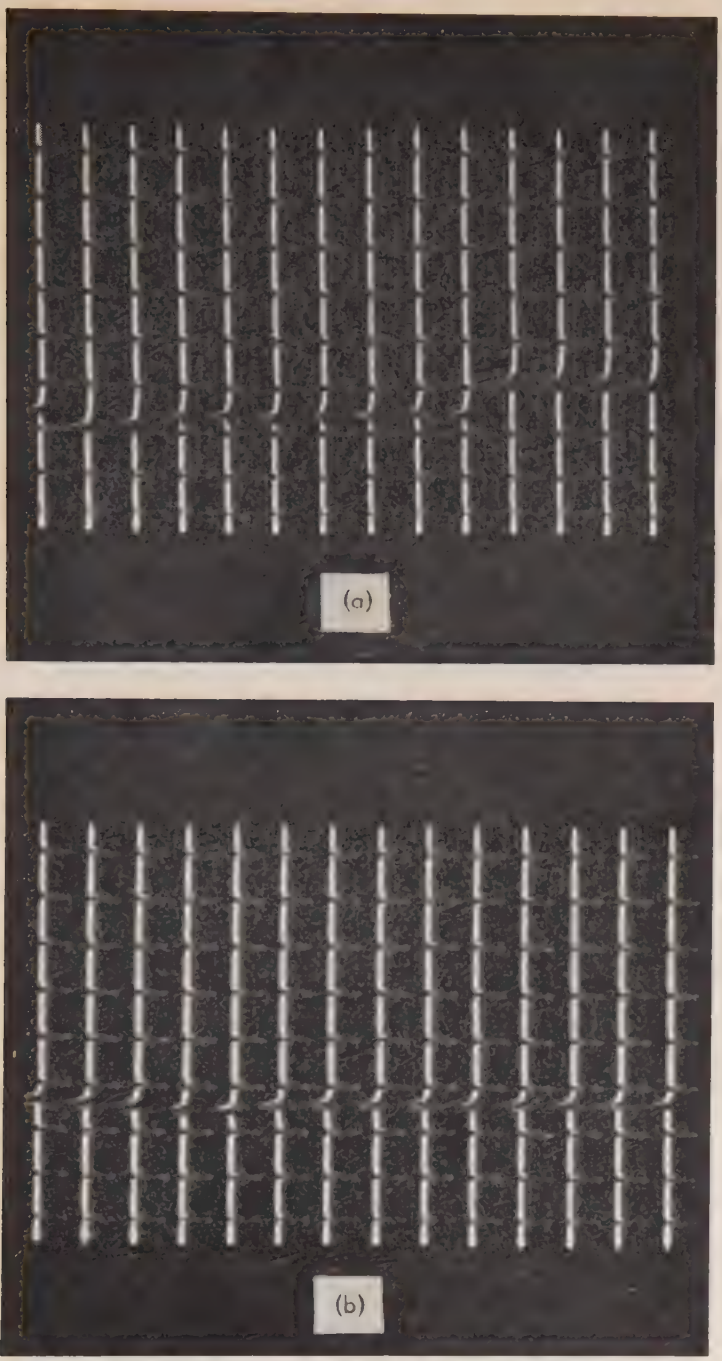

FIG. 4—Amplitude-modulated delay telemetering record for Aerobee No. 38 at (*a*) 104.7 sec time of flight = 104 km, and (*b*) 113.1 sec time of flight = 110 km

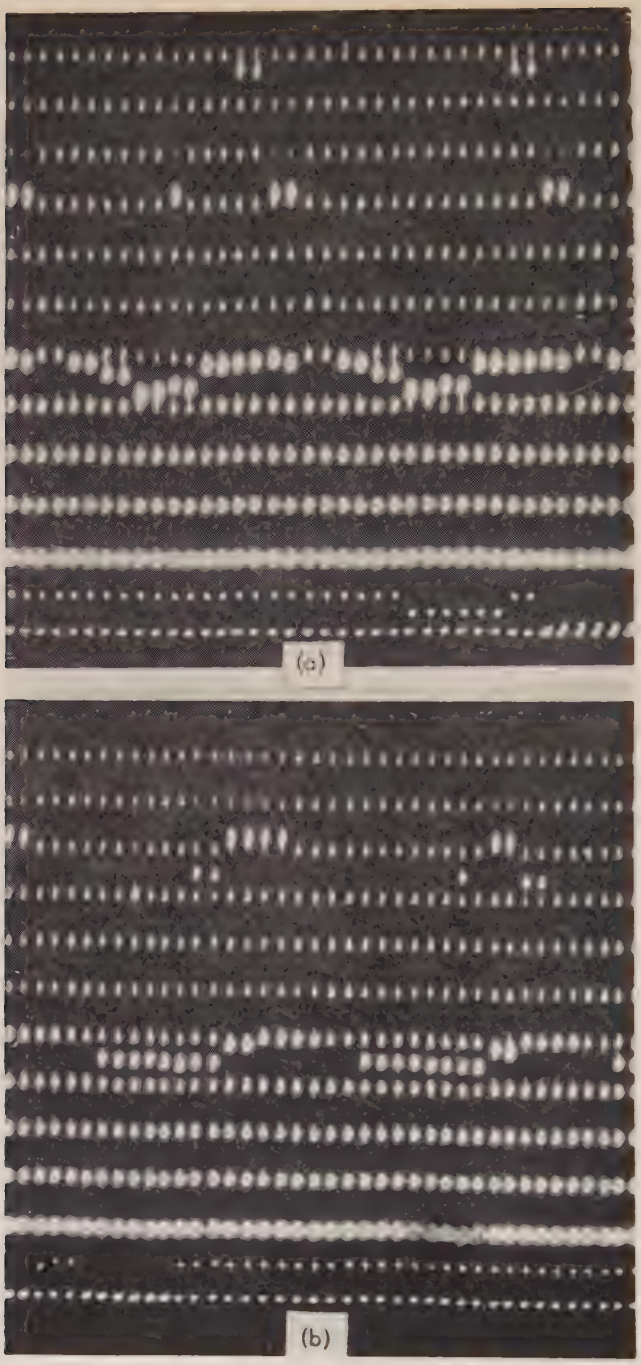

FIG. 5—Intensity-modulated delay telemetering record for Aerobee No. 38 at (*a*) 148.1 sec time of flight—128.25 km, and (*b*) 149.9 sec time of flight—129 km

of the system. The dots immediately above, occurring in groups of 14 with two blank spaces between, are due to the seven low-frequency pulses. The differences between these pulses and the beacon reply pulses indicate the relative delays of the seven frequencies. These differences are constant and constitute the zero or reference condition when the rocket is below the ionosphere. The frequency dependence of the delays is apparent here where the delays increase from the highest frequency on the left to the lowest frequency on the right. The dots immediately above the delayed pulses, occurring in groups of ten, result from a reflection of the 4- to 5-Mc pulses, probably from a sporadic-*E* cloud.

The upper half of the record in Figure 3 contains the second-channel telemetering data. The deflection upward of the pulses from the zero voltage or ground condition at the middle of the record is a measure of the performance of the rocket transmitting and receiving instrumentation. From these data, it was found that the 6-Mc transmitting tube failed at rocket launch, resulting in no downward transmission for this flight. Therefore, no mention is made about the recording style of the 6-Mc data pertaining to the downward transmission. Figure 6 of reference [5], however, shows examples of these recordings.

Since the delay data are rather difficult to read on the regular telemetering record, the same delay information is displayed by two other methods. These both have 100-μsec sweep lengths with 10-μsec markers, but in one the pulses and time markers intensity-modulate the scope while in the other they amplitude-modulate the scope.

An interesting example of the amplitude-modulated delay telemetering record from the Aerobee No. 38 flight is shown in Figures 4*a* and 4*b*. In Figure 4*a*, the delays are shown at 104.7 seconds time of flight, corresponding to a rocket altitude for this flight of 104 km. It will be noticed that the two lowest frequencies are significantly stepped upward compared with the other frequencies and appear just above the fourth 10-μsec marker. Figure 4*b* shows the more normal delay record, with a fairly uniform increasing delay with decreasing frequency. The delays of the two lowest, however, here at this altitude of 110 km, are less than those at 104 km. In a horizontally stratified ionosphere, this decrease in delay with increase in altitude is possible only in a special geometrical configuration and only with a limited gradient. This decrease in delays with increasing rocket altitude, also observed in other flights (Fig. 2 of reference [7]), is attributed to the "blobby" or irregular structure of the ionosphere.

Figure 5, an intensity-modulated delay telemetering record, shows an interesting example of the effect of the "blobby" structure for a higher altitude for this same rocket flight. In Figure 5*a*, the two highest frequencies and the three lowest frequencies are delayed more than the two middle frequencies. Figure 5*b*, with the rocket 0.75 km higher, shows the two highest frequencies have decreased in delay with the three lowest frequencies remaining stepped. This stepped condition has been observed and reported for another flight (Fig. 14 of reference [2]).

DELAY DATA REDUCTION

In deriving the upward-transmission delay curves for the analysis, any one of the three styles of recording at either of the stations can be used, provided it

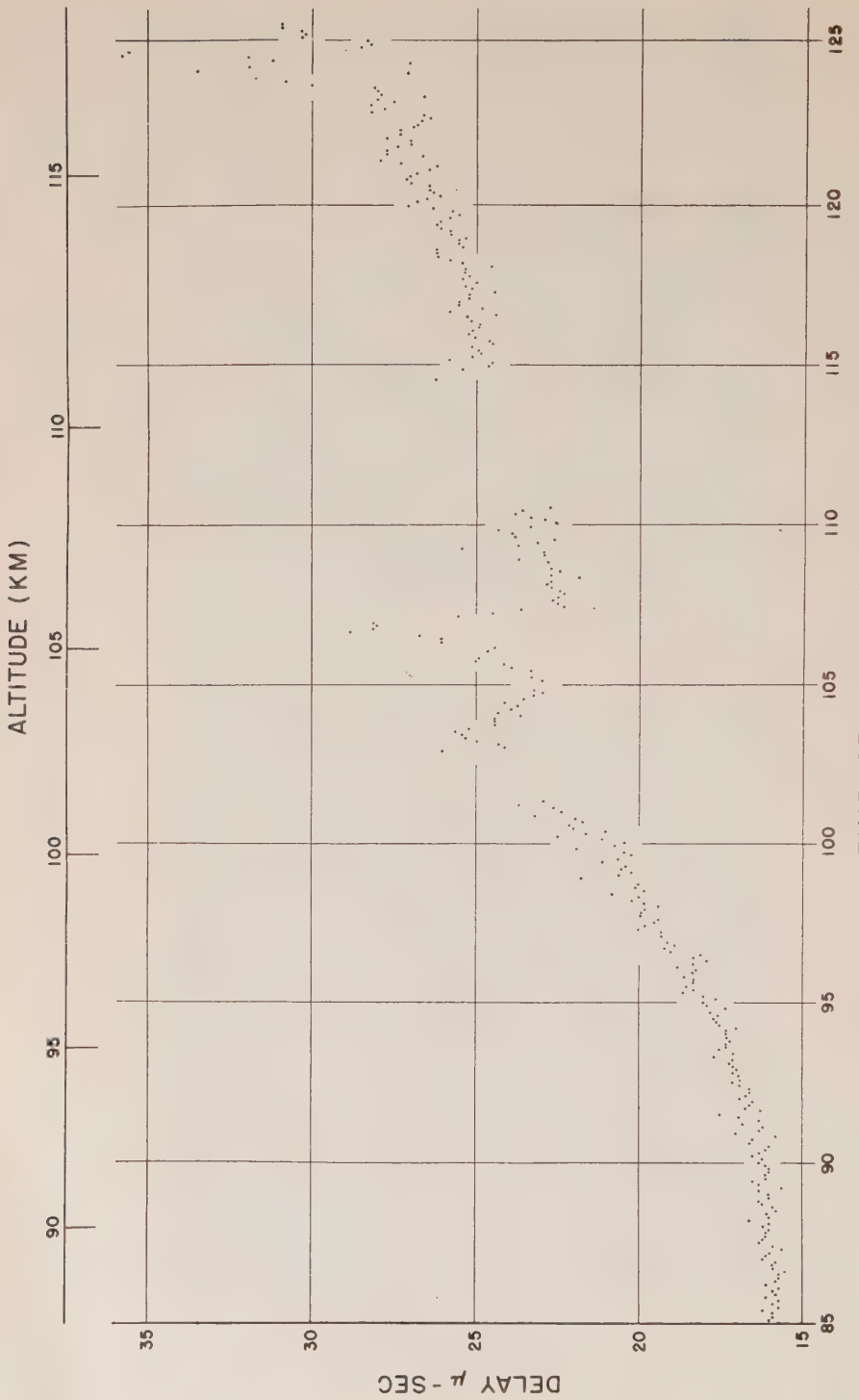

FIG. 6—Delay data from delay telemetering record at Two Buttes for 4.05-Mc frequency of rocket ascent of Aerobee No. 38

is a complete record of the delays. Usually, however, one record from each of the two stations is read, one to supplement the other because of gaps in the data resulting at times during the flight from poor antenna orientation. Of course, either the channel 1 intensity-modulated or amplitude-modulated delay telemetering are used whenever possible, since these records are more accurate than the regular telemetering record.

The actual reading of the film is accomplished very carefully by measuring magnified portions of the film with a micrometer arrangement that gives approximately 20 readings per microsecond deflection. Since the repetition rate of the system is 570 pps, the delay data for the upward transmissions at each frequency are recorded nearly 36 times per second. By reading a film from each of the two recording stations every tenth of a second, a little over half the data available is read. This gives, however, a range from approximately 20 readings per kilometer interval when the rocket is at the base of the ionosphere to a maximum of 80 readings per kilometer interval near zenith.

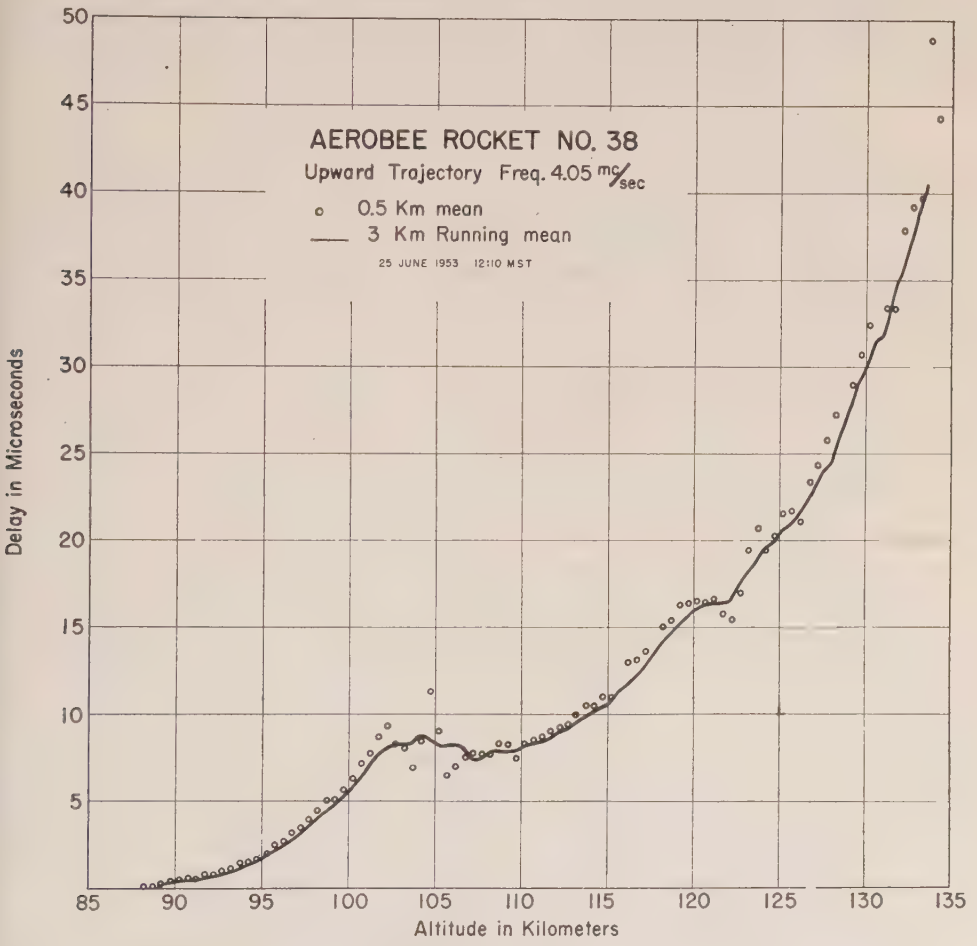

FIG. 7—0.5-km mean and 3-km running mean delay data for 4.05-Mc frequency of rocket ascent of Aerobee No. 38

Figure 6 shows the delay readings recorded at Two Buttes as a function of time of flight for the lowest frequency, 4.05 Mc, of the upward transmission for Aerobee No. 38. Gaps in the data from this amplitude-modulated delay telemetering recording are evident at various altitudes. These were filled in by data obtained from the recordings at Army 2. Examination of the data reveals a periodicity of the fluctuations of the readings which agrees with the rocket roll. From these data, it is evident that the missile rotates approximately one and one-half times per second, with an amplitude range of the fluctuations between $\frac{1}{2}$ and 1 microsecond. The delay data for this 6-Mc downward transmission from another rocket flight showed the missile rotated approximately two times per second, with an amplitude range of the fluctuations between $1\frac{1}{2}$ to 2 microseconds (Fig. 1 of reference [7]). This type of fluctuation can easily be eliminated by integrating over the period of the roll of the rocket.

Figure 7 shows how this fluctuation is eliminated when the mean value for $\frac{1}{2}$-km intervals is taken. This interval size is a consequence of the method of analysis, where the ionosphere is divided into equal layers of $\frac{1}{2}$-km thickness. The mean

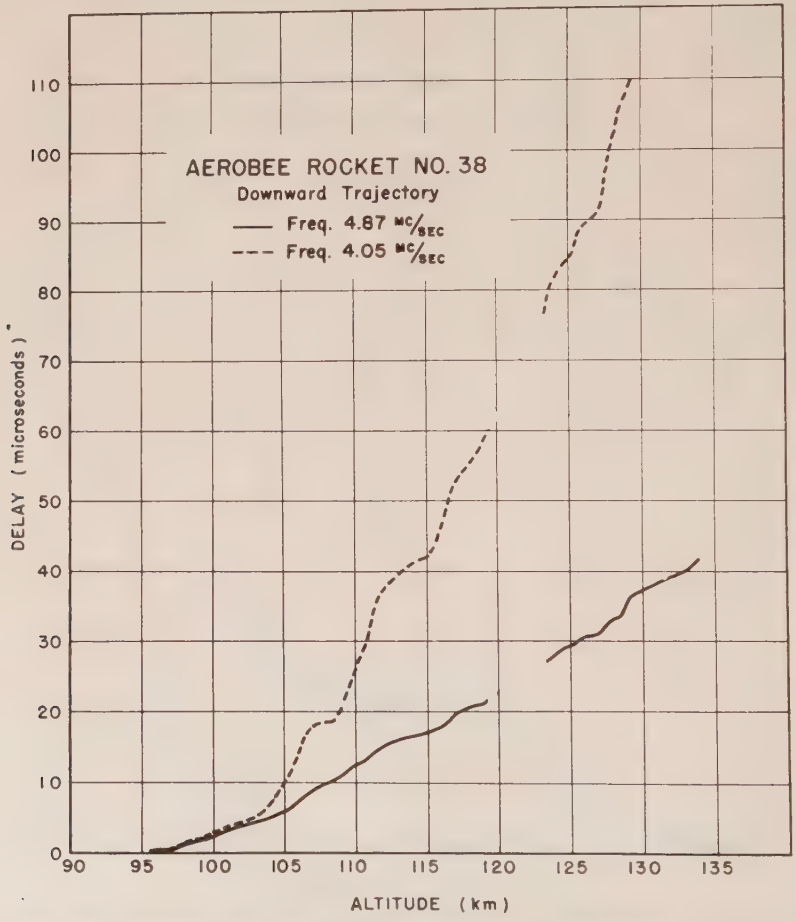

FIG. 8—3-km running mean delay data for 4.05- and 4.87-Mc frequencies of rocket descent of Aerobee No. 38

values, however, are still not regular enough to allow an analysis based on the concept of a smooth, stratified ionosphere. Irregularities are still evident at various altitudes, particularly noticeable at 102 and 105 km. The next step, therefore, in the analysis is to eliminate these by computing running means over 3-km intervals, shown by the solid line. In a like manner, the delay curve for the same frequency for the rocket descent and the delay curves for the highest of the seven frequencies, 4.87 Mc, for both the rocket ascent and descent, were obtained. These four delay curves were used in the analysis. For comparison, the delay curves for the two frequencies from the rocket descent are shown in Figure 8. Between 119 km and 123 km, the data were missing for both frequencies.

It is interesting also to compare the low-frequency curve from rocket ascent shown in Figure 7 with that shown here. The low-frequency delay data on rocket ascent are recorded to 134.5 km, while for rocket descent the data are missing from zenith to 129.5 km. The explanation for this becomes apparent when the other five frequency delay curves are examined. This reveals that the three lowest frequencies were being reflected in this height interval. The difference in delay readings at the same altitude for these two curves is due to the greater delays experienced by the pulses over the longer ray paths when the rocket is descending.

RESULTS FOR AEROBEE NO. 38

The four smoothed delay curves mentioned, that is, for the highest and lowest frequencies for rocket ascent and descent, have been used to compute the electron density exactly under the assumption of horizontal stratification. The method of analysis utilizes a ray-tracing technique developed for high speed computers by an extension of Poeverlein's graphical method [8]. The electron density has been computed in steps of $\frac{1}{2}$ km, using a trial-and-error method, whereby the departure angle of the ray and the electron density in the top layer of each ray are adjusted to hit the rocket and to meet the experimental delay time. In order to de-emphasize small details of no significance, the resulting step curve of $\frac{1}{2}$-km intervals of electron density *vs* altitude is smoothed out by a running, weighted mean over five such intervals, the weights used being 1, 0.8, and 0.4. The results for the two frequencies, 4.05 and 4.87 Mc, are shown for the rocket descent in Figure 9.

The agreement between the frequencies is good with respect to the shape of the curves, although the values at 107 and 114 km are noticeably different. These are attributed to the different effect the irregularities have on the two frequencies as a result of different ray paths and the smoothing process. Peaks in the curves occur at 106, 111, 117, and 128 km, with no data available from 119 to 123 km. The lack of data in this interval makes the values of electron density above 123 km questionable, but not the shape of the curves. The mean curve of Figure 9 compares favorably, with respect to the general shape and to the position of the peaks, with that obtained from the NRL Viking flight on 7 May 1954, as reported by Seddon, Pickar, and Jackson [9]. The two curves are shown in Figure 10.

The White Sands Ionospheric Station, about 30 miles away from the Aerobee launching tower, took a series of ionograms just prior to and immediately after the flight. The record taken at 1216 hours MST, rocket impact time, shown in Figure 11, is representative of conditions at White Sands during the rocket flight.

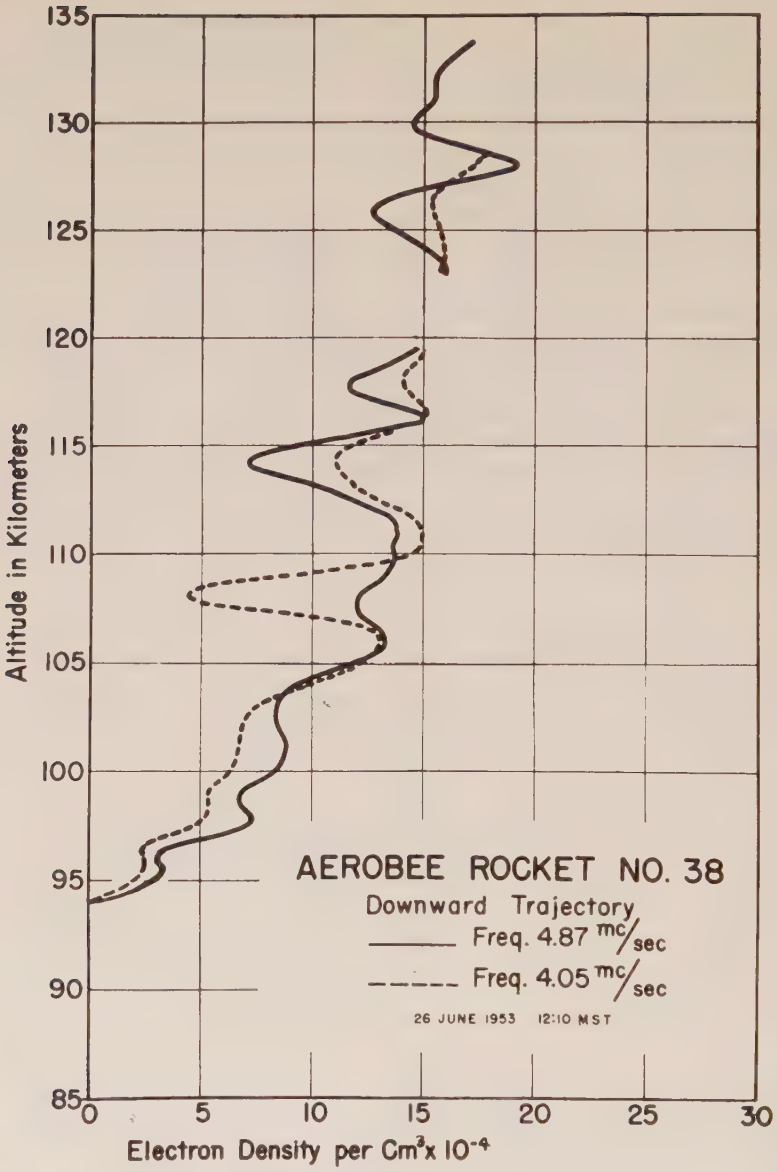

FIG. 9—Electron densities measured during rocket descent of Aerobee No. 38

For comparison purposes, this record and a P'-f record computed from the mean curve (somewhat modified below 105 km) of Figure 9 are shown in Figure 12. This P'-f record was computed using the curves supplied by and the method described by Jackson [10]. This record shows a series of critical frequencies at 3.2, 3.4, 3.5, 3.6, and 3.8 Mc, and of minimum virtual heights at 100, 124, 141, 171, and 153 km. In comparison, the P'-f record from White Sands shows the 3.5- and 3.8-Mc critical frequencies, with the trace from 3.2 to 3.5 Mc missing. The stratification at 128 km in Figure 9 has to be assumed with a steep rising slope so as to cause a

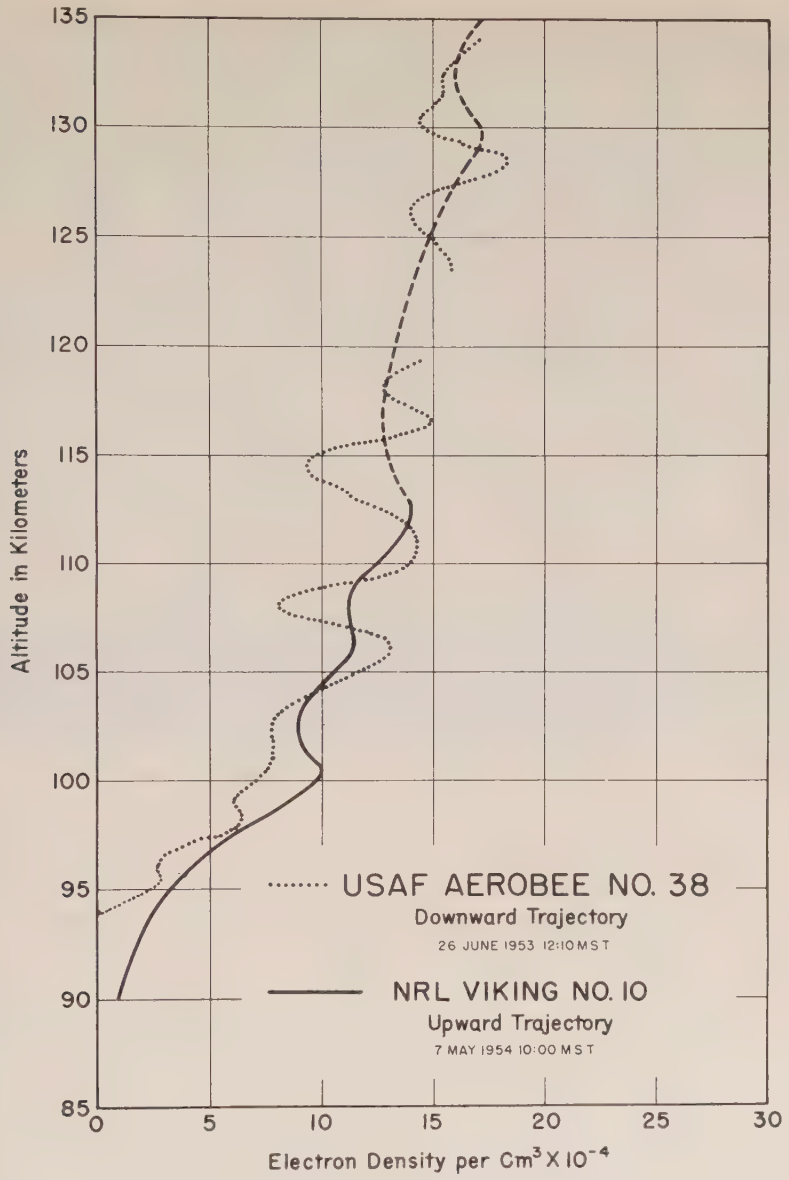

FIG. 10—Comparison of USAF Aerobee No. 38 and NRL Viking No. 10 results

partial reflection shown in the White Sands record around 130 km. This is a fine example of a case where one can have confidence in the analysis of the rocket experiment and where one can obtain much finer details of the structure than a *P'-f* record could provide.

On the other hand, the data from the rocket ascent of the same rocket flight demonstrate a major problem faced in the analysis. In Figure 7, it is shown how the 3-km running mean is used to eliminate the negative slopes, which are thought to be caused by the "blobby" structure of the ionosphere. Obviously, in this special

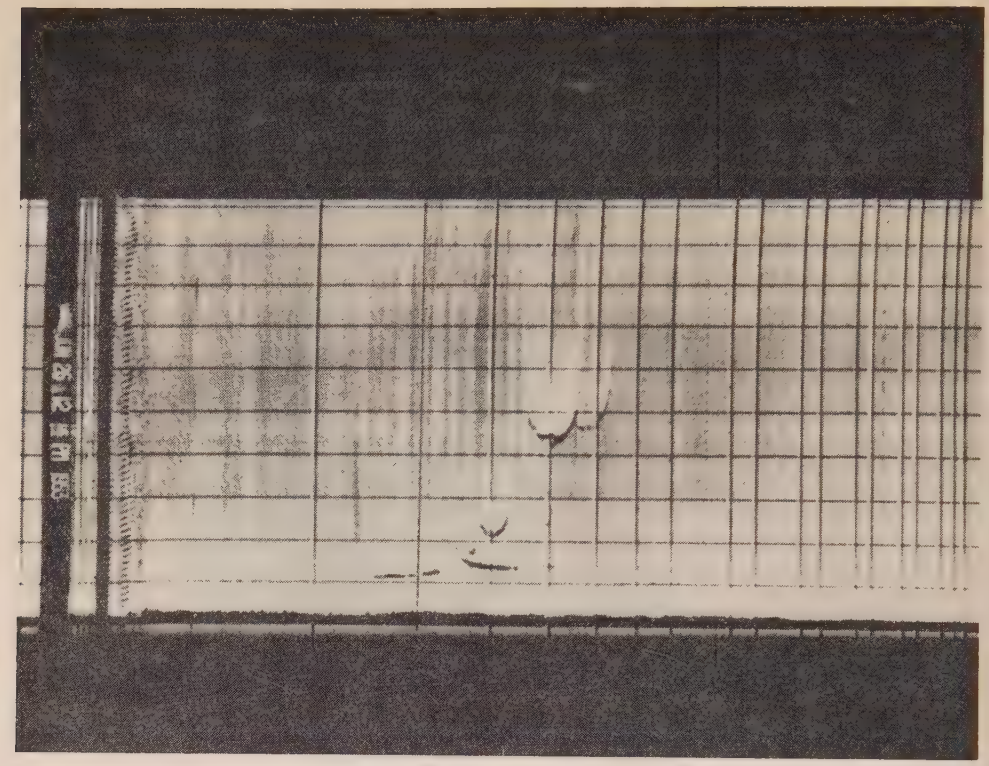

FIG. 11—P'-f record taken during Aerobee No. 38 flight, 1216 hours MST, 26 June 1953, White Sands Proving Ground, New Mexico

case, the desired effect has not been achieved, probably because a very intense irregularity was passed by the ray at about 100-km height of the rocket, causing increased delay, while later at 109-km height of the rocket the ray missed the irregularity and the delay went back to normal.

One way to handle such a case is to correct the delay curve by taking out the delay due to the blob on a more or less arbitrary basis. However, a more objective method was tried. The electronic computing machine was allowed to handle the slopes by allowing the results, that is, the electron densities, to become negative. The negative electron densities, of course, are fictitious. They are needed only to compensate the effect of the anomalous values in the layers below.

The results obtained this way are shown in Figure 13 for both frequencies. For comparison, the mean of the two frequency curves for the downward trajectory is plotted. This is considered to be the correct electron-density distribution for the smooth, stratified ionosphere. Note that the density is increased below 100 km and that it goes to negative values as expected around 105 km. It might be pointed out that the curve has been smoothed by taking weighted running means over 2.5 km of the group refractive index of the isotropic medium $1/\sqrt{1-x}$, the weight used again being 1, 0.8, and 0.4, and converting this curve to electron densities. The difference with respect to a smoothing by taking weighted running means of the electron density directly is a de-emphasizing of the large negative values of electron

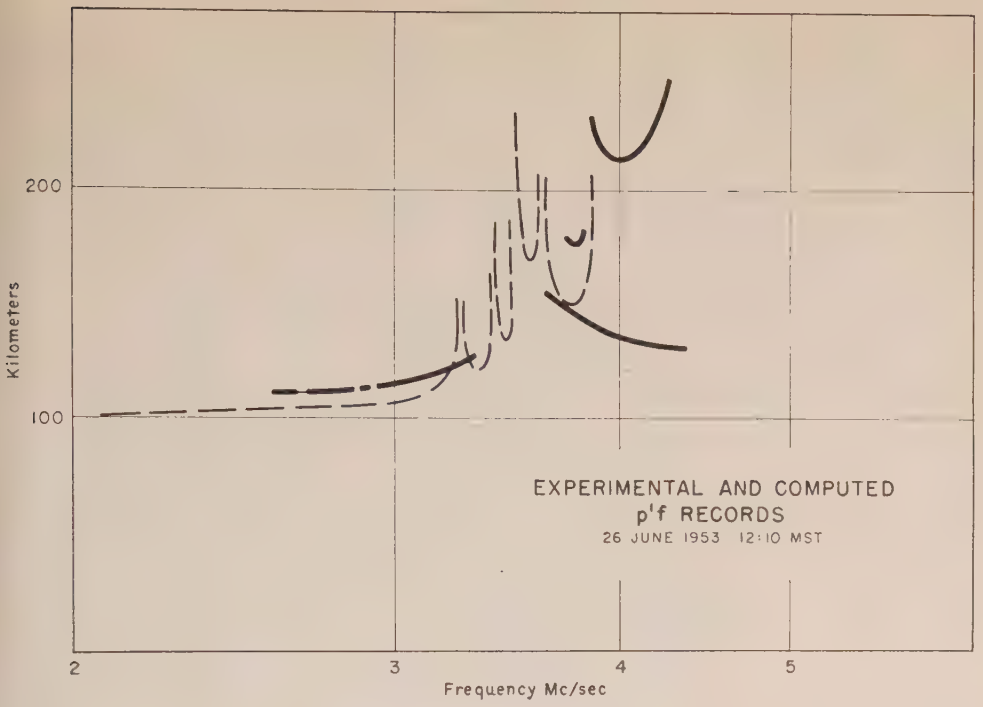

FIG. 12—Experimental and computed $p'f$ records

density, which appears reasonable, since these negative values have meaning only if applied to delay times.

The upper part of the two curves shows a good similarity with the mean curve of the downward trajectory insofar as the fluctuations are concerned. However, the average level of the electron density of these two curves is considerably lower around 110 km, just above the level of the compensating negative values, and reaches the proper level only when close to the top of the flight. Note that the error is largest for the low frequency.

DISCUSSION

From examination of the results of this rocket flight, it is evident how careful one has to be in the interpretation of measurements which are based on a transmission between rocket and ground. The resulting electron-density distribution can be just right to fit in a generally accepted picture of the ionosphere, as in the downward trajectory, or the computed distribution can be completely unrealistic, as in the upward trajectory, thus requiring a further explanation.

A single blob of high electron concentration was invoked as an explanation for this specific case. This might not be completely true, but it appears to be the simplest way for explaining the observations. The presence of irregularities of various sizes and intensities is normal in the ionospheric E region, although the occurrence of such intense ones probably is not often encountered.

The same upward trajectory of Aerobee rocket No. 38 has been analyzed

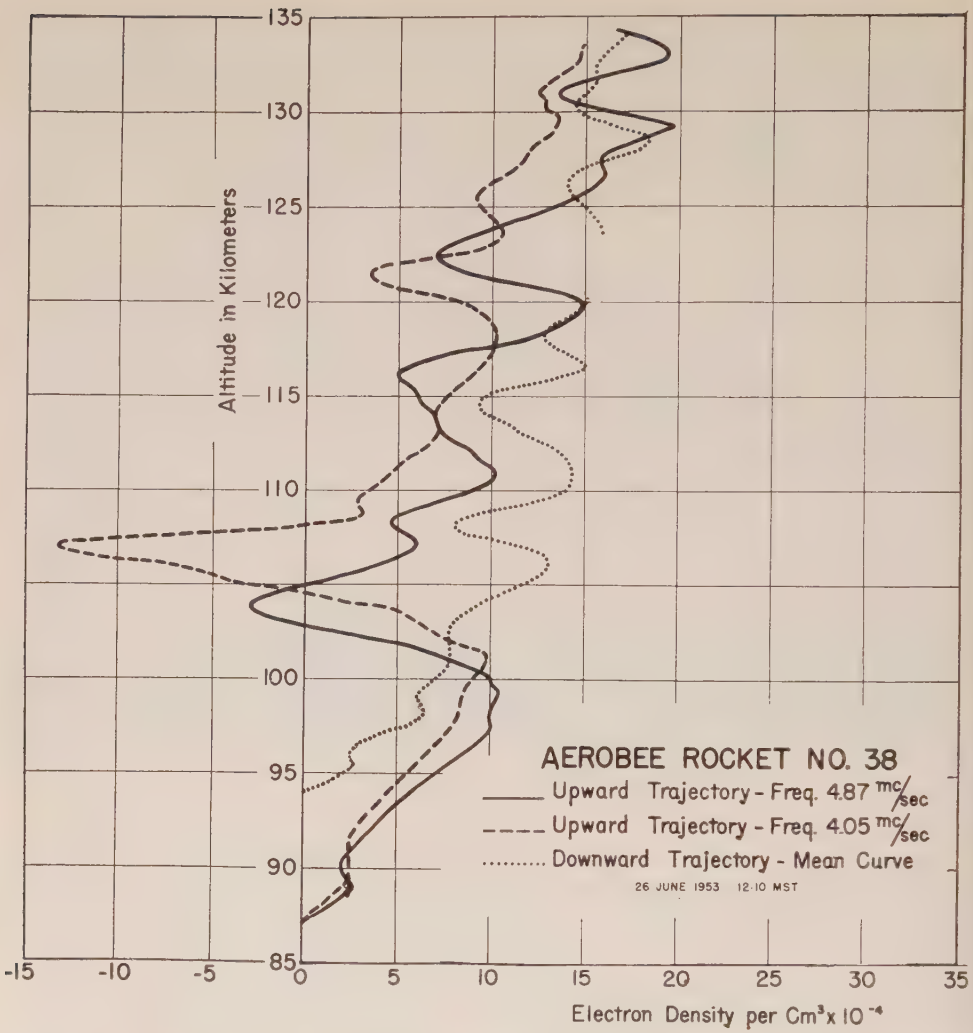

FIG. 13—Electron densities measured for Aerobee No. 38 for rocket ascent for two frequencies, 4.05 and 4.87 Mc, and for rocket descent the mean of the two frequencies

previously in a rough preliminary fashion, using only one of the four available delay records and a simplified method with respect to the effect of the earth's magnetic field [2]. These previous results are shown for comparison in Figure 14. The similarity with the new curves of Figure 13 is evident. A major difference is the absence of negative values for the electron density. This had been achieved by a judicious smoothing of the experimental delay data, which eliminates the negative slopes in the delay curve.

The early results from this rocket flight led to the conclusion of a bifurcation of the *E* layer, which seemed to be supported by the results of three other rocket flights, in spite of the technically somewhat lower quality of those data. It can be safely said that this conclusion was premature and that the explanation for this

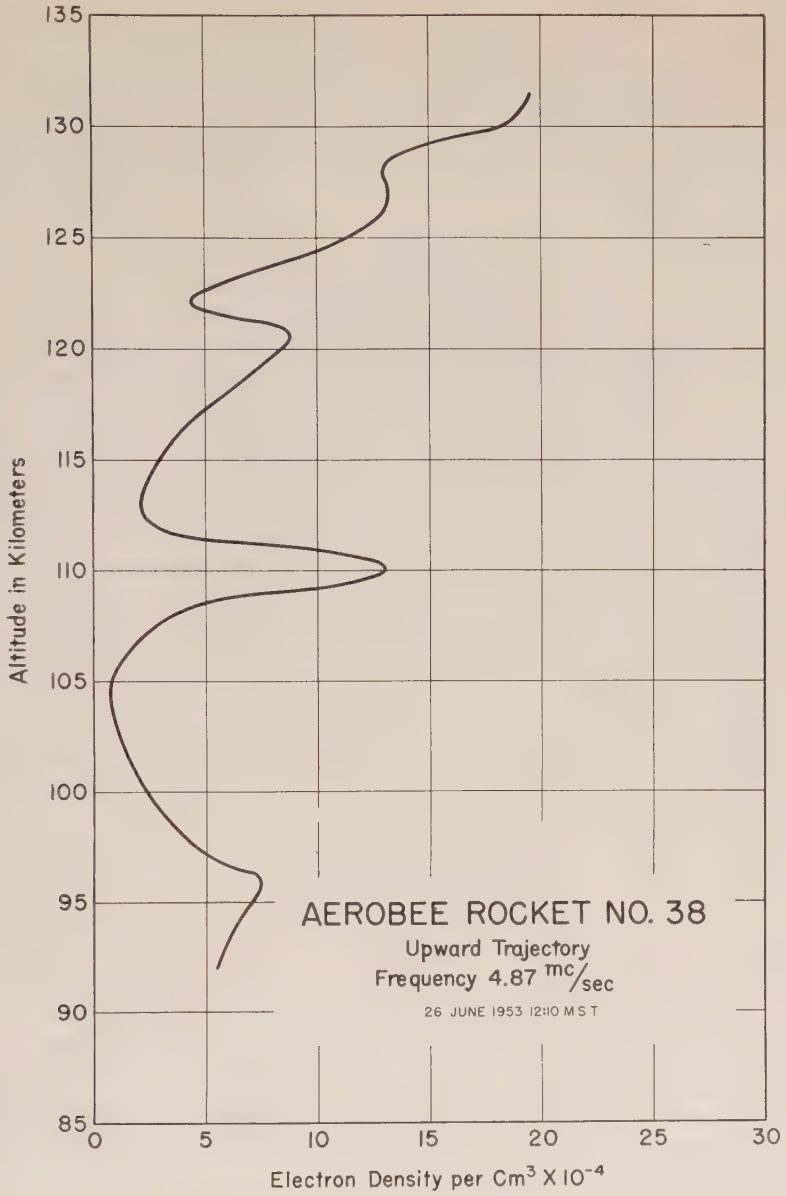

FIG. 14—Electron densities for Aerobee No. 38 rocket ascent as previously analyzed

peculiar apparent electron distribution must be sought in the effects of irregularities in the horizontal stratification. In a paper in preparation, it will be shown that the analysis of Aerobee rocket No. 39 of 1 July 1953 leads to an apparent bifurcation only if data from rocket descent and from the 6-Mc downward transmission are neglected.

It is clear that the irregular structure of the ionosphere causes fluctuations in the delay data. They complicate the analysis, which is primarily aimed to find

the mean electron density as a function of height. The mean should be taken over a horizontal area, large compared with the structure size of the irregularities. Obviously, the experiment is not designed to furnish an accurate mean value. This would require a large number of ray paths, spread evenly over a sufficiently large horizontal area. In the present case, only four sets of ray paths, which belong to the ascent and descent for two frequencies, each of the upward transmission, have been analyzed. In the case of a more successful experiment, the ray paths of the downward transmission for several receiving sites, for ascent as well as descent, could be added. This would give 12 or more sets of ray paths, and would enable the computation of reasonably good mean values from the 12 or more electron-distribution curves, provided the relationship between electron density and delay time can be considered as linear. As a further step, the deviations of the computed electron-density curves from the true mean curve could be studied and some interesting information about the size and intensity of the irregularities could be gained.

In view of the limited sets of delay curves available, the results of Figure 13 can be interpreted only tentatively. A reasonable assumption might be that the mean curve of the downward trajectory is the true mean electron-density distribution. A blob of high electron density may be assumed between the height level of 92 and 101 km, with a maximum density at 98 km. The blob affects the delay values as soon as the rocket reaches the 92-km level, until at a rocket position of 109 km the ray paths from the transmitting site miss the blob. The geometry of this situation enables the computation of a minimum horizontal extension of the blob of 3.5 km. The maximum intensity of the blob is about 6×10^4 electrons/cm^3, or about six times as high as the normal electron density at the 94-km level.

Figure 13 shows clearly that the effect of the blob below 100 km is considerably overcompensated by small electron densities above 100 km. The adoption of a smoothing process, as outlined before, for the computation of mean electron densities at each level would require that in the case of a single blob the results be correct whenever the ray misses the blob. This obviously is not the case in Figure 13, and the error becomes larger as the frequency approaches the critical frequency of reflection. It appears that the error is closely connected with the curvature of the rays, and that the error would be negligible if the refraction is small compared with the retardation. Therefore, it is desirable to increase the operating frequency. Unfortunately, this results also in small delays and, consequently, in a reduction of accuracy in the computed electron-density values due to the uncertainty in the delay readings. Nevertheless, it appears that a reasonable compromise in the choice of operating frequency is possible.

ACKNOWLEDGMENTS

Research, utilizing rockets such as reported in this paper, is an extensive and complicated operation, requiring the coordination and cooperation of many agencies. The late Dr. L. B. Linford and personnel from the University of Utah, under an Air Force contract, were responsible for the design, construction, and operation of the experimental instrumentation, and the receiving and recording of the delay data. The Rocket Sonde group at Holloman Air Development Center, with assistance from Oklahoma A. and M. contract personnel, recorded and pro-

vided the telemetering and trajectory data. Mr. J. Lien, Air Force Field Director for this rocket, and Mr. J. Downing, both of AFCRC, were responsible for the beacon performance. *P'-f* records were provided by Master Sgt. C. McDonald, of the Signal Corps WSPG Ionosphere Station. Messrs. T. J. Keneshea and J. A. Sandock of AFCRC programmed the method of analysis. The cooperation of all is greatly appreciated.

References

[1] E. Beth, Air Force Cambridge Res. Center, Geophys. Res. Papers No. 11, p. 255 (April 1952).
[2] J. R. Lien, L. B. Linford, *et al.*, Rocket Exploration of the Upper Atmosphere, edited by R. L. F. Boyd and M. Seaton, Interscience Publishers, Inc., New York (1954).
[3] J. C. Seddon and J. E. Jackson, Phys. Rev., **97**, 1183 (1955).
[4] W. Pfister, J. C. Ulwick, and R. J. Marcou, Phys. Rev., **97**, 1183 (1955).
[5] O. C. Haycock, Sci. Rep. No. 1, Upper Air Research Lab., University of Utah, Salt Lake City, ASTIA Document No. 117219 (1957).
[6] Upper Air Report No. 1, Air Material Command, Cambridge Field Station (Sept. 1947).
[7] W. Pfister, Scientific Uses of Earth Satellites, University of Michigan Press, Ann Arbor (1956).
[8] R. J. Marcou, W. Pfister, and J. C. Ulwick, J. Geophys. Res., **63**, 301 (1958).
[9] J. C. Seddon, A. D. Pickar, and J. E. Jackson, J. Geophys. Res., **59**, 513 (1954).
[10] J. E. Jackson, J. Geophys. Res., **61**, 107 (1956).

Journal of Geophysical Research Volume 63, No. 2 June, 1958

THE USE OF SWEEP-FREQUENCY BACKSCATTER DATA FOR DETERMINING OBLIQUE-INCIDENCE IONOSPHERIC CHARACTERISTICS

By R. Silberstein

National Bureau of Standards, Boulder, Colorado

(Received January 16, 1958)

ABSTRACT

The paper presents the results of comparisons of backscatter echoes, oblique-incidence pulse reception, and midpoint vertical-incidence echoes for a 2370-km path, following an earlier study for a 1150-km path. An attempt is made to find distinctive characteristics of those backscatter records that afford accurate values of MUF for the 2370-km path. Some sporadic intermediate-distance echoes are discussed, and some difficult night records are given. It is shown that present power and antennas are inadequate for obtaining $F2$-propagated echoes continuously, except on winter days.

It is concluded that the sweep-frequency backscatter technique is useful for obtaining maximum-usable-frequency data for instantaneous or prediction use over inaccessible areas, but that proper antennas and skilled personnel are very important.

1. *Introduction*

Results of sweep-frequency backscatter experiments on high frequencies performed at Sterling, Virginia, were described by the author [see 1 of "References" at end of paper]. Since that time, further experiments have been performed, both at Sterling, Virginia, and Boulder, Colorado.

Most of the later experiments had the advantages of receiving simultaneous sweep-frequency pulsed emissions over the Sterling-Boulder path, and a midpoint vertical-incidence sounding station, so that MUF determined from the backscatter could, for one distance, be checked by two independent means. The path used was the 2370-km path from Sterling, Virginia, to Boulder, Colorado, with a midpoint close to Carthage, Illinois. The modified C3 ionosphere recorders used at oblique incidence delivered about 2.5-kw peak pulse power to wave antennas in the middle of the frequency range. The pulse length for backscatter was 100 microseconds and the repetition rate 25 per second.

It is the purpose of this paper to describe some of the later results after a discussion of the factors involved in obtaining them. The paper also indicates how sweep-frequency backscatter echoes may be used to obtain routine maximum-usable-frequency data for inaccessible areas, thus affording not only information for instantaneous use, but also information for providing additional points needed for improved prediction of world MUF charts and maps.

2. *Amenability of Records to Correct Interpretation*

It is well known that much of the time it is possible, over certain ranges, to determine accurately the *F*2-layer skip distance by measuring the delay time of echoes assumed to be scattered back from the ground. References [1] to [6] and the references in each of those papers cover the field fairly well. Sometimes anomalous results are obtained (that is, scatter from the *E* region or elsewhere rather than from the ground at the *F*2-layer skip distance), as shown in reference [1]. Extended observations after the period of the above reference indicated that these anomalies did not occur as often as might be inferred by looking at the data for the limited number of observing days analyzed for the report. The proportion of the time the anomalous results prevail has still not been determined, and it is still not always possible to tell, without supporting data from the middle of any path studied, just when the records are anomalous. However, anomalous records are usually multi-branched, although all multi-branched records are not anomalous.

Figure 1 shows some typical backscatter sweeps observed at Boulder, Colorado, on antennas beamed on Sterling, Virginia. The abscissa scale is in megacycles, running from 3 to 25, and the ordinate scale is in hundreds of kilometers; the first marker, just barely visible above the solid line of the elongated transmitter pulse at the bottom, is the one-hundred kilometer marker. The 2370-km *F*2-layer MUF is scaled as the frequency, which gives a 2500-km slant range to the leading edge of the backscatter echo, corresponding to an assumed 300-km layer height. In each of the sweeps, the solid trace near the middle of the ordinate scale, terminating in a fairly constant range, is the Sterling pulse transmitter signal at an arbitrary video phase inadvertently recorded on the backscatter equipment. The normal record of those pulses was made on another recorder, using a more expanded time scale. The typical h'-f traces with multiples at the lower left-hand corner of each record are local h'-f records.

Figure 1(*a*) for February 7, 1955, at 1355 CST, is one of the more readily scalable sweeps. The *F*2-propagated backscatter echo starts at the second-order vertical-incidence echo at about 800 km and 8 Mc, and proceeds to increasing ranges and frequencies. The *F*2-layer 2370-km MUF by backscatter is 22.2 Mc. Figure 1(*b*), for the same day at 1319, is a split sweep, which gave correct results when scaled to the strongest echo—the portion of the split with the longer delay time [4]. The *F*2-layer 2370-km MUF by backscatter here is 20.1 Mc. Figure 1(*c*), for December 20, 1954, at 1113 CST, is a multi-branched sweep, from which it would not ordinarily be possible to obtain a maximum usable frequency.

In the earlier experiments at 1150 km [1], there was a period of a few days in which anomalous echoes were recorded, leading to an erroneous MUF determination, which could apparently be corrected by assuming that on those days the *F*2-propagated backscatter came from the distant *E* layer rather than from the distant ground. In the present set of experiments at 2370 km, anomalous records amenable to such a simple correction have not been seen. There exists in addition to the regular, smooth, single backscatter traces a variety of multi-branched types of echoes. For these longer distances, the experiment is apparently very sensitive to ionospheric irregularities in which focusing areas may direct the transmitted energy to one or more places off the main beam at any given time,

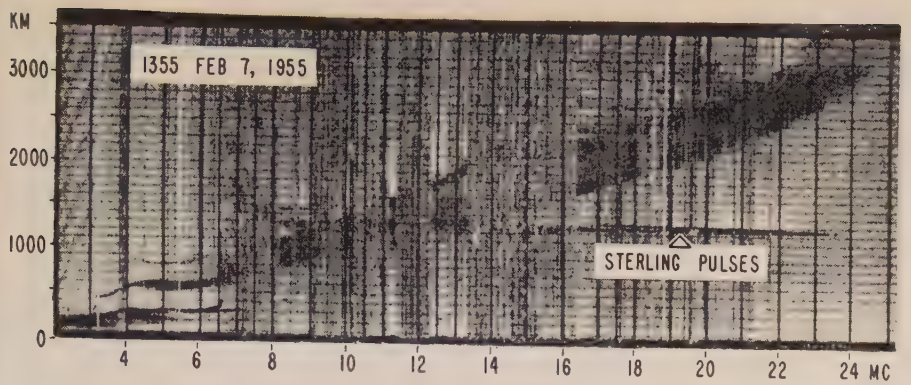

a. SCATTER ECHO WITH SHARP REGULAR LEADING EDGE, EASILY SCALED FOR MUF

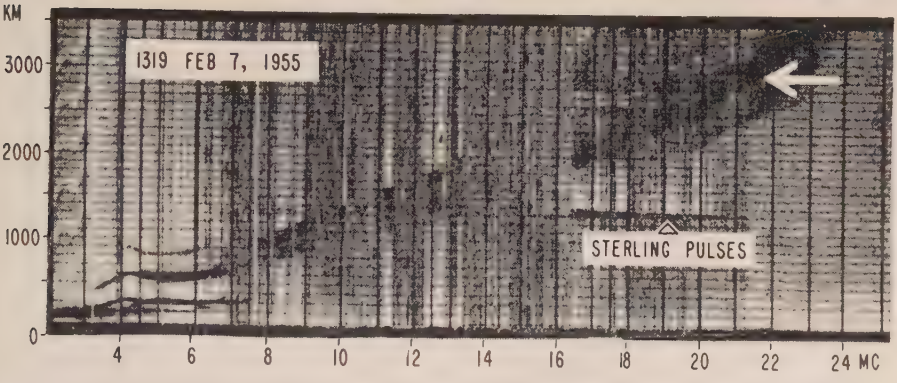

b. SCATTER ECHO DOUBLE; STRONGEST ECHO, MARKED BY ARROW, GIVES CORRECT MUF

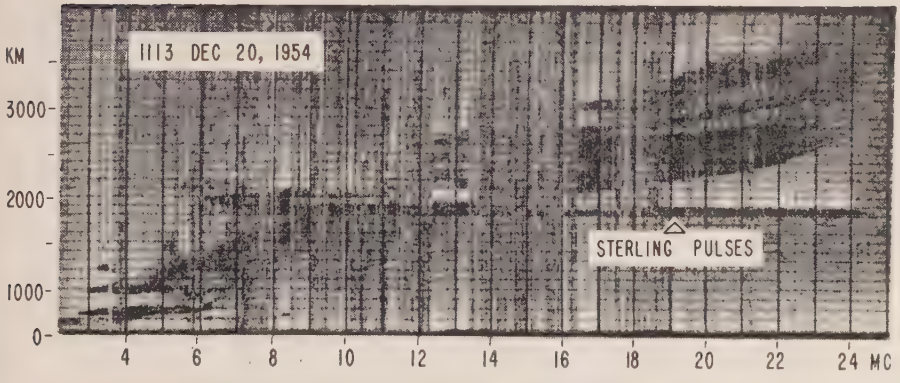

c. SCATTER ECHO WITH MANY BRANCHES, NOT USABLE FOR DETERMINING MUF

FIG. 1—A variety of winter daytime backscatter records made at Boulder, Colorado

emphasizing echoes at relatively fixed ranges. Or, perhaps at times, ionospheric focusing may favor auxiliary lobes in the antenna rather than the main lobe.

3. *The Antenna System*

The antenna system is much more important in backscatter (and especially sweep-frequency backscatter) experiments than in point-to-point experiments. In the latter case, the bulk of the energy received from the distance transmitter is transmitted over the great-circle path, even if there are side lobes or if the beam is not properly directed. In the former case, the energy is transmitted from the receiving location in any direction the transmitting antenna will send it and, with favorable propagation conditions, the backscatter is available to be received from any direction in which the receiving antenna has appreciable directivity. In fact, in reception, the energy coming in at a given delay time is the result of integrating the energy picked up by the receiving antenna at that delay time at all azimuths. Clearly, the best transmitting antenna design would be one affording a high-gain azimuthally-sharp main lobe with a minimum of side lobes over a wide frequency range. In the receiving antenna, requirements are similar, except that fairly high over-all losses can be tolerated, since the losses also affect external noise and interference. It is a good idea to use dissimilar antennas for transmitting and receiving, since the side lobes for the two will tend to occupy different angular positions at any frequency, while the main lobes, being the same, will have an additive effect. In the experiments at Boulder, the transmitting antenna was a horizontal vee, and the receiving antenna a standard Signal Corps Type A rhombic.

4. *Seasonal and Diurnal Limitations*

The best records are obtained on winter days, since ionospheric absorption is low and the usable frequencies are high, making it possible to obtain records with moderate power (2.5-kw peak output with 100-μsec pulses) and with standard rhombic antennas designed for optimum performance near 20 Mc. Also the fact that the $F1$ layer is absent or not very prominent simplifies the records.

In other seasons of the year, conditions are less favorable for continuous daytime reception of $F2$-propagated backscatter, for the following reasons:

a. During the middle of the day, ionospheric absorption is greater because the elevation of the sun is greater and the MUF is lower for a given skip distance.

b. The main lobes of antennas of convenient size are often too high at these lower frequencies.

c. In addition, E- and $F1$-layer maximum usable frequencies are higher, yielding records which are more difficult to interpret.

Thus, records for most of the day in spring, summer, and early fall, with small antennas, medium power, and pulses of the order of 100 μsec, may not show usable $F2$-propagated backscatter.

Figure 2(*a*) is an early spring record made at Sterling, Virginia, in a westward direction, on March 25, 1954, at 0938. The emissions from Boulder appear at an arbitrary relative delay of about 1400 km. The streaks going downward to the right are pulse interference. In the lower left-hand corner appear the first- and second-order vertical-incidence traces. The $F2$-propagated backscatter trace

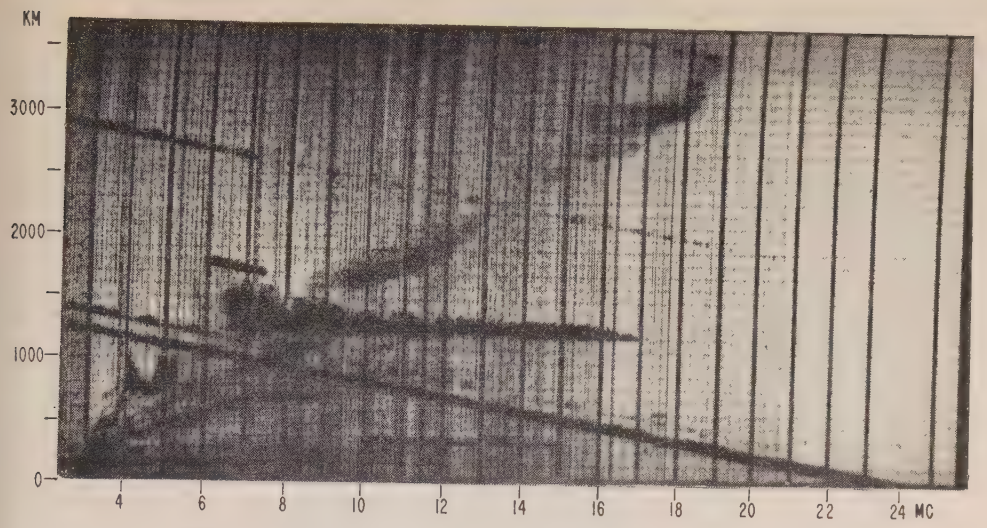

a. GROUND SCATTER PROPAGATED BY THE VARIOUS LAYERS IN SWEEP OBSERVED AT STERLING, VA., MARCH 25, 1954, AT 0938 CST

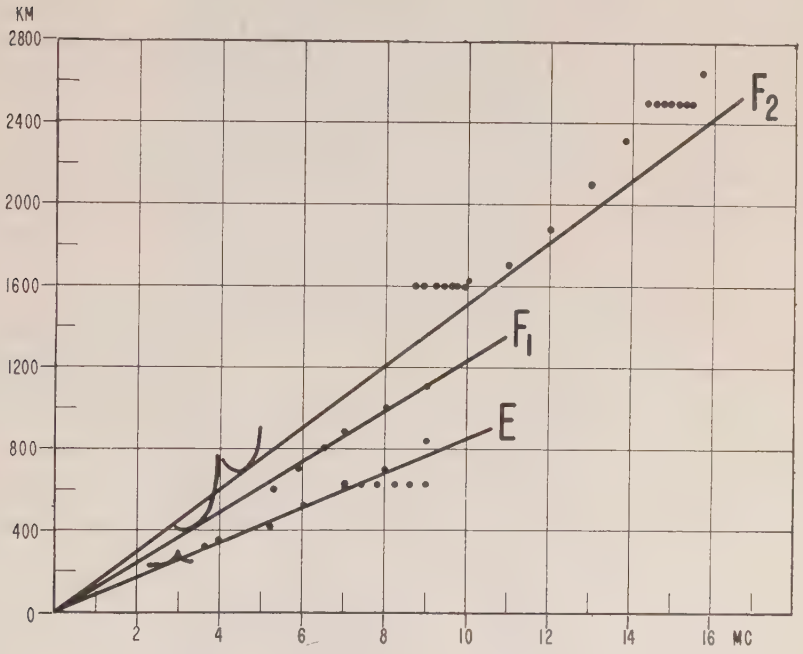

b. ANALYSIS OF ABOVE SHOWS ECHOES VIA E, F, AND F_2 LAYERS FALLING ALONG APPROPRIATE LINES THROUGH ORIGIN TANGENT TO SECOND-ORDER VERTICAL INCIDENCE ECHO FOR EACH LAYER

FIG. 2—Ground scatter propagated by E, $F1$, and $F2$ layers

moves upward to the right in its usual position, increasing in range as frequency increases. In addition, two closer traces with an upward slope represent $F1$- and E-layer propagated backscatter, being identified by the standard technique of Figure 4, reference [1], as illustrated in Figure 2(*b*).

5. *Night Records*

Night records may be difficult to obtain with small antennas in any season. In addition to having poor response at the desired vertical angles, the antenna may lose most of its directional characteristics at the lower frequencies.

Spread echoes, when present on winter nights, contribute additional complexities. Figure 3 illustrates some spread-echo records made at Boulder on the night of March 29–30, 1955. In these records can be seen scattered reflections corresponding to:

a. The first-order spread echo growing out of the first-order vertical-incidence $F2$ trace, the slope satisfying the requirement for "slant F" corresponding to "slant E," as described in Appendix II of reference [8]

b. The $F2$-propagated ground scatter growing out of the second-order vertical-incidence $F2$ trace

c. The second-order spread echo contaminating the $F2$-propagated ground scatter

d. Weak echoes apparently from the reverse direction

6. *Sporadic Backscatter Echoes*

One phenomenon noted in the original experiments was examined in some detail. Figures 10 and 11 of reference [1] illustrate an intermediate-distance echo which was attributed to ground scatter propagated by sporadic-E ionization. Figure 4 shows some similar sweeps.

Figure 4(a), for December 11, 1954, at 0939 CST, demonstrates the intermediate-distance echo, in considerable strength, stretching across the record below the Sterling sweep. During the winter of 1954-55, this type of echo was chiefly a morning phenomenon, and, although associated with sporadic-E ionization, appears to be assisted by the existence of auxiliary factors which may further enhance the ionization. Their appearance in the morning suggests the assistance of meteoric ionization. The period of the Geminid meteor shower, December 10-13, 1954, was characterized by heavy sporadic intermediate-distance echoes in the morning. The heaviest of these echoes observed during the winter, however, came on February 1, which was not a meteor-shower day, but one which was characterized by an intense solar-noise storm.

Figure 4(b) shows the echo on February 1, 1955, at 0637 CST. The leading edge of the main echo approaches 900 km in range at 18 to 20 Mc. There is also a shorter distance echo which, while not exactly at half the slant range, could be a direct echo from a higher level in the same sporadic-E region producing the more distant echo. The longer range echo, coming at approximately the same range whenever seen, would appear to be ground scatter, propagated *via* the portion of the E layer illuminated by the main lobe of the transmitting antenna. The possibility that the shorter range echoes are ground scatter, propagated in a similar manner by means of a higher lobe, should not be ruled out.

Figure 4(c), for December 14, 1954, at 0942 CST, shows the morning echo just disappearing below the Sterling sweep.

Figure 5 shows values of sporadic-E maximum frequency at Boulder plotted against time of morning periods for which data were available during December 10-19, 1954. For those days on which the sporadic morning echo was seen, the

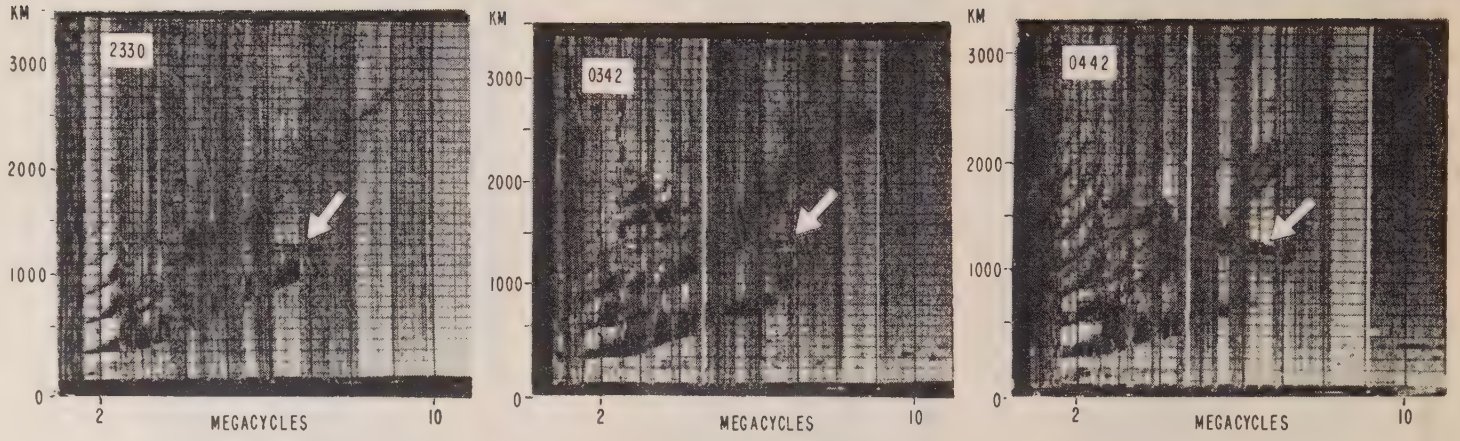

FIG. 3—Spread echoes at Boulder, Colorado, March 29-30, 1955 (arrow marks Sterling sweep)

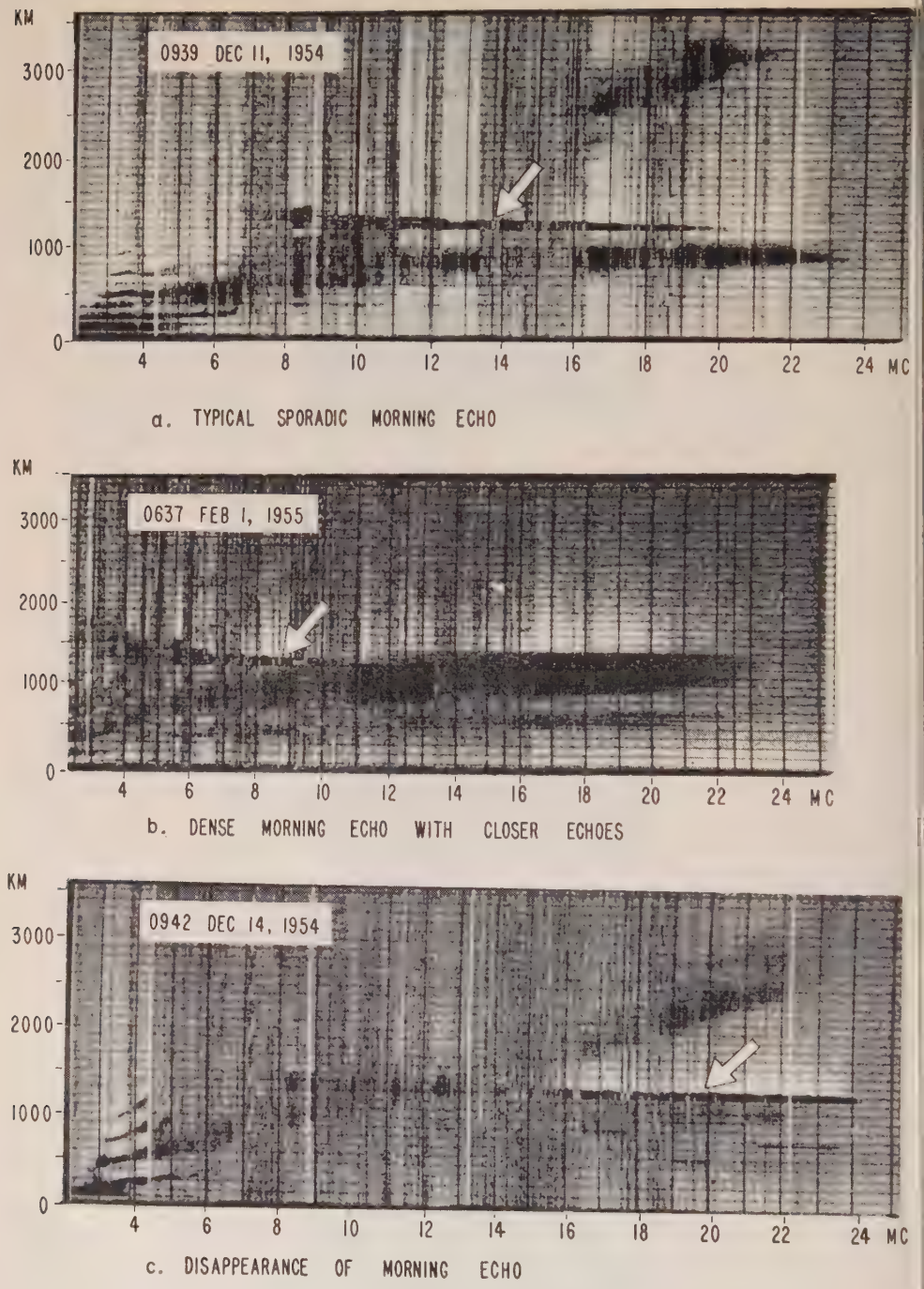

FIG. 4—Some sporadic morning echoes observed at Boulder, Colorado (arrow shows Sterling sweep)

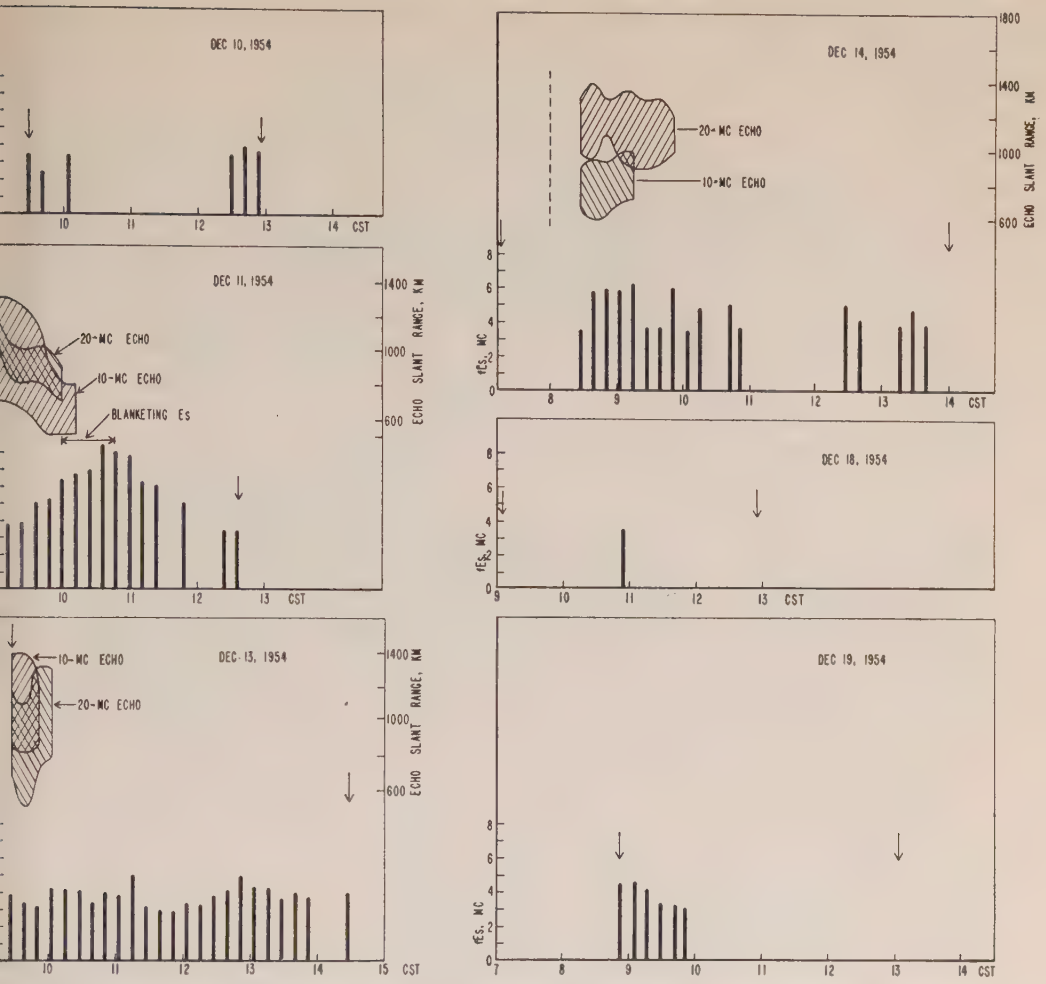

FIG. 5—Comparison of sporadic morning echoes with maximum vertical incidence sporadic-*E* frequency, Boulder, Colorado
(*Note:* Vertical arrows mark start and finish of observations)

range and breadth of the echo appearing on 10 and 20 Mc are plotted. The relation of the echoes to occurrence of intense sporadic-*E* ionization seems evident.

Figure 6 shows three representative days in February, the 1st having the most dense morning sporadic echoes seen during the winter, the 8th when the echoes were too weak to scale, and the 18th when the echoes were not seen. The presence of fairly dense sporadic-*E* on the 18th indicates that perhaps additional sources of ionization are needed to produce the morning echoes or that ionospheric absorption was high on this particular day.

In the test from 1109 CST, April 26, to 1109 CST, April 27 (not shown in a Figure), sporadic intermediate-distance echoes appeared and vanished from time to time throughout the 24 hours, but seemed to be most dense in the morning. During the night, there also appeared two-hop sporadic-*E* propagated pulses from Sterling

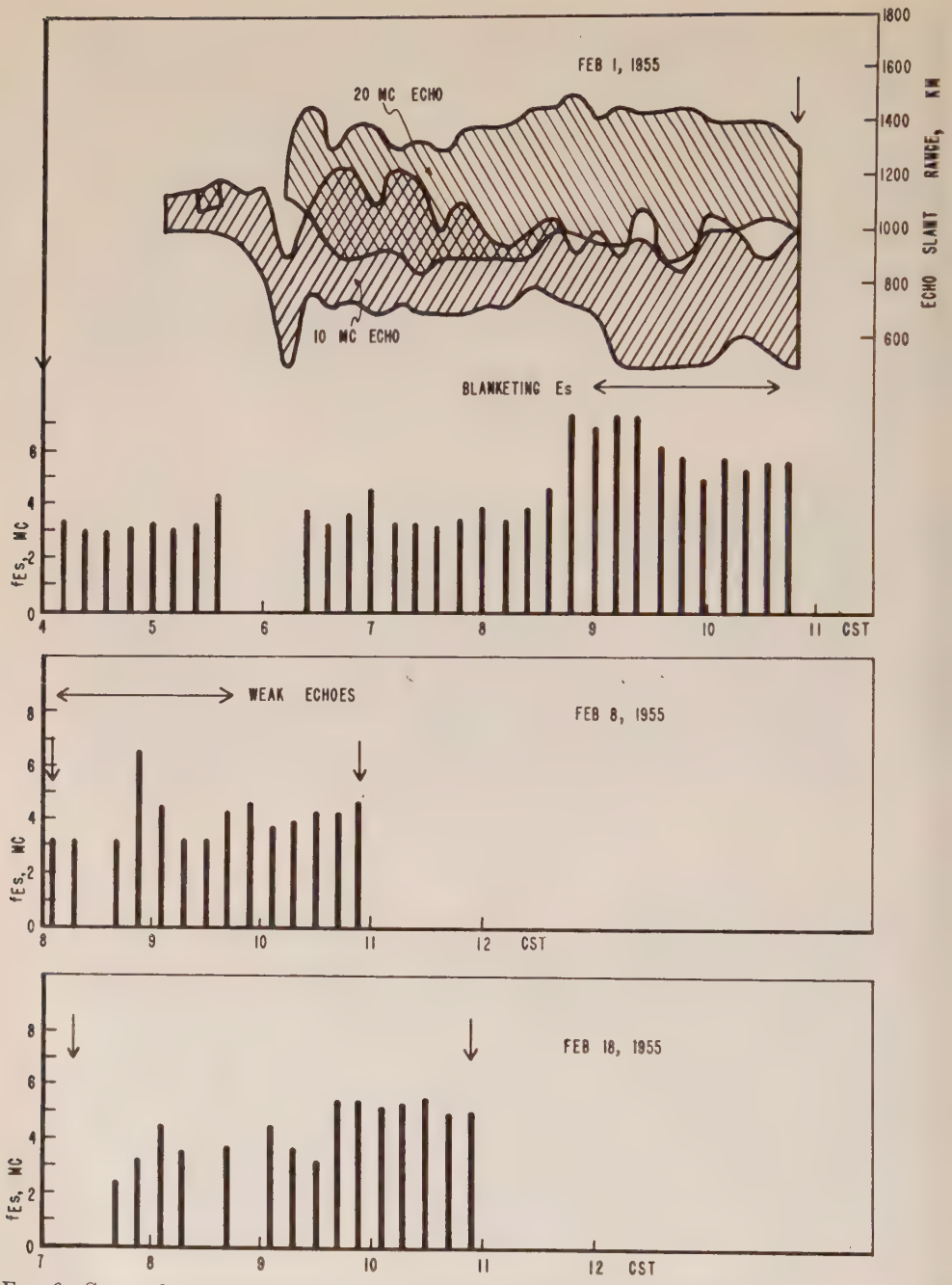

FIG. 6—Some plots of morning sporadic echoes and maximum vertical incidence sporadic-*E* frequency, Boulder, Colorado
(*Note:* Vertical arrows mark start and finish of observations)

at frequencies as high as 23 Mc. The period came after a weak radio-propagation disturbance and just before a stronger one. At 1105 CST on April 26, there was a 455-Mc solar-noise burst, accompanied by a sudden ionospheric disturbance

(SID). The North Atlantic circuits were disturbed from 1800 to 2400 CST. On April 27 at 1023, there was a geomagnetic "sudden-commencement" storm, and the worst of the disturbed period was from 1200 to 2100 CST, just after the end of the test.

7. *Determining and Predicting MUF at a Distance*

It is possible to use sweep-frequency backscatter to obtain directly, and with reasonable accuracy, hourly values of maximum usable frequency for a specified distance. The data obtained are radar-type slant ranges of echoes from the skip distance, which do not give virtual-height information, so that the slant range for a desired ground distance must be obtained by assuming virtual heights of the ionosphere. The error in assuming the wrong height becomes negligible as the distance increases. Sweep-frequency techniques are to be favored over fixed-frequency techniques, because a fixed skip distance must be chosen when a fixed control point is studied. With sweep frequency, this distance may appear on every sweep, whereas with fixed frequency it may appear only twice a day. Also anomalies may be identified more easily [1]. A fixed-frequency record with changing skip distances represents data for a shifting control point.

Skip distances from about 800 to 2500 km seem to be the most amenable to this type of experiment, the data being obtainable for geographical control points on a radius of one-half the specified distance. Distances beyond about 2500 km might be attenuated, because the wave angles are too low for feasible antennas and powers. Also, at very long distances, energy received at small angular de-

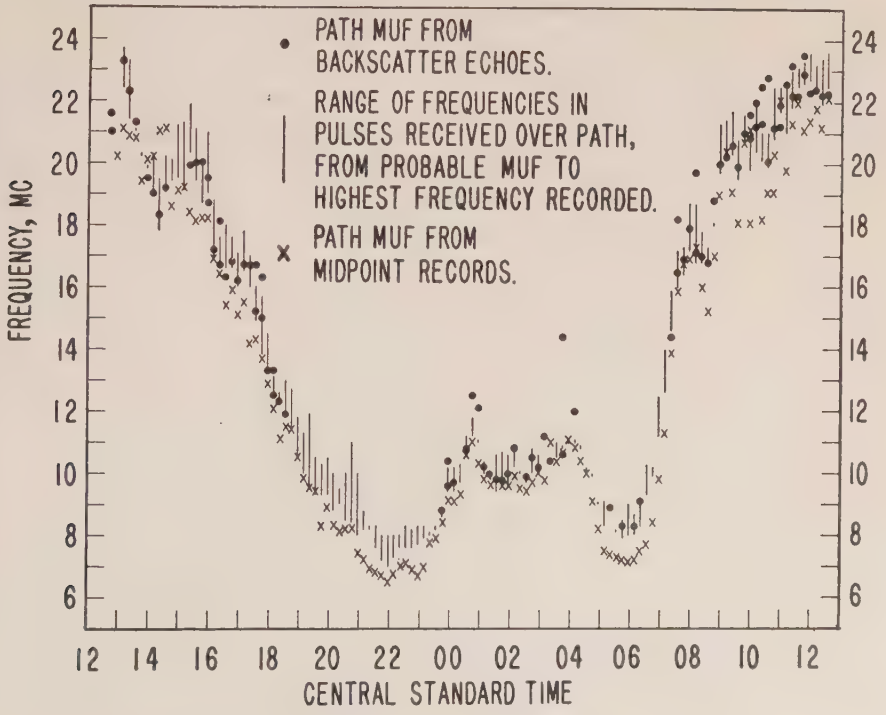

FIG. 7—*F*2-layer MUF for Sterling-Boulder path, November 29-30, 1954

parture from the great-circle path may arrive *via* control points far from the desired. At distances less than about 800 km, computations are made more complicated because of the "time-delay-focus" phenomenon [3]. Again, at very short distances, antenna azimuthal discrimination is poor.

Figure 7, for November 29-30, 1954, shows the *F*2-layer maximum usable frequencies for the Sterling-Boulder path, 2370 km, as determined by pulse propagation over the path, by vertical-incidence midpoint data, and by backscatter measurements. It is to be noted that in this test, night observations of backscatter were obtained during several hours after midnight, on frequencies as low as 5 Mc, although night observations are generally difficult to obtain. The range of values of MUF obtained for any oblique-incidence scaling is shown by a vertical straight line. It starts at the best estimated value of the "classical MUF" where the low and high rays appear to merge, and runs to the highest recorded frequency. The oblique-incidence data were scaled from relatively-high-resolution expanded-sweep records.

Figure 8, for the same day, demonstrates that it is possible to determine maximum usable frequencies for other distances, like 1500 and 3000 km, from these same backscatter records, assuming a fixed ionosphere height.

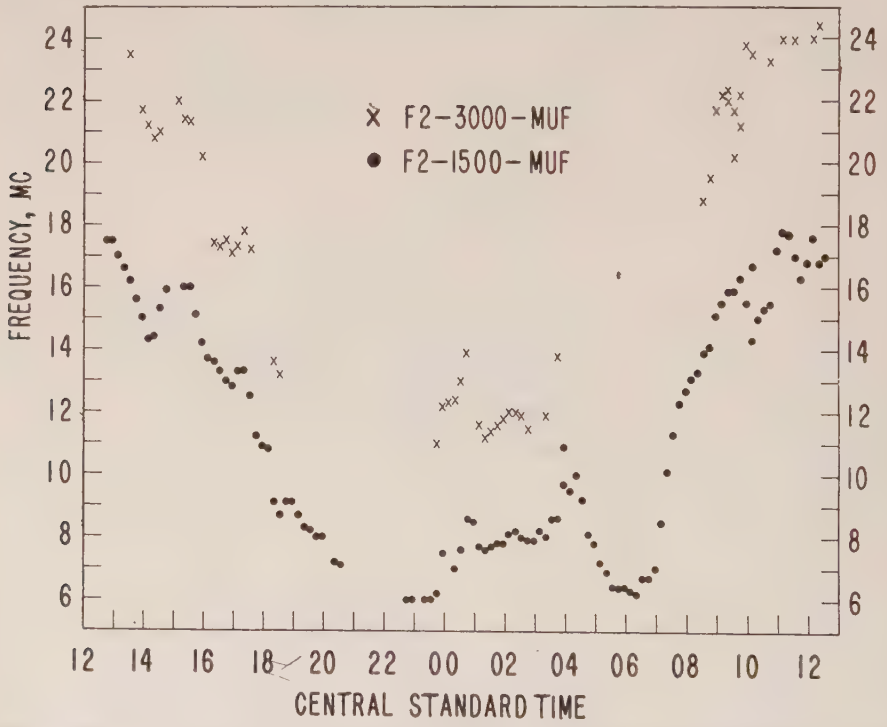

FIG. 8—*F*2 MUF derived from backscatter to east of Boulder, November 29-30, 1954

Figure 9 is a percent-difference distribution diagram, relating the MUF obtained by vertical-incidence scalings and the MUF obtained by backscatter measurements to the MUF scaled from oblique-incidence records made simultaneously on pulsed emissions from Sterling. If the latter were considered to be the true MUF, then

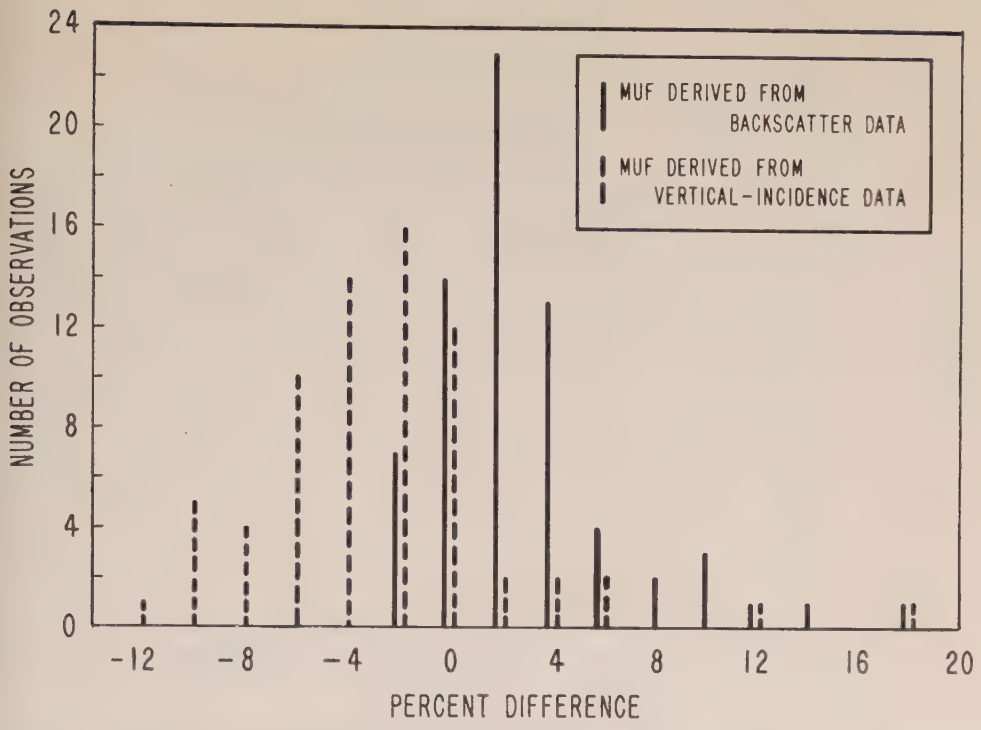

FIG. 9—Percent differences between derived MUF and oblique-incidence MUF, Sterling-Boulder path, November 29-30, 1954

the distribution diagram would describe the errors of the vertical-incidence and the backscatter methods. It is evident that on this day the backscatter gave even better results than the vertical-incidence data. The median percent difference for the vertical-incidence data is −3.0, and for the backscatter data is +1.8. In the former case, 90 percent of the percent differences lie between −9.5 and +6.3, and in the latter case between −1.8 and +9.6.

The sequence of data just discussed was about average relative to ease of interpretation. In the data for December 20-21, 1954, about 12 percent of the daytime records were not capable of being scaled and the backscatter echoes were too weak for night results. Figure 10 shows a plot of the daytime data, and Figure 11 the frequency distributions. Results are comparable to those of the superior November 29-30 period. In the December 20-21 data, the median percent difference for the vertical-incidence data is −1.8, and for the backscatter data is +1.4. In the former case, 90 percent of the percent differences lie between −9.7 and +5.0, and in the latter case between −3.8 and +7.0.

In the period January to April, 1954, many routine sweep-frequency backscatter records were made at Sterling, Virginia, using a modified C3 recorder. Vertical-incidence records were made at Carthage at the same time. Daytime results (1100-1630 CST) were analyzed in a manner similar to the way in which the November 29-30 and December 20-21 data were analyzed. Figure 12 shows the plots for each month and all months. Table 1A presents an analysis of the

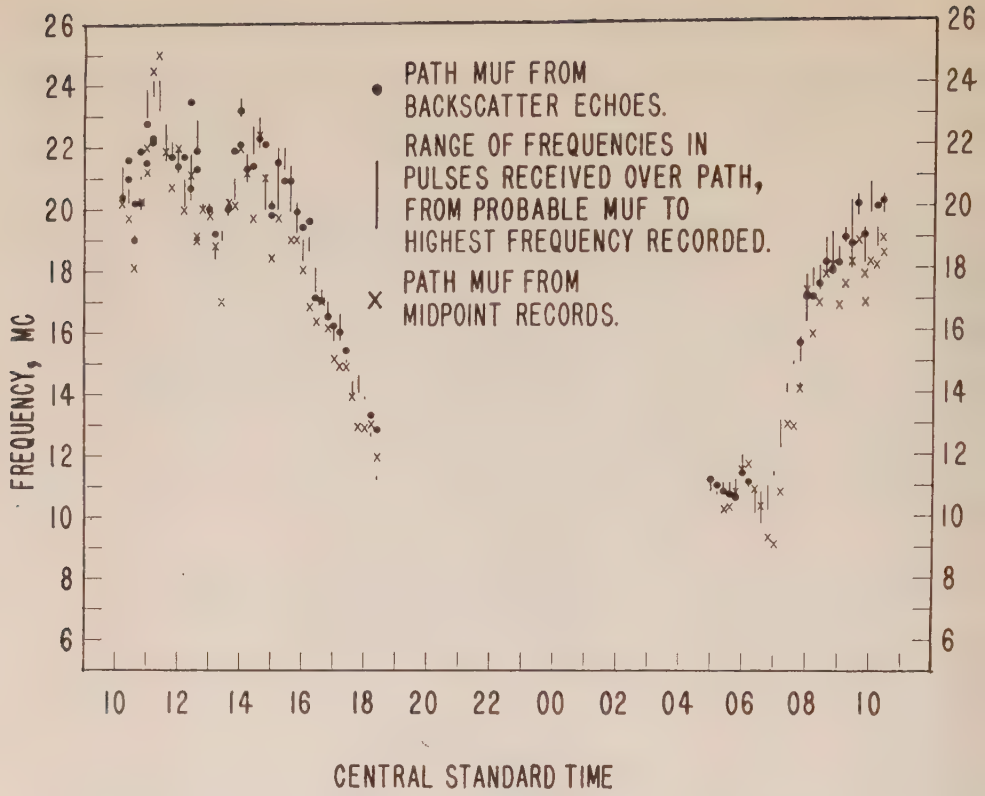

FIG. 10—*F*2-layer MUF for Sterling-Boulder path, December 20-21, 1954

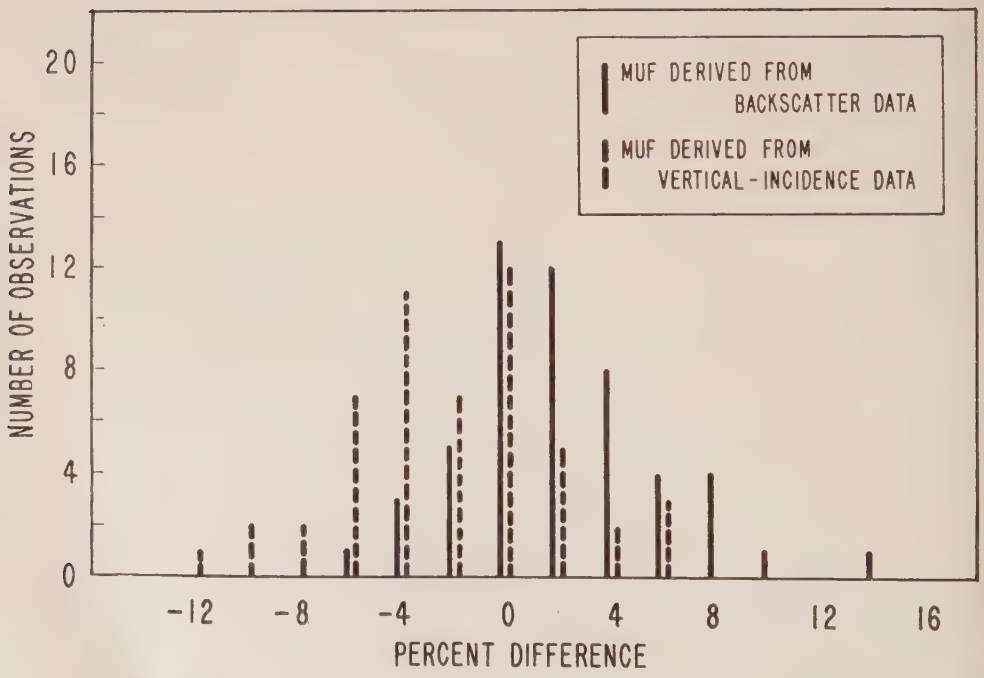

FIG. 11—Percent differences between derived MUF and oblique-incidence MUF, Sterling-Boulder path, December 20-21, 1954

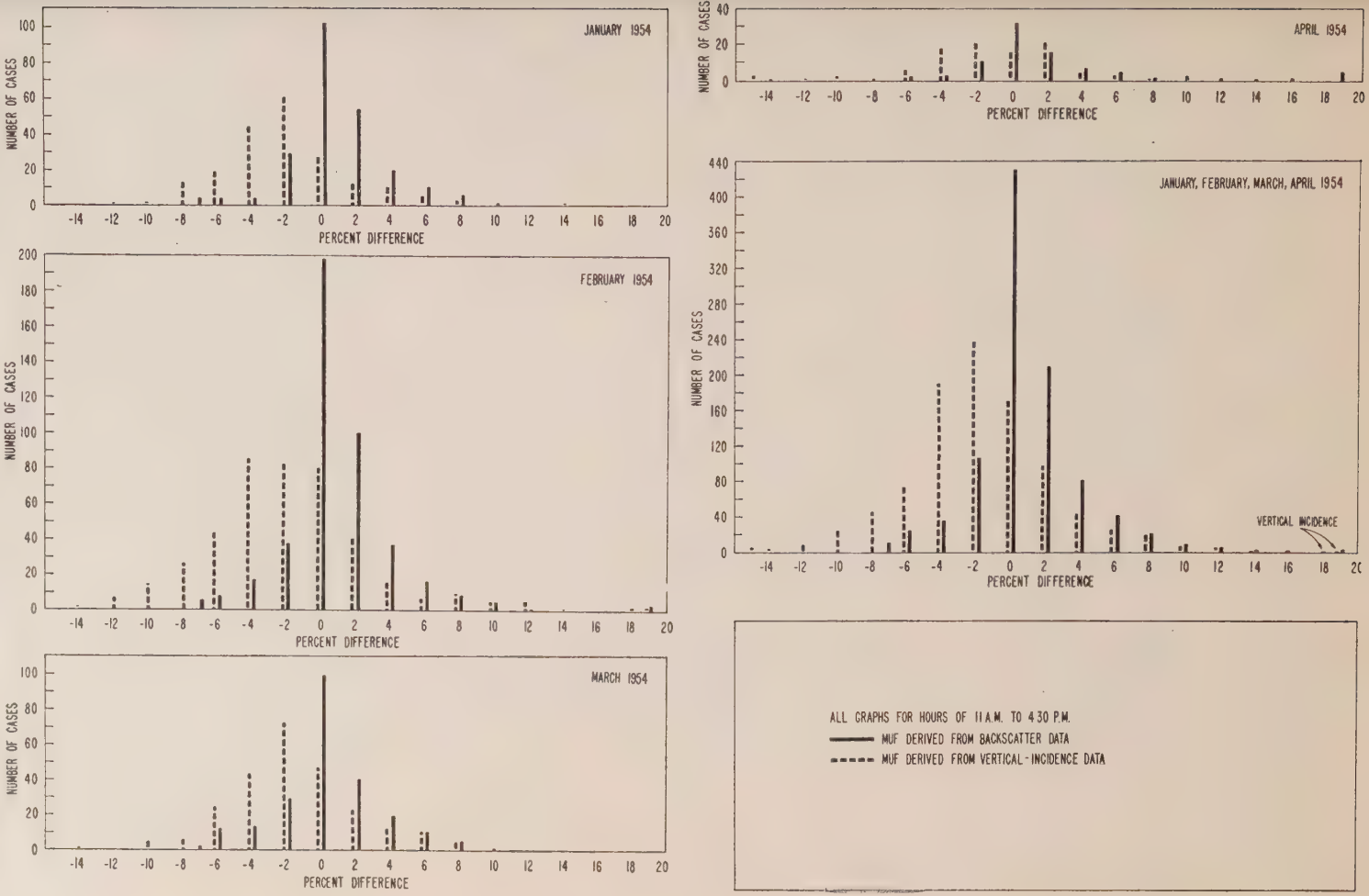

FIG. 12—Percent differences between derived MUF and oblique-incidence MUF, Sterling-Boulder path, January to April, 1954

results of comparing the backscatter MUF with the oblique-incidence MUF, and Table 1*B* a similar analysis for the oblique-incidence MUF and the vertical-incidence MUF.

TABLE 1

A. Percent differences bstween MUF obtained from backscatter data and from oblique-incidence data

Month	Median percent difference	Value exceeded 5% of the time	Values exceeded 95% of the time	No. of all data	No. of usable data	Percent of data usable
1954						
January	0.5	−4.1	6.3	280	234	83.4
February	0.5	−3.2	6.6	494	436	88.3
March	0.0	−5.9	6.1	335	230	68.8
April	0.7	−3.1	12.9	306	86	28.4
All months	0.5	−3.9	6.8	1736	986	56.8

B. Percent difference between MUF obtained from vertical-incidence data and from oblique-incidence data

Month	Median percent difference	Value exceeded 5% of the time	Values exceeded 95% of the time	No. of all data	No. of usable data	Percent of data usable
1954						
January	−2.1	−7.9	5.4	239	199	83.3
February	−2.2	−9.6	7.4	463	432	93.3
March	−1.6	−7.1	5.1	290	253	86.7
April	−1.3	−12.5	4.3	303	100	33
All months	−2.0	−8.7	5.4	1586	984	62

Note: Data are in simultaneously observed pairs.

There is seen to be great similarity between all the months. There is a small positive percent difference between the MUF determined by backscatter and that determined from oblique-incidence data, the value being only of the order of 0.5 percent. There is a larger negative difference between the vertical-incidence and the oblique-incidence MUF, but still median errors are only of the order of of 1 or 2 percent. The data are distributed more closely about the median in the backscatter case. Thus, for February, 90 percent of the backscatter MUF differences fall between −3.2 percent and +6.6 percent, whereas for the same month 90 percent of the vertical-incidence MUF differences fall between −9.6 percent and +7.4 percent.

During January and February, 80 percent to 90 percent of both the backscatter and vertical-incidence data were usable. As spring approached, the proportion of usable records declined to about 30 percent in April, there being a higher proportion of usable vertical-incidence records than usable backscatter records.

An attempt to establish a relationship between percent difference of backscatter MUF and oblique-incidence MUF and the operating frequency between 14 and 25 Mc did not yield any obvious trends.

8. *Vertical-Incidence Predictions*

Only oblique-incidence predictions can be made directly from backscatter records, because the equipment gives slant range *vs* frequency. As for vertical-incidence characteristics, at distances short enough for a flat-earth assumption, the addition of angle-of-arrival measurements would afford virtual-height information. Then, with some assumptions as to layer shape, critical frequencies might be calculated. However, time-delay focus and the possibility of seeing extraordinary-wave backscatter would make the results difficult to obtain.

9. *Conclusions*

It should be feasible by the use of sweep-frequency backscatter techniques to obtain regular observations of $F2$-layer maximum usable frequency over inaccessible areas for control points on radii of 400 to 1300 km or so, using switched antenna arrays. These data could be used for instantaneous skip-distance determination or for obtaining monthly medians.

In designing a station for such use, proper antennas are very important. The interpretation of the data should be made only by persons skilled in ionospheric work and thoroughly familiar, not only with backscatter characteristics and anomalies in general, but with the characteristics and anomalies prevailing in the region.

10. *Acknowledgments*

Successful performance of the experiments described here was made possible only through the coordinated efforts of the personnel of two oblique-incidence ionosphere stations and one vertical-incidence midpoint sounder. Their diligent cooperation is hereby acknowledged.

References

[1] R. Silberstein, Sweep-frequency backscatter—some observations and deductions, Trans. Inst. Radio Eng., **AP-2**, 56-63 (1954).

[2] C. F. Edwards and K. G. Jansky, Measurements of the delay and direction of arrival of echoes from nearby short-wave transmitters, Proc. Inst. Radio Eng., **29**, 322-329 (1941).

[3] A. M. Peterson, The mechanism of F-layer propagated backscatter echoes, J. Geophys. Res., **56**, 221-237 (1951).

[4] W. G. Abel and L. C. Edwards, The source of long distance backscatter, Proc. Inst. Radio Eng., **39**, 1538-1541 (1951).

[5] W. L. Hartsfield and R. Silberstein, A comparison of CW field intensity and backscatter delay, Proc. Inst. Radio Eng., **40**, 1700-1706 (1952).

[6] W. L. Hartsfield, Observations of distant meteor-trail echoes followed by ground scatter, J. Geophys. Res., **60**, 53-56 (1955).

[7] A. F. Wilkins and E. D. R. Shearman, Back-scatter sounding: An aid to radio propagation studies, J. Brit. Inst. Radio Eng., **17**, 601-616 (1957).

[8] E. K. Smith, Jr., On world-wide occurrence of sporadic E, Nation. Bur. Stan., Circ. No. 582 (available from U. S. Govt. Printing Office at $3.25).

JOURNAL OF GEOPHYSICAL RESEARCH VOLUME 63, No. 2 JUNE, 1958

FIELD METHOD FOR DETERMINING DIRECTION OF MAGNETIZATION AS APPLIED TO LATE CENOZOIC BASALTS, NORTHEASTERN NEW MEXICO*

BY WILLIAM R. MUEHLBERGER

Department of Geology, The University of Texas, Austin 12, Texas

AND

BREWSTER BALDWIN

New Mexico Bureau of Mines and Mineral Resources, Socorro, New Mexico

(Received February 4, 1958)

ABSTRACT

Placing a magnet parallel to a Brunton compass to cancel part of the earth's field at the compass will sensitize it so that field determinations of magnetic polarity of strongly magnetized rocks (for example, basalts) can be made. Late Cenozoic basaltic rocks in northeastern New Mexico do not show consistent direction of magnetization laterally in a single flow or vertically through the stratigraphic column when tested by this method.

Introduction

Paleomagnetic studies have been done mainly in laboratories with expensive equipment. The field technique described herein requires a compass and small bar or horseshoe magnet; it will give excellent results on strongly magnetic rocks, as, for example, most igneous rocks. Initially, we hoped to use this method as a stratigraphic tool to aid in subdividing and correlating the volcanic rocks of northeastern New Mexico into the known stratigraphic sequence in the Capulin Mountain region (Muehlberger, in preparation), and to relate the reversals of magnetic field with those of the basalts in Iceland, which in turn are interbedded with glacial moraines (Hospers, 1953, p. 475). We hoped to date our volcanic rocks in this manner, on the assumption that reversals of the earth's main geomagnetic field exist and therefore should be a world-wide device for dating rocks (Blackett, 1956, p. 8). Our work, as reported here, leads us to believe that the direction of magnetization of a particular specimen is valid, but it cannot be assumed to be the same throughout a single basalt flow or sequence of flows.

*This project was supported jointly by the Geology Foundation, The University of Texas, and the New Mexico Bureau of Mines and Mineral Resources. Publication authorized by the Director, New Mexico Bureau of Mines and Mineral Resources. The results reported herein were presented orally at the Annual Meeting of the Geological Society of America at Atlantic City, New Jersey, on November 5, 1957.

Procedure

The needle of a Brunton compass can be deflected only a few degrees by a piece of strongly magnetized basalt. Victor Vacquier, formerly of the New Mexico Institute of Mining and Technology, outlined the following procedure to increase the deflection.

Place the compass on a short pedestal and orient roughly. In our work, we used two one-foot wood blocks of 4″ × 4″ dimensions. On a line normal to the compass needle, place a magnet (bar or horseshoe) on another pedestal with its poles parallel to the compass poles. Move the magnet along the normal line until the earth's magnetic field is effectively canceled, leaving only a weak restoring field. This point can be recognized when the needle swings slowly in a wide arc. If the magnet is in reverse position, the needle will swing rapidly. Rotate magnet to make the needle home on north.

On the side opposite from the magnet, hold a rock sample level with the needle and a few inches away. Rotate specimen in all directions until the point of maximum repulsion of the north-seeking pole is found. In this position, place finger horizontally along rock, pointing toward the pole. The finger is now parallel with magnetic alignment of the rock, pointing toward its north pole. Rotate the rock sample back to its original field orientation. If the finger points north and down, magnetization is normal (for, at least, late Cenozoic rocks in North America; Hospers, 1955, p. 72). If the finger points south and up, magnetization is reversed.

By addition of protractors and standard axes of rotation (simplified universal stage), measurements of magnetic declination and inclination of reasonable accuracy ($\pm 5°$) could be done in the field. However, the work reported here was only concerned with whether the rocks were normally or reversely magnetized.

Geologic sketch of late Cenozoic basalts, northeastern New Mexico

In Union and eastern Colfax counties (Fig. 1), there is an extensive volcanic province which extends in an east-southeast direction onto the southern High Plains from the Rocky Mountain front. By geomorphic and stratigraphic position, basalts of this volcanic province were subdivided by Collins (1949, pp. 1022-1023) into three major groups, which he named from oldest to youngest, Raton basalts, Clayton basalts, and Capulin basalts.

The Raton basalts are possibly early Hemphillian (early upper Pliocene), based on the association of vertebrate remains with volcanic bombs and scoria in beds now cropping out along the east edge of the southern High Plains in the Texas Panhandle (Reed and Longnecker, 1932, p. 83).

The Capulin basalts, the youngest group, consist of a small number of cinder cones and associated flows, which by radiocarbon dates are found to be younger than Folsom Man (*ca.* 8000 B.C.) and older than 2500 B.C. (Muehlberger, 1955, pp. 1600-1601).

Other than being somewhere intermediate in age between the Raton and Capulin basalts, the Clayton basalts had no paleontologic or other control on dating. These we hoped to correlate by paleomagnetism.

Initial reconnaissance study

Two preliminary one-day reconnaissance trips by Muehlberger in February and

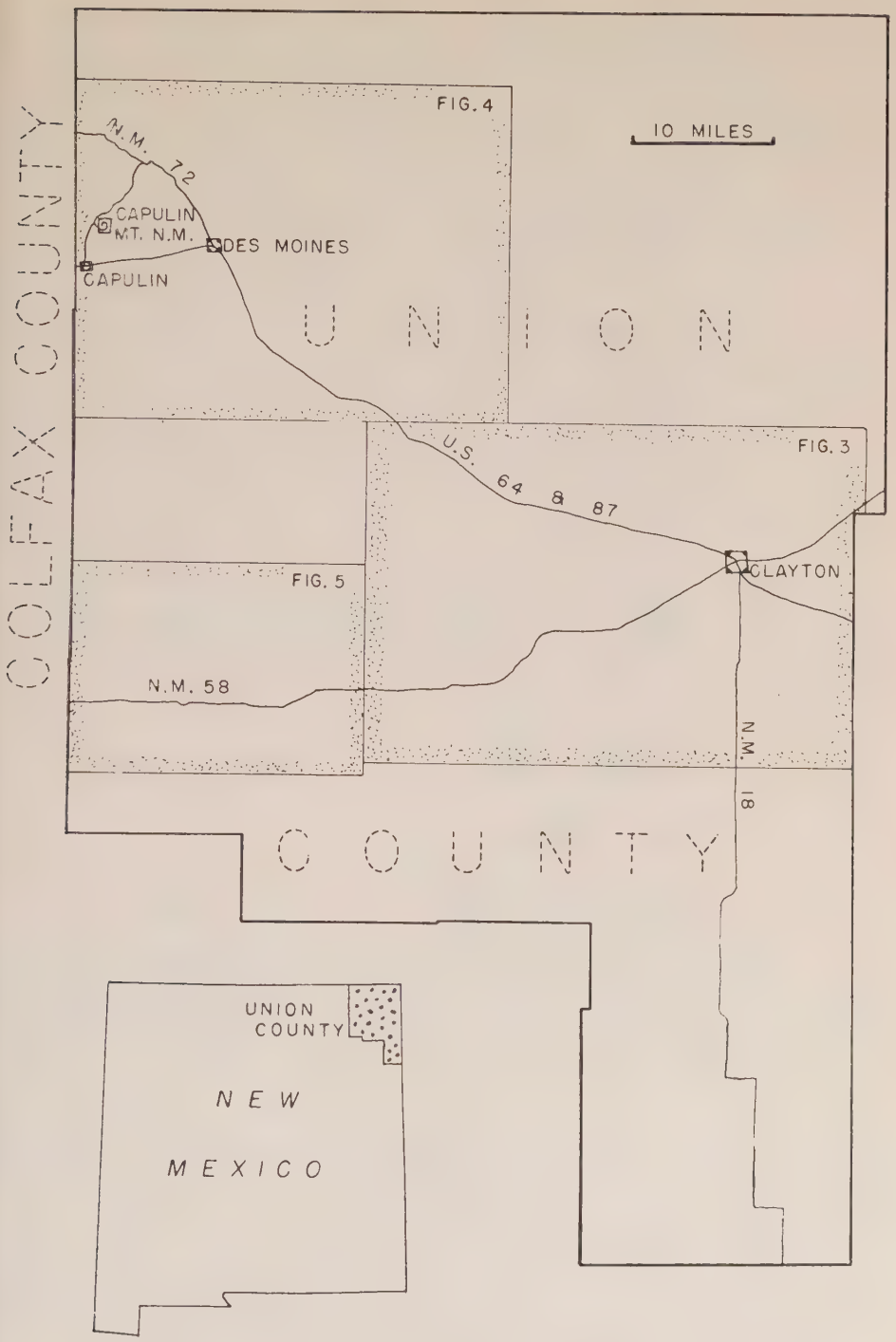

FIG. 1—Index map of Union County, New Mexico, showing location of Figures 3, 4, and 5

March, 1957, in the Capulin Mountain region, northwestern Union County and adjoining parts of Colfax county, led to the results summarized in Figure 2. Each

CAPULIN BASALTS	
Baby Capulin Mountain	N
Purvine Hills	N
Twin Mountain	
Capulin Mountain	N
CLAYTON BASALTS	
Folsom Vents	R
José Butte	
Robinson Mountain	R
Bellisle Mountain	R
Mud Hill	N
Augite Vents	N
Big Hill – East Big Hill	N f
Emery Peak – East Emery Peak	N f
Dunchee Hill	R
Gaylord Mountain	N
Purvine Mesa	N
Sierra Grande	N
RATON BASALTS	N f

FIG. 2—Results of paleomagnetic reconnaissance of the Capulin Mountain region volcanic rocks. Capulin basalts—Recent; Clayton basalts—late Pliocene (?) to early Pleistocene (?); Raton basalts—early upper Pliocene (?). Relative stratigraphic position within the Clayton basalt sequence is not known for the vents listed below Emery Peak. *N* = normal magnetization, *R* = reverse magnetization, *f* = very faint magnetization.

volcanic source was sampled from a single locality, in most cases from the vent itself, although a few were sampled from lava flows convenient to an access road. About five samples were tested at each station, and only the dominant magnetic direction was recorded. The occasional aberrant specimen was ignored.

The vents are listed in stratigraphic order from youngest at the top to oldest at the bottom. All Capulin basalts tested were normally magnetized. Incidentally, the specimens tested from Capulin Mountain were bombs taken from the cinder cone itself. This is taken as evidence of cooling below the Curie temperature after the bomb reached its present position on the cone.

The Clayton basalts showed a reversal in magnetic orientation between the eruption of Bellisle Mountain and Mud Hill. This reversal could then be correlated

with the Icelandic basalts where Hospers (1953, p. 475) shows a reversal occurring between basalts underlying and overlying the oldest glacial moraines. Thus, the Clayton basalts could be latest Pliocene to early Pleistocene in age. The stratigraphic positions of the Clayton vents listed below Emery Peak are not known with respect to the main list and are only put in to give the complete data. Sierra Grande is a complex vent, probably erupted at several times.

The Raton basalt samples tested were very faintly magnetic, and were obtained from the lower portion of one flow in road cuts near the east end of Johnson Mesa in eastern Colfax County (on N. M. State Highway 72).

Union County study

In his geologic mapping of Union County, Baldwin (Bushman and Baldwin, in preparation) has outlined several basalt flows that are 10 to 20 miles long. These appeared to be ideal for testing the consistency of results. Therefore, we spent a week in June, 1957, sampling the long flows at several locations. Eighty-five crudely oriented samples from thirty-two localities were kept; twice as many were tested in the field. The results will be discussed in the order studied. Figures 3, 4, and 5 summarize the work.

At each location, four or more samples were tested; if all specimens were consistent, only the preferred magnetization is shown; if inconsistent results were found, these are indicated by subscripts which indicate the approximate proportion of normal to reverse magnetization in the samples tested. All specimens with an obvious anomalous magnetic orientation (*A*) are noted, even though only

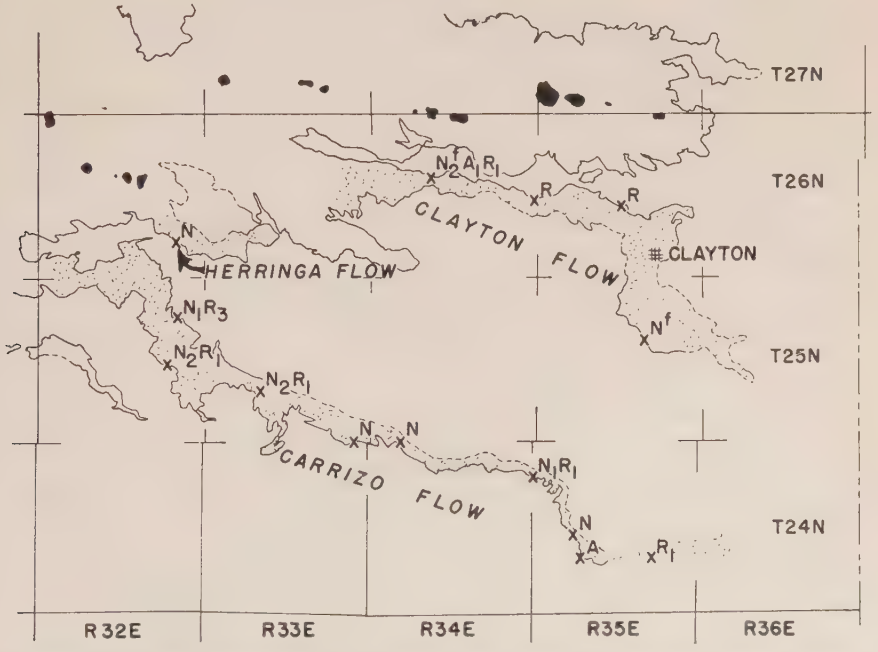

Fig. 3—Paleomagnetic observations on Clayton age basalts in eastern Union County, New Mexico. Subscripts indicate relative proportions of tested samples having *N*-normal magnetization, *A*-anomalous magnetization, *R*-reverse magnetization.

one or two specimens showed magnetization at strong angles to the main field. Practically all specimens were taken along the upper edges of the exposed flow. The basal portion of the flows, except in a few road cuts and on the walls of deep valleys, are always covered with talus, wind-blown and colluvial material.

Figure 3 shows the results of sampling on three Clayton age flows, including the type Clayton basalt. Both in hand specimen and in thin section, no differences can be found among any of these flows or between oppositely magnetized specimens from an individual locality. It is, therefore, possible that what are named here as three separate flows, the Clayton, Herringa, and Carrizo flows, may be from one magma and be parts of a single larger unit now partially buried by later volcanic action.

The Carrizo flow shows a tendency toward being normally magnetized. The easternmost locality probably should be excluded, because it is based on one sample taken from a small outcrop found in an area of low sand-dunes, and thus may be a large boulder. (The Herringa flow was sampled at only one locality, where all specimens were strongly normal.) The Clayton flow, on the other hand, shows a tendency toward reverse magnetization, especially when the faintness of magnetization of the normal specimens is compared with strong for the reverse specimens.

Figure 4 shows the results of sampling on the Gaps and Van Cleve flows, also Clayton age basalts. The Gaps flow is consistently normal. The localities of reverse magnetism in the western part of R. 30 E., along what appears to be a topographic-

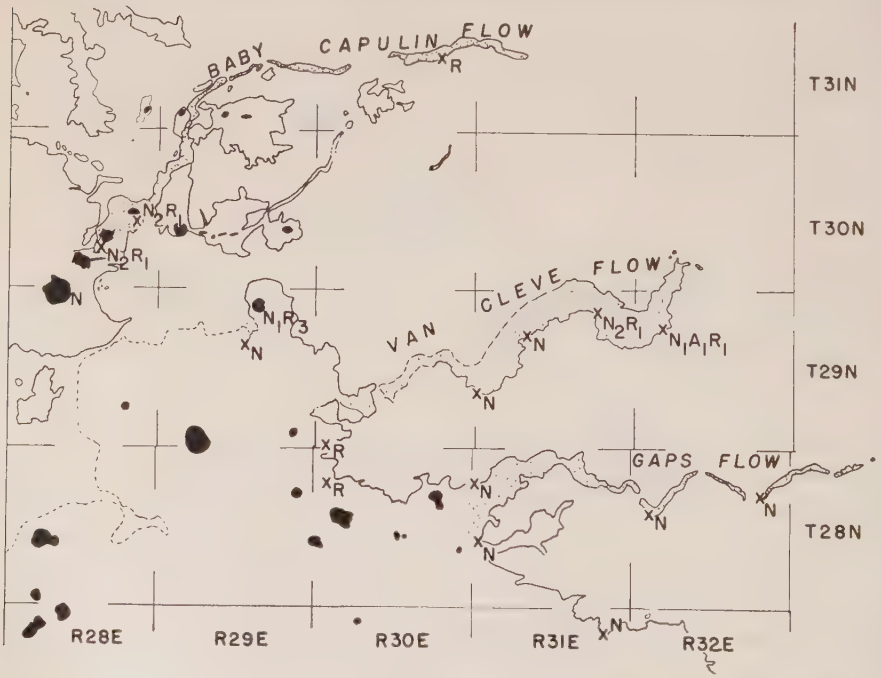

FIG. 4—Paleomagnetic observations on Clayton and Capulin basalts in northwestern Union County, New Mexico. Symbols same as Figure 3.

ally continuous portion of the Gaps flow, are probably from a different vent, as shown by the dissimilarity of hand specimens. The Van Cleve flow is completely normal at two localities and inconsistent at the other two locations. No source is known for either the Gaps or Van Cleve flows. They are each petrographically different from the other and from the Clayton flows of Figure 3.

Owing to the inconsistency of our results, we briefly revisited the Capulin Mountain region to resample a few locations as checks on the earlier reconnaissance (data shown in Fig. 2). Dunchee Hill, a Clayton age vent, was resampled, with results shown (N_1R_3 vent in northeast T. 30 N., R. 29 E.). The "*N*" station, two miles south of Dunchee Hill, is on a basalt flow that is part of the Sierra Grande complex (main vent is large vent shown on boundary between T. 29 N. and T. 30 N., R. 29 E.). These results agreed, in the main, with the earlier reconnaissance work (Fig. 2). Capulin Mountain once again gave consistently normal results (vent "*N*" on the boundary between T. 29 N. and T. 30 N., R. 28 E.).

We also sampled three locations on the lava field from Baby Capulin (second vent northeast of Capulin Mountain). Inconsistent results were obtained at all locations, and only reverse magnetization was observed at the locality near the end of the flow. This is especially noteworthy, because the basalt is petrographically the same wherever sampled, and the vent erupted less than 10,000 years ago, when the main geomagnetic field is supposed to have been in its present position.

We further tested the Raton basalts of Johnson Mesa in eastern Colfax County and obtained the following results: five normal, two anomalous, and one reverse sample.

The Don Carlos Hills (Fig. 5) form an eruptive entity in the southwest part of the county. A series of aligned vents and associated flows, they lie on a basalt

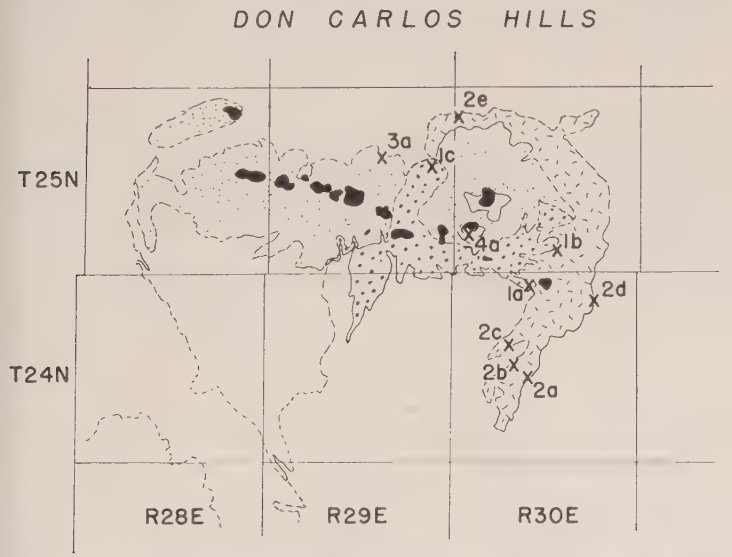

DC_4	4a	$N_1A_1R_2$
DC_3	3a	N_3
DC_2	2e	N_1^f R_2
	2d	$N_2A_1R_1$
	2c	N_3
	2b	N_2 R_1?
	2a	N_2A_1
DC_1	1c	A_1R_1
	1b	$N_1A_1R_1$
	1a	N_1 R_2

FIG. 5—Paleomagnetic observations on Don Carlos Hills, southwestern Union County, New Mexico. *DC*1 = Raton (?) basalt platform, *DC*2 = oldest flow on east side of hills, *DC*3 = youngest flows, *DC*4 = vent probably contemporaneous with *DC*3.

platform, here labeled *DC*1 (heavily dotted area), that are probably Raton in age. All *DC*2 specimens are from one flow, with the possible exception of 2*e*. *DC*3 (lightly dotted area) flows are the youngest in this sequence. *DC*4 is a single vent and flow that may be one of the youngest of the *DC*3 sequence. The inconsistency of results obtained may be easily seen in the tabulated data. The Don Carlos Hills eruptions appear to be dominantly normal in magnetization, and the older Raton (?) platform (*DC*1) is dominantly reversely magnetized.

Conclusions

The inconsistency of results observed when there is no obvious change in the rock leads us to doubt the usefulness of paleomagnetism as a field tool for stratigraphic subdivision or correlation. Possibly, if it were possible to sample all flows at the same position (top, middle, or bottom), some of the inconsistencies might disappear, although the reason for the inconsistencies would still be unknown.

Acknowledgments

Guy Smith, Marshall Perry (February); J. A. Wilson, Don Winston, R. E. Grant (March); and T. E. Longgood, Jr. (summer) assisted the authors in the field. Discussions with and editorial criticism by S. E. Clabaugh, J. L. Snyder, and T. E. Longgood, Jr., are gratefully acknowledged. Victor Vacquier suggested the use of the magnet to sensitize the compass needle.

References

Blackett, P. M. S. (1956); Lectures on rock magnetism, The Weizmann Science Press of Israel, Jerusalem.

Bushman, F. X., and B. Baldwin (in preparation); Geology and ground-water resources of Union County, New Mexico, New Mexico Bur. Mines and Min. Res. Ground-water Report.

Collins, R. F. (1949); Volcanic rocks of northeastern New Mexico, Bull. Geol. Soc. Amer., **60**, 1017-1040.

Hospers, J. (1953); Reversals of the main geomagnetic field, Proc. Kon. Nederland. Akad. Wetensch., B, **56**, 467-491.

——— (1955); Rock magnetism and polar wandering, J. Geol., **63**, 59-74.

Muehlberger, W. R. (1955); Relative age of Folsom Man and the Capulin Mountain eruption, Colfax and Union Counties, New Mexico, (abst.) Bull. Geol. Soc. Amer., **66**, 1600-1601.

——— (in preparation); Geology of the Capulin Mountain region, northeastern New Mexico, New Mexico Bur. Mines and Min. Res. Bull.

Reed, L. C., and O. M. Longnecker, Jr. (1932); The geology of Hemphill County, Texas, Univ. Texas Bull. No. 3231.

Journal of Geophysical Research Volume 63, No. 2 June, 1958

EFFECT OF STRESS ON THE REMANENT MAGNETISM OF MAGNETITE-BEARING ROCKS

By F. D. Stacey

Department of Geophysics, Australian National University, Canberra, Australia

(Received February 28, 1958)

ABSTRACT

An estimate is made of the effect of externally applied stress upon the remanent magnetic moment of an assembly of multi-domain magnetite grains. Magnetite is highly magnetostrictive and therefore very sensitive to stress, and it is estimated that remanent moments are changed by about 0.05 per cent per atmosphere of applied linear compression. Moments parallel to the direction of compression are reduced and those perpendicular to it are increased; moments with intermediate orientations are deflected away from the direction of compression.

I. INTRODUCTION

Graham and others [see 1, 2, and 3 of "References" at end of paper] have recently pointed out that magnetostriction, in its converse effect of stress upon magnetisation, may have an important influence on the remanent moments of rock samples used for palaeomagnetic investigations. The magnitude of the effect of stress has been adequately demonstrated by the experiment of Graham, Buddington, and Balsley [3], but the conclusions drawn from palaeomagnetic work are not necessarily invalidated. We require to know whether a rock acquiring thermoremanent magnetisation under a stress from which it is subsequently released has a moment differing in direction from the field in which it cooled. The present paper is an attempt to establish a theoretical approach to the problem, by considering the effect of isothermal compression on thermoremanent moments.

The general problem is very complex and depends upon data which are not available. However, the case of a rock containing magnetite as the only magnetic mineral can be examined by making an estimate of the magnetostriction of magnetite.

II. THE MAGNETOSTRICTION OF MAGNETITE DUE TO LOW FIELDS AND SMALL REMANENT MOMENTS

Heaps [4] has given results of measurements of the magnetostriction of a magnetite single crystal in three crystallographic directions. The measurements were made in high fields, but the magnetostriction due to small induced and remanent moments can be inferred from them.

A simple extrapolation to low fields of Heaps' magnetostriction curves might

suggest that magnetostriction varies linearly with field at sufficiently low fields. This is seen to be incorrect by considering the fundamental thermodynamic equation upon which the present discussion is based:

$$\left(\frac{\partial \lambda}{\partial H}\right)_p = -\left(\frac{\partial I}{\partial p}\right)_H \quad \ldots\ldots(1)$$

Here I is the magnetic moment per unit volume of material in field H, subjected to linear compression p. For compressions parallel to H, λ is the longitudinal magnetostriction (or fractional change in dimension) λ_L ; for p perpendicular to H, λ is the transverse magnetostriction λ_T . A convenient derivation of this equation is given by Bozorth [5, p. 632].

For a material with a small induced moment, $I = kH$, where k, the incremental or initial susceptibility, is independent of H to a good first approximation. Then for this material,

$$\left(\frac{\partial \lambda}{\partial H}\right)_p = -H\left(\frac{\partial k}{\partial p}\right)_H$$

so that λ varies as H^2. It is more convenient to write

$$\lambda = CI^2 \quad \ldots\ldots(2)$$

The significance of equation (2) in domain theory will appear in §III, where the variation of the constant C with p is considered.

Hysteresis of magnetostriction shows that λ is a function of I rather than H and that it is associated with remanent magnetic moments, I_R , as well as induced moments, (kH). Equation (2) will, therefore, be used for the magnetostriction accompanying total moments $(I_R + kH)$. It may be noted that where I_R and (kH) have different directions, I_R must be resolved parallel and perpendicular to H for the estimation of magnetostriction, but this anisotropy is not considered further here.

An examination of the experimental points given by Heaps in his Figures 1 and 2 suggests that at the lowest field used (~850 oersteds) his particularly hard specimen may have been near to the range of field over which equation (2) is valid. The constants listed in Table 1 were calculated on this assumption, using the value 1.2 for initial permeability, as estimated by Heaps for his specimen.

TABLE 1—*Low field magnetostriction constants* $C = \lambda/I^2$ *of magnetite, calculated from the data of Heaps* [4]

Crystal axis	Longitudinal constant C_L	Transverse constant C_T
100	-1.0×10^{-9}	$+1.6 \times 10^{-9}$
110	$+8.3 \times 10^{-9}$	-16.6×10^{-9}
111	$+4.2 \times 10^{-9}$	-13.6×10^{-9}

There are several reasons why the figures of Table 1 should be considered only as an order of magnitude for the magnetostriction of magnetite:

(i) Permeability is certainly a function of crystal direction.

(ii) The assumption that "initial magnetostriction," described by equation (2), extended to 850 oersteds may be at fault.

(iii) The easy direction of magnetisation appears to be (100), whereas Nagata [6, p. 30] gives (111).

(iv) From the Table, volume magnetostriction appears to be large. (Volume magnetostriction equals the longitudinal magnetostriction plus twice the transverse magnetostriction.) If this is correct, it is most unusual and implies a first order effect of hydrostatic pressure on magnetic moment.

A detailed analysis without more information about magnetostriction would be of little value. In the following sections, it is assumed that an assembly of multi-domain magnetite grains with random crystal directions behaves isotropically and has magnetostriction constants:

$$C_L = 10 \times 10^{-9}$$

$$C_T = -5 \times 10^{-9}, \text{ referred to pure magnetite}$$

These figures eliminate the anomaly of large volume magnetostriction, while retaining the sign and approximate values of the constants obtained from Heaps' data.

III. THE EFFECT OF COMPRESSION ON REMANENT MOMENTS

Substituting equation (2) into equation (1), we obtain

$$-\left(\frac{\partial I}{\partial p}\right)_H = \left(2CI\,\frac{\partial I}{\partial H}\right)_p = (2CIk)_p$$

where k is the incremental volume susceptibility, and

$$I = I_R + kH$$

Thus,

$$-\frac{\partial}{\partial p_H}(I_R + kH) = (2CkI_R + 2Ck^2H)_p$$

Since I_R is independent of H, this equation is separable:

$$-\left(\frac{\partial I_R}{\partial p}\right)_H = (2CkI_R)_p \quad \text{.....(3)}$$

$$-\left(\frac{\partial k}{\partial p}\right)_H = (2Ck^2)_p \quad \text{.....(4)}$$

Combining equations (3) and (4), we see that I_R and k vary with pressure in the same way:

$$\left(\frac{\partial I_R}{\partial k}\right)_H = \left(\frac{I_R}{k}\right)_p$$

from which we obtain

$$k = \frac{k_0}{I_{R_0}} \cdot I_R$$

The subscript 0 is used to denote values at zero pressure. This result is substituted into equation (3), giving:

$$-\left(\frac{\partial I_R}{\partial p}\right)_H = \frac{2k_0}{I_{R0}}(CI_R^2)_p \quad \ldots\ldots(5)$$

To proceed with the integration of equation (5), it is necessary to know the dependence of C upon p, for which an appeal is made to domain theory. Isothermal remanent magnetisation (IRM) and thermoremanent magnetisation (TRM) must be considered separately, as they have different domain structures.

In a magnetic body of many domains, IRM proceeds initially by 180° domain wall movements, not accompanied by magnetostriction, with very little 90° wall movements or domain rotations; this is in agreement with equation (2), which requires that magnetostriction be small for initial magnetisation. A small IRM may, therefore, be regarded as the expansion of domains in one direction at the expense of those oppositely directed, with the perpendicular moments very little affected. The reversible nature of initial IRM requires that the small magnetostriction which accompanies it should be due to 90° wall movements and not domain rotations. The magnetostriction is thus proportional to the area of 90° domain boundaries, which makes it difficult to handle mathematically. Further discussion is restricted to the geophysically more important TRM.

Although the detailed domain structure of TRM is different from that of IRM, the statistical distribution of domain directions is similar, as is necessary for equation (2) to apply to TRM. In a rock cooling through its Curie temperature, at which the spontaneous magnetisation σ is very small, magnetostriction is negligible, being proportional to σ^2. In a small external field, a magnetic moment is produced by a balance between the tendency of the field to turn the domains in one direction and the disordering influence of temperature. If the blocking temperature at which the domain structure becomes "frozen in" is near to the Curie point, the magnetostriction accompanying it does not appear until the material has cooled much further and therefore has only a secondary effect upon magnetisation. The Boltzmann probability for domain alignment is greatest parallel to the field, least antiparallel, and for perpendicular alignment is practically the same as for the unmagnetised material, as with IRM. The important point for the present discussion is that TRM is effectively produced by domain rotation.

Linear compression causes domain rotations either towards or away from the direction of compression, depending upon the sign of the magnetostriction of the material. For a body with a TRM, the ratio of the total resolved moments parallel and antiparallel to the net moment, I_R, remains constant, because compression causes a similar increase or decrease in the parallel and antiparallel components of the moments of domains which have partial alignments in the two directions. Thus, I_R is proportional to the total resolved moment, $M_\parallel$, in the direction of I_R, added without regard to sign.

$$\frac{I_R}{I_{R_0}} = \frac{M_\parallel}{M_{\parallel 0}} \quad \ldots\ldots(6)$$

where, as before, the subscript 0 refers to values at zero pressure.

It is important to note that the magnetostriction associated with I_R, required

for equation (5), does not include the change of dimension accompanying the domain rotation caused by compression, but only the much smaller effect due to magnetisation at constant pressure.

For a material compressed in the direction of I_R, the longitudinal magnetostriction λ_L, at any pressure is proportional to the total resolved moments parallel ($M_\parallel$) and perpendicular ($M_\perp$) to I_R, added without regard to sign in the case of $M_\parallel$ or direction in the perpendicular plane for $M_\perp$. Depending upon the direction of rotation, $M_\parallel$ and $M_\perp$ are measures of the ease of rotation (that is, moment already rotated) and the moment available for rotation. Thus, referring to values at zero pressure:

$$\frac{\lambda_L}{\lambda_{L_0}} = \frac{M_\parallel}{M_{\parallel_0}} \cdot \frac{M_\perp}{M_{\perp_0}} \qquad (7)$$

The quantities $M_\parallel$ and $M_\perp$ may be related by considering volume magnetostriction to be zero, so that transverse magnetostriction is given by

$$\lambda_T = -\tfrac{1}{2}\lambda_L$$

Since magnetostriction is due to a change in total moment in any direction, λ_L is proportional to the change $\Delta M_\parallel$ in $M_\parallel$ and to half the change $\Delta M_\perp$ in $M_\perp$. Thus,

$$\Delta M_\parallel + \Delta M_\perp = 0$$

$$M_\parallel + M_\perp = \text{constant} = M_{\parallel_0} + M_{\perp_0}$$

From which

$$\frac{M_\perp}{M_{\perp_0}} = \frac{M_{\parallel_0}}{M_{\perp_0}} + 1 - \frac{M_\parallel}{M_{\parallel_0}} \cdot \frac{M_{\parallel_0}}{M_{\perp_0}} \qquad (8)$$

The ratio $M_{\parallel_0}/M_{\perp_0} = \frac{1}{2}$, because at zero pressure the total resolved moments in the three mutually perpendicular directions are equal. Equations (6), (7), and (8) may then be used to obtain the relation between λ_L and I_R :

$$\frac{\lambda_L}{\lambda_{L_0}} = \frac{I_R}{I_{R_0}}\left(\frac{3}{2} - \frac{1}{2}\frac{I_R}{I_{R_0}}\right) \qquad (9)$$

Substituting this into equation (5) and noting that $\lambda_{L_0} = C_{L_0} I_{R_0}^2$, we obtain

$$\frac{\mathrm{d}}{\mathrm{d}p}\left(\frac{I_R}{I_{R_0}}\right) = -k_0 C_{L_0} \frac{I_R}{I_{R_0}}\left(3 - \frac{I_R}{I_{R_0}}\right)$$

which integrates to

$$\frac{3 - \dfrac{I_R}{I_{R_0}}}{2\dfrac{I_R}{I_{R_0}}} = \exp\left(3k_0 C_{L_0} p\right)$$

or

$$\frac{I_R}{I_{R_0}} = \frac{3}{1 + 2\exp\left(3k_0 C_{L_0} p\right)} \qquad (10)$$

Equation (10) gives the relative change in remanent moment, I_R , of a rock due to compression p parallel to I_R . The corresponding equation for compression perpendicular to I_R is

$$\frac{I_R}{I_{R_0}} = \frac{3}{2 + \exp(6k_0 C_{T_0} p)} \quad \text{.....(11)}$$

IV. COMPARISON WITH EXPERIMENT

A comparison of equations (10) and (11) with the results of Graham, Buddington, and Balsley [3] is an important test of the extent to which the magnetostrictive processes of rocks have been understood. For this purpose, Nagata's [6, p. 89] approximate figure for the initial susceptibility of magnetite occurring as grains in rocks, $k_0 = 2.5 \times 10^{-2}$, will be used with the values C_{L_0} , C_{T_0} of the magnetostriction constants given in §II.

If the moment M of a sample makes an angle θ with the direction of a subsequently applied stress p, it may be resolved into components ($M \cos \theta$) and ($M \sin \theta$) parallel and perpendicular to p. By equations (10) and (11), the resolved moments become, under compression:

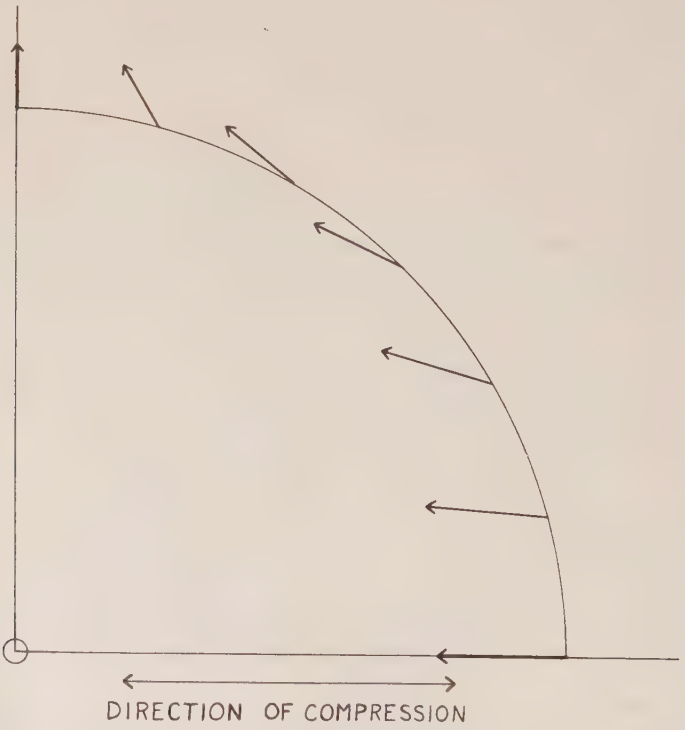

FIG. 1—Calculated fractional changes in magnetisation of magnetite-bearing rocks subjected to 500 atmospheres linear compression. Vectors from the origin to tails of arrows represent original magnetisation and vectors from origin to arrow heads represent magnetisation under pressure.

$$\left[\frac{3}{1 + 2 \exp (7.5 \times 10^{-10} p)}\right] \cdot M \cos \theta$$

$$\left[\frac{3}{2 + \exp (-7.5 \times 10^{-10} p)}\right] \cdot M \sin \theta$$

where p is in dyne $cm^{-2} = 10^{-6}$ atmosphere.

At 500 atmospheres, the factors in brackets are 0.767 and 1.12. These values have been used to calculate the vectorial changes in moment indicated in Figure 1, which is intended for comparison with Figure 2 of the paper by Graham, Budding-ton, and Balsley [3].

The calculated changes are comparable with those induced experimentally by about 200 atmospheres of compression. The discrepancy of a factor of two or three in not serious, in view of the crude manner of estimating the constants C_0 and the fact that the value of k_0 could have been in error by this factor for the rocks examined. In fact, the rocks were metamorphic and not typical of specimens used for palaeomagnetic work. Of the specimens in which the magnetic minerals were most nearly pure magnetite, A, F, and M, only F and M show reasonable agreement with the theory presented. Specimen A behaved in almost the opposite manner. This discrepancy is more serious and does not have an obvious explanation.

V. MAGNETOSTRICTION AND PALAEOMAGNETISM

The present paper is an attempt to establish a theoretical basis for an examination of the importance of magnetostriction in palaeomagnetism. The problem examined is the isothermal application of pressure to rocks with thermoremanent moments. The effect is expected to be almost completely reversible as long as the compression is elastic. If permanent deformation or fracture occurs, the problem becomes more difficult, but is nevertheless important, as a field test of magnetic stability [7] depends upon the folding of rocks after magnetisation.

However, it will be of considerable interest to examine the process of thermo-remanent magnetisation under elastic compression, from which the samples are released for measurement.

At the Curie point of a mineral, its magnetostriction is zero, so that compression does not have an effect upon the directions of the domains as they are originally formed. It is, therefore, possible, as suggested by Graham [1] that TRM acquired under compression assumes the direction of the field inducing it and that the release of pressure has an effect exactly opposite to the application of pressure considered in this paper.

Néel [8] has pointed out that, even for multi-domain grains, TRM is not "frozen in" until the rock has cooled to a blocking temperature significantly lower than the Curie point. A question to be answered is, therefore, whether the blocking temperature is sufficiently lower to allow the magnetostrictive effect of pressure to influence the domain formation. The effect would then be qualitatively similar to isothermal compression, being at least partially reversible. For palaeomagnetism to be relieved of the doubt which has been aroused by magnetostriction, it is necessary that quantitative considerations show that this reversibility is almost complete.

References

[1] J. W. Graham, Paleomagnetism and magnetostriction, J. Geophys. Res., 61, 735-739 (1956).
[2] J. W. Graham, The role of magnetostriction in rock magnetism, Adv. Phys. (Quarterly Supplement of Phil. Mag.), 6, 362-363 (1957).
[3] J. W. Graham, A. F. Buddington, and J. R. Balsley, Stress-induced magnetizations of some rocks with analyzed magnetic minerals, J. Geophys. Res., 62, 465-474 (1957).
[4] C. W. Heaps, The magnetostriction of a single magnetite crystal, Phys. Rev., 24, 60-67 (1924).
[5] R. M. Bozorth, Ferromagnetism, D. Van Nostrand Co., Inc., New York (1951).
[6] T. Nagata, Rock Magnetism, Maruzen Co., Ltd., Tokyo (1953).
[7] J. W. Graham, The stability and significance of magnetism in sedimentary rocks, J. Geophys. Res., 54, 131-167 (1949).
[8] L. Néel, Some theoretical aspects of rock magnetism, Adv. Phys. (Quarterly Supplement of Phil. Mag.), 4, 191-243 (1955).

JOURNAL OF GEOPHYSICAL RESEARCH VOLUME 63, No. 2 JUNE, 1958

3303 A EMISSION FROM SODIUM EJECTED INTO THE UPPER ATMOSPHERE*

BY C. DEWEY COOPER

Physics Department, University of Georgia, Athens, Georgia

AND

EDWARD R. MANRING AND JOHN F. BEDINGER

Geophysics Research Directorate, Air Force Cambridge Research Center, Air Research and Development Command, L. G. Hanscom Field, Bedford, Massachusetts

(Received March 8, 1958)

ABSTRACT

The emission of both 5893 A and 3303 A has been observed from a sodium cloud in the upper atmosphere. The yellow line is at least 100 times more intense than the ultraviolet line. The appearance of the 3303 A line with the observed intensity proves conclusively that the sodium twilight flash results from resonance scattering.

OBSERVATIONS

During the early morning twilight on November 26, 1957, two kilograms of sodium were vaporized [see 1 of "References" at end of paper] from a rocket over an altitude range of 75 to 200 km above Sacramento Peak, New Mexico. The sodium was ejected between 0557 and 0600 MST. The yellow cloud, which was visible for 30 minutes, was tracked with two visible, f/2 and f/2.8, and one ultraviolet, f/2, spectrograph. With the aid of telescopic sights, the spectrographs were directed at the upper portion of the cloud.

In the visible region the only radiation recorded from the cloud on Type 103A-F and 103A-G film, for an exposure time of 20 minutes, was the very strong 5893 A atomic line. In the ultraviolet region, very weak emission lines were observed at 3303 A and 4045 A on Type 103A-O film with an exposure time of 13 minutes. The 3303 A line results from the 4P-3S transition in sodium and the 4045 A line is the corresponding line of potassium. A laboratory spectrographic test of the sodium used for the experiment showed a strong 4045 A line which resulted from an impurity of potassium.

Relative intensity measurements of the 5893 A and 3303 A lines were not accurately determined, because different spectrographs and films were used for the two regions. Also, our tracking of the narrow twisted sodium cloud did not insure that our spectrographic optics were always filled with light. Rough measurements show that the intensity of the yellow line is at least 100 times greater than that of the ultraviolet line.

*This research was supported by Contract No. AF 19(604)1562 with the Air Force Cambridge Research Center.

THEORY AND DISCUSSION

If the 3303 A line resulted from ionic recombination, we would have observed the higher members of the diffuse and strong series in the visible region. If some chemical process excites the 3P level, then only 5893 A could be observed; and if only the 4P level is excited, then the 5893 A line should be about two to three times as intense as the 3303 A line [2]. The resonance scattering theory permits us to calculate the relative intensities of the 5893 A and 3303 A lines, since all of the necessary oscillator strengths are known [3]. We may write:

$$\frac{I_y}{I_v} = \frac{\rho(\nu)_y}{\rho(\nu)_v} \frac{\nu_y}{\nu_v} \frac{B_{3\,S\text{-}3P}}{B_{3\,S\text{-}4P}} \left[\frac{A_{4P\text{-}4\,S} + A_{4P\text{-}3\,S}}{A_{4P\text{-}3\,S}} \right] \exp\left[h(\beta_v - \beta_y)\right]$$

Here the symbols have the following meanings:

I_y	=	ground intensity of 5893 A
I_v	=	ground intensity of 3303 A
$\rho(\nu)_y$	=	energy density per frequency unit at 5893 A
$\rho(\nu)_v$	=	energy density per frequency unit at 3303 A
ν_y and ν_v	=	frequencies of the 5893 A and 3303 A lines
A and B	=	Einstein transition probabilities between the indicated levels
h	=	reduced height of the atmosphere above Sacramento Peak, New Mexico [4]
β_y	=	Rayleigh scattering coefficient [4] for 5893 A, and
β_v	=	Rayleigh scattering coefficient [4] for 3303 A

In deriving the above equation, we assumed:

1. $A_{4P-4\,S}$ is 50 times greater than A_{4P-3D} ; therefore, we can neglect the 4P-3D transition [2].

2. The number of excited 3P levels per second will be proportional to $\rho(\nu)_y B_{3\,S-3P}$ and each will emit a 5893 A photon.

3. The number of excited 4P levels per second will be proportional to $\rho(\nu)_v B_{3\,S\text{-}4P}$ and the fractional portion $A_{4P-3\,S}/(A_{4P-4\,S} + A_{4P-3\,S})$ of these will emit a 3303 A photon.

4. The increase in the number of excited 3P levels which results from the 4P-4S, 4S-3P transitions is small in comparison to those produced by the direct absorption of 5893 A.

The equation is further simplified if we substitute $\rho(\nu) = \rho(\lambda)\lambda/\nu$. The $\rho(\lambda)$ values for the continuum of the sun are listed by Minnaert [5], but they do not include the effects of Fraunhofer absorptions. According to Shane [6], 95 per cent of the 5893 A radiation is absorbed in the atmosphere of the sun. Using his value and the oscillator strengths along with Minnaert values for the continuum, we find the relative energy density to be $\rho(\lambda)_y/\rho(\lambda)_v = 0.063$ for the 5893 A and 3303 A wavelengths when they strike the earth's atmosphere. Using the usual relation between the oscillator strengths and the transition probabilities, we obtain $I_y/I_v = 70$. In these calculations, the theoretical value of $A_{4P-4\,S}/A_{4P-3\,S}$ was 2.1. Berry and Rollefson [2] obtained an experimental value of 3.4 for this ratio. If we use their experimental value, we obtain $I_y/I_v = 100$.

In the above calculations, the scattering of the light before it strikes the sodium

cloud and the ozone absorption has been neglected. It is recognized that the minimum distance of the incoming radiation above the earth will definitely reduce the light intensity in the incident beam. This will tend to reduce the intensity of the 3303 A radiation relative to the 5890 A and probably accounts for our failure to observe the 3303 A line in an earlier experiment [7].

CONCLUSION

The relative intensity of the first two resonance lines of sodium has been calculated assuming resonance scattering of the sunlight from a sodium cloud in the upper atmosphere. These calculations show that the 5893 A line should be at least 70 times more intense than the 3303 A line. Experimentally, the yellow line was measured to be at least 100 times greater than the ultraviolet line. No experimental evidence of ionic recombination in the cloud was observed. The observations of the 3303 A line with an intensity of less than 10^{-2} of the 5893 A line provide conclusive proof that the sodium twilight flash results from the resonance scattering of sunlight.

References

[1] H. D. Edwards, J. F. Bedinger, E. R. Manring, and C. D. Cooper, The Airglow and the Aurorae (edited by E. S. Armstrong and A. Dalgarno), Pergamon Press, Ltd., London (1955); p. 122.

[2] N. E. Berry and G. K. Rollefson, Phys. Rev., **38**, 1599 (1931).

[3] E. U. Condon and G. H. Shortley, The Theory of Atomic Spectra, Cambridge, University Press (1951); p. 149.

[4] H. C. van de Hulst, The Atmosphere of the Earth and Planets (edited by G. P. Kuiper), University of Chicago Press, Chicago (1952); pp. 51 and 55.

[5] M. Minnaert, The Sun (edited by G. P. Kuiper), University of Chicago Press, Chicago (1953); p. 95.

[6] C. D. Shane, Lick Obs. Bull., **19**, 119 (1941).

[7] J. F. Bedinger, E. R. Manring, and S. N. Ghosh, J. Geophys. Res., **63**, 19 (1958).

A STUDY OF THE DISTRIBUTION OF RADON, THORON, AND THEIR DECAY PRODUCTS ABOVE AND BELOW THE GROUND

By Stanley L. Jaki and Victor F. Hess

Fordham University, New York, New York

(Received March 8, 1958)

ABSTRACT

The respective concentrations of radon, thoron, and their decay products have been measured immediately above the earth and below the ground, and a study of their correlation with meteorological conditions has been carried out.

It was found that the concentration of radon and thoron in the vicinity of the earth's surface depends primarily on the dryness of the ground.

Measurements at and below the ground level were carried out by an indirect method, collecting the decay products of radon and thoron on the inner surface of an aluminum cylinder charged to −600 volts.

From November 16, 1956, to May 7, 1957, 239 experiments were made. It was found that the concentration of thoron below the ground seems to reach a maximum value at a depth of about 75 cm, whereas the concentration of radon shows a continuous increase within the range investigated. Comparison with other experiments shows that the cylinder method can be used for investigating the exhalation of both radon and thoron at the surface of the ground. The mean value obtained for radon is 6×10^{-18} curie per cm^2 sec. The measurements presented here give the first data on the exhalation of thoron through the air-soil interface.

I. INTRODUCTION

Among the radioactive substances, radon, thoron, and their decay products are the principal ionizing agents in the lower atmosphere. Since their half-lives are relatively short, their rather constant concentration above the ground must be due to a continuously active replenishing source: exhalation from the ground.

In the past, much work was done on the ionizing effect of radon and its concentration above the ground. Much less attention, however, has been given to thoron. Still the relatively few early results sufficiently substantiated the view that thoron and its decay products contribute somewhat less to the ionization of the atmosphere near the ground than radon and its decay products.

The data concerning the relative amounts of radon and thoron in the soil gas are too scarce to justify a general conclusion.

It seemed, therefore, to be of interest to determine more closely the relative amounts of radon and thoron in the lowest part of the atmosphere and in the soil gas itself.

II. SURVEY OF THE METHODS

There are several methods which can be used for the quantitative determination of the relative concentration of radon and thoron in the atmosphere or in the soil gas. The direct methods are based on the introduction of a known amount of air or soil gas into a large ionization chamber and the subsequent measurement of the ionization produced therein. In the case of an air sample, such procedure is feasible only if the background ionization due to cosmic rays and to the local gamma radiation is considerably reduced. This can be achieved either by surrounding the chamber by at least 10 cm of iron, or by using the differential-chamber technique.

In our experiments, the two following methods were used: for measurements above the ground, the direct air-intake method was found most suitable; for measurements at and below the ground level, a new arrangement of the electrostatic method was devised. Both are described in detail in the following sections.

III. MEASUREMENTS ABOVE THE GROUND

1. *Experimental procedure and theory*

To measure the ionization produced by radon, thoron, and their decay products in the free air at about one meter above the ground,* a very large ionization chamber was used.

Before the introduction of the air sample, the chamber (volume 43.7 liters) was evacuated and then carried to an open field in front of the Physics Building. The opening of the intake-valve was kept at about one meter above ground. In order to protect the amber insulation of the chamber from the effects of water vapor, the air was made to pass through a tube, containing freshly cut small cubes of sodium, as drying agent. To assure proper drying, the filling time was made to last from 10 to 15 minutes. After filling, the chamber was placed in an iron house (wall thickness 10 cm), which was set up in the basement of the Physics Building. The ionization current was measured with a Lindemann electrometer whose fiber system was directly connected to the inner electrode of the chamber. The readings were taken in the following manner. A 3-volt auxiliary battery in connection with a potentiometer and voltmeter made it possible to add any voltage from 0 to -3 volts to the 135-volt sweep voltage. In this way, an opposite charge was induced on the floating needle of the electrometer to keep the needle always at or close to zero potential. Therefore, any insulation leakage of the electrometer was practically eliminated.

The total amount of this compensating voltage ΔV, added to the sweep voltage during the time Δt of reading, is directly proportional to the ionization, q, expressed in ion-pairs/cc/sec. This can be written in the following way:

$$\text{the current } I = C\frac{\Delta V}{\Delta t} = keWq$$

where e = elementary charge, W = volume of the chamber, C = capacity between

*This height was chosen because most atmospheric electrical measurements are made at this level.

the guard-ring system and the inner electrode of the chamber, k = Duane-Laborde correction-factor.† Therefore,

$$q = \frac{C \cdot \Delta V}{300keW \cdot \Delta t}$$

where ΔV is measured in volts and the remaining quantities are given in electrostatic units. The first readings were taken at about three hours after the introduction of the air sample into the chamber. A fraction of q (number of ion-pairs/cc/sec), as measured at about three hours after filling, is due to radon, RaA and RaC.‡ Let this fraction be denoted by x. The remaining part of q is evidently produced by ThC and ThC′.** This can be expressed by the following relationship:

$$q = xq + (1 - x)q$$

The first term of the right-hand side of this equation will diminish with the half-life of radon and the second term with the half-life of ThB. If then a measurement is taken at a time t, about 12 to 24 hours later, the corresponding ionization q' can be expressed by the following equation:

$$q' = xqe^{-\lambda_1 t} + (1 - x)qe^{-\lambda_2 t}$$

where λ_1 = decay constant of radon and λ_2 = decay constant of ThB. Rearranging the terms, one obtains:

$$x = \frac{(q'/q) - e^{-\lambda_2 t}}{e^{-\lambda_1 t} - e^{-\lambda_2 t}}.$$

The value of x expresses the ratio of the ionization due to all the three alpha emitters in the radon branch to the ionization produced by ThC and ThC′ and by radon, RaA and RaC.

Since the number of ions produced by each alpha particle of ThA is 1.92×10^5, of ThC 1.71×10^5, and of ThC′ is 2.54×10^5, while it is 1.23×10^5 for thoron itself, and since ThC′ amounts to 65 per cent while ThC amounts to 35 per cent of the branched products, the average ratio f of the ionization produced by (ThB + ThC) to thoron plus successive products is

$$f = \frac{\frac{1}{2}[(0.35 \times 1.71) + (0.65 \times 2.54)] \times 10^5}{1.23 + \frac{1}{2}[1.92 + (0.35 \times 1.71) + (0.65 \times 2.54)] \times 10^5} = \frac{1.124}{3.315} = 0.339$$

Therefore, if we obtain, for instance, an average of x = 79.5 per cent for the radon family and $(1 - x)$ = 20.5 per cent for (ThB + ThC), the latter value

†Since the alpha rays emitted from points near the wall of the chamber, and moving toward the wall, have not sufficient range to produce the maximum number of ion-pairs, it is customary to include the correction-factor k due to Duane and Laborde (1910). It is given by the empirical formula: $(1 - 0.572A/W)$, where A denotes the inner surface of the chamber. In our case, this factor amounts to 0.905.

‡The beta- and gamma-emitter members of both the radon and thoron branch are not taken into consideration, because their ionizing effect can at the best be estimated to a small fraction, perhaps a few per cent, of the ionization produced by each of the alpha emitters.

**Thoron and ThA decay completely in a few minutes.

would have to be raised if we want to include thoron and ThA, which were not measured, on account of their rapid decay.

The content of radon plus decay products was found to be $67.7 \times 10^{-18} \times 0.795 = 53.8 \times 10^{-18}$ curie/cm^3.

Therefore, the equivalent of thorium products, including thoron, would be

$$\frac{67.7 - 53.8}{0.339} = \frac{13.9}{0.339} = 41.0 \times 10^{-18} \quad \text{equivalent curies per cm}^3$$

The computation of the radon equivalent in curies per cm^3 from the ionization observed one to three hours after filling the chamber is based on values given in Meyer and Schweidler's book on radioactivity (B. G. Teubner, Leipzig, 1927, p. 629): 1 curie (radon) per cm^3 in equilibrium with RaA $\cdots$ RaC would give a saturation current of 2.75×10^6 esu multiplied with a factor $[1.55 + \frac{1}{2}(1.70 + 2.20)]/1.55 = 6.21 \times 10^6$ esu.

The factor $\frac{1}{2}$ has to be used, since the RaA and RaC atoms are deposited on the walls by the electric field and therefore only one half of their ionizing power is effective.

Therefore, the amount of 10^{-16} curie of radon corresponds to

$$\frac{6.21 \times 10^6 \times 10^{-16}}{4.8 \times 10^{-10}} = 1.29\, I$$

("I" denotes the number of ions produced per cm^3 per sec.)

The average "radon equivalent" of atmospheric air at Fordham given below represents practically the annual mean value, since measurements from July 1956 to April 1957 were used for this average.

The percentage of thorium products (ThB + ThC) was computed in all those cases where the total ionization measured was conveniently high so that the effect could be detected at a subsequent time with sufficient accuracy.

In order to obtain the value of the ionization due to radon and its decay products at time zero, measurements were taken also at 48 and 72 hours after filling. By that time, the ThC and ThC′ atoms have decayed to a negligible amount. Therefore, the fundamental radioactive decay law will yield directly the time-zero ionization value due to radon and its decay products.

In the same manner, a set of values can be computed for the difference between the total ionization and the ionization due to radon and its decay products. The resulting values show a decrease with time in accordance with the half-life of ThB. Consequently, the time-zero ionization due to ThC and ThC′ can easily be obtained.

2. *Results of the experiments*

The following Table gives the results of 69 experiments,

TABLE 1—*Results of measurements at one meter above ground*

No.	Date	Time	q	x
	1956			
1	July 2	10.35	1.03	81.0
2	8	11.30	1.25	78.7
3	16	10.00	0.85	80.5
4	21	13.45	0.34	100.0
5	23	10.15	1.20	84.0
6	31	8.00	1.05	80.5
7	Aug. 14	9.00	0.58	100.0
8	20	7.45	1.60	82.5
9	24	14.00	1.15	88.1
10	27	7.45	1.63	94.0
11	30	9.35	0.52	100.0
12	Sept. 1	12.40	0.55	100.0
13	2	13.45	0.43	100.0
14	5	9.15	0.98	85.5
15	9	11.30	0.52	100.0
16	11	9.30	1.45	87.5
17	15	12.30	1.02	87.1
18	18	8.30	0.45	100.0
19	20	12.45	0.48	100.0
20	21	7.30	0.49	100.0
21	27	9.00	0.90	83.5
22	30	12.10	0.94	79.2
23	Oct. 3	14.30	0.92	84.7
24	6	14.30	1.14	77.6
25	10	11.05	1.26	81.6
26	13	9.00	0.95	69.4
27	16	14.30	0.99	60.9
28	19	14.10	0.86	61.2
29	22	13.30	0.84	78.2
30	25	14.30	1.09	93.1
31	28	16.00	0.85	82.8
32	Nov. 4	16.15	0.95	79.3
33	7	16.15	0.81	80.8
34	10	16.15	1.08	91.4
35	13	16.15	0.78	100.0
36	20	15.15	1.01	85.6
37	24	15.15	0.81	83.9
38	28	15.15	1.07	74.1
39	Dec. 4	15.15	0.94	89.5
40	8	15.15	0.82	93.2
41	18	15.00	0.99	85.6
42	26	14.30	0.91	92.5
43	31	14.00	0.56	100.0

Explanation of symbols: q = number of ion-pairs/cc/sec., at time-zero; and x = fraction due to radon and decay products, in per cent.

TABLE 1—*Results of measurements at one meter above ground* (continued)

No.	Date	Time	q	x
	1957			
44	Jan. 2	13.30	0.50	100.0
45	6	14.00	0.94	81.1
46	15	13.30	0.55	100.0
47	19	12.45	0.51	100.0
48	20	14.30	0.49	100.0
49	22	15.30	0.97	86.3
50	26	13.15	0.59	100.0
51	30	16.30	0.95	74.9
52	Feb. 2	15.15	0.56	100.0
53	6	16.15	0.85	71.2
54	12	13.15	0.93	91.3
55	16	9.15	0.70	88.5
56	20	17.00	0.97	89.8
57	25	14.15	1.21	85.5
58	Mar. 3	17.00	1.01	89.3
59	6	16.30	0.82	85.2
60	12	9.15	1.02	80.8
61	18	8.15	1.09	75.7
62	23	14.15	1.12	75.2
63	28	14.30	1.05	93.0
64	Apr. 3	14.15	1.04	80.7
65	11	16.30	1.31	84.3
66	15	9.30	1.25	79.5
67	19	10.00	0.64	100.0
68	22	14.15	1.16	76.3
69	25	13.15	1.28	73.6

Explanation of symbols: q = number of ion-pairs/cc/sec., at time-zero; and x = fraction due to radon and decay products, in per cent.

Several average values of these results are given in the following Table.

TABLE 2—*Average values of measurements at one meter above ground*

Number of exper.	q	x	Weather conditions, when air sample was taken
		per cent	
69	0.91 $\bar{\Delta}$ 0.224 24.6%	86.95	All weather
53	1.02 $\bar{\Delta}$ 0.13 12.75%	83.0	Dry-ground condition: air sample was taken at least 24 hours following the last rainfall
9	0.50 $\bar{\Delta}$ 0.066 13.2%	100.0	During or shortly after rainfall
4	0.54 $\bar{\Delta}$ 0.037 6.85%	100.0	Snow-covered ground
3	0.54 $\bar{\Delta}$ 0.023 4.27%	100.0	Frozen ground

Explanation of symbols: $\bar{\Delta}$ = mean deviation from the average value, both in absolute and in percentage units.

3. *Discussion of the results*

The above data show clearly that the ionization obtained in fair weather is about twice the amount of that observed in rainy weather, or under typical winter conditions, such as with snow-covered or frozen ground.

Since the average variation of x is small when the ground is sufficiently dry, both thoron and radon have a rather constant concentration in the vicinity of the ground under such a condition. The variation of the concentration of radon in rainy or typically winter weather was also small.

(*a*) *Effect of meteorological factors*

The effect of rain is rather complicated. By clogging the capillaries of the earth, the rain prevents the diffusion of soil gas into the atmosphere. Consequently, the radon and thoron present in the air continue their decay without being replenished from the earth. Evidently the amount of thoron diminishes rapidly and drops within a few minutes to a negligible quantity. Because of the greater half-life of radon, the change in its amount would not be significant for the first few hours after rain started. The increased turbulence caused by the falling droplets, however, produces a greater mixing effect in the lower layers of the atmosphere, where even under normal conditions the concentration of radon falls to half of its ground-level value in 13 meters (Priebsch, 1931). Samples taken during rainfall show

clearly the large decrease in the total ionization and the absence of thoron in the air (experiments 11 and 12).

The clogging of the capillaries persists for 10 to 20 hours, even after not particularly heavy precipitation. This was clearly observed with samples taken in such periods of time. No thoron activity was detected in such cases, and similarly the radon content was rather small.

Samples taken at least 24 hours after rainfall show the reappearance of thoron activity, together with an increased radon content.

When rainy days are followed by a longer period of dry weather, as in October of 1956, it appears that the maximum ionization is reached four to six days after the precipitation ended. Evidently a dry period of four to six days opens the capillaries to such a depth that the soil gas accumulated in the lower layers can escape and in the subsequent days a lower rate of exhalation sets in (experiments 25 to 28).

Snow and frozen ground—There are two other specific winter phenomena, which prevent effectively the escape of radon and thoron into the free air: the freezing of the ground and the snow. Samples taken under such circumstances show again a lower total ionization and the complete absence of thoron in the air (experiments 43, 44, 46-48, 50, and 52.). It is true that freshly fallen snow displays a much greater activity than rain (Jaufmann, 1905), but the decay curves show only the presence of RaA, RaB, and RaC, which act as condensation nuclei. Consequently, freshly fallen snow does not carry along radon atoms from the higher layers of the atmosphere to compensate in this way for the diminution of radon near the ground caused by the clogging of the capillaries. On the other hand, it was found that snow laying on the ground contains radon arising from the soil (Jaufmann, 1905). This fact indicates also how effectively the snow prevents the passage of soil gas into the air.

(*b*) *Comparison with data obtained with other methods*

Former determinations of the relative concentration of radon and thoron in the air near the ground were made most often with the electrostatic method. Their results are usually given as the ratio of the number of radon and thoron atoms. The computation of this ratio is based on the law of equilibrium: $N_1/N_2 = \lambda_2/\lambda_1$.

When the same amount of ionization is produced by the decaying radon and thoron atoms, the concentration of the radon atoms is 6,950 times greater than that of the thoron atoms. This number is obtained by taking into account the number of ion-pairs produced by the alpha particles emitted by thoron and radon atoms (1.78×10^5 and 1.55×10^5, respectively). Therefore,

$$\frac{\text{Number of Rn atoms}}{\text{Number of Th atoms}} = \frac{1.27 \times 10^{-2}\ \text{sec}^{-1} \times 1.78 \times 10^5}{2.097 \times 10^{6}\ \text{sec}^{-1} \times 1.55 \times 10^5} = 6{,}950$$

The results of most of the early experiments of other authors, however, cannot be safely used for comparison, because they are based only on a fractional collection of the radioactive elements in the air. Furthermore, the collecting wire was usually exposed at 6 to 10 meters above ground, where the concentration of thoron is only a very small fraction of that at one meter above ground. Only one set of

experiments was carried out with a wire extended at 1.5 meter (Kinoshita, 1910). The mean value of these measurements indicated 6,500 radon atoms for each thoron atom.

The experiments of Aliverti (1932), based on an improved form of Sella's apparatus, indicated a smaller thoron content of the air in Torino: 19,000 radon atoms for each thoron atom. The air samples were taken at one meter above ground.

Macek and Illing (1934) obtained the number 45,000 in Innsbruck. This very small thoron content was observed in air samples taken at 0.5 meter above ground. In fact, only 25 per cent of the samples yielded a measurable thoron content.

Among other early experiments, the work of Eve (1911) offers the most reliable data for comparison. He measured the concentration of radon and thoron in a large container with a volume of 18.7 cubic meters filled with fresh air at one meter above ground. According to him, 61.8 per cent of the total ionization in the air samples is due to radon and its decay products.

On the basis of theoretical considerations, Hess (1934) calculated that radon and its decay products account for about 62 per cent of the ionization of the air by radon, thoron, and their decay products at one meter above ground. The experiments carried out by himself (1953) and with Vancour (1950) provided an excellent confirmation of this view.

IV. MEASUREMENTS AT AND BELOW THE GROUND

1. *Experimental procedure*

In the second group of experiments, an attempt was made to determine the respective amount of thoron and radon at the ground and in the soil gas. The area investigated was that of the Seismic Garden, adjacent to the Physics Building of Fordham University.

The indirect or electrostatic method was used in the following arrangement: an aluminum sheet (20 × 42 cm) was bent into the form of a cylinder and placed into a circular pit of 25 cm in diameter, the lower edge of the cylinder being about 4 cm from the bottom of the pit. A glass rod, which served also as an insulator, supported the cylinder charged to −600 volts. This voltage was provided by a battery of dry cells. The pit was covered by an asbestos plate and a sheet of aluminum to keep its temperature close to that of the surrounding ground and to protect it from the disturbing effects of rain and wind. The electric field in the interior of the cylinder was made uniform by a brass rod, mounted vertically at the center of the bottom of the pit. A number of such pits, 25, 50, and 75 cm deep, were used.

When measurements were taken at the surface of the ground, a somewhat different arrangement was used: the cylinder was supported by a small metal stand and insulated from it by a piece of hard rubber. A central brass rod completes the experimental set-up, which is protected from rain and wind by a cone-shaped iron cover.

Such an arrangement has several advantages: by eliminating the disturbing air-currents, it can operate with a relatively small voltage. Furthermore, no undue accumulation of soil gas is taking place in the pit, since the asbestos plate does not close it air-tight. Finally, no pumping is needed to collect the sample and therefore

the natural diffusion rate of the soil gas at the bottom of the pit is not changed.

Radon and thoron diffusing through the capillaries of the soil find their way into the space surrounded by the cylinder and decay there subsequently. It is well established that the decay products RaA and ThA are positively charged immediately after being produced by the alpha emission of radon and thoron. Consequently, they are drawn toward the negatively charged cylinder by the field. The average potential gradient in the pit was 100 volts/cm.

The RaA and ThA atoms being deposited on the cylinder undergo subsequent disintegrations, and after a certain time an equilibrium state is established. The time required to reach this equilibrium state is about four hours for RaA and its decay products, and about 48 hours for ThA and its decay products. Furthermore, the amounts deposited on the cylinder in two days are within one per cent of the maximum amount which would be obtained after an infinite time of exposure (Kurz, 1909). Accordingly, the cylinders were kept exposed for at least two days.

2. *Technique and theory of the measurements*

Since during the measurements the cylinder is pressed against the wall of the ionization chamber, only the decay products deposited on the inner surface of the cylinder produce ionization in the chamber. The radius of the chamber was sufficient to obtain the maximum ionization due to alpha rays. The corresponding effect of the beta and gamma rays was again, as in the former set of experiments, considered negligible.

The ionization was measured with a vibrating-reed electrometer together with an Esterline-Angus self-recording instrument, and recorded continuously for at least four hours in each case. Out of the four operating ranges, only two (100 mv, 1,000 mv) were used with a 10^{12}-ohm input resistance.

The ionization due to radon and thoron and their decay products was computed in the following way: both groups of decay products on the cylinder are assumed to be in equilibrium at the beginning. If the ionization due to one of these substances in each branch can be determined at a certain time, the corresponding time-zero value can easily be obtained. From this time-zero value of the ionization due to that particular substance, the total ionization of all the alpha emitters in that branch can be derived, since the respective alpha energies are known, and in the equilibrium state the number of atoms decaying per second is the same for each subsequent decay product.

The differential equations concerning the case when RaA, RaB, and RaC, being in equilibrium at time zero, are separated from their radon source and left to decay, are well known.

RaA decays completely in 15 minutes, and only RaC remains active as an alpha emitter for one to three hours. The solutions show that the number of RaC atoms, and consequently the ionization due to RaC atoms at 35 minutes,* is only 76.6 per cent of the time-zero value. The value of the ionization by RaC atoms at 35 minutes is obtained from the ionization curve recorded on the Esterline-

*This time was chosen, because usually it took about five minutes to transfer the cylinder from the pit into the ionization chamber and to start the recording of the ionization current. Therefore, at 35 minutes, the recording was already 30 minutes in progress.

Angus chart in the following way: since after four hours all the RaC atoms have decayed, the remaining ionization is due to the alpha emitters ThC and ThC′, which decay with the half-life of ThB. Therefore, subtracting the background ionization from the total ionization at four hours, the ionization due to ThC and ThC′ is obtained and the time-zero and the 35-minute values can be computed from the exponential law of decay. The difference between the total ionization at 35 minutes minus the background ionization, and the ionization due to ThC and ThC′ at the same time, yields the corresponding ionization value of the RaC atoms.

The ratio of the number of ion-pairs produced by alpha particles emitted by RaC atoms to the number of ion-pairs produced by the alpha particles emitted by Rn, RaA, and RaC is 0.314. Therefore, if the time-zero value of the ionization due to RaC is divided by 0.314, the total ionization by radon and its decay products is obtained. In a similar way, the time-zero value of the ionization due to ThC and ThC′ should be divided by 0.339, to get the ionization due to thoron and its decay products.

Such a procedure is based, as it was stated before, on the assumption that the state of equilibrium is reached on the collecting cylinder between ThA, RaA, and their respective decay products. Our experiments provided clear evidence that this assumption is correct.

Since the half-lives of RaA, RaB, and RaC do not differ too much, their respective amount present on the cylinder at the end of the exposure is of the same order of magnitude. Consequently, the number of the alpha-emitter RaC atoms whose ionization is measured is a function also of the RaA and RaB atoms present at any time. Therefore, the number of RaC atoms diminishes not simply with the half-life of RaC (19.7 m), but in the well-known more complicated way.

3. *Results of the measurements*

From November 16, 1956, to May 7, 1957, 229 measurements were carried out. Their results are listed in the following Table.

TABLE 3—*Average values of the measurements taken at and below the ground at five locations (A to E)*

Level		Location of the pits				
		A	*B*	*C*	*D*	*E*
0 cm	*T*	4.90	5.97	6.68	5.42	5.70
	R	1.21	0.80	2.02	1.10	1.27
	I	6.11	6.77	8.69	6.52	6.97
	X	19.80%	11.82%	23.25%	16.87%	18.22%
	N	(10)	(10)	(10)	(11)	(10)
25 cm	*T*	17.32	12.26	24.81	29.43	15.72
	R	2.92	5.17	19.53	5.42	2.94
	I	20.24	17.43	44.34	34.85	18.56
	X	14.43%	29.66%	44.04%	15.55%	15.84%
	N	(32)	(16)	(12)	(22)	(12)
50 cm	*T*	31.04	12.31	26.68	38.06	20.65
	R	31.43	12.40	41.02	13.40	10.15
	I	62.47	24.71	67.70	51.46	30.80
	X	50.31%	50.18%	60.59%	26.04%	32.95%
	N	(10)	(23)	(10)	(10)	(10)
75 cm	*T*	.....	12.73	33.33	.....	.....
	R	.....	24.82	73.45	.....	.....
	I	.....	37.55	106.78	.....	.....
	X	.....	66.09%	68.79%	.....	.....
	N	.....	(11)	(10)	.....	.....

Explanation of symbols: T = the average time-zero ionization due to thoron and its decay products; R = the average time-zero ionization due to radon and its decay products; I = the average total time-zero ionization; $X = R/I$; and N = the number of measurements taken in a given pit. All ionization values are given in units of 10^{-14} amp.

4. *Discussion of the results*

(*a*) *Effect of change in depth*

The measurements indicate that the total ionization increases linearly with depth. But the thoron and radon components of the total ionization do not increase with depth in the same manner. The thoron content tends to approach a maximum value at a depth of about 75 cm (see Fig. 1), whereas the increase of the radon content with depth (see Fig. 2) shows no such indication within that range.

It seems that thoron, because of its short half-life, decays before it can be carried away too far in the capillaries by the soil gas. Therefore, all the decay products of thoron, collected on the inner surface of the cylinder, are due to thoron which is contained in the soil gas diffusing from a thin layer of soil at the bottom of the pits. It is reasonable to assume that such a thin layer would contain the same amount of thorium X at different depths in a uniform soil. Consequently, it is not surprising that the maximum thoron content of the soil gas is attained at about 75 cm below ground.

The change of the concentration of radon with depth was extensively analyzed on theoretical grounds (Israël-Köhler and Becker, see "Reference" at end of

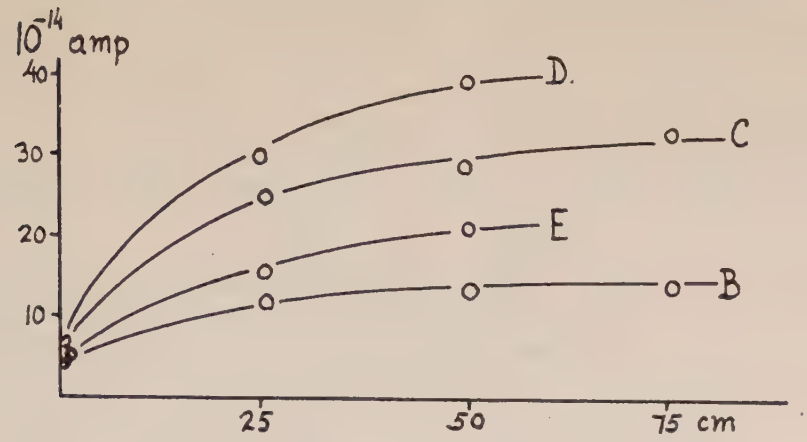

FIG. 1—Variation of the ionization by thoron with depth

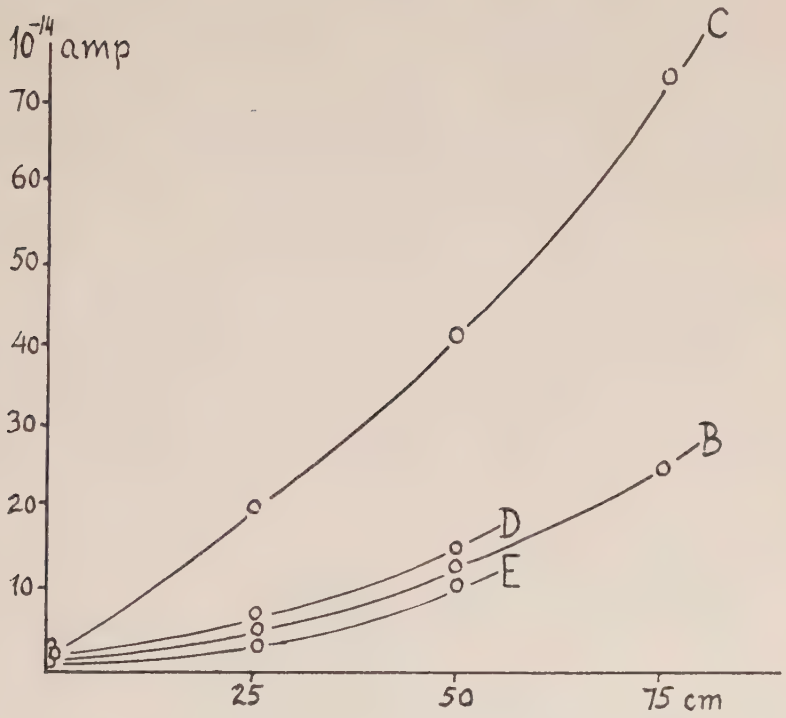

FIG. 2—Variation of the ionization by radon with depth

paper). Assuming a rather thick (15 to 20 meters) uniform soil, the concentration of radon would reach its maximum at about 8 meters below the surface of the ground. Between the surface and the 8-meter level, the concentration of radon would change according to the following pattern.

An increase of the concentration of radon for the first meter would be followed by a linear increase down to about 6 meters. From there on, the maximum value would be approached asymptotically. The slight concave curvatures shown by

the radon lines in Figure 2 agree very well with the above-mentioned pattern within the first 75 cm.

Since Israël-Köhler and Becker carried out only a few measurements, our experiments seem to be the first detailed confirmation of their conclusions, at least within the indicated range. Continuation of the measurements with the cylinder method at deeper levels could provide interesting data in this respect.

(b) *Effect of the quality of the soil*

The results show an evident variation of both the total and the relative amounts of radon and thoron in the soil gas at the same levels at different places (see Figs. 1 and 2). The upper layers of the Seismic Garden consist of a mixture of humus, clay, and sand, occurring at different ratios from place to place. This is due to leveling and gardening work done there prior to the last ten years. The pits of group *C* are located in an area consisting mostly of humus, whereas there is more clay and sand in the area where groups *B* and *E* are located. Since it is known that clay and sand contain much less radium and thorium X than ordinary top soil, such as humus (Satterly, 1911), the considerably smaller amounts of thoron and radon in the areas *B* and *E* can easily be accounted for.

Furthermore, different soils show different porosity. Since the porosity of the ground is greater in humus, such a soil permits a more unimpeded circulation of radon. This would explain the larger amount of radon observed in the pits of group *C*.

(c) *Effect of meteorological factors*

Meteorological factors have an effect on the capillaries of the soil and this, in turn, influences the radon and thoron concentration in the soil gas below the surface. Therefore, one would expect fluctuations in the radon and thoron content. These fluctuations can most suitably be expressed in terms of the mean deviations from the average value of all the measurements taken in a given pit. The following Tables list these values expressed as the percentage of the corresponding average values.

TABLE 4—*Mean percentage deviations of the time-zero ionization due to thoron and its decay products*

Level	Location of the pits				
	A	*B*	*C*	*D*	*E*
cm	*per cent*	*per cent*	*per cent*	*per cent*	*per cent*
0	26.6	20.2	19.8	16.1	17.2
25	19.7	19.8	14.6	14.2	15.3
50	7.6	27.5	15.6	16.5	14.7
75	....	22.2	9.3	....	....

TABLE 5—*Mean percentage deviations of the time-zero ionization due to radon and its decay products*

Level	Location of the pits				
	A	*B*	*C*	*D*	*E*
cm	*per cent*	*per cent*	*per cent*	*per cent*	*per cent*
0	55.2	43.8	41.0	30.7	43.3
25	61.1	49.4	23.6	51.7	40.6
50	41.7	39.3	18.3	28.1	16.2
75	....	33.5	17.9	....	....

In general, the concentration of thoron in the soil gas shows much smaller variations than the concentration of radon. This is due to the fact that thoron cannot diffuse to as great a distance as can radon. Were not this the case, the concentration of thoron would be affected just as much by the changing conditions of the capillaries as is the concentration of radon.

Snow and frozen ground tend to close the capillaries at the surface of the soil and prevent the escape of the soil gas into the free air. As a result, the amount of radon and thoron increases below the surface. Since the half-life of radon is much longer than that of thoron, a larger maximum value can be expected for radon than for thoron. Under such circumstances, increases of as much as 100 per cent have been observed in the mean value of radon content. The corresponding increases of the thoron content were not found to be greater than 40 per cent.

Rain soon clogs the capillaries, even at a depth of 25 cm, and produces a sharp 75 to 100 per cent drop in the radon content at that level. The same is also true for quickly melting snow. The thoron content is again much less affected. This may explain that the largest mean percentage deviations of the radon content occurred always in the 25-cm deep pits.

Similar effects were observed in the 50- and 75-cm deep pits only when the precipitation was very heavy. In these pits, a normal precipitation increased the amount of radon usually by about 50 per cent.

The clearing of the capillaries is evidently hastened by stronger wind and higher temperature, which increase the rate of evaporation of water. By this process, the clogging of the capillaries is removed. Consequently, the radon, which is the product of radium salts previously dissolved in the precipitation, finds an easier way to escape when these solutions evaporate.

(*d*) *Effect of voltage applied*

It is well known that in free air the amount of decay products collected on a negatively charged wire varies according to the voltage applied and reaches a maximum only with 10 to 15 kilovolts (Kurz, 1909). But in the pits, well protected from disturbing air currents, no similar variation with voltage was observed. As a result of 63 experiments, it was found that no more radioactive matter is collected on the cylinders when the voltage is increased from −600 volts to −6,000 volts.

Aside from the magnitude of the voltage, its polarity also deserves discussion. Experiments carried out under various conditions show that positively charged

plates collect only a very small quantity of the decay products of radon and thoron. The fact that these decay products, due to alpha emission, become immediately positively charged has not yet been fully explained. Neither did our experiments yield any clue for a possible explanation. Perhaps the best approach to the satisfactory explanation should take into account the fact that the energies corresponding to nuclear decay are so large compared to the energies of the valence electrons that it is quite easy for these electrons to be stripped off in the process. This otherwise plausible explanation fails to account for the fact that RaC and ThC, ThC′ atoms are not collected on the negatively charged plate, like RaA and ThA. Otherwise the observed decay curves would have a different shape.

(e) *Comparison with data obtained with other methods*

By the cylinder method, only that amount of the decay products of radon and thoron is collected which is due to radon and thoron diffusing naturally through the bottom of the pits or through the surface of the ground. Therefore, the results obtained indicate the amount of radon and thoron at the corresponding spot. It is of interest to know how they compare with results obtained with other methods.

Several experiments were carried out in the past to determine the amount of radon exhaled through the air-soil interface. The rather recent experiments of Cullen (1951) at Fordham University yielded a mean value of 5×10^{-18} curie/cm^2/sec. An estimate of the average exhalation of radon from the surface can be arrived at in the following way: In our experiment, the average value of the saturation current produced by the deposit of RaA + RaB + RaC on the aluminum cylinder, at the ground level, was 1.28×10^{-14} amp $= 3.84 \times 10^{-5}$ esu. One curie of radon alone gives a saturation current of 2.75×10^{6} esu, and in equilibrium with (RaA + $\cdots$ + RaC) 6.21×10^{6} esu. The difference, 3.46×10^{6} esu, corresponds to the activity produced by (RaA + RaC). Therefore, our value corresponds to

$$\frac{3.84 \times 10^{-5}}{3.46 \times 10^{6}} = 1.11 \times 10^{-11} \quad \text{curie}$$

Assuming that this activity is collected on the aluminum cylinder in four hours (14,400 sec), the total activity collected per second would be $1.11 \times 10^{-11} : 14{,}400 = 0.877 \times 10^{-15}$ curie per second coming from an area of 146 cm^2 (surface of the bottom of the pit corresponding to the cross-section of the activated cylinder).

The mean exhalation rate of the soil in the Seismic Garden at Fordham, therefore, is

$$\frac{0.877 \times 10^{-15}}{146} = 6 \times 10^{-18} \quad \text{curie per cm}^2 \cdot \text{sec}$$

which agrees with the direct measurements of Cullen.

Our experiments on the surface of the ground yielded a rather novel result: the preponderance of thoron over radon in the soil gas passing through the air-soil interface. The mean value of the fraction X* at the five points on the surface where measurements were taken is 18.0 per cent; on the other hand, the mean value of the fraction X is 62.3 per cent at one meter above ground. The difference

*The fraction X denotes the percentage of radon products in the total activity collected.

between these two values is explained by the decrease of the concentration of thoron in the air in the first meter elevation. As Priebsch (1931) has shown, the concentration of thoron at one meter drops to about one-eighth of its value at one cm above ground, whereas the change in the concentration of radon is negligible within the same range. Consequently, the fraction X will change from 18 per cent to about 60 per cent with a change in height of one meter, in very good agreement with our measurements.

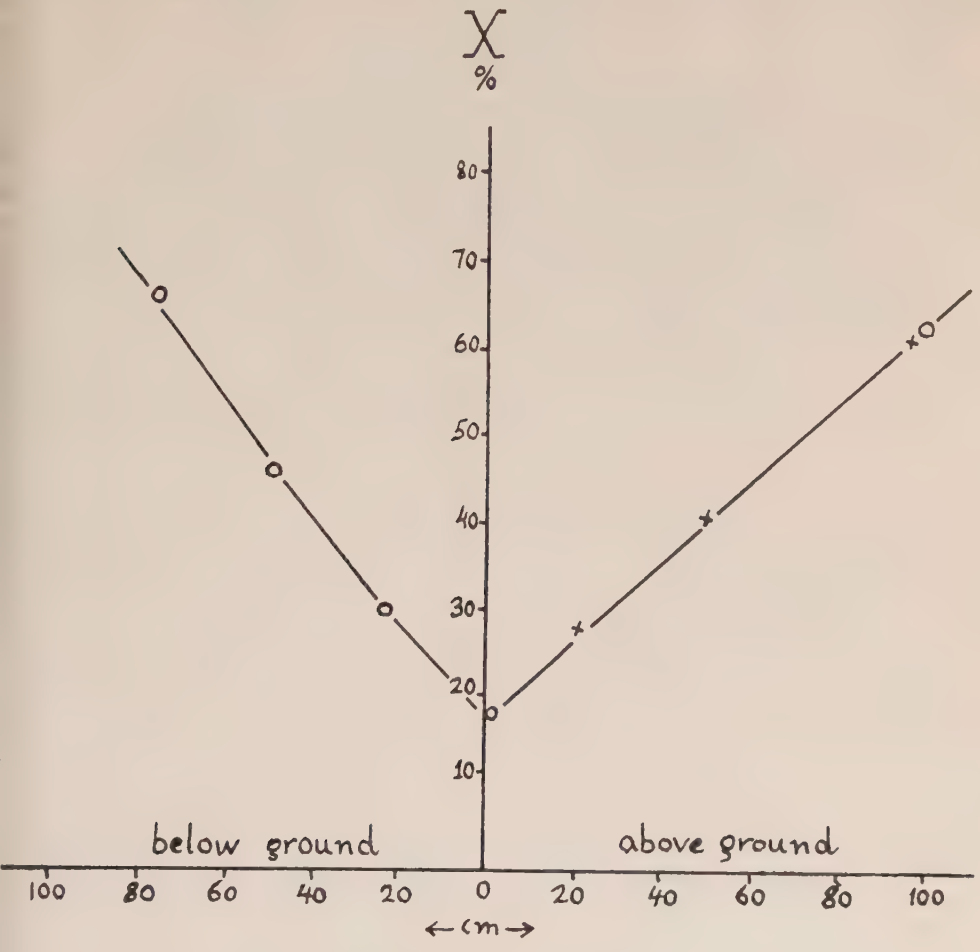

FIG. 3—Variation of the fraction X below and above the ground

Using the results obtained by Priebsch with respect to the drop of the concentration of thoron in the air at 20 cm and 50 cm above ground, the variation of the fraction X above ground can be plotted. These values are shown in Figure 3, together with the values of the fraction X below the ground as measured by the cylinder technique. This new comprehensive picture shows that the fraction X has its minimum at the surface level and increases linearly in both directions within the range investigated.

References

[1] G. Aliverti, Nuovo Cimento, 8, 233 (1931); and **9**, 313 (1932).
[2] T. L. Cullen, Thesis, Fordham University, New York, N. Y. (1951).
[3] W. Duane and A. Laborde, Paris, C.-R. Acad. sci., **150**, 1421 (1910).
[4] A. S. Eve, Phil. Mag., **10**, 98 (1905); **14**, 724 (1907); and **21**, 26 (1911).
[5] V. F. Hess, J. Atmos. Terr. Phys., **3**, 172 (1953).
[6] H. Israël-Köhler and F. Becker, Beitr. Geophysik, **48**, 13 (1936).
[7] S. Kinoshita, S. Nishikawa, and S. Ono, Phil. Mag., **22**, 821 (1911).
[8] K. Kurz, Habilitationschrift, University of Munich (1909).
[9] O. Macek and W. Illing, Beitr. Geophysik, **43**, 388 (1935).
[10] J. Priebsch, Physik Zs., **32**, 622 (1931).

JOURNAL OF GEOPHYSICAL RESEARCH VOLUME 63, No. 2 JUNE, 1958

THE ROLE OF *F*-LAYER TILTS IN DETECTION OF AURORAL IONIZATION

BY SIDNEY STEIN*

Radio Propagation Laboratory, Stanford University, Stanford, California

(Received December 21, 1957)

ABSTRACT

An important ionospheric mode for detection of powerful long-range auroral reflections at Stanford depends upon appropriate tilts in the *F* layer to the north. Auroral reflections received *via* this mode have been reported as originating from prevalent, strongly reflecting ionized structures at great heights, between 300 km and 1,200 km above the surface of the earth. This interpretation is rejected as a plausible explanation of the radio data. An explicit distinction is made between these auroral reflections and newer classes of radio reflections observed at high and middle latitudes arising from field-aligned ionization in the *E* and *F* regions.

I. INTRODUCTION

Ground-backscatter equipment at the relatively low geomagnetic latitude of Stanford has registered a great number of radio reflections from the northern auroral zone attributable to ionization associated with the aurora [see 1 and 2 of "References" at end of paper]. These auroral reflections appear on low-power ionospheric radars operating on radio frequencies between 6 Mc and 30 Mc. The relationship of Stanford (geomagnetic latitude of 43.8°) to the auroral zone permits many effective ionospheric propagation paths, some of considerable complexity, into the heart of the auroral zone, paths by which auroral reflections may be received. Indeed, auroral reflections may be received at any point on the earth's surface *via* suitable ionospheric propagation modes.

Out of the great number of possible ionospheric modes for detection of auroral ionization, this paper will examine one particular mode that is peculiarly important because of the unusual properties ascribed to auroral ionization detected *via* this mode. This particular mode depends upon the occurrence of appropriate tilts in the *F* layer to the north of Stanford. Auroral reflections propagated *via* this mode have been reported as originating from prevalent, strongly reflecting ionized structures at great heights, between 300 km and 1,200 km above the surface of the earth [2]. Furthermore, it has been proposed that primary auroral particles spiraling in along the earth's magnetic field lines are responsible for these ionization formations [2]. While these auroral reflections do give the appearance of originating high

*Now at the Ionosphere Research Laboratory, The Pennsylvania State University, University Park, Pennsylvania.

above the F layer in the outer atmosphere of the earth, this paper will show that they are, nevertheless, comprehensively explainable in terms of auroral ionization in the E region over the auroral zone—provided the consequences of reflection from a tilted F layer are not neglected. What appear to be prevalent, strongly reflecting ionized structures at great heights above the surface of the earth are explainable as the virtual images of auroral structures in the E region mirrored in the tilted reflecting F layer. The implications of this result on other ionospheric phenomena will be discussed.

II. THE ROLE OF F-LAYER TILTS

The deviation of an ionospheric layer from spherical symmetry, often expressed as horizontal gradients of ion density or simply as layer tilts, can have a first-order effect on oblique radio propagation as a consequence of the sphericity of the earth [3, 4]. Low-angle rays reflected from a properly oriented, sufficiently tilted ionospheric layer do not impinge upon the ground, but pass over the earth's surface and illuminate the ionosphere again. Such rays may be reflected several times before encountering a region of reduced ion density in the layer and escape into space. On the other hand, a group of rays may encounter a properly oriented layer tilt so that a restricted region on the earth's surface is illuminated. Trajectories which terminate on the earth's surface are designated ${}^{n}X$, where n is the number of layer reflections and X is the ionospheric layer involved. Detection at a middle-latitude station, such as Stanford, of auroral ionization in the E region over the auroral zone *via* an ionospheric mode involving one F-layer reflection, as shown in Figure 1, is of principal importance in this study, irrespective of whether another ionospheric reflection occurs further out. This type of mode is called ${}^{1}F$.

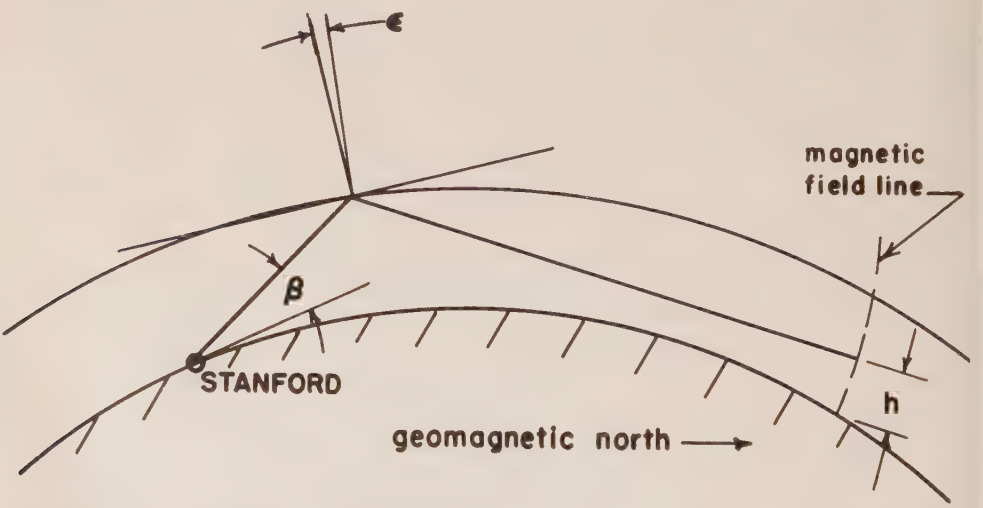

FIG. 1—Geometry of ${}^{1}F$ mode. F-layer reflection is simulated by tilted mirror reflection.

Observations of auroral ionization on VHF normally occur by line-of-sight and consequently do not incur the uncertainties inherent in ionospheric propagation. But even on VHF, auroral phenomena are complex. Results to date have

produced a surprising conflict of ideas as to the proper interpretation of the basic radio data [5, 6, 7, 8, 9]. Nevertheless, some widely but by no means universally accepted interpretations have emerged to explain major characteristics of auroral reflections. Basic properties of reflecting auroral structures appear to be their alignment to a greater or lesser extent along the magnetic field lines of the earth and their principal occurrence at E-region heights [8, 10].

Radiation reflected from a tilted F layer generating ^1F rays illuminates a far larger volume of the E region at longer distances from the transmitter site than is possible by downcoming radiation that has been reflected from a spherically symmetric F layer. The structure of the F layer north of Stanford is often appropriate for illumination of the E region over the auroral zone *via* ^1F propagation, principally as a consequence of the increased obliquity of the sun's rays as the polar region is approached. If ^1F rays make perpendicular intersection with the magnetic field lines of the earth in the E region over the auroral zone, then auroral echoes are anticipated at the transmitter site *via* this propagation mode.

The essential character of the geometry of intersection between the earth's field lines and ^1F trajectories from Stanford can adequately be shown with the following gross simplifications: First, F-layer reflection is simulated by mirror reflection at a constant height of 350 km; the deviation of the ionospheric layer from spherical symmetry is approximated by a tilt of the mirror. Second, the axis of tilt is kept perpendicular to the plane of propagation. Consequently, the geometrical path lies entirely within a plane containing the center of the earth, intersecting a great circle on the earth's surface. Third, the terrestrial magnetic field is assumed adequately represented by a dipole field. Fourth, the plane of propagation is taken as the meridian plane (propagation in the geomagnetic-north direction), the plane containing the geomagnetic pole and the station site. In addition, the geometry of intersection for paths with two-layer reflections and an intervening ground reflection, called $1F^1F$ (tilts are introduced only at the second mirror reflection point), has also been investigated. Figure 2 presents the loci of perpendicular intersection for the ^1F and $1F^1F$ modes.

Each mode has a family of curves generated by using the tilt angle as a parameter; equal take-off angles are connected by broken lines. The altitude of perpendicular intersection between a ray and a magnetic field line is plotted against the slant range of the geometrical path from the station to the intersection. Two "cut-off" curves are introduced into the graphs: "pole cut-off" terminates the ray at the geomagnetic pole; "ground cut-off" eliminates those rays which strike the earth.

Both the ^1F and $1F^1F$ modes provide exact-perpendicular intersection within the E region over the auroral zone. An 8° take-off ray after F-layer reflection has its perpendicular intersection at an altitude of 120 km for a tilt of 2°; at 80 km for a tilt of approximately $1\frac{1}{2}$°. The corresponding slant ranges of the geometrical paths are 3,981 and 4,060 km, respectively. Rays with intervening ground reflection propagate long distances into the north and consequently require larger tilts to make a perpendicular intersection on the station side of the pole. By ray tracing through a realistic ionospheric model, it can be established whether tilts of the right order of magnitude occur. Alternatively, if auroral reflections are shown to be received by way of ^1F rays, then tilts of the order of 1° to 2° may be inferred.

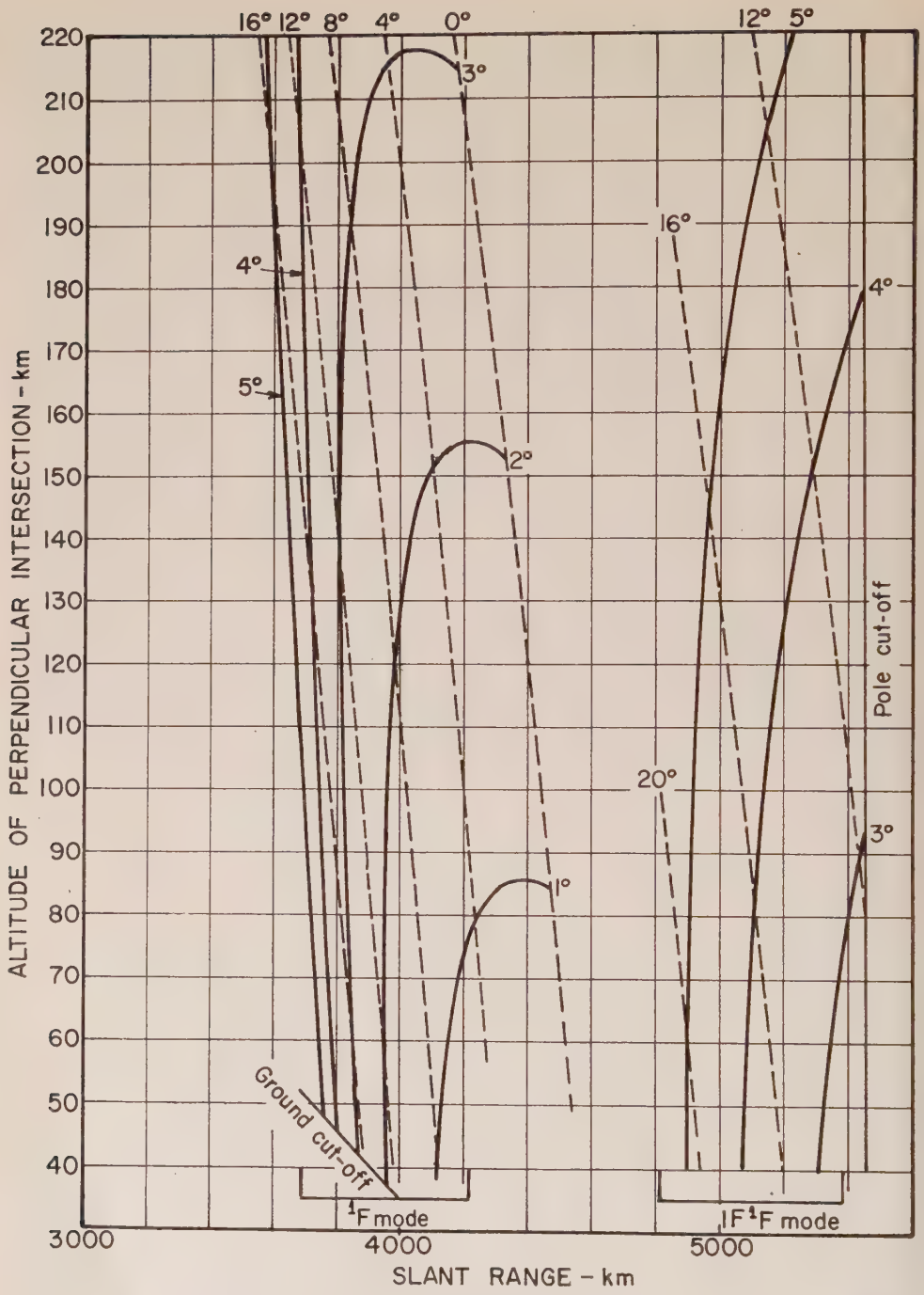

FIG. 2—Loci of exact-perpendicular intersection for ^1F and $1F^1F$ modes: constant mirror reflection height at 350 km; station site at geomagnetic latitude 44.8°; propagation in the geomagnetic-north direction. Solid lines connect equal tilt angles; broken lines connect equal take-off angles.

The latter alternative has been chosen in the present study since the character of the given class of auroral reflections does give important and discernible clues as to the mode of propagation, clues that initiated great interest in the effects of layer tilts on long-range radio propagation.

The part of the reflected ray system that misses the earth, the ^1F rays, cannot return ground backscatter unless another ionospheric reflection occurs further out. The earth is illuminated at grazing angles by energy leaving the transmitter at slightly greater take-off angles than for the ^1F rays, unless the skip ray is fortuitously ^1F also. The part of the ray system that is intercepted at grazing angles by the ground is ineffective in giving detectable ground backscatter because of the rapid change in path length across the ground. PPI scans showing no ground backscatter in the direction of an auroral reflection at ranges of the order of 4,000 km are consistent with the interpretation of ^1F propagation. However, a sufficiently dense layer, with or without horizontal gradients, will give detectable ground backscatter near the skip distance since equivalent tilts have a gross effect, as far as equivalent path lengths are concerned, only on low take-off rays.

Ground-reflected rays at grazing incidence on the earth's surface do not make a perpendicular intersection with magnetic field lines in the E region for propagation northward from Stanford; grazing rays impinge upon the ground at latitudes greater than 70°. An undeviated ray from the ground at latitude 70° cannot make perpendicular intersection with the field lines above an altitude of 50 km [13]. From this consideration, it is expected that grazing ground-reflected rays would not be effective for ionospheric detection of auroral ionization. However, the grazing ground-reflected rays and the ^1F rays simultaneously illuminate a common region forming a radar multipath. The assumption of a near-perpendicular requirement between the ionospheric path and the magnetic field lines implies that the outgoing and incoming paths are nearly *coincident*. Furthermore, energy impinging on an auroral target may be strongly scattered in other than the direction of arrival. For the geometry and long ranges involved in ^1F propagation, slight deviations in backscatter angle can easily couple the energy into the grazing ground-reflected mode, and *vice versa*. Whatever the statistical occurrence of each case, however, it is horizontal gradients that are instrumental in providing strong illumination at grazing angles. Of interest is the fact that ^1F rays may remain entirely above and avoid the long path through the polar D region encountered by grazing ground-reflected rays [4].

Auroral reflections are often detected at great ranges, slant ranges up to 5,000 km, without any detectable intervening ground backscatter between ground-zero and the place of occurrence of the echo on the PPI. It is clear that if powerful long-range auroral reflections are received *via* ^1F (or coupled ^1F and grazing ground-reflected) paths without any intervening ground backscatter, then an analysis based upon a spherically symmetric F layer, that is, neglect of F-layer tilts, must necessarily conclude that these auroral reflections result from ionized structures high above the F region. (See section IV.)

III. BACKSCATTER OBSERVATIONS

Typical examples of auroral reflections without ground backscatter are shown

in Figure 3, a sequence of 17.31-Mc PPI scans for the morning of 18 December 1952. The equipment operated with nominal 2 kilowatts output, 2-millisecond

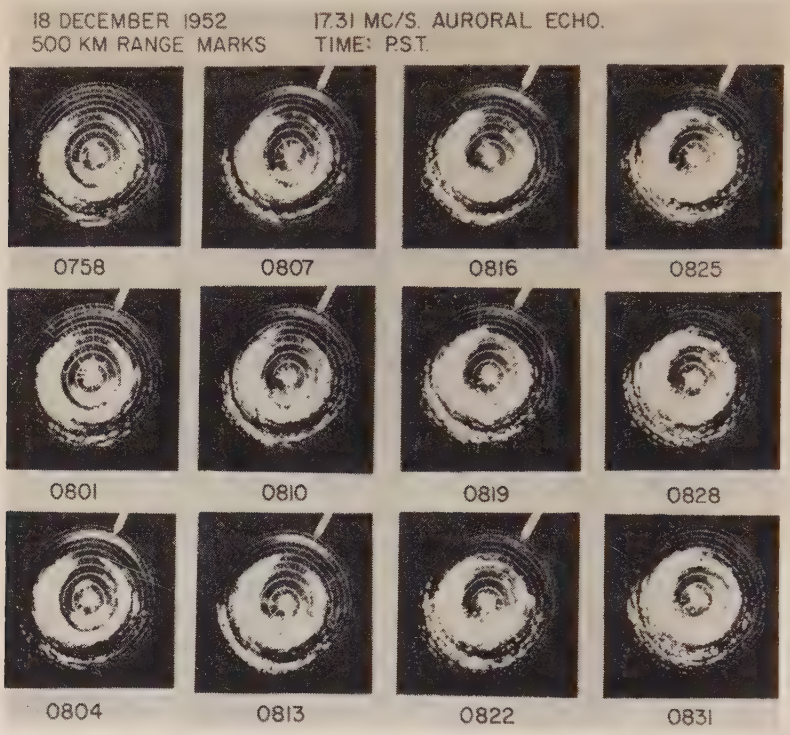

FIG. 3—Morning sequence, showing appearance of auroral reflections as ground-backscatter ring closes in the northern direction. Auroral reflections occur at 4,100 km.

pulses, 5,000-km sweep range, and a rotating three-element Yagi antenna [11]. The auroral display appears at range 4,000 km in the direction of the open sector in the ground-backscatter pattern. The reflections disappear when ground backscatter is detected to the north as well as to the south of the station. The disappearance can be attributed to break-up of the reflecting structure, but more likely is due to an alteration in the ^1F ray system as the over-all ion density in the F layer increases. Another sequence of PPI scans, showing the occurrence of auroral reflections in the direction of the open sector in the ground-backscatter pattern, this time in the afternoon, is shown in Figure 4. In the second example the ion density in the F layer is waning, in contrast to the situation in the morning sequence.

On Stanford scatter-sounders, auroral reflections are often as strong or stronger than F-layer-propagated ground-backscatter signals [1]. Part of the surprising amplitude of auroral echoes received *via* F-layer reflection can be attributed to a focusing effect of the layer. Low-angle F-layer reflection will give some increase over free-space propagation for comparable equivalent path lengths, of the order of several db each transit [12]. If the entire reflected ray system misses the earth, auroral structures may be illuminated by a pencil of rays near the caustic and strong reflections are anticipated, considering the large slant ranges of the echoes.

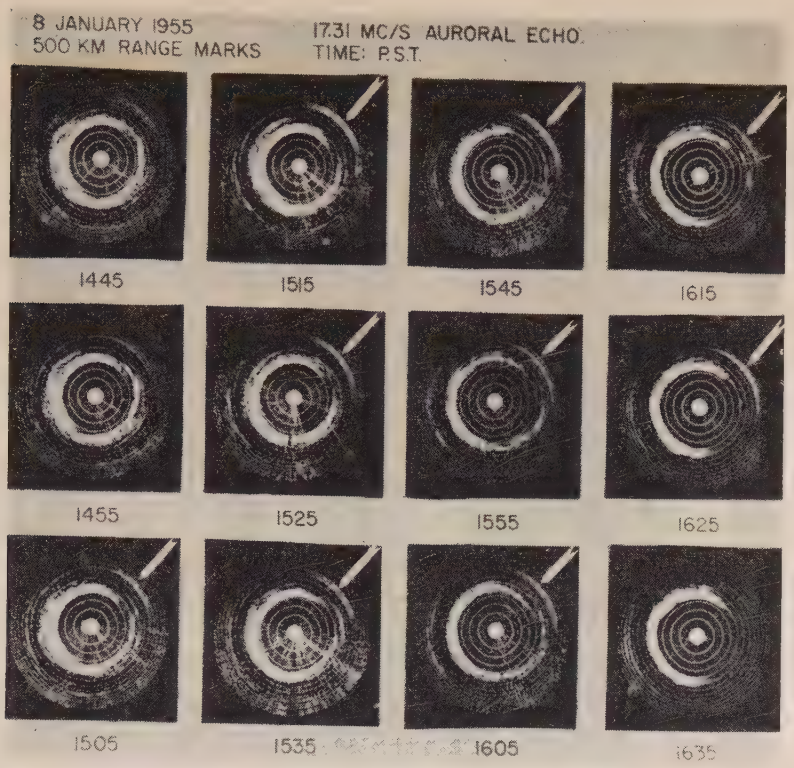

FIG. 4—Afternoon sequence, showing appearance of auroral reflections as ground-backscatter ring opens. Auroral reflections occur at 4,000 km.

Leadabrand has scaled the range and time of occurrence of auroral echoes during the period October 1952 to March 1953; Leadabrand's results are shown in Figures 5 and 6 [2]. Average $f^{\circ}F2$ values for Winnepeg are shown on the activity histogram to demonstrate the controlling influence of F-layer ionization. These statistics were scaled from records obtained during a period of low solar activity; as the sunspot cycle progresses, changes in ionospheric characteristics can cause *radical* changes in auroral statistics obtained on a given observational frequency. For example, no auroral echoes were detected on 30 Mc during the period October 1952 to March 1953 as a consequence of the low $f^{\circ}F2$ values such that 30-Mc radiation to the north was not reflected by the F layer. As the sunspot cycle progressed toward its maximum, the critical frequency of the F layer increased and ground-backscatter patterns on 30 Mc during the day became similar to the daytime patterns on 17 Mc some years previously. When this occurred, auroral reflections were detected on 30 Mc, too. Auroral reflections on 30 Mc became prevalent at Stanford during 1956, the 30-Mc statistics repeating the 17-Mc statistics for the years during sunspot minimum.

The peak in the range histogram, Figure 5, occurs at 3,500 to 4,000 km. Now the slant range of the geometrical path of ^1F rays used to compute the loci of perpendicular intersection, Figure 2, is a useful first-order measure of the time delay (in km) along the actual ionospheric trajectory. The slant ranges for per-

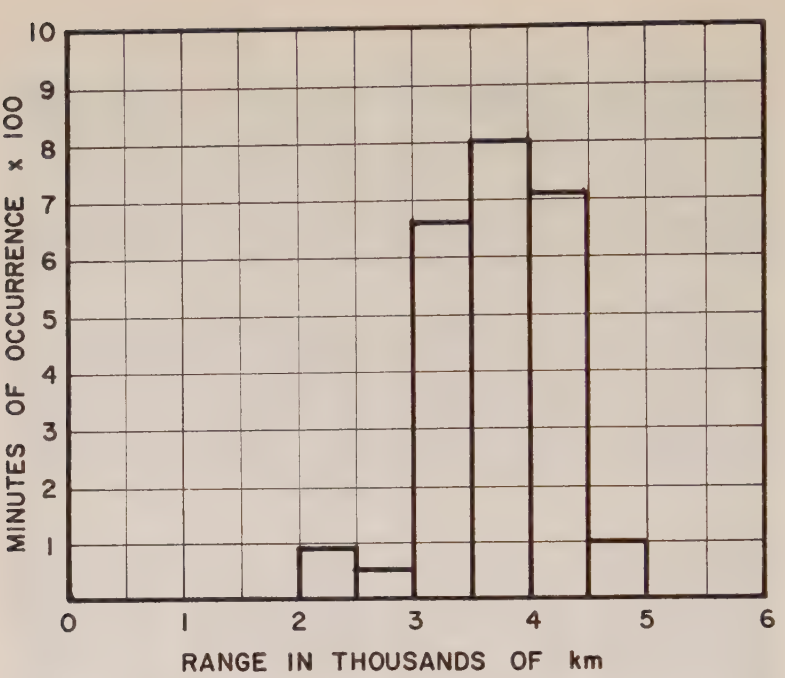

FIG. 5—Range histogram of 17.31-Mc auroral reflections for the period October 1952 to March 1953. (After Leadabrand, reference [2], Fig. 8.)

pendicular intersection between ^1F trajectories to the north and the earth's magnetic field lines in the E region agree very well with the experimental range histogram. The minor subsidiary peak at 2,000 to 2,500 km is consistent with the interpretation ascribing more than one mode as contributing to the total occurrence of auroral reflections. At the time of scaling, however, several other types of backscatter reflections, now known, went undiscovered; the subsidiary peak may represent an impurity in the data.

Figure 6 shows *no* auroral reflections during the night. During the period in which these statistics were accumulated, the F layer north of Stanford was normally transparent to 17-Mc radiation at night. Consequently, ionospheric-propagated auroral reflections were not received.

IV. REJECTION OF SUPRA-F-REGION ORIGIN

The absence of auroral reflections at times of low sunspot activity on 17 Mc during the night or on 30 Mc during the day and night has been attributed to a transparent F layer. The other explanation that has been advanced claims that auroral structures giving rise to this particular class of echo are situated high above the F layer, detection occurring only when the F layer is severely refractive. This argument is based upon the fact that sufficient deviation of low-angle rays penetrating the F layer north of Stanford will place the rays into a more propitious orientation for detection of auroral structures above the F layer, permitting reflection at lower altitudes and nearer to a right-angle intersection with the earth's magnetic field lines. This explanation, referred to as the "penetration" hypothesis,

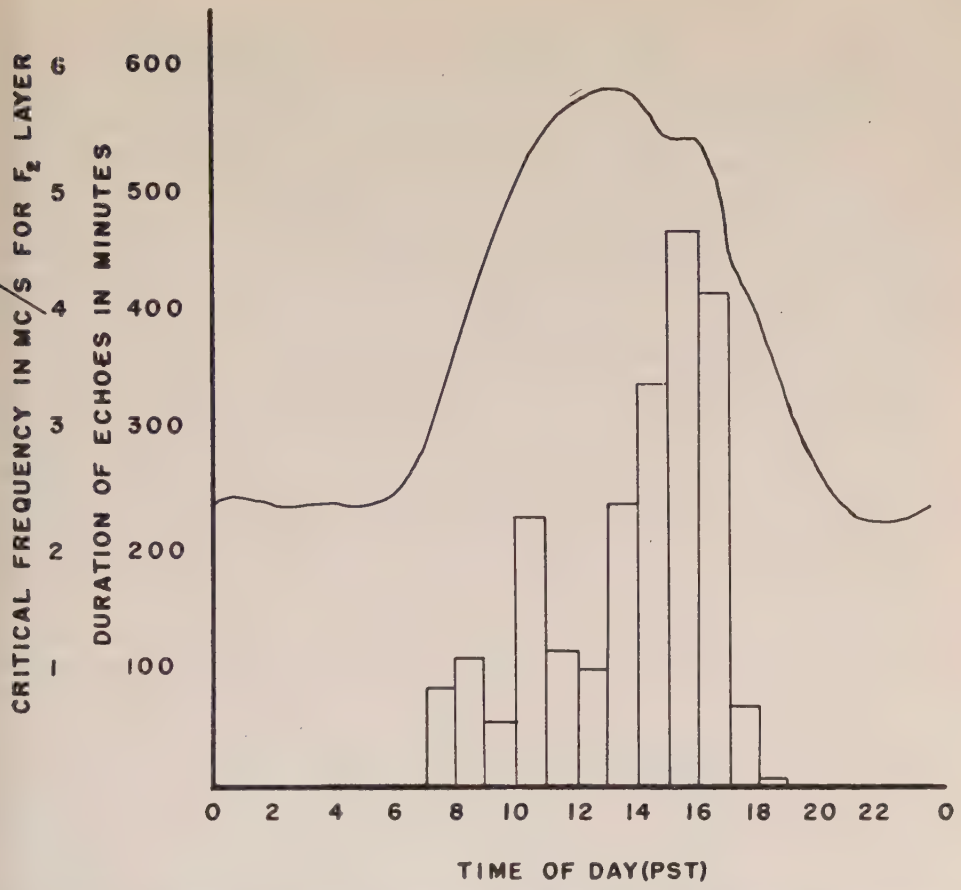

FIG. 6—Activity histogram for auroral reflections registered in Figure 5. Median *F*-layer critical frequencies at Winnipeg for the same period are also shown. (After Leadabrand, reference [2], Fig. 8.)

assumes *ad hoc* the existence of strongly reflecting ionized structures high above the *F* region. The "penetration" hypothesis is rejected as an explanation of the experimental data for the following reasons.

First, for penetrating rays Leadabrand has shown that the maximum amount of deviation that can be expected from a spherically symmetric layer corresponds to an effective zero take-off angle for low-angle rays from practical antenna installations.* Heavy refraction yields very moderate expected deviations principally because the severely deviated rays are eliminated in the analysis due to severe defocusing.** Thus, the deviation that can be expected is small to begin with and it is not apparent why a small deviation should be all-important in detection.

Second, it does not follow that deviations in the ionosphere necessarily result in closer to right-angle intersection with the terrestrial field lines high above the *F* layer. For propagation in the geomagnetic north direction in the presence of a

*Note that spherical symmetry is a legitimate first-order approximation for this calculation though it is not for the reflecting case.

**This is analogous to neglecting the severely defocused upper rays in the reflecting case.

spherically symmetric parabolic layer, deviation of a given ray penetrating the layer results in further from a right-angle intersection at a *fixed* reference height above the layer than would be the case if the layer were absent. This layer displaces the ray toward the pole, where the magnetic field lines are oriented closer to the local vertical, but does not alter the orientation of the ray with respect to the local horizontal once the ray emerges from the layer (Bouger's law). In the actual case, the "tail" of ionization above the F-layer maximum determines the characteristics of magnetic intersection.† In particular, we are left with the fact that low-angle, long-range paths of 3,500 to 4,000 km, distances which correspond to the peak of the range distribution, intersect the magnetic field lines at angles in excess of 10° even after the expected deviations in the F layer.

Third, no satisfactory explanation is evident for the range statistics, Figure 5. If the assumption of prevalent, strongly reflecting auroral structures above the F layer is true, then it is reasonable to expect that the range histogram would peak at a smaller range because: (*a*) the auroral activity maximum is considerably closer to Stanford than at slant ranges 3,500 to 4,000 km, (*b*) sensitivity of detection is increased, (*c*) the intersection with the magnetic field lines is more nearly perpendicular, (*d*) collisional probabilities for ion formation are much greater lower in the ionosphere.

Fourth, the geometry of the scattering volume implied by the "penetration" hypothesis is highly artificial. Since auroral reflections are not visible when the F layer is not sufficiently refractive, auroral structures giving rise to these reflections are all situated beneath the "effective" radio horizon, according to the "penetration" hypothesis. Furthermore, the spread in range, as in Figure 5, implies that the radio horizon is a boundary of the scattering volume. But a major portion of the volume above the radio horizon, within line-of-sight of Stanford, is above the auroral zone. Thus, the radio horizon at Stanford is given the peculiar property of dividing the ionosphere high above the auroral zone into two, one volume in which strongly reflecting auroral structures occur and one in which none occur. It is not possible to claim with consistency that auroral structures within line-of-sight of Stanford remain invisible as a consequence of improper geometry of intersection between straight-line paths and the terrestrial field lines since near-perpendicular intersection is not insisted upon by the "penetration" hypothesis in the first place.

Fifth, multiple auroral reflections may appear in the azimuth of the open sector in the ground-backscatter pattern. Occasionally, two echoes may have strikingly similar shapes, one echo lying exactly behind the other. The behavior of these split echoes may *sometimes* be attributed to detection of both a lower-ray and an upper-ray packet. Upper-lower splitting is not expected to be frequently observable on the Stanford equipment because the pulse length of 2 milliseconds, corresponding to a radar range of 300 km, can easily hide moderate upper-lower splitting and the narrow bandwidth of 3 kilocycles does not permit resolution of wave packets closer than about 100 km. In addition, the attenuation of upper-ray reflections becomes severe as the delay differential increases. For an approximately spherical layer, there are two rays emanating from the transmitter that intersect at any point beyond the skip edge beneath the layer (for operating frequencies

†This theory is important in a novel method for deducing the altitude of genuine field-aligned ionization structures situated above the F-layer maximum. See section IV.

above the critical frequency of the layer). Only one ray from the transmitter reaches any given point above the layer, neglecting the trapped rays circumventing the earth which are enormously defocused. Positive identification of split echoes due to upper-lower splitting would be further evidence in support of the theory attributing auroral reflections to structures beneath the *F* layer.

No contention is being made that radio echoes cannot be received from auroral ionization in the outer atmosphere of the earth on low-power broad-beam radars similar to those used in this study [11]. It is even possible that such echoes have been received at Stanford but have not been isolated from the bulk of auroral reflections. As the length of observation time and the beam power of radars are increased, echoes are anticipated from markedly off-perpendicular angles and from very high altitudes, especially during periods of peak sunspot activity. However, a conclusion of this study is that the prevalence of such echoes is *drastically less* than has hitherto been reported. *Bona-fide* echoes from great heights could be of great importance for the study of aurora and the outer atmosphere. It remains desirable to determine the conditions for detection and isolation of auroral-type echoes originating from great heights above the earth's surface [13]. Observations of exceptional value, bearing directly on the issues raised in this paper, can be obtained from high-power, narrow-beam radars operating at sufficiently high frequencies to insure line-of-sight surveillance. A manyfold increase in over-all system sensitivity over the present 17-Mc and 30-Mc scatter-sounders is readily obtainable.

V. ASPECT-SENSITIVE REFLECTIONS FROM FIELD-ALIGNED IONIZATION IN THE *E* AND *F* REGIONS

An important consequence of this study is the separation of recently discovered classes of radio reflections that have been unjustifiably connected by the "penetration" theory with radio reflections arising from *E*-region ionization over the auroral zone. In September 1955, Stanford researchers announced the discovery of aspect-sensitive radio reflections detected at middle latitudes from field-aligned ionization in the *E* and *F* regions [14]. Subsequently, considerable effort was expended to discover an explanation for the formation of these ionization structures and to explore their effects on other ionospheric phenomena. The occurrence of these new classes of radio reflections from field-aligned ionization in the *E* and *F* regions was interpreted by extending the conclusions of the "penetration" theory. The formation of columnar ionization irregularities in the *E* and *F* regions was considered a manifestation of low-latitude, low-intensity auroral activity in view of their night-time occurrence and their alignment with respect to the earth's magnetic field. The nature of the field-aligned ionization was attributed to charged particle bombardment, offering a possible explanation for the production of night-time sporadic-*E* ionization at middle latitudes [2].

In this connection, it is worth reporting that a rare "red aurora" was seen in the Palo Alto area early Saturday morning, February 25, 1956. This aurora was recorded on the Stanford 17- and 30-Mc recorders as aspect-sensitive echoes of exceptionally great intensity, resembling the aspect-sensitive echoes which are seen almost nightly. Widespread visual and photographic observations elsewhere have established that the aurora occurred at *F*-region heights, and was situated

in the same northern geographical regions from which the Stanford echoes were returned. As a result of this incident, it is possible to say that at least one type of visible aurora produces radio reflections similar to low-latitude aspect-sensitive backscatter, except in respect to intensity. A crucial question is whether these radio reflections arise from ionization irregularities composed in part of *new* ionization as a consequence of particle bombardment or from irregularities resulting from a "disturbance" of ionization normally present. On the basis of direct connection between unusual auroral activity and intense aspect-sensitive reflections, it was widely contended that the very frequent aspect-sensitive echoes which are seen almost nightly are, in fact, manifestations of weak, low-latitude auroral effects.

On the other hand, Gallagher has done an especially thorough investigation of the *E*-region field-aligned ionization detected at Stanford latitudes [15]. Gallagher concluded that the best interpretation of known experimental facts (May, 1956) calls for a horizontal arrangement of non-isotropic scatterers individually elongated at least several wavelengths (at 23 Mc) along the direction of the earth's magnetic field. He concluded that, although the echo behavior in many respects is suggestive of a low-latitude extension of the aurora, the evidence favors a distinctly separate cause for the new scatter phenomena. Gallagher further concludes that, in all likelihood, the scatter region owes its origin to electron clusters interacting with the earth's magnetic field when they are subjected to various hydrodynamic forces in the ionosphere. He finds that the new scatter correlates closely with local sporadic-*E* but not with meteoric ionization, geomagnetic, sunspot, or auroral activity. He suggests the hypothesis that in most cases sporadic-*E* and the new radio scattering are different manifestations of a common phenomenon; both manifestations can be observed simultaneously under a specified, but not unusual, set of conditions.

All experimental observations (known to the author) subsequent to the publication of Gallagher's work have supported his conclusions in every essential detail.

The main results of the author's investigation of *F*-region field-aligned ionization are now summarized. Detection of aspect-sensitive reflections from the *F* region has been associated, on various occasions, with a variety of different disturbances.* In particular, the prevalent field-aligned ionization structures seen almost every night at Stanford are, in all likelihood, not due to primary particle bombardment, but to hydrodynamic forces in the ionosphere. The interpretation of activity histograms of aspect-sensitive reflections must not neglect the presence of underlying layers. Effects were discovered where echoes could not be received because of bending by the *F* layer. On the other hand, *F*-layer bending is necessary for detection of *F*-region field-aligned ionization under some conditions. Such effects, while interesting for many reasons, provide a means for calculating the altitude of field-aligned ionization. This is the "penetration" hypothesis.** But in this case, it has been applied to known field-aligned structures in a situation

*These echoes should not be confused with another class of back reflections from traveling disturbances.

**It is the "deviation" and not the "penetration" of the rays that should be emphasized in this case.

where, after deviation, the ray trajectories can intersect the magnetic field lines in the F region at right-angles; furthermore, this effect is operative at high take-off angles. Finally, the F-region field-aligned ionization irregularities have been identified, on a phenomenological basis, as closely related to the irregularities that produce radio star scintillations.

VI. CONCLUSIONS

Long-range auroral reflections, hitherto attributed to auroral structures located at great heights, between 300 and 1,200 km above the surface of the earth, are explainable on the basis of E-region ionization observed *via* reflection from a tilted F layer. The bulk of the echoes recorded in Figures 5 and 6 are attributed to ^1F and coupled ^1F with grazing ground-reflected paths. Naturally, on other radio frequencies or at other periods of solar activity, other modes may be more prevalent. While it certainly cannot be stated that radar echoes cannot be received from auroral ionization in the outer atmosphere of the earth, the prevalence of such echoes is drastically less than has hitherto been reported.

An explicit distinction has been made between auroral reflections propagated *via* the ^1F mode and newer classes of radio reflections observed at high and middle latitudes arising from field-aligned ionization in the E and F regions.

VII. ACKNOWLEDGMENTS

This study is one chapter of a thesis submitted in partial fulfillment of the requirements for the Ph.D. degree at Stanford University.

The film records for the auroral work in this study were made available by the Radio Propagation Laboratory of Stanford University and are due to the effort of many workers. The principals are A. M. Peterson, O. G. Villard, Jr., R. L. Leadabrand, and R. D. Egan.

References

[1] A. M. Peterson and R. L. Leadabrand, Long-range radio echoes from auroral ionization, J. Geophys. Res., **59**, 306 (1954).

[2] R. L. Leadabrand, Radio echoes from auroral ionization detected at relatively low geomagnetic latitudes, Radio Propagation Laboratory, Stanford University, Tech. Rep. No. 98 (1955).

[3] O. G. Villard, Jr., S. Stein, and K. C. Yeh, Studies of transequatorial ionospheric propagation by the scatter-sounder method, J. Geophys. Res., **62**, 399 (1957).

[4] S. Stein, The role of ionospheric-layer tilts in long-range high-frequency radio propagation, J. Geophys. Res., **63**, 217 (1958).

[5] R. B. Dyce, Auroral echoes observed north of the auroral zone on 51.9 Mc/sec, J. Geophys. Res., **60**, 317 (1955).

[6] H. G. Booker, C. W. Gartlein, and B. Nichols, Interpretations of radio reflections from the aurora, J. Geophys. Res., **60**, 1 (1955).

[7] B. W. Currie, P. A. Forsyth, and F. E. Vawter, Radio reflections from aurora, J. Geophys. Res., **58**, 179 (1953).

[8] H. G. Booker, A theory of scattering by nonisotropic irregularities with application to radar reflections from the aurora, J. Atmos. Terr. Phys., **8**, 204 (1956).

[9] K. Bullough and T. R. Kaiser, Radio reflections from aurorae, J. Atmos. Terr. Phys., **5**, 189 (1954).

[10] C. G. Little, W. M. Rayton, and R. B. Roof, Review of ionospheric effects at VHF and UHF, Proc. Inst. Radio Eng., **44**, 992 (1956).
[11] A. M. Peterson, A scatter-sounder for the study of sporadic ionization in the upper atmosphere, Radio Propagation Laboratory, Stanford University, Tech. Rep. No. 1 (1953).
[12] L. H. Bixby, Jr., Calculation of high frequency radio field intensity over a 4000-kilometer ionospheric path, Report of the Radio Propagation Laboratory, Stanford University (1953).
[13] S. Chapman, The geometry of radio echoes from aurorae, J. Atmos. Terr. Phys., **3**, 1 (1953).
[14] A. M. Peterson, O. G. Villard, Jr., R. L. Leadabrand, and P. B. Gallagher, Regularly-observable aspect-sensitive radio reflections from ionization aligned with the earth's magnetic field and located within the ionospheric layers at middle latitudes, J. Geophys. Res., **60**, 497 (1955).
[15] P. B. Gallagher, Analysis of a new type of radio scattering from the ionospheric *E*-region, Radio Propagation Laboratory, Stanford University, Tech. Rep. No. 107 (1956).

JOURNAL OF GEOPHYSICAL RESEARCH VOLUME 63, NO. 2 JUNE, 1958

THE PROPAGATION VELOCITY OF WORLD-WIDE SUDDEN COMMENCEMENTS OF MAGNETIC STORMS

BY A. J. DESSLER

Lockheed Aircraft Corporation, Missile Systems Division, Palo Alto, California

(Received April 5, 1958)

ABSTRACT

The following model is presented for the propagation of a world-wide sudden commencement of a magnetic storm: A longitudinal hydromagnetic wave will be generated by the impact between a plasma cloud ejected from the sun and the earth's magnetic field. This wave will travel from the point of impact both east and west around the geomagnetic equator and carry the magnetic effect of the impact to the back side of the earth. It is shown that this hydromagnetic wave will be stable at an altitude of about 400 km and travel with a velocity of about 130 km/sec. Thus, it is proposed that sudden commencements do not occur simultaneously over the earth. Rather, about two minutes are required for a sudden commencement to be propagated around the world.

I. INTRODUCTION

It is observed that in low geomagnetic latitudes the world-wide sudden commencement of a geomagnetic storm is *always* characterized by an increase in H, the horizontal component of the magnetic intensity. In this paper, it will be assumed that the sudden commencement occurs when the earth collides with a plasma cloud or stream which has been ejected from the sun. Since an increase in H would be caused by a downward motion of the ionosphere, the question arises as to the mechanism whereby a collision with a plasma cloud on one side of the earth can push down the ionosphere on the opposite side of the earth so as to cause a world-wide increase in H. It is suggested here that the increase in H is propagated from the impact area around to the other side of the earth by longitudinal hydromagnetic waves [see 1 of "References" at end of paper]. That is, the impact of the plasma cloud only directly affects the geomagnetic field on one side of the earth and hydromagnetic waves transmit the effect of the impact completely around the earth with a wave velocity which is calculated to be approximately 130 km/sec.

II. A MODEL FOR WORLD-WIDE SUDDEN COMMENCEMENT OF MAGNETIC STORMS

It has been shown that the earth's dipole field is probably confined within a distance of about 6 to 10 earth radii [3, 4]. The dipole character of the magnetic

field is terminated at about this distance due to the relative motion of the earth and the coronal gas. When a plasma cloud or stream collides with the earth's magnetic field, the interaction first takes place at the 6 to 10 earth radii distance. The plasma will push closest to the earth in the equatorial region of the dipole field, since the magnetic pressure $B^2/2\mu$, is a minimum there [4]. (MKS units are used throughout this paper.) By thus displacing a portion of the earth's field, an increase in magnetic intensity will be propagated to the earth as a longitudinal hydromagnetic wave with a velocity $v = B/\sqrt{\mu\rho}$, where ρ = density of charged particles in kg/meter^3. The neutral particle density is not included in ρ because the mean free path is so long that only charged particles will contribute to the hydromagnetic wave motion.

Table 1 and Figure 1 give the velocity of a hydromagnetic wave as a function of altitude. The charged particle density and molecular weight *vs* altitude are given by Johnson [5]. The general shape of this curve is not sensitive to the exact values taken for the charged particle density or molecular weight as a function of altitude. Starting from the highest altitude down to about 1,000 km, the wave velocity will increase downward as $1/r^3$ (that is, directly with B), since the ion density will be approximately constant in this region. Below about 1,000 km, the atmosphere is supported hydrostatically. In the hydrostatically supported region, the atmospheric density increases exponentially downward; hence the ion density also increases exponentially downward, since the percentage ionization remains approximately constant. This exponential increase in ion density overcomes the $1/r^3$ increase in B, so that below this level the wave velocity decreases downward until the $F2$ region is reached. At about this level (that is, 300 km), the exponential increase in ion density ceases due to the rapidly decreasing fraction of gas ionized. Therefore, the hydromagnetic wave velocity increases downward below the $F2$ region.

The minimum in the velocity curve near 400 km implies that this altitude region is a stable one for hydromagnetic wave propagation, since a wave will be refracted away from the higher velocity regions both above and below the minimum velocity level. The principle of refraction away from a region of higher velocity will also cause the wave to be confined to an equatorial belt, because the wave velocity at constant altitude will increase toward the poles with the increase in magnetic field intensity.

Therefore, the result of an impact between a plasma cloud from the sun and the earth will be longitudinal hydromagnetic waves traveling both east and west around the geomagnetic equator at an altitude of 400 km and with a velocity of about 130 km/sec. This velocity is sufficient to carry the effect of the impact to the back side of the earth in about two minutes. Even though the wave is confined to a narrow region, its effect will be felt on the ground as an increase in total magnetic intensity (that is, an increase in H at low latitudes).

Experimental evidence [6, 7, 8] suggests a velocity of propagation of a sudden commencement of 100 to 200 km/sec. The agreement with the derived value of 130 km/sec is perhaps fortuitous, for it appears that the measurements were not sufficiently precise in time to accurately determine a velocity of propagation. Furthermore, the data consisted mainly of sudden-commencement times measured

TABLE 1.—*Hydromagnetic wave velocity vs altitude; equatorial magnetic field at surface of earth taken as* 3×10^{-5} *weber/meter*^{2} (0.3 *gauss*) *for this Table*

Altitude	No. charged particles/meter^3	Molecular weight	$v = B/\sqrt{\mu\rho}$
km			*meter/sec*
32,000	10^9	1.0	0.95×10^5
6,000	10^9	1.0	2.8×10^6
1,200	10^9	1.0	1.24×10^7
1,050	10^9	1.0	1.33×10^7
900	1.3×10^9	5.	5.5×10^6
750	3×10^9	18.	2.0×10^6
600	3×10^{10}	18.7	6.7×10^5
400	10^{12}	18.7	1.26×10^5
300	10^{12}	18.7	1.32×10^5
200	5×10^{11}	21.6	1.8×10^5

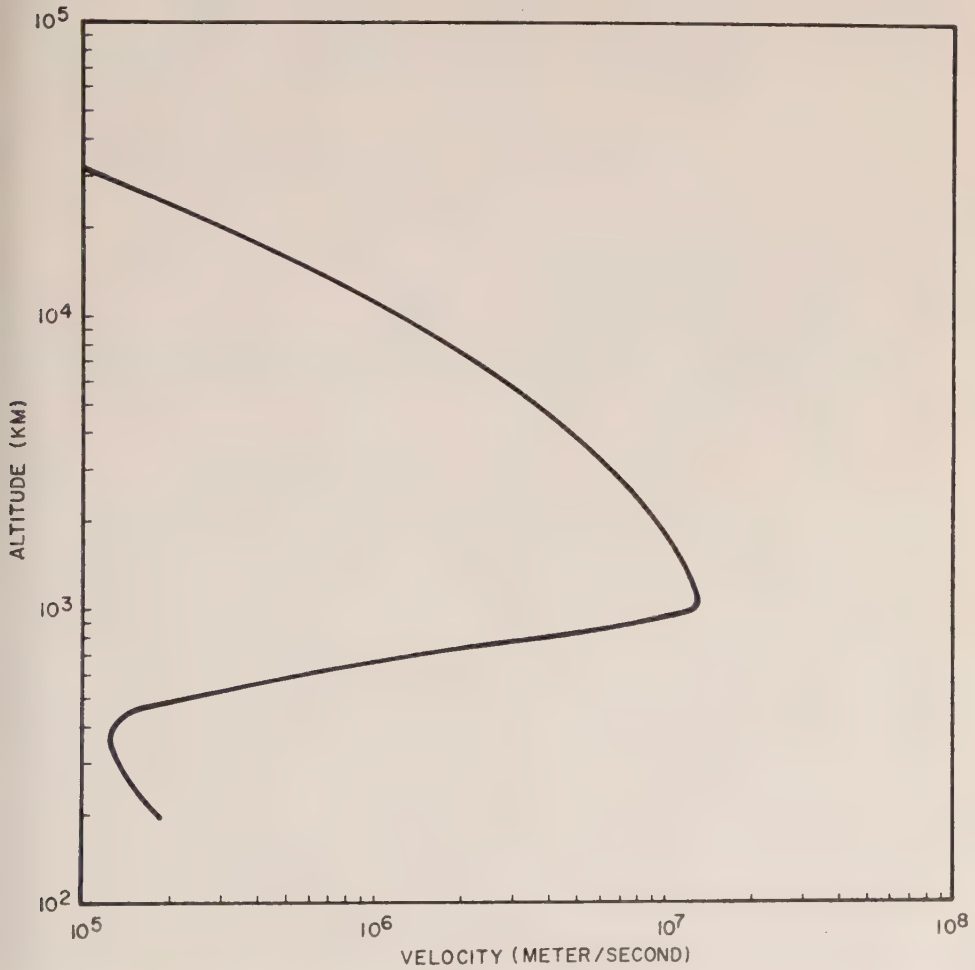

FIG. 1—Hydromagnetic wave velocity as a function of altitude above the surface of the earth

by middle- and high-latitude stations. It is possible that these data would not show a consistent propagation velocity, since hydromagnetic waves may arrive at polar stations by paths other than one which determines the equatorial sudden commencement (for example, transverse hydromagnetic waves traveling down the lines of force). If the model presented here is correct, the equatorial stations would be the ones to most clearly show the propagation velocity phenomenon.

It would be possible to measure the velocity of propagation of a sudden commencement with sensitive, high-speed magnetometers placed around the geomagnetic equator. Radio time-signals should enable the magnetometer time-bases to be synchronized to a fraction of a second. The recently developed proton free-precession magnetometer is ideal for this experiment, since it can easily be built with a magnetic field resolution of better than one gamma and a time resolution of less than one second.

III. ACKNOWLEDGMENTS

I wish to gratefully acknowledge the encouragement and aid of F. S. Johnson in the preparation of this paper. Also, my thanks are due to W. B. Hanson, R. K. M. Landshoff, and E. N. Parker for stimulating discussions of the phenomena involved.

References

[1] L. Spitzer, Physics of Fully Ionized Gases, Interscience Publishers, Inc., New York (1956); p. 57.
[2] F. Hoyle, Phys. Rev., **104**, 269 (1956).
[3] E. N. Parker, submitted for publication in Physics of Fluids.
[4] E. N. Parker, J. Geophys. Res., **61**, 625 (1956).
[5] F. S. Johnson, private communication.
[6] L. A. Bauer and J. W. Peters. Terr. Mag., **30**, 45 (1925).
[7] A. Tanakadate, C.-R. Assemblée de Lisbonne, Sept. 17-25, 1933, Union Géodésique et Géophysique Internationale Association de Magnétism et Électricité, Bull. No. 9 (1934); p. 149.
[8] T. Okada, *ibid.*, p. 276.
[9] L. Rhodes and D. la Cour, *ibid.*, p. 157.

GEOMAGNETIC AND SOLAR DATA

FINAL RELATIVE SUNSPOT-NUMBERS FOR 1957

The final sunspot-numbers are based on observations made at the Zurich Observatory and its two branch stations at Arosa and Locarno, and supplemented by series furnished by a large number of cooperating observatories. The most important of these are: Royal Greenwich Observatory, Herstmonceux; Observatoire d'Astronomie physique, Meudon; Observatoire Royal de Belgique, Uccle; Astrophysikalisches Observatorium Potsdam; Sonnenobservatorium Kanzelhöhe, Kärnten; Statne Observatorium Skalnaté Pleso; Observatoire de Belgrade; Observatoire National, Athens; Observatorium Istanbul; Observatory of the American University of Beirut; Osservatorio Astrofisico, Arcetri; Osservatorio Astronomico Monte Mario, Rome; Osservatorio Astrofisico, Catania; Observatorio del Ebro, Tortosa; Observatorio Astronomico de Madrid; Observatorio Astronomico de Cartuja, Granada; John Payson Williston Observatory, Mt. Holyoke, South Hadley; U.S. Naval Observatory, Washington; Tokyo Astronomical Observatory.

TABLE 1—*Final relative sunspot-numbers for the whole disk of the sun for 1957*

Day	Jan.	Feb.	Mar.	Apr.	May	June	July	Aug.	Sep.	Oct.	Nov.	Dec.
1	160	108	155	140	124	158	185	144	244	236	266	230
2	189	120	164	152	121	163	194	148	225	234	250	217
3	211	102	137	135	118	180	204	162	190	242	232	230
4	224	110	128	160	106	169	235	163	173	217	214	243
5	226	110	124	138	92	159	213	158	171	219	201	266
6	252	123	147	108	138	194	226	163	160	227	182	245
7	224	138	147	138	140	170	192	157	137	234	177	190
8	207	151	144	160	150	145	152	141	172	244	158	197
9	166	157	180	163	162	168	162	121	215	267	192	152
10	153	142	186	150	195	158	135	89	240	264	226	148
11	151	136	210	121	211	140	107	96	245	232	232	151
12	155	132	224	114	204	160	93	116	253	236	231	157
13	134	122	228	143	197	178	97	104	252	244	221	161
14	121	130	175	122	214	158	136	135	251	232	210	167
15	86	142	156	162	210	225	156	157	247	264	177	174
16	100	153	146	181	196	239	184	195	252	268	179	187
17	112	140	150	202	179	252	203	197	258	251	181	205
18	143	132	147	205	185	272	218	196	273	222	185	225
19	170	123	147	207	173	274	223	186	290	217	194	249
20	170	117	122	208	182	272	238	170	302	230	207	284
21	177	123	120	214	205	265	250	138	334	237	234	299
22	193	130	137	218	159	242	255	114	302	241	263	316
23	191	132	152	226	180	232	265	108	268	254	251	343
24	209	134	145	248	186	235	265	110	238	276	238	355
25	184	139	160	251	150	208	227	132	234	240	211	355
26	168	131	170	223	132	212	206	164	215	293	199	337
27	150	141	155	215	132	220	173	181	226	280	201	275
28	141	129	152	221	143	190	158	204	242	317	215	260
29	132		154	177	162	180	142	236	242	334	215	275
30	107		172	155	179	204	159	252	224	317	184	274
31	108		145		179		150	261		299		255
Mean	165.0	130.2	157.4	175.2	164.6	200.7	187.2	158.0	235.8	253.8	210.9	239.4

TABLE 2—*Daily number of sunspot-groups for 1957*

Day	Jan.	Feb.	Mar.	Apr.	May	June	July	Aug.	Sep.	Oct.	Nov.	Dec.
1	9	9	11	12	11	13	13	10	11	20	21	15
2	11	13	11	13	11	12	14	11	12	20	20	14
3	13	9	9	12	12	11	13	13	10	21	19	17
4	13	11	10	13	10	10	18	12	11	20	19	20
5	16	8	12	12	8	10	13	11	12	17	19	19
6	20	10	16	11	11	14	19	15	11	20	19	20
7	17	8	13	12	9	11	15	14	10	18	19	15
8	15	10	12	11	8	12	11	12	13	19	16	16
9	13	11	13	10	8	16	13	13	14	22	19	14
10	13	11	15	9	9	12	13	12	13	19	22	14
11	13	11	20	8	10	11	13	12	14	15	17	12
12	13	11	22	9	9	13	9	11	16	17	20	14
13	12	11	22	14	9	14	10	10	20	18	16	12
14	12	13	15	11	13	11	13	13	18	17	15	16
15	10	13	15	14	14	16	15	17	16	16	14	14
16	8	14	11	16	13	15	20	21	17	18	16	16
17	8	12	11	18	15	16	16	16	16	17	14	16
18	12	11	13	19	15	18	18	18	16	15	16	17
19	12	8	14	14	15	17	19	15	18	16	11	20
20	11	9	9	19	16	16	19	14	16	18	12	19
21	13	9	10	18	15	17	18	13	16	18	17	18
22	14	10	12	15	12	14	20	13	16	17	17	19
23	14	9	13	18	16	14	20	9	16	21	17	22
24	14	8	12	20	14	12	17	9	18	20	17	20
25	15	11	13	20	11	12	14	11	16	17	16	24
26	12	10	14	17	11	14	12	11	15	21	17	23
27	13	10	12	17	11	14	11	11	14	20	16	19
28	14	9	13	20	11	14	12	12	14	22	17	21
29	12		12	16	12	12	13	11	15	21	17	23
30	9		15	13	14	12	13	11	17	22	14	24
31	12		14		15		10	10		22		21
Mean	12.7	10.3	13.4	14.4	11.9	13.4	14.6	12.6	14.7	18.8	17.0	17.9

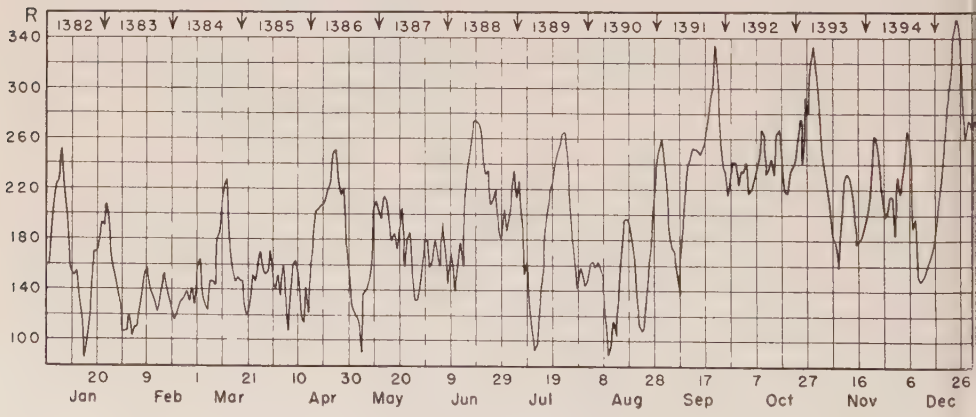

Fig. 1- DAILY RELATIVE SUNSPOT-NUMBERS FOR 1957

The final sunspot-numbers for the whole disk of the sun are given in Table 1. The exceptionally large increase of the solar activity since 1955 continued also throughout 1957. The maximum of solar activity falls on the second half of the year 1957 yet; the exact date can be determined definitively toward the middle of 1958 only. Figure 1 gives a graphical representation of the daily relative sunspot-

numbers for 1957. The limits of the successive solar rotations are indicated by vertical arrows in the upper edge of Figure 1. The yearly mean of the relative numbers amounts to 190.2 against 141.7 in 1956. This is by far the highest yearly mean hitherto observed; the next highest amounts to 154.4 and concerns the year 1778; the third—amounting to 151.6—was recorded in 1947. The absolute highest values of the relative numbers (355) were observed on December 24 and 25. Table 2 gives the numbers of sunspot-groups on each day for the year 1957. The yearly mean of the group-numbers is 14.3 against 10.8 in 1956. The present sunspot-maximum is remarkable by its exceptional intensity, by the wanting of extremely large spot-groups, and by the distribution of the activity to all heliographic latitudes from the equator to $\pm$ 50°. The solar activity was consequently less concentrated to some single large centres than rather distributed to large fields of the sun's surface and to many small to middle-sized spot-groups.

More details about the solar activity and the distribution and development of the individual spot-groups will be given in "Die Sonnenaktivität im Jahre 1957" (Astron. Mitt. der Eidgen. Sternwarte Zürich Nr. 215) and in "Heliographische Karten der Photosphäre für das Jahr 1957" (Publ. Eidgen. Sternwarte Zürich, **11**, Fasc. 2).

M. Waldmeier

Swiss Federal Observatory
Zurich, Switzerland, March 11, 1958

INTERNATIONAL DATA ON MAGNETIC DISTURBANCES

Geomagnetic planetary three-hour-range indices *Kp*, preliminary magnetic character-figures *C*, average amplitudes *Ap*, and final selected days, October to December, 1957, are given in Table 1 on the following pages, Monthly mean values of *Ci*, *Cp*, and *Ap* are given in Table 2. For explanations. please refer to previous reports in this Journal (Vol. 54, No. 3, 295, 1949; and Vol. 59, No. 3, 423, 1954).

It is hoped that the usual data on sudden commencements and solar-flare effects prepared by Dr. Romañá will appear in the next report (September 1958 issue).

TABLE 1—*Geomagnetic planetary three-hour-range indices Kp, preliminary magnetic character-figures C, average amplitudes Ap (unit 2γ), and final selected days, October to December, 1957*

October 1957									
E	1	2	3	4	5	6	7	8	Sum
1	4+	4o	3o	2o	4−	2+	4+	4−	27+
2	4−	4−	2−	2−	3−	2+	2−	3o	20+
3	3−	2o	1+	3+	4−	5−	4+	3o	25o
4	3o	3o	2+	3−	2+	3−	3o	3−	22−
5	3o	3o	2−	2+	2o	3−	3−	2o	19+
6	2−	0+	1o	1−	0o	0o	0+	0+	4+
7	1o	2o	2−	2−	2−	1−	2o	1+	12o
8	2−	0o	1o	1−	0+	0+	0+	0+	5−
9	0+	2−	2+	2−	2+	2+	2o	2+	15o
10	3o	4o	4o	3o	2+	3o	4−	3−	26−
11	3+	4+	3+	4+	4−	3o	2+	2+	27−
12	2+	3o	3−	4−	3−	3−	2−	3+	22o
13	5o	5+	3o	2+	3−	2+	4+	4o	29o
14	4+	6+	6−	5o	4+	5+	4o	5o	40o
15	3+	2o	2−	2+	3o	3−	3+	2o	20+
16	1+	0+	0+	1−	1+	1+	2−	0+	7+
17	1+	1+	1+	3o	3−	2o	1o	1+	14o
18	2−	1+	2−	1+	1−	2−	3−	1+	12+
19	1−	1+	3−	3+	2−	2+	3−	2−	16+
20	2o	2+	1+	2o	2o	3o	3−	4o	19+
21	3+	3−	3−	2−	3−	4o	4−	7−	27+
22	4+	3o	4−	4−	2+	3+	3−	4−	27−
23	5o	3−	4−	3o	1+	2o	4o	4−	25+
24	2o	2−	2o	2+	3−	2−	4−	1o	17o
25	2o	2−	2o	3o	2o	1+	2o	2+	16+
26	3o	2o	1+	2+	2o	1+	2−	2o	16−
27	2o	2o	2o	3−	4o	3+	2o	2+	20+
28	4o	2o	3+	3+	2o	3o	3−	1o	21+
29	4−	3o	4−	3o	3+	3−	3+	4−	26+
30	3o	4−	5−	3o	3−	2o	3−	1+	23o
31	1o	1+	2−	2o	4−	1o	2−	2−	14o

November 1957									
1	2	3	4	5	6	7	8	Sum
1+	3+	2+	2+	2−	2o	2−	2−	16+
1+	2−	2o	2o	2−	1o	2−	3+	15−
3+	1+	3o	3+	3+	3o	2+	1o	21−
1+	0o	1o	1−	0+	2−	1+	1+	8−
0+	1−	1−	1−	1o	2−	1+	1o	7+
0o	0o	1+	1+	2o	3−	6−	6+	19+
7o	4+	3+	4−	3+	3−	2+	1o	28−
1−	3−	4−	4−	4−	3o	3o	4+	25−
4o	4+	5−	3+	4+	4o	4−	4+	33−
5o	4+	4o	4−	4−	4−	3+	3o	31−
4o	4−	4o	4−	4o	3−	3−	4−	28+
4−	3−	3−	4−	4o	4−	2o	3−	25o
3−	2−	2+	3−	3o	2+	2+	3o	20o
4−	3−	3o	4o	4o	4o	4−	4−	29−
4o	4o	4o	4o	3o	3+	3−	3−	28−
3−	2+	2+	3−	3−	3−	2+	1+	19o
2−	2−	1o	1+	2−	1−	1−	3o	12−
4−	4o	4o	4+	5−	4o	3o	2+	30o
2−	3o	3−	3−	3o	1o	2o	2o	18o
2o	2o	1+	3−	3o	3o	3−	2+	19o
0+	0o	1+	0+	1+	1o	1+	2o	8−
2o	1+	1o	1o	2o	2+	2o	0+	12o
0+	1−	2−	2−	3−	2+	1+	3o	14−
3o	3+	2+	2o	3−	3o	3−	2+	21+
3+	4o	5+	4+	3+	4o	4o	4+	33−
5o	5o	5o	4−	4+	7−	7−	6+	43−
6+	6+	5o	5o	3+	4o	3+	4o	37+
4o	4+	5o	4+	4o	3+	3+	3+	32−
4−	4o	2+	3+	3+	3+	2o	2+	24+
3−	3o	2+	2+	3o	2+	2o	1o	19−

December 1957									
E	1	2	3	4	5	6	7	8	Sum
1	5−	6−	5−	4−	3o	3−	2+	4o	31−
2	3o	4−	4−	4−	4−	3o	2o	2o	25−
3	2o	2+	3+	3+	4−	3−	2o	2+	22−
4	3o	2−	3o	3o	2o	2−	1−	2+	17+
5	4o	4o	4o	3+	3+	4−	5−	4+	31+
6	4o	5−	4−	5−	4o	4+	4−	3−	32−
7	3−	3−	5−	4o	5−	3−	3−	3o	27o
8	3o	3o	3−	3−	2o	2−	2+	2+	20−
9	3+	3o	3−	4−	4−	4−	2+	4o	27−
10	4−	4−	3−	3+	3+	4+	4−	4+	29o
11	4−	6−	5+	4+	4+	4−	5−	5+	37o
12	4+	4+	4o	5−	3+	4o	4+	4o	33o
13	3+	3+	3−	5o	3+	5−	3o	1o	26+
14	3o	3−	2+	2−	2−	1o	2−	2+	16+
15	3−	3o	3o	4+	5−	5−	3o	1+	27−
16	3o	3−	2+	2+	3−	2+	3+	4−	22+
17	4−	4+	5−	2+	2o	3o	3+	3+	27−
18	3+	3−	2+	3o	3−	3−	1+	2o	20o
19	3−	3o	3−	4o	4−	3o	4+	4−	27o
20	4−	5−	3o	3o	3o	3−	3+	4−	27o
21	3−	5−	4o	2+	2o	2o	2o	2o	22−
22	2+	2+	1o	1−	1−	1−	1o	0o	9−
23	1+	1+	1o	1+	1o	1−	1−	1−	8o
24	1−	1+	1−	3−	2+	2−	2+	2−	13+
25	1+	3+	4−	3−	3o	2+	4−	4−	24−
26	3−	4+	3+	4−	4o	3o	3o	2−	26−
27	2o	2−	1o	1+	2+	1+	2o	2+	14o
28	1o	1+	1−	1−	1o	1o	1+	1+	8+
29	0+	1−	1−	1+	2+	1+	1+	3o	11o
30	3+	3o	4o	5−	4o	2o	1o	1+	23+
31	4o	5o	6−	5+	5−	5+	6−	6−	41+

Preliminary *C*, 1957		
Oct.	Nov.	Dec.
1.1	0.4	1.2
0.8	0.4	0.9
1.0	0.7	0.8
0.8	0.1	0.5
0.7	0.2	1.1
0.1	1.3	1.1
0.2	1.2	1.1
0.0	1.5	0.5
0.5	1.3	1.0
1.0	1.2	1.1
1.1	1.1	1.4
0.9	1.0	1.1
1.2	0.8	1.0
1.5	1.1	0.3
0.8	1.0	1.1
0.1	0.6	0.8
0.4	0.2	1.0
0.2	1.2	0.5
0.5	0.6	1.1
0.7	0.7	1.1
1.3	0.2	0.7
1.1	0.2	0.1
1.1	0.4	0.1
0.5	0.8	0.4
0.4	1.3	1.0
0.4	1.8	1.0
0.7	1.5	0.4
0.7	1.2	0.1
1.0	0.9	0.4
0.9	0.6	1.0
0.5		1.6

Average amplitude *Ap*		
Oct.	Nov.	Dec.
21	8	29
12	7	16
19	13	13
12	4	10
10	4	26
2	24	28
6	31	21
3	18	11
7	29	18
18	26	22
19	21	41
13	17	29
26	11	22
50	22	8
12	21	22
4	10	13
7	6	20
6	25	11
9	10	20
11	10	20
28	4	14
19	6	4
20	7	4
9	12	7
8	30	16
8	64	18
12	47	6
14	28	4
18	16	6
16	10	18
8		53

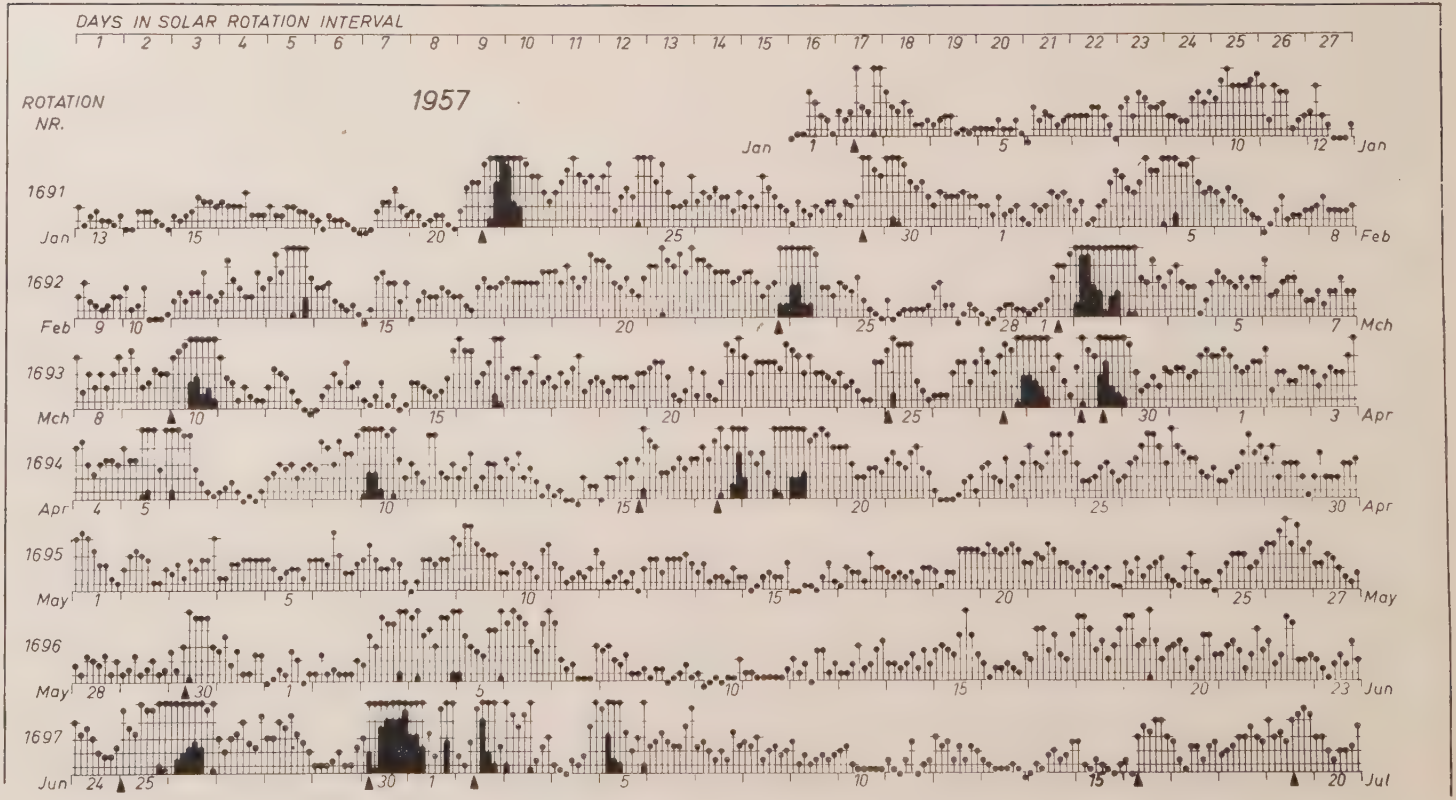
DAYS IN SOLAR ROTATION INTERVAL
1 2 3 4 5 6 7 8 9 10 11 12 13 14 15 16 17 18 19 20 21 22 23 24 25 26 27
ROTATION NR.
1957
Jan 1 5 10 12 Jan
1691
Jan 13 15 20 25 30 1 5 8 Feb
1692
Feb 9 10 15 20 25 28 1 5 7 Mch
1693
Mch 8 10 15 20 25 30 1 3 Apr
1694
Apr 4 5 10 15 20 25 30 Apr
1695
May 1 5 10 15 20 25 27 May
1696
May 28 30 1 5 10 15 20 23 Jun
1697
Jun 24 25 30 1 5 10 15 20 Jul

TABLE 1A

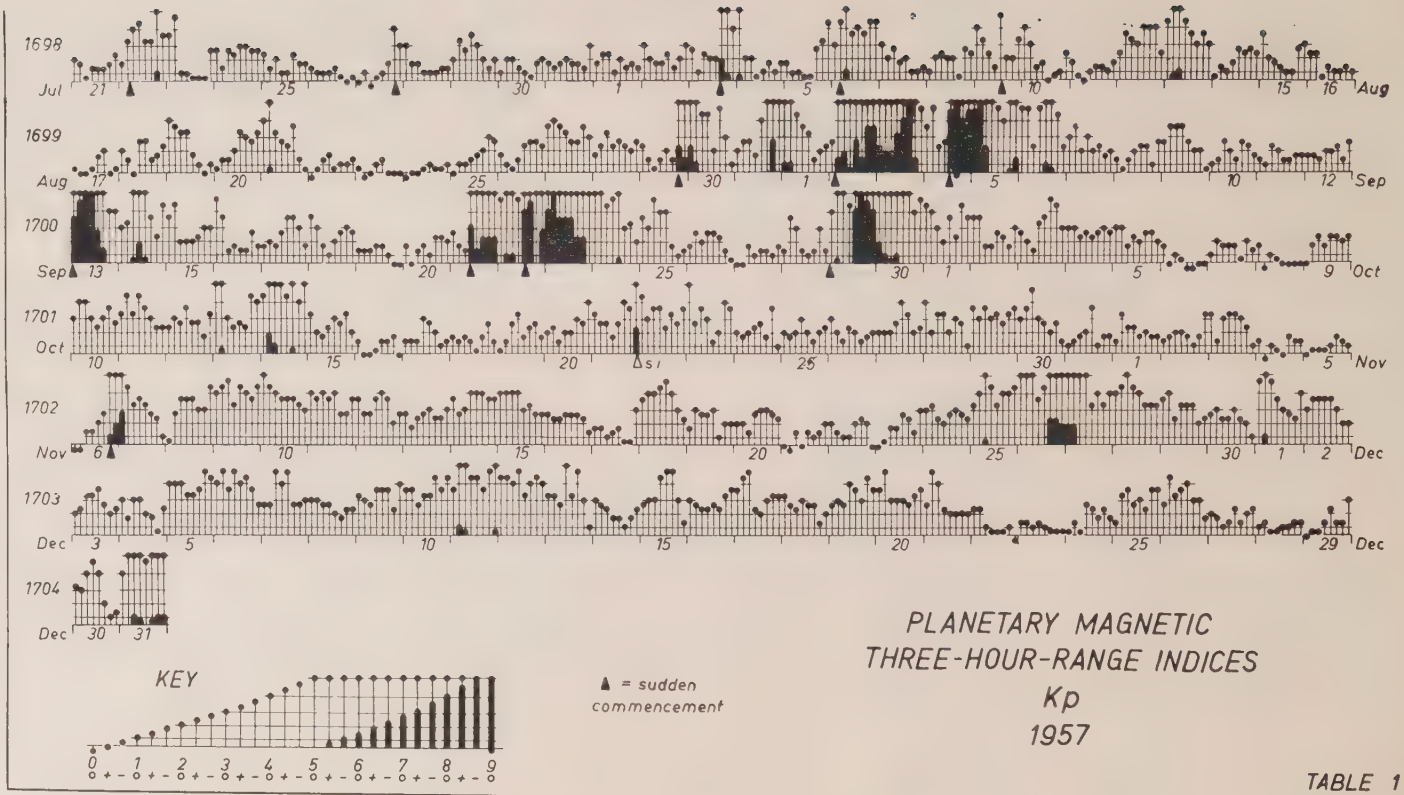
1698
Jul 21 25 30 1 5 10 15 16 Aug
1699
Aug 17 20 25 30 1 5 10 12 Sep
1700
Sep 13 15 20 25 30 1 5 9 Oct
1701
Oct 10 15 20 SI 25 30 1 5 Nov
1702
Nov 6 10 15 20 25 30 1 2 Dec
1703
Dec 3 5 10 15 20 25 29 Dec
1704
Dec 30 31
KEY
0 0+ 1- 1o 1+ 2- 2o 2+ 3- 3o 3+ 4- 4o 4+ 5- 5o 5+ 6- 6o 6+ 7- 7o 7+ 8- 8o 8+ 9- 9o
▲ = sudden commencement
PLANETARY MAGNETIC
THREE-HOUR-RANGE INDICES
Kp
1957

TABLE 1B

TABLE 1—(Concluded)—*Final selected days, October to December, 1957*

Month	Five quiet days	Ten quiet days	Five disturbed days
1957			
October	6 7 8 16 18	6 7 8 9 16 17 18 25 26 31	1 11 13 14 21
November	4 5 17 21 22	1 2 4 5 17 19 21 22 23 30	9 25 26 27 28
December	22 23 27 28 29	4 8 14 18 22 23 24 27 28 29	1 6 11 12 31

TABLE 2—*Monthly mean values of Ci, Cp, and Ap, October to December, 1957*

Index	October 1957	November 1957	December 1957
Mean *Ci*	0.72	0.85	0.82
Mean *Cp*	0.68	0.81	0.84
Mean *Ap*	14	18	18

The magnetic activity for the year 1957, as indicated by the planetary three-hour-range indices *Kp* is shown in Figures 1*A* and 1*B*, arranged in solar rotations of 27 days for the study of recurrence tendencies.

COMMITTEE ON CHARACTERIZATION OF MAGNETIC DISTURBANCES

J. BARTELS, *Chairman*
University
Göttingen, Germany

J. VELDKAMP
Kon. Nederlandsch Meteorologisch Instituut
De Bilt, Holland

PROVISIONAL SUNSPOT-NUMBERS FOR JANUARY TO MARCH, 1958

(Dependent on observations at Zurich Observatory and its stations at Locarno and Arosa)

Day	Jan.	Feb.	Mar.
1	214	138	109
2	213	148	90
3	200	146	140
4	217	144	185
5	191	148	203
6	192	156	215
7	205	156	220
8	210	157	187
9	232	164	177
10	252	157	181
11	253	165	168
12	255	177	156
13	262	163	145
14	270	174	158
15	284	154	165
16	290	129	155
17	247	135	164
18	230	137	162
19	212	139	155
20	190	145	154
21	171	152	156
22	173	150	163
23	192	160	187
24	137	145	204
25	137	187	180
26	143	160	194
27	182	141	226
28	160	118	292
29	130		302
30	110		338
31	132		342
Means.....	202.8	151.6	189.5
No. days.....	31	28	31

Mean for quarter: **182.3** (**90** *days*)

M. WALDMEIER
Observer-in-Charge

SWISS FEDERAL OBSERVATORY
Zurich, Switzerland

FREDERICKSBURG THREE-HOUR-RANGE INDICES *K* FOR JANUARY TO MARCH, 1958

[$K9 = 500\gamma$; scale-values of variometers in γ/mm: $D = 2.7$; $H = 2.5$; $Z = 2.8$]

Gr. day	January 1958		February 1958		March 1958	
	Values *K*	Sum	Values *K*	Sum	Values *K*	Sum
1	6543 3343	31	2132 2122	15	3110 1101	8
2	4333 3221	21	2334 2110	16	0232 2000	9
3	1101 1221	9	1111 3122	12	1232 3354	23
4	1110 1112	8	2013 4333	19	5433 3333	27
5	3211 2211	13	4433 4344	29	3454 3334	29
6	1232 3222	17	4434 4434	30	6543 4333	31
7	1221 2121	12	3334 3333	25	3443 3333	26
8	1122 2211	12	3444 3344	29	4443 3222	24
9	2112 3223	16	3421 2233	20	4323 3322	22
10	4222 2322	19	3322 2334	22	3422 3332	22
11	3222 3322	19	8899 7665	58	3112 3424	20
12	3332 3223	21	5554 4465	38	6655 4333	35
13	3332 2232	20	3134 3322	21	3455 5432	31
14	1133 2324	19	3432 2321	20	2002 5433	19
15	1332 3432	21	1002 2222	11	2443 4332	25
16	1223 2333	19	1112 2333	16	5322 1233	21
17	2333 3233	22	4433 4443	29	4355 3331	27
18	4335 4231	25	4544 4333	30	3442 4443	28
19	1222 3222	16	4343 3244	27	4533 4445	32
20	2133 3334	22	4333 4233	25	4433 3233	25
21	5633 3221	25	3443 3244	27	3433 4434	28
22	2333 4232	22	5322 3224	23	5512 2224	23
23	3333 4342	25	4433 3322	24	3433 2343	25
24	1213 4221	16	1323 2121	15	4432 4333	26
25	3234 4321	22	0132 1111	10	5243 3534	29
26	3442 1221	19	2131 2122	14	3224 4433	25
27	2211 1123	13	2111 2233	15	4223 2334	23
28	1122 2222	14	2234 4223	22	2322 2323	19
29	3332 1221	17			3310 1112	12
30	1332 3220	16			1134 5444	26
31	1213 2233	17			3432 3323	23

ROBERT E. GEBHARDT
Observer-in-Charge

FREDERICKSBURG MAGNETIC OBSERVATORY
Corbin, Virginia, U. S. A.

PRINCIPAL MAGNETIC STORMS

(Advance knowledge of the character of the records at some observatories as regards disturbances)

Observatory (Observer-in-Charge)	Greenwich date	Storm-time GMT of begin.	Storm-time GMT of ending[1]	Sudden commencement Type[2]	Amplitudes[3] D	H	Z	C-figure, degree of activity[4]	Maximal activity on K-scale 0 to 9 Gr. day	Gr. 3-hr. period	K-index	Ranges D	H
(1)	(2)	(3)	(4)	(5)	(6)	(7)	(8)	(9)	(10)	(11)	(12)	(13)	(14)
	1958	*h m*	*d h*		′	γ	γ					′	γ
College	Jan.	None											
(C. J. Beers)	Feb. 4	11 15	9 05	.....	.....	.....	.....	ms	6	6	7	220	1380
	Feb. 10	10 40	14 21	.....	.....	.....	.....	s	11	1,4	9	†	†
	†(*Note:* Maximum ranges unobtainable for this storm; insensitive recorder inoperative. However, ranges at Big Delta were D = 320′, H = 5000γ, and Z = 2400γ; while at Healy they were D = 440′, H = 5320γ, and Z = 2320γ)												
	Feb. 16	10 09	24 03	.....	.....	.....	.....	ms	23	4	7	170	1370
	Mar. 3	08 00	8 15	.....	.....	.....	.....	ms	6	4	7	230	1430
	Mar. 11	11 56	14 02	.....	.....	.....	.....	ms	12	3	7	240	1590
	Mar. 19	10 45	20 04	.....	.....	.....	.....	ms	19	5,6,7	6	170	1220
	Mar. 25	07 00	25 21	.....	.....	.....	.....	ms	25	3,6	7	250	1340
Sitka	Jan. 17	08 ..	19 00	.....	.....	.....	.....	ms	18	4,5	6	58	496
(J. L. Bottum)	Jan. 20	07 32	21 11	s.c.	−1	+3	0	ms	21	2	7	90	410
	Jan. 22	06 ..	23 21	.....	.....	.....	.....	ms	23	5	6	47	285
	Jan. 25	08 55	25 21	s.c.	−5	−11	+6	m	25	5,6	5	32	230
	Feb. 4	11 09	9 05	s.c.	+1	+1	0	ms	5	5	7	55	600
	Feb. 11	01 26	13 01	s.c.*	+47	+486	−156	s	11	1,3,4,5	9	353	3900
	Feb. 13	08 37	14 19	s.c.	−5	+5	0	ms	13	5	6	40	345
	Feb. 16	16 41	19 21	s.c.*	−4	−2	0	ms	17	5	6	93	444
	Feb. 20	09 46	22 15	s.c.	−3	+7	+6	ms	21	5	6	60	499
	Feb. 23	00 ..	23 13	.....	.....	.....	.....	ms	23	4	6	38	244
	Mar. 3	09 ..	4 23	.....	.....	.....	.....	ms	4	4,5	6	47	487
	Mar. 5	05 ..	8 17	.....	.....	.....	.....	s	5	3	8	79	879
	Mar. 9	08 57	9 19	s.c.	+6	+22	−10	ms	9	4	6	33	377
	Mar. 11	11 58	12 21	s.c.*	−1	−10	0	s	12	3	8	136	1064
	Mar. 13	03 ..	13 23	.....	.....	.....	.....	s	13	5	8	120	1329
	Mar. 14	12 12	15 19	s.c.*	−11	+76	+10	ms	15	4,5	6	50	473
	Mar. 17	06 ..	17 21	.....	.....	.....	.....	ms	17	3	7	62	512
	Mar. 18	06 ..	22 05	.....	.....	.....	.....	ms	19	5	7	77	720
	Mar. 24	04 36	24 20	s.c.	−1	+7	0	ms	24	4	6	34	355
	Mar. 25	07 22	26 02	s.c.	+3	+14	−16	ms	25	3	7	62	538
	Mar. 26	09 ..	27 01	.....	.....	.....	.....	ms	26	4,5,6	6	32	279
	Mar. 30	08 12	30 22	s.c.	+2	+4	−8	ms	30	5,6	6	58	430
Fredericksburg	Jan. 16	05 ..	19 21	.....	.....	.....	.....	m	18	4	5	25	107
(R.E.Gebhardt)	Jan. 20	11 ..	23 22	.....	.....	.....	.....	ms	21	2	6	32	124
	Feb. 11	01 26	12 15	s.c.	+18	+160	−35	s	11	3,4	9	171	2155
	Feb. 16	16 42	23 21	s.c.*	+4	+15	−5	m	18	2	5	28	120
									22	1	5		
	Mar. 3	09 30	8 15	s.c.	+1	+7	−1	ms	6	5	6	30	132
	Mar. 11	22 ..	13 20	.....	.....	.....	.....	ms	12	1,2	6	41	98
	Mar. 14	12 13	16 05	s.c.*	−5	+31	+6	m	15	5	5	23	104
	Mar. 17	05 38	17 21	s.c.	+1	+7	−1	m	17	3,4	5	19	89
	Mar. 18	02 01	22 05	s.c.	0	+3	0	m	20	2,8	5	29	126
									22	1,2	5		
	Mar. 30	08 ..	.. ..	.....	.....	.....	.....	(Storm continuing)					
Tucson	Jan. 17	16 ..	18 21	.....	.....	.....	.....	m	18	4	5	17	80
(R. F. White)	Jan. 20	07 37	23 22	.....	.....	.....	.....	m	20	8	5	19	128
									21	2	5		
	Feb. 4	10 00	9 06	.....	.....	.....	.....	m	5	7	5	14	102
									6	6	5		
	Feb. 11	01 26	13 05	s.c.	+8	+86	+7	s	11	1,2,3,4	8	44	546
	Feb. 16	16 41	22 07	s.c.	−1	+6	+1	m	21	3	5	16	127

[1]Approximate time of ending of storm construed as the time of cessation of reasonably marked disturbance movements in traces; more specifically, when the K-index measure diminished to 2 or less for a reasonable period.

[2]s.c. = sudden commencement; s.c.* = small initial impulse followed by main impulse (the amplitude in this case is that of *main impulse only*, neglecting the initial brief pulse; . . . = gradual commencement.

[3]Signs of amplitudes of D and Z taken algebraically; D reckoned positive if towards the east and Z reckoned positive if ve cally downwards.

[4]Storm described by three degrees of activity: *m* for moderate (when K-index as great as 5); *ms* for moderately severe (wh K = 6 or 7); *s* for severe (when K = 8 or 9).

PRINCIPAL MAGNETIC STORMS—Continued

)bservatory (Observer-n-Charge)	Green-wich date	Storm-time GMT of begin.	Storm-time GMT of ending[1]	Sudden commencement Type[2]	Amplitudes[3] D	H	Z	C-figure, degree of activity[4]	Maximal activity on K-scale 0 to 9 Gr. day	Gr. 3-hr. period	K-index	Range D	H	Z
(1)	(2)	(3)	(4)	(5)	(6)	(7)	(8)	(9)	(10)	(11)	(12)	(13)	(14)	(15)
	1958	*h m*	*d h*		′	γ	γ					′	γ	γ
:son	Mar. 3	09 30	8 09	s.c.	−1	+12	+1	ms	5	3	6	18	111	76
Continued	Mar. 11	12 10	13 21	.....	....	....	....	m	12	1,2,3,4	5	15	154	72
F. White)									13	3,4,5	5			
	Mar. 14	12 12	15 18	s.c.	+1	+24	+1	m	14	6	5	14	81	49
									15	3	5			
	Mar. 17	05 37	22 04	.....	....	....	....	ms	18	6	6	20	142	65
	Mar. 25	15 40	27 03	s.c.*	+6	+15	+1	ms	25	6	6	17	138	30
	Mar. 30	08 ..	31 18	.....	....	....	....	m	30	4,6	5	13	115	46
nolulu	Jan.	None												
L. Cleven)	Feb. 11	01 26	13 01	s.c.	+	+	+	s	11	2	9	16	670	110
	Mar.	None												
tituto	Jan. 20	14 20	21 22	.....	....	....	....	ms	20	7,8	6	10	379	69
ofisico de	Feb. 4	13 05	4 21	.....	....	....	....	ms	4	6	7	9	340	36
ancayo	Feb. 5	07 50	6 23	.....	....	....	....	ms	5	6,7	6	11	354	44
A. Giesecke,	Feb. 11	01 25	12 13	s.c.	+2	+167	+21	s	11	1	9	28	990	103
and M.	Feb. 16	11 20	17 22	.....	....	....	....	ms	17	5,7	6	8	391	41
averde)	Mar. 3	09 30	4 04	.....	....	....	....	ms	3	7	7	7	442	38
	Mar. 5	05 37	6 03	.....	....	....	....	m	5	3,5,6,7	5	6	423	41
	Mar. 13	09 37	13 20	.....	....	....	....	ms	13	6	6	7	212	37
	Mar. 14	12 12	14 22	s.c.*	−2	+139	+6	ms	14	6	7	10	364	56
	Mar. 17	07 51	17 21	.....	....	....	....	ms	17	6	6	6	187	42
	Mar. 18	12 00	18 22	.....	....	....	....	ms	18	6	7	6	315	31
	Mar. 25	12 03	26 02	.....	....	....	....	ms	25	6	7	9	404	52
	Mar. 30	11 00	30 22	.....	....	....	....	ms	30	6	7	10	383	44
rmanus	Jan. 15	10 30	15 16	.....	....	....	....	m	15	5	5	14	53	52
M.	Jan. 18	07 ..	18 15	.....	....	....	....	m	18	5	5	15	103	42
an Wijk)	Jan. 20	21 43	21 11	bs	....	....	....	m	20	8	5	20	100	74
	Jan. 25	10 50	25 18	s.c.*	+2	+16	+13	m	25	5	5	13	72	108
	Feb. 4	13 03	8 21	bs	....	....	....	m	4	7	5	29	138	96
									5	4,5,8	5			
									7	4,5	5			
	Feb. 11	01 26	13 01	s.c.	+11	+110	+84	s	11	1	9	86	880	573
	Feb. 16	16 42	19 12	s.c.	+1	+16	+12	m	17	5	5	23	127	69
	Feb. 20	18 ..	20 23	.....	....	....	....	m	20	7	5	15	41	71
	Feb. 21	17 ..	22 14	.....	....	....	....	m	21	8	5	22	73	84
	Feb. 28	07 ..	28 15	.....	....	....	....	m	28	4	5	26	79	66
	Mar. 3	09 30	4 13	s.c.*	+½	+13	+7	m	3	7	5	27	98	112
									4	1	5			
	Mar. 5	03 ..	6 15	.....	....	....	....	ms	5	3	6	30	122	94
	Mar. 11	16 ..	13 19	.....	....	....	....	ms	12	2	6	27	135	103
	Mar. 14	12 12	14 18	s.c.*	+8	+54	+52	m	14	5	5	20	58	124
	Mar. 15	02 58	15 18	.....	....	....	....	m	15	2,3	5	24	100	80
	Mar. 18	07 ..	22 08	.....	....	....	....	m	18	7,8	5	30	117	128
									19	6,7,8	5			
									20	5,8	5			
									22	1	5			
	Mar. 23	09 53	23 11	sfe	....	....	....	ms	23	4	6	($K' = 2$)		
	Mar. 24	08 ..	25 03	.....	....	....	....	m	24	7,8	5	27	71	96
									25	1	5			
	Mar. 25	15 40	26 03	s.c.	+1	+21	+13	m	25	6	5	7	49	30
	Mar. 30	07 ..	30 23	.....	....	....	....	m	30	4,5	5	38	104	116
	1957													
heroo	Dec. 31	01 16	2 01	.....	....	....	....	m	31	1	5	22	150	144
M.	*1958*													
Gregor)	Jan.	None												
	Feb. 11	01 26	12 22	s.c.*	−13	−122	−36	s	11	1,4	9	96	561	579
	Mar.	None												

Observatory (Observer-in-Charge)	Greenwich date	Storm-time GMT of begin.	Storm-time GMT of ending[1]	Sudden commencement Type[2]	Amplitudes[3] D	H	Z	C-figure, degree of activity[4]	Maximal activity on K-scale 0 to 9 Gr. day	Gr. 3-hr. period	K-index	Ranges D	H	2
(1)	(2)	(3)	(4)	(5)	(6)	(7)	(8)	(9)	(10)	(11)	(12)	(13)	(14)	(1
	1957	*h m*	*d h*		′	γ	γ					′	γ	
Toolangi	Dec. 31	01 17	3 06	s.c.	+1	−3	0	ms	1	2	6	23	268	1
(C. A. van der Waal)	*1958*													
	Jan.	None												
	Feb. 11	01 25	13 06	s.c.	−21	−142	−12	s	11	1	9	105	751	5
	Mar. 3	09 31	8 13	s.c.	+3	+19	+4	ms	5	3	6	24	281	
	Mar. 14	12 12	16 11	s.c.	+4	+58	+9	m	14	5	5	20	131	
									15	2,3,4,6	5			
	1957													
Amberley	Dec. 29	20 00	2 15	.....	.....	.....	.....	ms	1	2	6	24	300	1
(A. L. Cullington)	*1958*													
	Jan. 20	01 00	24 07	.....	.....	.....	.....	m	21	2	5	21	160	1
	Feb. 4	11 20	.. ..	s.c.	+1	+14	−4	m	5	7	5	.....	.....	
		(*Note:* Record for storm of Feb. 4 incomplete)												
	Feb. 11	01 25	14 19	s.c.	+23	+120	+77	s	11	1,5	9	79	1210	8
	Feb. 16	16 42	22 16	s.c.*	+3	+9	−9	m	17	1,2,7	5	20	150	
									21	2	5			
	Mar. 5	01 ..	6 09	.....	.....	.....	.....	m	5	3,4	5	20	164	
	Mar. 11	12 ..	13 23	.....	.....	.....	.....	m	12	3	5	28	146	1
									13	4,6	5			
	Mar. 25	15 40	27 06	s.c.*	+8	+23	−18	m	25	6	5	16	130	
Macquarie Island (B. G. Cook)	*1956*	*N.B.* In 11 instances in the original report, the values given under the heading of "Ranges" for Macquarie Island were approximate ones; in 20 cases, generally in Z and H, the values were given as "more than" a specified quantity (for example, in the first entry H = >811). Tabular space does not permit these indications in the compilation.												
	Jan. 10	04 00	11 24	.....	.....	.....	.....	m	11	4	7+	154	811	5
	Jan. 17	23 45	20 02	(Obscured)				m	19	5	6+	112	806	4
	Jan. 23	17 10	25 16	.....	.....	.....	.....	m	24	6	7+	157	781	7
	Jan. 27	09 00	30 08	.....	.....	.....	.....	m	27	7	6+	97	1050	4
									28	1,2,5	6+			
									29	5	6+			
	Feb. 25	03 07	26 16	s.c.*	−12	+50	−39	ms	25	2 to 6	7	230	1604	8
	Feb. 29	00 00	29 24	(Obscured)				ms	29	6	8	190	1550	8
	Mar. 2	23 42	4 18	s.c.	−16	+49	−39	ms	3	3,5 to 8	7	187	1612	8
	Mar. 20	10 30	23 09	.....	.....	.....	.....	m	22	3	7+	247	1105	8
	Apr. 21	08 00	23 13	.....	.....	.....	.....	m	21	4	8	164	1391	7
	Apr. 26	03 45	28 16	.....	.....	.....	.....	s	27	4	9	338	2129	13
	Apr. 28	17 27	29 22	s.c.	?	+26	−18	m	29	1 to 5	5	109	551	4
	Apr. 30	01 37	1 19	s.c.*	−18	+114	−70	m	1	4	7	67	1088	7
	May 12	00 00	13 21	.....	.....	.....	.....	m	12	5	7	158	1312	8
									13	3,4	7			
	May 14	07 ..	17 19	.....	.....	.....	.....	s	16	6	9	313	2239	14
									17	3	9			
	May 23	08 ..	25 19	.....	.....	.....	.....	ms	25	3	8	140	1476	9
	June 23	18 06	25 21	s.c.*	0	−8	+10	m	24	6	7	178	1109	5
	Aug. 23	00 ..	26 24	.....	.....	.....	.....	m	23	5	7	100	1488	5
									24	4,5,6	7			
	Sep. 2	01 17	3 20	s.c.	−20	−12	+13	ms	2	2	8+	100	1691	8
	Sep. 8	07 ..	8 24	.....	.....	.....	.....	ms	8	5,6	7	142	994	5
	Sep. 20	02 ..	22 24	.....	.....	.....	.....	m	22	4	7	82	945	4
	Oct. 20	02 45	22 08	.....	.....	.....	.....	m	20	3,5	7	93	1229	5
	Oct. 26	12 ..	29 04	.....	.....	.....	.....	m	26	8	7	131	1451	5
									28	3	7			
	Nov. 9	20 30	13 07	s.c.*	−20	−62	+44	ms	10	7	8	250	1946	8
	Nov. 13	21 38	16 24	s.c.	−7	−36	+28	m	15	1,2,3	7	200	1306	8
	Nov. 20	23 10	23 22	.....	.....	.....	.....	m	21	3	7	124	1010	6
	Nov. 25	06 ..	26 05	.....	.....	.....	.....	m	25	5	7	207	1701	7
(J. R. Cleary)	Dec. 25	07 55	26 12	.....	.....	.....	.....	m	25	4,6	6	90	726	5
	Dec. 27	15 02	29 04	s.c.	+15	−212	+113	ms	28	5,6	7	91	1115	4
	1957													
	Jan. 2	09 10	3 01	s.c.*	+6	+138	−71	m	2	7	7	75	890	4
	Jan. 9	12 22	10 24	s.c.	+3	−100	+71	ms	9	5	6	91	1030	4
									10	2 to 6	6			

PRINCIPAL MAGNETIC STORMS—Continued

Observatory (Observer-in-Charge)	Greenwich date	Storm-time GMT of begin.	Storm-time GMT of ending[1]	Sudden commencement Type[2]	Amplitudes[3] D	H	Z	C-figure, degree of activity[4]	Maximal activity on K-scale 0 to 9 Gr. day	Gr. 3-hr. period	K-index	Ranges D	H	Z
(1)	(2)	(3)	(4)	(5)	(6)	(7)	(8)	(9)	(10)	(11)	(12)	(13)	(14)	(15)
	1957	*h m*	*d h*		′	γ	γ					′	γ	γ
cquarie	Jan. 11	07 32	11 15	s.c.	+6	+50	−42	m	11	4,5	6	77	656	386
sland	Jan. 21	08 21	25 09	s.c.	+38	+63	−49	s	21	6,7,8	8	160	2080	1040
Continued	Jan. 29	09 50	31 19	.....	....	....	....	ms	29	5	7	91	1330	490
R. Cleary)	Feb. 4	10 52	5 17	s.c.*	−5	+19	+14	ms	4	4	7	123	1210	663
									5	5	7			
	Feb. 12	18 51	14 08	s.c.	+3	+19	−15	ms	13	5	7	93	1130	600
	Feb. 21	07 57	24 15	s.c.	+19	−88	+21	ms	21	6	7	130	1150	620
									24	1	7			
	Mar. 1	09 42	3 20	.....	....	....	....	s	2	2	8	150	1590	790
	Mar. 10	00 24	11 07	s.c.*	−14	+60	−60	ms	10	4,5,6	7	115	1300	920
	Mar. 24	21 15	25 16	.....	....	....	....	m	25	3,4,5	6	68	850	510
	Mar. 26	11 29	28 17	.....	....	....	....	ms	28	2	7	160	1000	700
	Mar. 29	03 36	30 05	s.c.*	+4	+80	−50	ms	29	5	8	110	1570	1040
	Apr. 1	00 45	1 21	s.c.	+3	+40	−30	m	1	6	6	75	760	360
	Apr. 6	06 11	6 17	s.c.*	−11	−250	+180	m	6	3,4	6	77	800	400
	Apr. 9	01 36	10 19	.....	....	....	....	ms	10	3,4	7	104	1020	750
	Apr. 17	11 36	18 05	s.c.*	+5	+50	+20	m	17	5	6	85	540	250
	Apr. 18	15 09	19 21	s.c.	−4	+60	−40	ms	19	7	7	130	1160	570
	May 9	00 58	9 16	.....	....	....	....	m	9	2,3,5	5	55	640	330
	May 30	08 22	30 22	s.c.*	+2	+75	−40	m	30	6	6	80	540	360
	June 3	02 36	5 19	.....	....	....	....	m	3	4,6,7	6	79	660	520
									4	4	6			
	June 5	23 20	6 23	s.c.	+2	+40	−40	m	6	3,4,5	6	65	680	390
	June 25	00 46	27 03	s.c.*	−7	0	0	ms	26	4,5	7+	....	....	....
	June 30	04 06	1 11	.....	....	....	....	s	30	4,6,7	7+	....	....	....
	July 2	08 59	2 21	s.c.*	−9	+175	−105	ms	2	4,5	7	105	990	750
	July 5	00 43	5 12	s.c.*	+16	+275	−55	ms	5	4	7	120	880	410
	July 16	07 15	16 21	s.c.	+3	+35	−20	m	16	4,6,7	5	41	530	280
	July 22	04 20	23 06	.....	....	....	....	m	22	7	6	61	540	400
	Aug. 6	05 09	6 21	s.c.*	+5	−20	+15	ms	6	3,4	7	....	920	....
	Aug. 13	03 10	13 15	s.c.	+1	0	0	ms	13	3,4	7	140	1000	720
	Aug. 20	13 26	21 18	s.c.	−3	+25	−20	m	20	7	5	89	780	275
									21	2,6	5			
	Aug. 29	19 20	30 13	s.c.*	−7	+30	−20	m	30	4	7	88	850	470
	Aug. 31	12 29	1 16	s.c.	−4	+25	−15	ms	31	7	7	63	950	570
	Sep. 2	03 15	4 06	s.c.*	−3	+140	−95	s	3	4,5	8	190	1750	1200
	Sep. 4	12 59	7 05	s.c.*	+18	−75	+55	s	4	6	9	....	2200	1160
	Sep. 13	00 45	15 06	s.c.*	+33	+140	−120	s	13	2	8	290	1910	880
	Sep. 21	10 05	25 15	s.c.*	+30	−390	+120	s	23	2	9	270	2400	1350
	Sep. 29	00 16	1 05	s.c.	+7	−40	+25	s	29	7	8	143	2200	980
	Oct. 3	10 19	4 02	s.c.	−2	0	0	m	3	4,6	6	84	560	360
	Oct. 9	13 30	15 21	s.c.	+4	−25	+15	ms	14	3,6	7	144	1270	580
	Oct. 21	11 50	23 24	.....	....	....	....	m	21	8	6	76	490	370
	Nov. 6	18 20	7 19	s.c.*	−7	+110	−100	m	6	7,8	6	125	910	440
									7	1,5	6			
	Nov. 8	04 26	12 19	.....	....	....	....	ms	8	4	6	92	1040	450
									9	5	6			
									10	2,5	6			
	Nov. 13	09 25	16 20	.....	....	....	....	m	13	4	6	68	830	430
									15	1,2,3	6			
	Nov. 18	01 50	19 15	.....	....	....	....	m	18	4,5,6	6	98	1000	430
	Nov. 24	14 10	29 18	.....	....	....	....	ms	25	4,7	7	151	1830	680
									26	4,6,7	7			
									27	1,3	7			

PRINCIPAL MAGNETIC STORMS—Concluded

Observatory (Observer-in-Charge)	Greenwich date	Storm-time GMT of begin.	Storm-time GMT of ending[1]	Sudden commencement Type[2]	Amplitudes[3] D	H	Z	C-figure, degree of activity[4]	Maximal activity on K-scale 0 to 9 Gr. day	Gr. 3-hr. period	K-index	Ranges D	H	
(1)	(2)	(3)	(4)	(5)	(6)	(7)	(8)	(9)	(10)	(11)	(12)	(13)	(14)	(1
	1958	*h m*	*d h*		′	γ	γ					′	γ	
				Additional reports received later										
Witteveen (D. van Sabben)	Jan. 20	21 00	21 07	.....	.....	.....	.....	ms	20	8	6	25	195	
	Feb. 11	01 26	12 22	s.c.	−24	+185	−11	s	11	1,3	9	175	980	4
	Mar. 3	20 31	4 07	s.c.*	−7	+28	0	ms	3	7	6	20	150	
	Mar. 11	18 00	12 08	.....	.....	.....	.....	ms	11	7	6	40	170	1
									12	1	6			
	Mar. 13	10 00	13 21	.....	.....	.....	.....	ms	13	7	6	20	185	1
	Mar. 14	12 12	14 18	s.c.*	−12	+60	−6	ms	14	5	6	20	125	
	Mar. 19	15 00	22 03	.....	.....	.....	.....	ms	19	8	6	45	160	1
									20	1,7,8	6			
	Mar. 25	15 40	25 24	s.c.	−5	+76	−3	ms	25	6	6	20	135	
	Mar. 30	11 00	30 23	.....	.....	.....	.....	ms	30	6	6	30	140	
San Juan (M. Vazquez)	Jan.	None												
	Feb. 11	01 27	13 01	s.c.	+4	+75	−30	s	11	1	9	34	649	
	Mar.	None												
	(*Note:* There were several periods of rough magnetic conditions throughout March, but sufficient to be considered storms)													
Elisabethville/ Karavia (A. Alexandre)	Jan.	Pas d'orage important												
	Feb. 2	01 53	.. ..	.....	.....	.....	.....	...	..	...	...	.....	.....	
	Mar.	Par d'orage important												
Apia (J. G. Keys)	Jan. 9	09 ..	20 21	.....	.....	.....	.....	m	10	8	5	11	138	
									18	1	5			
	Jan. 20	21 42	24 06	s.c.	0	+29	−7	m	20	8	5	13	174	
									21	1,2	5			
	Jan. 25	10 50	26 23	s.c.	0	+13	−4	m	26	2	5	11	148	
	Feb. 11	01 26	14 18	s.c.	+2	+81	−47	s	11	1	9	25	862	
	Feb. 16	16 41	24 13	s.c.	0	+3	−2	ms	17	2	6	12	206	
	Mar. 5	05 37	11 04	s.c.	0	+13	−5	ms	5	3	6	5	167	
	Mar. 11	23 17	13 22	s.c.	0	+10	−4	m	12	1,2,3,4,5	5	6	206	
									13	5	5			
	Mar. 14	12 12	16 06	s.c.	−1	+25	−10	ms	15	2	6	7	140	
	Mar. 17	07 52	22 06	s.c.	.....	.....	.....	m	18	8	5	8	118	
									22	1	5			
	Mar. 25	15 40	29 07	s.c.	−1	+21	−9	m	25	6	5	8	129	
Binza (J. Dodson)	Jan. 20	21 47	21 04	s.c.	+0	+38	−2	m	20	8	...	8	101	
	Feb. 11	01 33	12 12	s.c.	+2	+131	−7	ms	11	1	...	22	850	
	Feb. 11	02 06	12 12	s.c.	+8	+465	−16	s	11	1	...	.....	.....	
	Feb. 16	16 43	17 06	s.c.	+0	+25	−3	m	17	1	...	3	68	
	Mar. 14	12 15	15 12	s.c.	+1	+63	−5	m	14	5	...	10	161	
	Mar. 25	15 37	25 24	s.c.	+2	+46	−5	m	25	6	...	3	55	

NOTES

(14) *Launching of United States Vanguard satellite*—On March 17, 1958, at Cape Canaveral, Florida, the U. S. Navy launched a Vanguard test satellite into orbit around the earth. This second U.S. satellite was hurtled some 2500 miles out into space, the highest yet attained by a man-made satellite. It is expected to remain there from five to ten years. The Vanguard project forms part of the United States International Geophysical Year program. Navy plans now call for the launching of a full-size Vanguard instrumented satellite, a 21-pound sphere measuring 20 inches in diameter.

(15) *Third United States artificial satellite*—From Cape Canaveral, Florida, on March 26, 1958, the U. S. Army placed in orbit another Explorer satellite, using the Jupiter-C rocket. The 31-pound sphere, a duplicate of Explorer I successfully launched on January 31, 1958, attained a strange, unplanned orbit, and because of its perigee (around 110 miles) may have a relatively brief life span. Valuable scientific information is expected to be obtained from it, however.

(16) *Navy book on tracking missiles*—The U. S. Navy has released a booklet telling radio amateurs how to track the Vanguard earth satellite. The booklet describes two systems. The booklet is titled "PB 131330, Project Vanguard Report No. 21, Minitrack Report No. 2—the Mark II Minitrack System," and is available at the Office of Technical Services, U.S. Department of Commerce, Washington 25, D.C., at a cost of $1.00.

(17) *Special issue on radio astronomy, IRE*—The January 1958 number (Vol. 46, No. 1) of the Proceedings of the Institute of Radio Engineers brings together 50 papers on radio astronomy. It is the first publication to deal comprehensively with the engineering and equipment phases of this 25-year old subject, and it also presents new findings in astrophysics, for example, in connection with radio sources among the planets. Contributions came from Australia, Japan, Canada, England, France, Belgium, Alaska, Hawaii, and the United States, and the list of authors includes a majority of the leading workers in this field. The issue was 21 months in preparation.

(18) *Publication of proceedings of the Polar Atmosphere Symposium (AGARD)*—The proceedings of the Polar Atmosphere Symposium (Part II, Ionospheric Section), held at Oslo, Norway, July 2-8, 1957, have been published as a Special Supplement to the Journal of Atmospheric and Terrestrial Physics. The symposium was held under the auspices of the Advisory Group for Aeronautical Research and Development (AGARD) of the North Atlantic Treaty Organization. Some 20 papers are included in the publication, which was received by subscribers (March 24, 1958) as part of their subscription for 1957.

(19) *Royal Astronomical Society's new Geophysical Journal*—To meet the rapid increase of research work in geophysics in recent years, the Royal Astronomical Society (London) began the publication in March 1958 of "The Geophysical Journal," a new quarterly containing original papers, short notes and letters, and

articles on the progress of geophysics. The "Geophysical Supplement to the Monthly Notices" (last number appeared towards the end of 1957) will be incorporated in the new Journal.

(20) *Magnetic observatories for the IGY*—As part of the geomagnetic program for the International Geophysical Year, two field magnetic stations have been set up by the India Meteorological Department to study the daily variation of magnetic elements near the geomagnetic equator which passes through the southern part of India. These two magnetic observatories, which are on either side of the geomagnetic equator, are located at Trivandrum (geographical coordinates 08° 28′ north, 76° 57′ east; geomagnetic, 0°.9 south, 146°.3 east) and Chidambaram (Annamalainagar) (geographical coordinates 11° 24′ north, longitude 79° 41′ east; geomagnetic, 1°.8 north, 149°.4 east).

(21) *Reports of Soviet IGY activities*—A weekly report of Soviet bloc activities in connection with the International Geophysical Year is being published by the Office of Technical Services (OTS), U.S. Department of Commerce, Washington 25, D.C. The reports contain information selected and translated from foreign-language publications regarding Soviet bloc plans and endeavors in rockets and artificial earth satellites, upper atmosphere, meteorology, oceanography, latitude, seismology, glaciology, the Antarctic, and other subjects. Prepared primarily for the information of U.S. Government scientists, the reports are being published by OTS for the benefit of non-Government scientists, who may subscribe to the series for $10. The series runs from February 14, 1958, to January 2, 1959. Back issues to February 14 will be supplied to subscribers regardless of the date of their order.

(22) *Subscription to IGY Bulletin*—The National Academy of Sciences has announced that the "IGY Bulletin," official monthly publication of the U.S. National Committee for the International Geophysical Year, is now available by subscription. It includes brief articles and reports on projects and experiments in a dozen different scientific fields covered by the U.S.-IGY program, as well as available news of IGY activities in other countries. The monthly issues of the Bulletin comprise at least 16 pages and are illustrated with charts, tables, and diagrams. Subscription to the Bulletin is $4. This will include all back issues, dating from July 1957, together with all future issues. (The Bulletin will be published at least through December 1958 and possibly through June 1959.) Subscriptions should be sent to the Publications Office, National Academy of Sciences, 2101 Constitution Avenue, Washington 25, D.C.

(23) *Results of conference for creation of a national center for coordination of scientific and technical information*—Western Reserve University's conference on this matter recommended a "crash" study program of the technical and other problems involved in the establishment of such a center. The U.S. National Academy of Sciences will be asked to sponsor the study so that the recommendations will have the national recognition necessary to win the approval and support of industry, government, academic institutions, and the foundations.

(24) *Recent book "Agricola on Metals," by Bern Dibner*—This is a distillation of the first scientific text-book on mining, metallurgy, and geology, "De Re Metallica," by Agricola (Latin version of his original German name, Bauer). Georgius Agricola, receiving his degree in medicine in Italy in 1526, returned to Germany and settled as a practicing physician in the mining region of the Harz Mountains,

his object being partly "to fill in the gaps in the art of healing" and partly to test what had been written about mineralogy by careful observation of ores and the methods of their treatment. The original publication in 1556 of his 586-page treatise, "De Re Metallica," was in Latin, followed by translations into German and Italian. In 1912, Herbert Clark Hoover (later to become President of the United States) and his wife Lou Henry Hoover translated it into English. Agricola's masterful writings influenced succeeding generations of engineers, industrialists, and scientists. Bern Dibner, Director of the Burndy Library, Norwalk, Connecticut, has reproduced in this latest book over 70 absorbing illustrations from the original 291 woodcuts, at the same time conveying a message of timeless appeal to a large audience. The solutions of the problems of pumping, ventilation, handling bulky and heavy materials, testing minerals and metals, organizing and managing large groups of workmen developed in the 1500's, which Agricola described and illustrated, were in succeeding centuries adapted to the needs of manufacturing industries from textiles to automobiles and electrical appliances. Sixteenth century Germany used on a considerable scale power-operated machinery, assembly-line methods, and other paraphernalia suggestive of today's economy of mass production. Dibner dedicated his new book: "To these men who delved beneath the earth's surface and published their findings, of whom Agricola was the first, we owe an eternal debt—for they created the geological sciences. Whereas the most ancient of our sciences, astronomy, has been extending our known universe to limitless space, geology, this newest of sciences, now reveals to us the very great age of the world we have yet to know."

(25) *Symposium on Satellite Observations*—A Symposium on Satellite Observations, sponsored by the American Geophysical Union, was held on the afternoon of May 6, 1958, at the National Academy of Sciences Building, Washington, D.C. Speakers at the Symposium included L. V. Berkner, president of Associated Universities, Inc., N. Dubin and R. A. Minzner of the Geophysics Research Directorate, G. F. Schilling of the Smithsonian Institution Astrophysical Observatory, H. W. Wells of the Carnegie Institution of Washington, and P. W. Swenson of the University of Illinois. Topics discussed at the Symposium included upper atmosphere densities as deduced from satellite observations; and meteoric incidences determined from *Explorer* I and III observations and radio-wave propagation from *Sputniks* I and II.

(26) *Geomagnetic activities of the United States Coast and Geodetic Survey*—Captain E. B. Roberts, Chief of the Geophysics Division, was official United States delegate for geomagnetism at the eighth consultation of the Commission on Cartography, PAIGH, at Havana in February.

Mr. A. J. Bilik continued the magnetic survey of repeat stations in southwestern United States.

Messrs. J. V. Hastings and C. A. Harris are making a magnetic survey of repeat stations in southeastern United States. A portable variograph is being used as a control station.

Four volumes of the MHV series of publications were issued, giving hourly values and reproductions of magnetograms for 1952 for Honolulu and for 1953 for Sitka, Tucson, and San Juan.

The staff of the College Magnetic Observatory received as a group the Depart-

ment of Commerce Meritorious Service Award for the successful completion of the IGY Alaskan construction program. In addition to their routine duties, they established within the period of allotted time two new primary observatories and five variograph stations throughout Alaska, and installed much additional equipment at the College and Barrow magnetic observatories.

Mr. James H. Nelson, Chief of the Geomagnetism Branch, received the Exceptional Service Award of the Department of Commerce "for exceptionally significant technical leadership and inventive accomplishments having far-reaching effect upon the geomagnetic activities of the Coast and Geodetic Survey, and on the national and international relationships of the United States Department of Commerce."

(27) *Personalia*—Dr. *Aden B. Meinel* has been appointed director of the new National Astronomical Observatory, the site for which is to be selected in Arizona. Dr. Meinel has been associate director of the Yerkes and McDonald observatories since 1953, but recently he has been on leave to work on the program of the new observatory. He will direct work on the observatory from his present field office in Phoenix, Arizona, until such time as a site has been definitely selected.

Dr. *Ellis A. Johnson*, director of the Operations Research Office, Johns Hopkins University, has received the U. S. Army's Distinguished Civilian Service Medal "for his distinguished ability and performance."

Dr. *J. O. Thomas*, of the Radio Group, Cavendish Laboratory, University of Cambridge, England, arrived in the United States for a two-month visit on April 7, 1958. During his stay in this country, he visited the ionosphere groups at the Pennsylvania State University, the Department of Terrestrial Magnetism of the Carnegie Institution of Washington, and the Central Radio Propagation Laboratories, Boulder, Colorado. The main purpose of his visit was for consultations on the coordinating of the British and American IGY programs for the reduction of ionospheric $h'(f)$ records to electron density-height profiles using electronic digital computers.

NO STONE UNTURNED?

The vigorous activity and interest that is being manifested today throughout the world in geophysical phenomena of the earth, air, and outer space is both inspiring and gratifying. This JOURNAL receives numerous requests for back issues and sets of "Terrestrial Magnetism and Atmospheric Electricity" and its continuation, the "Journal of Geophysical Research." Wanted are complete copies of the following issues:

Vol.1-No.1 (1896;) Vol.2-No.1 (1897); Vol.3-Nos.2 and 4 (1898);
Vol.4-Nos.3 and 4 (1899); Vol.5-Nos.2,3, and 4 (1900);
Vol.6-Nos.1,2,3, and 4 (1901); Vol.14-Nos.3 and 4 (1909);
Vol.15-No.3 (1910); Vol.16-Nos.2,3, and 4 (1911);
Vol.17-Nos.1,2,3, and 4 (1912); Vol.18-Nos.2 and 3 (1913);
Vol.19-Nos.1 and 2 (1914); Vol.20-No.3 (1915); Vol.21-No.1 (1916);
Vol.23-No.1 (1918); Vol.28-Nos.1,2,3, and 4 (1923); Vol.29-

Nos.1 and 2 (1924); Vol.30-No.3 (1925); Vol. 31-Nos.3 and 4 (1926);
Vol.32-No.1 (1927); Vol.33-Nos.3 and 4 (1928); Vol.34-Nos.1,2,3, and 4 (1929);
Vol.35-No.1 (1930); Vol.37-No.1 (1932);
Vol.40-No.1 (1935); Vol.41-Nos.1,2,3, and 4 (1936);
Vol.43-Nos.1,2,3, and 4 (1938); Vol.44,No.1 (1939); Vol.45-Nos.1 and 3 (1940);
Vol.46-Nos.1 and 3 (1941); Vol.52-Nos.1,2,3, and 4 (1947);
Vol.53-Nos.1,2,3, and 4 (1948); Vol.54-No.1 (1949).

Those who have copies of any of the above numbers for sale are invited to send particulars to the Editorial Office of this JOURNAL, 5241 Broad Branch Road, N.W., Washington 15, D.C., U.S.A.

NOTICE

The Pergamon Institute, a non-profit Foundation for the furtherance and dissemination of scientific knowledge, is urgently in need of a complete set of "Terrestrial Magnetism and Atmospheric Electricity" and its successor, the "Journal of Geophysical Research," from the first volume (1896) to the end of 1957. Readers who have back volumes or numbers and wish to dispose of them should send a list of their holdings to the Pergamon Institute, 4 and 5 Fitzroy Square, London, W. 1, England.

LIST OF RECENT PUBLICATIONS

By W. E. Scott

Department of Terrestrial Magnetism,
Carnegie Institution of Washington,
Washington 15, D. C.

(Received April 2, 1958)

A—*Terrestrial Magnetism*

Abisko. Results of geomagnetic observations at Abisko 1946-1950, with a summary of annual means 1921-1953. By Kjell Borg. Stockholm, Kungl. Sjöfartsstyrelsen, Jordmagnetiska Pub. No. 17, 38 pp. (1957).

Andrade, E. N. da. The early history of the permanent magnet. Endeavour, **17**, No. 65, 22-30 (1958).

Blackett, P. M. S. Rock magnetism and the movement of continents. Proc. R. Inst., **36**, Pt. 2, No. 163, 370-373 (1957).

Cahill, L. J., Jr., and J. A. Van Allen. New rocket measurement of ionospheric currents near the geomagnetic equator. J. Geophys. Res., **63**, No. 1, 270-273 (1958). [Letter to Editor.]

Deutsch, E. R. The remanent magnetism of some lavas in the Deccan Traps. Phil. Mag., **3**, No. 26, 170-184 (1958).

Dodson, H. W., and E. R. Hedeman. Geomagnetic disturbances associated with solar flares with major premaximum bursts at radio frequencies $\leq$ 200 Mc/s. J. Geophys. Res., **63**, No. 1, 77-96 (1958).

Eleman, F. A 16 mm film recorder for studies of rapid geomagnetic variations. Stockholm, Kungl. Sjöfartsstyrelsen, Jordmagnetiska Pub. No. 16, 12 pp. (1957).

Finch, H. F., and B. R. Leaton. The earth's main magnetic field—epoch 1955.0. Mon. Not. R. Astr. Soc., Geophys. Sup., **7**, No. 6, 314-317 (1957).

Gebhardt, R. E. Fredericksburg three-hour-range indices K for October to December, 1957. J. Geophys. Res., **63**, No. 1, 248 (1958).

Helwan Observatory. Magnetic report for the year 1947. Published under the direction of Prof. A. H. Samaha, Director of Helwan Observatory, Cairo University Press, 54 pp. (1957).

Irving, E., and R. Green. The palaeomagnetism of the Kainozoic basalts of Victoria. Mon. Not. R. Astr. Soc., Geophys. Sup., **7**, No. 6, 347-359 (1957).

Kato, S. Time characteristics of magneto-hydrodynamical dynamos. J. Phys. Earth, **5**, No. 1, 15-24 (1957).

Leaton, B. R. Improving world magnetic charts. Mon. Not. R. Astr. Soc., Geophys. Sup., **7**, No. 6, 318-323 (1957).

Lovö. Ergebnisse der Beobachtungen des magnetischen Observatoriums zu Lovö (Stockholm) im Jahre 1955. Von Folke Eleman und Kjell Borg. Stockholm, Kungl. Sjöfartsstyrelsen, 30 pp. (1957).

Maeda, H. Horizontal wind systems in the ionospheric E region deduced from the dynamo theory of the geomagnetic S_q variation. Part III. J. Geomag. Geoelectr., **9**, No. 2, 86-93 (1957).

Maeda, H. Wind systems for the geomagnetic S_d field. J. Geomag. Geoelectr., **9**, No. 2, 119-121 (1957).

Nagata, T., T. Oguti, and K. Momose. Preliminary report of geomagnetic observations at Prince Harald Coast, Antartica. Rep. Ionosphere Res. Japan, **11**, No. 2, 41-49 (1957).

Nairn, A. E. M. A palaeomagnetic study of Jurassic and Cretaceous sediments. Mon. Not. R. Astr. Soc., Geophys. Sup., **7**, No. 6, 308-313 (1957).

Romañá, A., J. Bartels, and J. Veldkamp. International data on magnetic disturbances, third quarter, 1957. J. Geophys. Res., **63**, No. 1, 243-247 (1958).

Thailand. Report on the operations of the Royal Survey Department, Ministry of Defence, for the year 1951-52. Printing Office, Royal Survey Dept., 32 pp. (rec'd Feb. 24, 1958). [Contains some results of magnetic field observations, 1951-52.]

Theis, H. Über erdmagnetische Pulsationen. D. Hydrogr. Inst., Hamburg (Spec. Pub. No. 4, D. Hydrogr. Zs.), 29 pp. + 1 table (1957).

Tromsø, Auroral Observatory. Observations 1955. Bergen, Norska Inst. Kosmisk Fysikk, No. 40, 31 pp. (1957). [Contains results of magnetic, ionospheric, and ozone observations for the year 1955; also annual means of *D*, *H*, and *Z* for the years 1930-1955.]

United States Coast and Geodetic Survey. Magnetograms and hourly values, Tucson, Arizona, 1953. Washington, D. C., U. S. Coast Geod. Surv., No. MHV-Tu53, 140 pp. (1957).

Uyeda, S. Thermo-remanent magnetism and coercive force of the ilmenite-hematite series. J. Geomag. Geoelectr., **9**, No. 2, 61-78 (1957).

Watson, G. S., and E. Irving. Statistical methods in rock magnetism. Mon. Not. R. Astr. Soc., Geophys. Sup., **7**, No. 6, 289-300 (1957).

Wingst Observatorium. Magnetogramme Wingst 1955—1. Januar bis 31. Dezember. D. Hydrogr. Inst., Hamburg, Pub. No. 2503, 98 pp. (1957).

Witteveen Magnetic Observatory. Yearbook 1953—one hundred and fifth volume. B—Geomagnetism. 'S-Gravenhage, K. Nederlands Met. Inst., No. 98, v + 28 pp. (1957). [Contains hourly values of the magnetic elements for 1953 at Witteveen.]

B—*Terrestrial Electricity*

Chalmers, J. A. Point-discharge current, potential gradient and wind-speed. J. Atmos. Terr. Phys., **11**, Nos. 3/4, 301-302 (1957). [Letter to Editor.]

Kraakevik, J. H. The airborne measurement of atmospheric conductivity. J. Geophys. Res., **63**, No. 1, 161-169 (1958).

Miranda, H. A., Jr. The ionization due to beta radiation from the atmosphere. J. Geophys. Res., **63**, No. 1, 147-155 (1958).

Murphy, T. The formation and disappearance of fog in photo-electric nucleus counters. Geofisica pura e appl., **36**, 35-40 (1957).

Pawsey, J. L. Radar observations of lightning on 1.5 metres. J. Atmos. Terr. Phys., **11**, Nos. 3/4, 289-290 (1957).

Pollak, L. W. Methods of measuring condensation nuclei. Geofisica pura e appl., **36**, 21-26 (1957).

Pollak, L. W., and J. Daly. A condensation nucleus counter with stereo-photomicrographic recording. Geofisica pura e appl., **36**, 27-34 (1957).

Pollak, L. W., and A. L. Metnieks. Photo-electric condensation nucleus counters of high precision for measuring low and very low concentrations of nuclei. Geofisica pura e appl., **37**, 174-180 (1957).

Pollak, L. W., and A. L. Metnieks. The fog in the photo-electric nucleus counter. Geofisica pura e appl., **38**, 181-203 (1957).

Rönicke, G. Zur Methodik luftelektrischer V: Über eine Radiosonde zur Messung des Potentialgefälles in der freien Atmosphäre. Beitr. Geophysik, **66**, Heft 4, 313-322 (1957).

Sivaramakrishnan, M. V. Point discharge current, the earth's electrical field and rain charges during disturbed weather at Poona. Indian J. Met. Geophys., 8, No. 4, 379-384 (1957).

Twomey, S. Electric charge separation in subfreezing cumuli. Tellus, **9**, No. 3, 384-393 (1957).

Woessner, R. H., W. E. Cobb, and R. Gunn. Simultaneous measurements of the positive and negative light-ion conductivities to 26 kilometers. J. Geophys. Res., **63**, No. 1, 171-180 (1958).

C—*Cosmic Rays*

Barton, J. C., and J. H. Stockhausen. Time variations of the cosmic ray intensity in Jamaica. Phil. Mag., **3**, No. 25, 55-62 (1958).

Beiser, A. Cosmic-ray trapping in interplanetary space. J. Geophys. Res., **63**, No. 1, 1-17 (1958).

Boischot, A., et J.-F. Denisse. Les émissions de type IV et l'origine des rayons cosmiques associés aux éruptions chromosphériques. Paris, C.-R. Acad. sci., **245**, No. 25, 2194-2197 (1957).

Chapman, N. G., and N. V. Ryder. Time variations of cosmic rays at Wellington, New Zealand. J. Atmos. Terr. Phys., **11**, Nos. 3/4, 291-292 (1957). [Research note.]

Conforto, A. M., and J. A. Simpson. The 24-hour intensity variations of the primary cosmic rays. Nuovo Cimento, **6**, No. 5, 1052-1063 (1957).

Danielson, R. E., and P. S. Freier. Geomagnetic effects on heavy primary cosmic radiation at 42°N. Phys. Rev., **109**, No. 1, 151-157 (1958).

Kodama, M., I. Kondō, and M. Wada. Cut-off rigidities of cosmic-ray particles calculated for the eccentric dipole model of the earth's magnetic field. J. Sci. Res. Inst., Tokyo, **51**, 138-157 (Sept. 1957).

Missert, R. F. High-altitude intensities of the medium and heavy cosmic-ray nuclei and of the star-producing component over a 25-hour interval. Phys. Rev., **108**, No. 5, 1327-1330 (1957).

Miyazaki, Y. Comparison of cosmic-ray intensity variations observed at different altitudes. J. Sci. Res. Inst., Tokyo, **51**, 97-106 (Sept. 1957).

Pomerantz, M. A., S. P. Agarwal, and V. R. Potnis. Direct observation of periodic variation of primary cosmic-ray intensity. Phys. Rev., **109**, No. 1, 224-225 (1958). [Letter to Editor.]

Schaefer, H. J. Extra-atmospheric cosmic ray dosage during the large solar flare of 23 February 1956. Science, **127**, 186-187 (Jan. 24, 1958). [Report.]

Storey, J. R., A. G. Fenton, and K. G. McCracken. Effective magnetic meridian for cosmic rays. Nature, **181**, 34 (Jan. 4, 1958). [Letter to Editor.]

Young, O. B., and F. E. Harvey. Charge spectrum, mean free path, and flux of heavy primary cosmic rays at the top of the atmosphere. Phys. Rev., **109**, No. 2, 529-532 (1958).

D—*Upper Air Research*

Adams, R. M., N. McCumber, and M. Brinkman. Processed observational data for USSR satellites 1957 Alpha and 1957 Beta. Smithsonian Inst., Astrophysical Obsy, IGY Project No. 30.10, Spec. Rep. No. 10, 120 pp., mim. (March 1, 1958).

Annals of the International Geophysical Year. IGY Instruction Manual—Part I: Ozone. Pergamon Press, London-New York-Paris, Vol. 5, Pts. 1, 2, and 3, 244 pp. (1957).

Ashbrook, J., G. F. Schilling, and T. E. Sterne. Glossary of astronomical terms for the description of satellite orbits. Smithsonian Inst., Astrophysical Obsy., IGY Project No. 30.10, Spec. Rep. No. 4, 9 pp., mim. + reprint from Sky and Telescope, **17**, 66-68, 1957, "Celestial mechanics of artificial satellites," by T. E. Sterne (Nov. 30, 1957).

Barber, N. Timing errors in an equilateral array of receivers. J. Atmos. Terr. Phys., **11**, Nos. 3/4, 299-300 (1957). [Research note.]

Bates, D. R., and M. R. C. McDowell. Atmospheric helium. J. Atmos. Terr. Phys., **11**, Nos. 3/4, 200-208 (1957).

Bauer, S. J. An apparent ionospheric response to the passage of hurricanes. J. Geophys. Res., **63**, No. 1, 265-269 (1958). [Letter to Editor.]

Bedinger, J. F., E. R. Manring, and S. N. Ghosh. Study of sodium vapor ejected into the upper atmosphere. J. Geophys. Res., **63**, No. 1, 19-30 (1958).

Booker, H. G. The controversy concerning ionospheric turbulence at the meteoric level. J. Geophys. Res., **63**, No. 1, 97-107 (1958).

Bullough, K., T. W. Davidson, T. R. Kaiser, and C. D. Watkins. Radio reflections from aurora—III. The association with geomagnetic phenomena. J. Atmos. Terr. Phys., **11**, Nos. 3/4, 237-254 (1957).

Campbell, L., Jr., and J. A. Hynek. Visual observations of Alpha One made by MOONWATCH stations during lifetime of the object. Smithsonian Inst., Astrophysical Obsy., IGY Project No. 30.9, Spec. Rep. No. 6, 50 pp., mim. (Dec. 17, 1957).

Chandrasekhar, S. The partition of energy in hydromagnetic turbulence. Annals of Physics, 2, No. 6, 615-626 (1957).

Chapman, J. The waveforms of atmospherics and the propagation of very low frequency radio waves. J. Atmos. Terr. Phys., **11**, Nos. 3/4, 223-236 (1957).

Chvojková, E. Propagation of radio waves from cosmical sources. Nature, **181**, 105 (Jan. 11, 1958). [Letter to Editor.]

Couderc, P. Le satellite artificiel. Astronomie, **71**, 431-439 (novembre 1957).

Couderc, P. Les satellites artificiels. Astronomie, **71**, 453-470 (décembre 1957).

Dagg, M. The origin of the ionospheric irregularities responsible for radio-star scintillations and spread-*F*—I. Review of existing theories. J. Atmos. Terr. Phys., **11**, Nos. 3/4, 133-138 (1957).

Dagg, M. The origin of the ionospheric irregularities responsible for radio-star scintillations and spread-*F*—II. Turbulent motion in the dynamo region. J. Atmos. Terr. Phys., **11**, Nos. 3/4, 139-150 (1957).

Evans, J. V. The electron content of the ionosphere. J. Atmos. Terr. Phys., **11**, Nos. 3/4, 259-271 (1957).

Eyfrig, R. A critical discussion about special ionospheric characteristics. J. Atmos. Terr. Phys., **11**, Nos. 3/4, 163-176 (1957).

Ferraro, V. C. A. The coefficient of diffusion of ions in the *F*2 regions. J. Atmos. Terr. Phys., **11**, Nos. 3/4, 296-298 (1957). [Research note.]

Fleagle, R. G. Inferences concerning the dynamics of the mesosphere. J. Geophys. Res., **63**, No. 1, 137-146 (1958).

Gibbons, J. J., and B. Ramachandra Rao. Calculation of group indices and group heights at low frequencies. J. Atmos. Terr. Phys., **11**, Nos. 3/4, 151-162 (1957).

Goodwin, G. L. The movements of sporadic-*E* layer clouds. J. Atmos. Terr. Phys., **11**, Nos. 3/4, 177-186 (1957).

Gregory, J. B. Medium-frequency observations of the lower ionosphere during sudden disturbances. J. Geophys. Res., **63**, No. 1, 273-275 (1958). [Letter to Editor.]

Groves, G. V. Determination of impact point of a vertically-falling body by acoustical observations. J. Atmos. Terr. Phys., **11**, Nos. 3/4, 284-288 (1957).

Harrison, A. W., and W. Vallance Jones. Measurements of the absolute intensity of the aurora and night airglow in the 0.9-2.0 μ region. J. Atmos. Terr. Phys., **11**, Nos. 3/4, 192-199 (1957).

Heeschen, D. S. Neutral hydrogen in M32, M51, and M81. Astroph. J., **126**, No. 3, 471-479 (1957).

Heppner, J. P., and L. H. Meredith. Nightglow emission altitudes from rocket measurements. J. Geophys. Res., **63**, No. 1, 51-65 (1958).

Jacchia, L. G. Basic orbital data for satellite 1957 Beta One. Smithsonian Inst., Astrophysical Obsy., IGY Project No. 30.10, Spec. Rep. No. 9, 7 pp., mim. (Feb. 21, 1958).

Jackson, J. E., and J. C. Seddon. Ionosphere electron-density measurements with the Navy Aerobee-Hi rocket. J. Geophys. Res., **63**, No. 1, 197-208 (1958).

Jarrett, A. H., and P. L. Byard. On the possibility of observing aurorae in the daytime. J. Atmos. Terr. Phys., **11**, Nos. 3/4, 295-296 (1957). [Research note.]

Kato, S. Horizontal wind systems in the ionospheric *E* region deduced from the dynamo theory of the geomagnetic *Sq* variation. Part IV. J. Geomag. Geoelectr., Kyoto, **9**, No. 2, 107-115 (1957).

Keary, T. J., and H. J. Wirth. The random occurrence of meteors in the upper atmosphere. J. Geophys. Res., **63**, No. 1, 67-75 (1958).

Kellogg, P. J. Mechanism for production of x-rays by ion clouds striking the earth. Phys. Rev., **108**, No. 4, 1093-1094 (1957). [Letter to Editor.]

King, G. A. M. Relation between virtual and actual heights in the ionosphere. J. Atmos. Terr. Phys., **11**, Nos. 3/4, 209-222 (1957).

Lange-Hesse, G. Einfluss der erdmagnetischen Unruhe auf die Durchschnittsabweichungen der *F*1-Schicht-Tagesgrenzfrequenzen. J. Atmos. Terr. Phys., **11**, Nos. 3/4, 293-294 (1957) [Research note.]

Manning, L. A. The initial radius of meteoric ionization trails. J. Geophys. Res., **63**, No. 1 181-196 (1958).

Manring, E. R., and H. B. Pettit. The 5577A emission of [OI] in the night airglow from Sacramento Peak, New Mexico. J. Geophys. Res., **63**, No. 1, 39-49 (1958).

Massey, H. S. W., and R. L. F. Boyd. Scientific observations of the artificial earth satellites and their analysis. Nature, **181**, 78-80 (Jan. 11, 1958).

Meadows, R. W. The attenuation of radio waves reflected from the *E*-region of the ionosphere. Proc. Inst. Elec. Eng., **105**, Pt. B, No. 19, 22-26 (1958).

Meadows, R. W. The effect of the earth's magnetic field on absorption for a single-hop ionospheric path. Proc. Inst Elec. Eng., **105**, Pt. B, No. 19, 33-37 (1958).

Meadows, R. W., and A. J. G. Moorat. The effect of fading on the accuracy of measurement of ionospheric absorption. Proc. Inst. Elec. Eng., **105**, Pt. B, No. 19, 27-32 (1958).

Miranda, H. A., Jr. The radon content of the atmosphere in the New York area as measured with an improved technique. J. Atmos. Terr. Phys., **11**, Nos. 3/4, 272-283 (1957).

Munro, G. H. Travelling disturbances in the ionosphere: changes in diurnal variation. Nature, **180**, 1252-1253 (Dec. 7, 1957). [Letter to Editor.]

Murgatroyd, R. J. Winds and temperatures between 20 km and 100 km—a review. Q.J.R. Met. Soc., **83**, No. 358, 417-458 (1957).

Nichols, B. Drift motions of auroral ionization. J. Atmos. Terr. Phys., **11**, Nos. 3/4, 292-293 (1957). [Research note.]

Öpik, E. J. Problems in the physics of meteors. Amer. J. Phys., **26**, No. 2, 70-80 (1958).

Pobedonosçev, Yu. A. Laws of motion of an earth-satellite. Priroda, No. 1, 19-25 (1958). [Translation by E. R. Hope, Directorate of Scientific Information Service, Defence Research Board of Canada, Pub. No. T 283 R, March 1958.]

Purslow, B. W. Ionospheric drift in the *F*2 region near the magnetic equator. Nature, **181**, 35-36 (Jan. 4, 1958). [Letter to Editor.]

Reber, G. Between the atmospherics. J. Geophys. Res.,**63**, No. 1, 109-123 (1958).

Rumsey, N. J. Curvature-induced error in the analysis of fading records. J. Atmos. Terr. Phys., **11**, Nos. 3/4, 255-258 (1957).

Sato, T. Disturbances in the ionospheric *F*2 region associated with geomagnetic storms. III. Auroral latitudes. Kyoto, J. Geomag. Geoelectr., **9**, No. 2, 94-106 (1957).

Schilling, G. F. Soviet orbit information for USSR satellites 1957 Alpha Two and Beta One. Smithsonian Inst., Astrophysical Obsy, IGY Project No. 30.10, Spec. Rep. No. 8, 14 pp., mim. (Jan. 31, 1958).

Schilling, G. F., and E. S. Fergusson. Soviet orbit predictions and orbital information for USSR satellites 1957 Alpha One, Alpha Two, and Beta. Smithsonian Inst., Astrophysical Obsy., IGY Project No. 30.10, Spec. Rep. No. 5, 51 pp., mim. (Dec. 4, 1957).

Schilling, G. F., and T. E. Sterne. Preliminary orbit information for USSR satellites Alpha One and Alpha Two. Smithsonian Inst., Astrophysical Obsy., IGY Project No. 30.10, Spec. Rep. No. 1, 20 pp., mim. (Oct. 14, 1957; reissued Dec. 2, 1957).

Seddon, J. C. Differential absorption in the *D* and lower-*E* regions. J. Geophys. Res., **63**, No. 1, 209-216 (1958).

Stein, S. The role of ionospheric-layer tilts in long-range high-frequency radio propagation. J. Geophys. Res., **63**, No. 1, 217-241 (1958).

Sterne, T. E., and G. F. Schilling. Some preliminary values of upper atmosphere density from observations of USSR satellites. Smithsonian Inst., Astrophysical Obsy., IGY Project No. 30.10, Spec. Rep. No. 3, 10 pp., mim. (Nov. 15, 1957).

Sterne, T. E., B. M. Folkart, and G. F. Schilling. An interim model atmosphere fitted to preliminary densities inferred from USSR satellites. Smithsonian Inst., Astrophysical Obsy., IGY Project No. 30.10, Spec. Rep. No. 7, 8 pp. + 3 figs., mim. (Dec. 31, 1957).

Tandberg-Hanssen, E. Variations in the height of ionospheric layers during magnetic storms. J. Geophys. Res., **63**, No. 1, 157-160 (1958).

Wait, J. R. An extension to the mode theory of VLF ionospheric propagation. J. Geophys. Res., **63**, No. 1, 125-135 (1958).

Warren, E., and E. L. Hagg. Single-hop propagation of radio waves to a distance of 5,300 km. Nature, **181**, 34-35 (Jan. 4, 1958). [Letter to Editor.]

Warwick, J. W., and H. Zirin. Diurnal absorption in the *D*-region. J. Atmos. Terr. Phys., **11**, Nos. 3/4, 187-191 (1957).

Zelikoff, M., F. F. Marmo, J. Pressman, E. R. Manring, L. M. Aschenbrand, and A. S. Jursa. An attempt to measure atomic nitrogen by rocket release of ethylene at 105 and 143 km. J. Geophys. Res., **63**, No. 1, 31-37 (1958).

E—*Radio Astronomy*

Aarons, J., W. R. Barron, and J. P. Castelli. Radio astronomy measurements at VHF and microwaves. Proc. Inst. Radio Eng., **46**, No. 1, 325-332 (1958).

Akabane, K. A polarimeter in the microwave region. Proc. Inst. Radio Eng., **46**, No. 1, 194-19 (1958).

Barrett, A. H. Spectral lines in radio astronomy. Proc. Inst. Radio Eng., **46**, No. 1, 250-25 (1958).

Blum, E. J., J. F. Denisse, and J. L. Steinberg. Radio astronomy at the Meudon Observatory Proc. Inst. Radio Eng., **46**, No. 1, 39-43 (1958).

Booker, H. G. The use of radio stars to study irregular refraction of radio waves in the ionosphere Proc. Inst. Radio Eng., **46**, No. 1, 298-314 (1958).

Bracewell, R. N. Radio interferometry of discrete sources. Proc. Inst. Radio Eng., **46**, No. 1 97-105 (1958).

Bracewell, R. N. Restoration in the presence of errors. Proc. Inst. Radio Eng., **46**, No. 1, 106 111 (1958).

Cameron, W. S. A unique high-latitude sunspot group. Pub. Astr. Soc. Pac., **69**, No. 411, 561 563 (1957). [Notes from Observatories.]

Christiansen, W. N., and D. S. Mathewson. Scanning the sun with a highly directional array Proc. Inst. Radio Eng., **46**, No. 1, 127-131 (1958).

Coates, R. J. Measurements of solar radiation and atmospheric attenuation at 4.3-millimeter wavelength. Proc. Inst. Radio Eng., **46**, No. 1, 122-126 (1958).

Cohen, M. H. Radio astronomy polarization measurements. Proc. Inst. Radio Eng., **46**, No. 1 172-183 (1958).

Cohen, M. H. The Cornell radio polarimeter. Proc. Inst. Radio Eng., **46**, No. 1, 183-190 (1958)

Coutrez, R., J. Hunaerts, and A. Koeckelenbergh. Radio emission from Comet 1956 h o 600 mc. Proc. Inst. Radio Eng., **46**, No. 1, 274-279 (1958).

Dodson, H. W. Studies at the McMath-Hulbert Observatory of radio frequency radiation at th time of solar flares. Proc. Inst. Radio Eng., **46**, No. 1, 149-159 (1958).

Drake, F. D., and H. I. Ewen. Broad-band microwave source comparison radiometer for ad vanced research in radio astronomy. Proc. Inst. Radio Eng., **46**, No. 1, 53-60 (1958).

Emberson, R. M., and N. L. Ashton. The telescope program for the National Radio Astronom Observatory at Green Bank, West Virginia. Proc. Inst. Radio Eng., **46**, No. 1, 23-35 (1958)

Erickson, W. C. A mechanism of non-thermal radio-noise origin. Astroph. J., **126**, No. 3, 480 492 (1957).

Field, G. B. Excitation of the hydrogen 21-cm line. Proc. Inst. Radio Eng., **46**, No. 1, 240-25 (1958).

Findlay, J. W. Noise levels at the National Radio Astronomy Observatory. Proc. Inst. Radi Eng., **46**, No. 1, 35-38 (1958).

Callagher, P. B. An antenna array for studies in meteor and radio astronomy at 13 meters Proc. Inst. Radio Eng., **46**, No. 1, 89-92 (1958).

Gibson, J. E. Lunar thermal radiation at 35 kmc. Proc. Inst. Radio Eng., **46**, No. 1, 280-28 (1958).

Haddock, F. T. Introduction to radio astronomy. Proc. Inst. Radio Eng., **46**, No. 1, 3-12 (1958)

Heeschen, D. S., and N. H. Dieter. Extragalactic 21-cm line studies. Proc. Inst. Radio Eng. **46**, No. 1, 234-239 (1958).

Hey, J. S., and V. A. Hughes. A method of calibrating centimetric radiometers using a standar noise source. Proc. Inst. Radio Eng., **46**, No. 1, 119-121 (1958).

Horner, F. Radio noise from planets. Nature, **180**, 1253 (Dec. 7, 1957). [Letter to Editor.]

Jansky, C. M. The discovery and identification by Karl Guthe Jansky of electromagnetic radi ation of extraterrestrial origin in the radio spectrum. Proc. Inst. Radio Eng., **46**, No. 1 13-15 (1958).

Jasik, H. A wide-band antenna system for solar noise studies. Proc. Inst. Radio Eng., **46**, No. 1 135-142 (1958).

Jayaraman, A. Radio astronomy. Curr. Sci., Bangalore, **26**, No. 12, 369-374 (1957).

Kerr, F. J., and J. V. Hindman. Mass distribution of galactic neutral hydrogen. Pub. Astr Soc. Pac., **69**, No. 411, 558-560 (1957). [Notes from Observatories.]

Ko, H. C. The distribution of cosmic radio background radiation. Proc. Inst. Radio Eng., 46 No. 1, 208-215 (1958).

KRAUS, J. D. Radio telescope antennas of large aperture. Proc. Inst. Radio Eng., **46**, No. 1, 92-97 (1958).

KRAUS, J. D. Planetary and solar radio emission at 11 meters wavelengths. Proc. Inst. Radio Eng., **46**, No. 1, 266-274 (1958).

LAWRENCE, R. S. An investigation of the perturbations imposed upon radio waves penetrating the ionosphere. Proc. Inst. Radio Eng., **46**, No. 1, 315-320 (1958).

LILLEY, A. E., AND E. F. MCCLAIN. Absorption techniques as a tool for 21-cm research. Proc. Inst. Radio Eng., **46**, No. 1, 221-229 (1958).

LITTLE, C. G., AND H. LEINBACH. Some measurements of high-latitude ionospheric absorption using extraterrestrial radio waves. Proc. Inst. Radio Eng., **46**, No. 1, 334-348 (1958).

MARSHALL, L. A galactic model for production of cosmic rays and radio noise. Proc. Inst. Radio Eng., **46**, No. 1, 215-220 (1958).

MAXWELL, A., AND G. SWARUP. A new spectral characteristic in solar radio emission. Nature, **181**, 36-38 (Jan. 4, 1958). [Letter to Editor.]

MAXWELL, A., G. SWARUP, AND A. R. THOMPSON. The radio spectrum of solar activity. Proc. Inst. Radio Eng., **46**, No. 1, 142-148 (1958).

MAYER, C. H., T. P. MCCULLOUGH, AND R. M. SLOANAKER. Measurements of planetary radiation at centimeter wavelengths. Proc. Inst. Radio Eng., **46**, No. 1, 260-266 (1958).

MCCOY, C. T. Present and future capabilities of microwave crystal receivers. Proc. Inst. Radio Eng., **46**, No. 1, 61-66 (1958).

MEDD, W. J., AND A. E. COVINGTON. Discussion of 10.7-cm solar radio flux measurements and an estimation of the accuracy of observations. Proc. Inst. Radio Eng., **46**, No. 1, 112-118 (1958).

MENON, T. K. Hydrogen line study of stellar associations and clusters. Proc. Inst. Radio Eng., **46**, No. 1, 230-234 (1958).

MILLS, B. Y., A. G. LITTLE, K. V. SHERIDAN, AND O. B. SLEE. High resolution radio telescope for use at 3.5 M. Proc. Inst. Radio Eng., **46**, No. 1, 67-84 (1958).

PENFIELD, H. A phase tracking interferometer. Proc. Inst. Radio Eng., **46**, No. 1, 321-325 (1958).

PIDDINGTON, J. H. Cosmical electrodynamics. Proc. Inst. Radio Eng., **46**, No. 1, 349-355 (1958).

RAIMOND, E., AND L. M. J. S. VOLDERS. Preliminary observations of 21-cm emission from M33. Bull. Astron. Inst. Netherlands, **14**, No. 480, 19-20 (1957).

REBER, G. Early radio astronomy at Wheaton, Illinois. Proc. Inst. Radio Eng., **46**, No. 1, 15-23 (1958).

ROMAN, N. G., AND B. S. YAPLEE. Radio sources and the Milky Way at 440 mc. Proc. Inst. Radio Eng., **46**, No. 1, 199-204 (1958).

ROSSELAND, S., AND E. TANDBERG-HANSSEN. On some solar disturbances on 18 August and 24 September 1956. Astroph. Norvegica, **5**, No. 11, 279-287 + 4 pls. (1957).

SCHMIDT, M. The distribution of mass in M31. Bull. Astron. Inst. Netherlands, **14**, No. 480, 17-19 (1957).

SEEGER, C. L., G. WESTERHOUT, AND R. G. CONWAY. Observations of discrete sources, the Coma cluster, the moon, and the Andromeda Nebula at a wave length of 75 cm. Astroph. J., **126**, No. 3, 585-588 (1957). [Note.]

SHAIN, C. A. The Sydney 19.7-mc radio telescope. Proc. Inst. Radio Eng., **46**, No. 1, 85-88 (1958).

STRUM, P. D. Considerations in high-sensitivity microwave radiometry. Proc. Inst. Radio Eng., **46**, No. 1, 43-53 (1958).

SUZUKI, S., AND A. TSUCHIYA. A time-sharing polarimeter at 200 mc. Proc. Inst. Radio Eng., **46**, No. 1, 190-194 (1958).

TREXLER, J. H. Lunar radio echoes. Proc. Inst. Radio Eng., **46**, No. 1, 286-292 (1958).

TUOMINEN, J., AND M. KARRAS. A lunar occultation of the Crab Nebula at wave length 3.7 meters. Ann. Acad. Sci. Fennicae, A, VI, Physica 6, 8 pp. (1957).

VAN DE HULST, H. C., E. RAIMOND, AND H. VAN WOERDEN. Rotation and density distribution of the Andromeda nebula derived from observations of the 21-cm line. Bull. Astron. Inst. Netherlands, **14**, No. 480, 1-16 (1957).

WELLS, H. W. Flux measurements of Cassiopeia *A* and Cygnus *A* between 18.5 mc and 107 mc. Proc. Inst. Radio Eng., **46**, No. 1, 205-208 (1958).

Wild, J. P., and K. V. Sheridan. A swept-frequency interferometer for the study of high intensity solar radiation at the meter wavelengths. Proc. Inst. Radio Eng., **46**, No. 1, 160 171 (1958).

Yaplee, B. S. Radar echoes from the moon at a wavelength of 10 cm. Proc. Inst. Radio Eng **46**, No. 1, 293-297 (1958).

F—*Earth's Crust and Interior*

Aten, A. H. W. The calculation of the age of the elements. Physica, **23**, No. 12, 1073-1086 (1957)

Balakrishna, S. Elastic behaviour of rocks. Curr. Sci., Bangalore, **26**, No. 12, 377-379 (1957)

Båth, M. A continental channel wave, guided by the intermediate layer in the crust. Geofisic pura e appl., **38**, 19-31 (1957).

Båth, M. Shadow zones, travel times, and energies of longitudinal seismic waves in the presenc of an asthenosphere low-velocity layer. Trans. Amer. Geophys. Union, **38**, No. 4, 529-53 (1957).

Båth, M., and A. Vogel. Continental dispersion of seismic surface waves. Geofisica pura e appl **38**, 10-18 (1957).

Bolt, B. A. Earth models with continuous density distribution. Mon. Not. R. Astr. Soc., Geo phys. Sup., **7**, No. 6, 360-368 (1957).

Bolt, B. A. On taking means of density distributions in the earth. Mon. Not. R. Astr. Soc. Geophys. Sup., **7**, No. 6, 369-371 (1957).

Bolt, B. A. Earth models with chemically homogeneous cores. Mon. Not. R. Astr. Soc., Geophys Sup., **7**, No. 6, 372-378 (1957).

Curtis, G. H., and J. H. Reynolds. Notes on the potassium-argon dating of sedimentary rocks Bull. Geol. Soc. Amer., **69**, No. 2, 151-159 (1958).

Egyed, L. The magnetic field and the internal structure of the earth. Geofiz. Közl., Budapest **6**, Nos. 3-4, 3-8 (1957). [Abstract in English.]

Gutenberg, B. Zur Frage der Gebirgswurzeln. Geol. Rdsch., **46**, Heft 1, 30-38 (1957).

Hatherton, T. Shallow subsurface prospecting by the electrical resistivity method at Balclutha N. Z. J. Sci. Tech., B, **38**, No. 8, 807-819 (1957).

Lipson, J. Potassium-argon dating of sedimentary rocks. Bull. Geol. Soc. Amer., **69**, No. 2, 137 149 (1958).

G—*Miscellaneous*

Jefferies, J. T. Temperatures and electron densities in flares as derived from spectroscopic data Mon. Not. R. Astr. Soc., **117**, No. 5, 493-504 (1957).

Jensen, E., and T. S. Ringnes. The variation of the penumbra-umbra ratio of regular sunspot across the solar disk. Astroph. Norvegica, **5**, No. 10, 259-278 (1957).

Okhoçimski, D. Ye., T. M. Eneyev, G. P. Taratynova, and I. M. Yaçunski. Orbital pertur bations of artificial satellites. Uspekhi Fiz. Nauk, **63**, No. la, 33-50, 51-58, 59-71 (1957). [Translation by E. R. Hope, Directorate of Scientific Information Service, Defence Research Board of Canada, Pub. No. T 270 R, 42 pp., mim., Dec. 1957.]

Rogerson, J. B., Jr. Project Stratoscope—Solar photographs from 80,000 feet. Sky and Tele scope, **17**, No. 3, 112-115 (1958).

Urey, H. C. Diamonds, meteorites and the origin of the solar system. Proc. R. Inst., **36**, Pt. 2 No. 163, 451-455 (1957).

Waldmeier, M. Provisional sunspot-numbers for October to December 1957. J. Geophys. Res. **63**, No. 1, 248 (1958).

LETTERS TO EDITOR

ELECTRICAL CONDUCTIVITY IN THE GEOMAGNETIC STORM EFFECT

Hines[1] has recently argued that it is possible for the magnetic field of a ring ırrent to penetrate rapidly through the electrically conducting gas surrounding ıe earth because the geomagnetic field greatly reduces the conductivity per- əndicular to the lines of force. In this way, he argues that a ring current can very ıickly cancel (dissipate) part of the geomagnetic field at the surface of the earth › yield the main phase of a geomagnetic storm.

Now it was first pointed out by Schlüter,[2] and has since been discussed by 'ungey,[3] and by Cowling,[4] that the decay or dissipation of a magnetic field is *ɔt* enhanced by the reduction of conductivity perpendicular to **B**. As Cowling puts , one is justified in discussing the conductivity only if at the same time he considers ıe effective electric field.

The cancellation or dissipation of one magnetic field by another is merely a ıestion of Joule dissipation. And such dissipation, depending only upon the ectron collision frequency, is unaffected by magnetic fields. To take an extreme ıse by way of illustration, consider an ionized gas so tenuous that collisions may › neglected. Formally, the conductivity in the direction of an electric field **E**, hich is perpendicular to **B**, vanishes, for **E** results only in the electric drift velocity

$$\mathbf{v} = c\mathbf{E} \times \mathbf{B}/B^2 \qquad (1)$$

ıd is the same for both ions and electrons. From (1), it follows that $\mathbf{E} = -\mathbf{v} \times$ $/c$, and Maxwell's equation becomes the familiar hydromagnetic equation in

$$\partial \mathbf{B}/\partial t = \nabla \times (\mathbf{v} \times \mathbf{B})$$

which the lines of force are *permanently* connected in the frame of reference oving with **v**. Thus we see that when the perpendicular conductivity vanishes, ssipation of **B** vanishes and the field behaves as though in a *perfect* conductor.

From these facts, it may be seen that the time required for the field of a ring rrent to diffuse in to the surface of the earth—and there partially cancel the omagnetic field—is to be computed using the conductivity in the absence of agnetic fields. And the old difficulty[5] with the ring current remains: At least onths, and more probably years or centuries, are required for the diffusion of e ring-current field through the conducting gas around the earth to cancel the omagnetic field and produce a geomagnetic storm.

[1] C. O. Hines, J. Geophys. Res., 62, 491 (1957).
[2] A. Schlüter, Zs. Naturf., 5a, 72 (1950).
[3] J. W. Dungey, J. Atmos. Terr. Phys., 6, 88 (1954).
[4] T. G. Cowling, Magnetohydrodynamics, Interscience Publishers, Inc., New York (1957); 104.
[5] E. N. Parker, J. Geophys. Res., 61, 625 (1956).

The only ways in which one might attempt to weaken this argument agains the ring current would seem to be with Sweet's mechanism, as discussed elsewhere, or else by postulating a large abundance of neutral atoms in the vicinity of th earth, which would enhance the dissipation of the magnetic field, as discussed b Cowling[4,7] and Piddington.[8]

Otherwise it is necessary to seek geomagnetic storm processes alternative t the ring-current model, as, for instance, heating the gas above the ionosphere discussed elsewhere.[5]

E. N. Parker

Enrico Fermi Institute for Nuclear Studies,
University of Chicago,
Chicago, Illinois, December 30, 1957
(Received January 2, 1958)

[6]E. N. Parker, J. Geophys. Res., **62**, 509 (1957).
[7]T. G. Cowling, Mon. Not. R. Astr. Soc., **116**, 114 (1956).
[8]J. H. Piddington, Mon. Not. R. Astr. Soc., **116**, 314 (1956)

IONOSPHERIC PARAMETERS DEDUCED FROM THE FARADAY ROTATION OF LUNAR RADIO REFLECTIONS

The total electron content of the ionosphere has been determined by Browne, *t al.*,[1] and Evans[2,3] by deducing the rotation of the plane of polarization (Faraday ffect) of lunar radio echoes from fading curves of two closely spaced frequencies. 'he Faraday rotation arising from the double passage of linearly polarized radio 'aves through the ionosphere is given by

$$\phi = 4.72 \times 10^4 \cdot f^{-2} \cdot B \cdot \cos\theta \sec\delta \int_{h_1}^{h_2} N \, dh \text{ (radians)}$$

'here f is the frequency in cps, B the magnetic induction in gauss at ionospheric evels, θ the angle between the propagation path and the earth's magnetic field, δ he zenith angle of the propagation path, N the number of electrons per cm^3, dh height element in cm, and h_1 and h_2 the lower and upper limit, respectively, of he ionized region contributing to the Faraday rotation. Since ϕ is ambiguous in ıultiples of π, determination of absolute values of the total electron content of he ionosphere requires the use of two frequencies to resolve this ambiguity or a ıngle frequency high enough (>400 Mc/s) to have a total Faraday rotation less ıan π radians at the time of minimum electron concentration.

Measurements of the Faraday rotation at a frequency of 151.11 Mc/s have ecently been made by the writers,[4] using Belmar, New Jersey, as the transmitting te, Urbana, Illinois, as the receiving site, and the moon as reflector. Although ıese measurements do not give absolute values of total electron content directly, ıey provide a relatively sensitive measure of changes in electron content. The araday rotation ϕ measured in thirty-degree steps during the night of January -9, 1958, from 23:30 to 05:30 CST, was used to compute the change in total ectron content for that time period. For comparison purposes, the total electron ontent was also computed for a parabolic layer model, using Fort Monmouth, ew Jersey, ionosphere data. Figure 1 shows a plot of the change of total electron ontent n_F derived from Faraday rotation measurements which has been adjusted) an absolute scale on the basis of considerations outlined below. The total elec- on content for a simple parabolic layer model is also shown. Since vertical sound- g ionosphere data were available only for the transmitter location, while the araday rotation data were obtained over an oblique path, the plot for the para- olic layer was prepared by taking the resultant of two identical smoothed curves total electron content for a parabolic layer, having a time delay of one hour orresponding to the time difference between receiver and transmitter location).

The total electron content of the ionosphere may be expressed by

$$\int_{h_1}^{h_2} N \, dh = \int_{h_1}^{h_m} N \, dh + \int_{h_m}^{h_2} N \, dh$$

[1] I. C. Browne, J. V. Evans, J. K. Hargreaves, and W. A. S. Murray, Proc. Phys. Soc., B, **69**, 1 (1956).

[2] J. V. Evans, Proc. Phys. Soc., B, **69**, 953 (1956).

[3] J. V. Evans, J. Atmos. Terr. Phys., **11**, 259 (1957).

[4] F. B. Daniels and S. J. Bauer, Nature, to be published (1958).

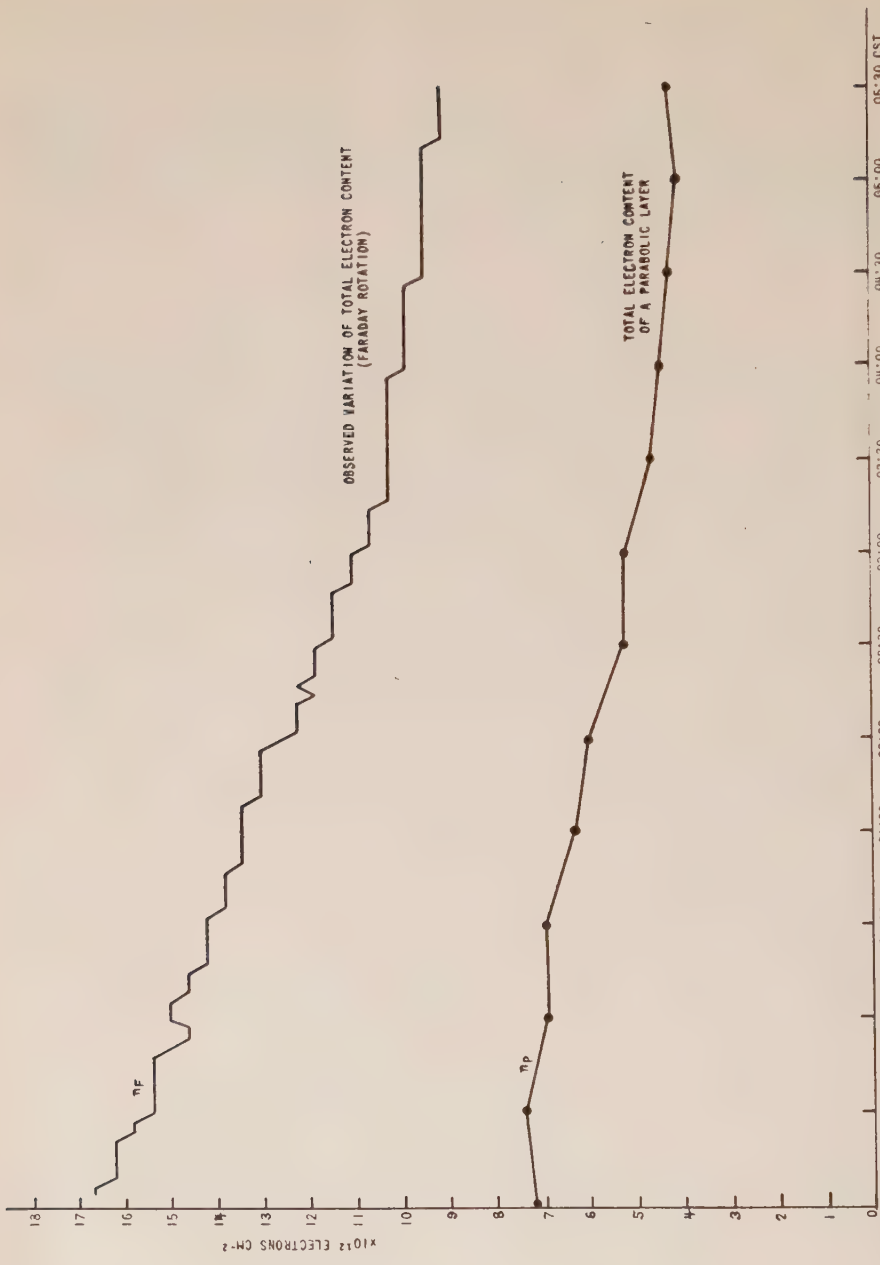

FIG. 1—Total electron content in a vertical column of 1 cm² cross-section through the ionosphere; n_F = total electron content

which may be rewritten

$$n = n_1 + n_2$$

where the first term on the right-hand side represents the electron content belo
the maximum electron density occurring at height h_m, while the second ter
represents the same quantity above the maximum.

For a simple parabolic layer, the total electron content can be expressed by

$$n_p = 2n_1$$

where $n_1 = 8.25 \times 10^{-9}(f^0F2)^2 \cdot y_m$. n_1 is given in quantities known or derivable from vertical sounding records (f^0F2 is the critical frequency in cps and y_m the semi-thickness of the parabolic layer in cm).

For night-time conditions, the continuity equation, assuming a linear law of electron loss and neglecting diffusion, can be written*

$$\frac{dn}{dt} = -\beta \cdot n$$

From Faraday rotation measurements, we can obtain $\Delta n_F/\Delta t$ and from the parabolic layer model $\Delta n_p/\Delta t$, that is, the average rate of change of total electron content.

Because of the departure of the true electron distribution from a parabolic layer, we will have

$$\frac{\Delta n_F}{\Delta t} = k \cdot \frac{\Delta n_p}{\Delta t}$$

and from the approximation of the continuity equation, assuming β = const,

$$n_F \cong k \cdot n_p$$

where n_F and n_p are understood to be the mean values over the time interval Δt. This relation can be used to adjust the absolute scale of total electron content (Fig. 1) obtained from Faraday rotation measurements on a single frequency, provided all the assumptions made hold for the case under consideration. Thus, in the case when the electron content below the maximum can be approximated by a simple parabolic layer model using available ionosphere data, the ratio of the number of electrons above the maximum to the number below the maximum can be expressed by

$$\frac{n_2}{n_1} \cong 2k - 1$$

since $n_1 + n_2 = n_F$ and also $n_F \cong k \cdot n_p = 2k \cdot n_1$.

Gledhill and Szendrei[5] and Burkard[6] have pointed out that the above ratio depends on the temperature distribution in the ionosphere. Thus, observational knowledge of this ratio should allow the testing of various ionospheric models, especially the one proposed by Burkard,[6,7] who considers a variable temperature gradient.

*If the logarithm of the total electron content (derived from Faraday rotation measurements) is plotted as a function of time, a straight line results, thus indicating that a linear law of electron loss actually holds. The slope of this line gives a numerical value of 3×10^{-5} sec^{-1} for β.

[5] J. A. Gledhill and M. E. Szendrei, Proc. Phys. Soc., B, **63**, 927 (1950).

[6] O. Burkard, Geofisica pura e appl., **22**, 1 (1952).

[7] O. Burkard, Geofisica pura e appl., **37**, 145 (1957).

In our case, the change in total electron content throughout the night measured by means of the Faraday rotation is 7.7×10^{12} electrons cm^{-2}, while the change over the same time interval of six hours for the parabolic model is 3.5×10^{12} electrons cm^{-2}. Thus, $k \approx 2.2$, and therefore during the night there are, on the average, about 3.4 times as many electrons above the maximum as below. This value is in good agreement with the results of Evans.[2,3]

Siegfried J. Bauer
Fred B. Daniels

U. S. Army Signal Engineering Laboratories,
Fort Monmouth, New Jersey, March 28, 1958
(Received April 1, 1958)

ION COMPOSITION OF THE ARCTIC IONOSPHERE

This is a brief summary of the preliminary ion composition results obtained from the IGY air and ion composition experiments flown at Fort Churchill, Manitoba, Canada. Three Aerobee-Hi rockets, identically instrumented with Bennett radio-frequency ion-mass spectrometers, were launched on 20 November 1956,[1] 21 February 1958, and 23 March 1958, their peak altitudes being 251, 225,* and 202* km, respectively. The November 1956 flight was at night, into an overcast which prevented observations of the overhead sky. The February 1958 flight was at night and entered an auroral display. The March 1958 flight was at noontime.

Positive and negative ions were detected on all flights. Figure 1 shows the distribution *vs* altitude of masses 32^+, 30^+, and 16^+ AMU, the major positive ions above Fort Churchill, Canada. The distribution for each flight is the average of ascent and descent data taken at approximately eight-second intervals, one-sixth of the total number of spectra. The relative abundance of an ion at a particular altitude is represented by the horizontal width of the area assigned to each ion. For example, the mass 16^+ AMU ion does not appear below 130 km, but becomes the predominant ion above 200 km on all flights. Beside the appearance of 16^+ at approximately 130 km, the following general features of the distribution are noteworthy. First, the relative abundance of 16^+ on both night-time flights is identical, and that for the daytime flight 16^+ increases more rapidly with altitude. Second, mass 30^+ AMU is the predominant positive ion in the night-time below 200 km, but during the daytime is supplanted by 32^+ below 100 km and by 16^+ above 150 km.

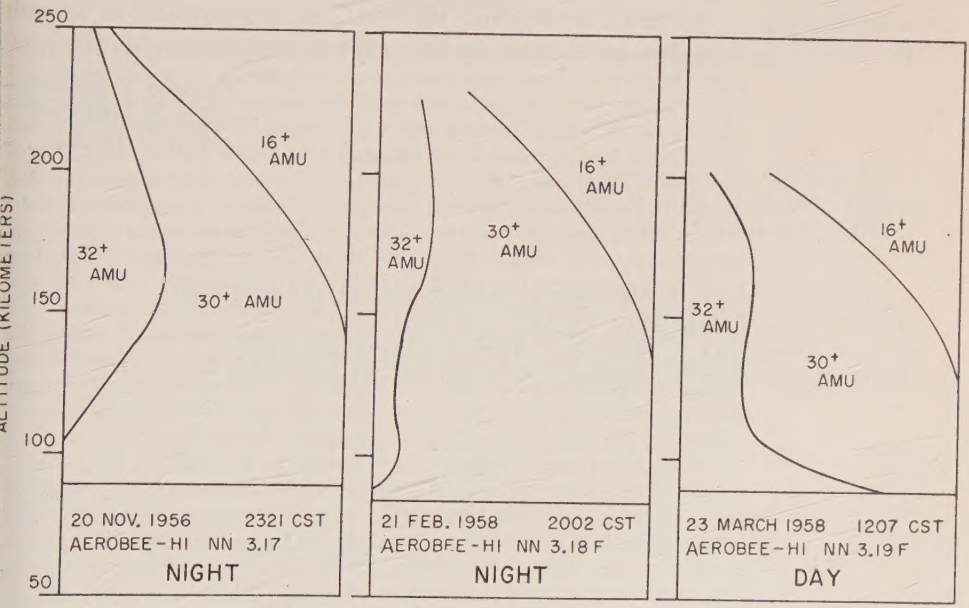

FIG. 1—Distribution of the major positive ions above Fort Churchill, Canada

[1]C. Y. Johnson, J. P. Heppner, J. C. Holmes, and E. B. Meadows, Ann. Géophys. (to be published).

*Preliminary data.

In addition to masses 32^+, 30^+, and 16^+ AMU, ions of masses 28^+, 18^+, and 14^+ AMU were detected on all flights. Their total maximum abundance is approximately 3 per cent. The major exception to this latter statement is that when NN3.18F was in an auroral display the relative abundance of the ions 32^+, 30^+, and 28^+ AMU became approximately equal in the 100-105 km region. This particular feature is not shown in Figure 1.

A negative ion in the region of mass 46^- AMU was detected on all Fort Churchill flights throughout most of the altitude range covered. This ion has now been detected on all flights in which a negative ion spectrometer was flown. (Reexamination of the Aerobee 23 flight record revealed a negative ion peak in the region of mass 46^- AMU.[1])

In view of the consistent results from the Fort Churchill flights, a few remarks about the ion composition results obtained at White Sands Proving Ground, New Mexico, seem appropriate. In the Viking 10 experiment,[2] a single positive-ion spectrometer was flown, but because of the negative charge acquired by the rocket and the evolution of gas from the rocket it was felt that the spectra obtained did not accurately represent the ambient ion composition; however, subsequent flights have detected some of the ions found on this flight. Vacuum-tight rockets, improved instrumentation, and the use of harmonic analysis[3] to determine the absolute mass of the ions have eliminated the difficulties encountered in the Viking 10 experiment. The identification of the single positive ion detected during the Aerobee 23 flight[4] as mass 28^+ AMU is still in accordance with the laboratory calibration of the experiment. For Aerobee 24,[5] the absence of positive ions, as stated previously, is particularly striking. However, an instrumental or systems failure, which was not detectable from the telemeter record, cannot be ruled out.

CHARLES Y. JOHNSON
EDITH B. MEADOWS
JULIAN C. HOLMES

U. S. NAVAL RESEARCH LABORATORY,
Washington 25, D. C., April 15, 1958
(Received April 17, 1958)

[2]C. Y. Johnson and E. B. Meadows, J. Geophys. Res., **60**, 193–203 (1955).
[3]C. Y. Johnson, J. Appl. Phys., **29**, 740 (April 1958).
[4]C. Y. Johnson and J. P. Heppner, J. Geophys. Res., **60**, 533 (1955).
[5]C. Y. Johnson and J. P. Heppner, J. Geophys. Res., **61**, 575 (1956).

NOTICE

When available, single unbound volumes can be supplied at $6 each and single numbers at $2 each, postpaid.

Charges for reprints and covers

Reprints can be supplied, but prices have increased considerably and costs depend on the number of articles per issue for which reprints are requested. It is no longer possible to publish a schedule of reprint charges, but if reprints are requested approximate estimates will be given when galley proofs are sent to authors. Reprints without covers are least expensive; standard covers (with title and author) can be supplied at an additional charge. Special printing on covers can also be supplied at further additional charge.

Fifty reprints, without covers, will be given to institutions paying the publication charge of $8 per page.

Alterations

Major alterations made by authors in proof will be charged at cost. Authors are requested, therefore, to make final revisions on their typewritten manuscripts.

Orders for back issues and reprints should be sent to Editorial Office, 5241 Broad Branch Road, N.W., Washington 15, D. C., U.S.A.

Subscriptions are handled by The Editorial Office, 5241 Broad Branch Road, N.W., Washington 15, D. C., U.S.A.

CONTENTS—Concluded

JOURNAL OF GEOPHYSICAL RESEARCH